Year : 2014

Role of the Epithelial Sodium Channel (ENaC) and its regulator CAPl/Prss8 in colon

Malsure Sumedha

Département de Pharmacologie et Toxicologie

Role of the Epithelial Sodium Channel (ENaC) and its regulator CAP1/*Prss8* in colon

Thèse de doctorat en sciences de la vie (PhD)

Présentée à la Faculté de biologie et de médecine
de l'Université de Lausanne

par

Sumedha Malsure

Master of Veterinary Pharmacology and Toxicology, Mumbai, India

Jury

Privat-docent Edith Hummler, Directeur de thèse
Prof. Bernard Rossier, Expert interne
Prof. Christoph Korbmacher, Expert externe
Prof. Sanjiv Luther, Président

Lausanne 2014

UNIL | Université de Lausanne
Faculté de biologie
et de médecine

Ecole Doctorale

Doctorat ès sciences de la vie

Imprimatur

Vu le rapport présenté par le jury d'examen, composé de

Président	Monsieur	Prof. Sanjiv	**Luther**
Directeur de thèse	Madame	Prof. Edith	**Hummler**
Experts	Monsieur	Prof. Bernard	**Rossier**
	Monsieur	Prof. Christoph	**Korbmacher**

le Conseil de Faculté autorise l'impression de la thèse de

Madame Sumedha Malsure

Master en sciences vétérinaires de Bombay Veterinary college, Mumbay, Inde

intitulée

**Role of the Epithelial Sodium Channel (ENaC)
and its regulator CAP1/*Prss8* in colon**

Lausanne, le 17 janvier 2014

pour Le Doyen
de la Faculté de Biologie et de Médecine

Prof.   Sanjiv Luther

Contents

Acknowledgements

Summary

In aldosterone-responsive epithelial cells of kidney and colon, the epithelial sodium channel (ENaC) plays a critical role in the control of sodium balance, blood volume, and blood pressure. The role of ENaC is well characterized in kidney and lung, whereas role of ENaC and its positive regulator channel-activating protease 1 (CAP1/*Prss8*) on sodium transport in colon is largely unknown. We have investigated the importance of ENaC and CAP1/*Prss8* in colon for sodium and potassium balance. Mice lacking the αENaC subunit (*Scnn1a*^{KO} mice) in intestinal superficial cells were viable and did not show any fetal or perinatal lethality. Under regular (RS) or low salt (LS) diet, the amiloride sensitive rectal potential difference (ΔPD_{amil}) was drastically decreased and its circadian rhythm blunted. Under regular salt (RS) or high salt (HS) diets or under potassium loading, plasma and urinary sodium and potassium were not significantly changed. However, upon LS, the *Scnn1a*^{KO} mice lost significant amounts of sodium in their feces, accompanied by very high plasma aldosterone and increased urinary sodium retention. Mice lacking the CAP1/*Prss8* (*Prss8*^{KO}) in intestinal superficial cells were viable and did not show any fetal or perinatal lethality. Upon RS and HS diets, however, *Prss8*^{KO} exhibited a significantly reduced ΔPD_{amil} in the afternoon, but its circadian rhythm was maintained. Upon LS diet, sodium loss through feces was accompanied by higher plasma aldosterone levels. Thus, we have identified the channel-activating protease CAP1/*Prss8* as an important *in vivo* regulator of ENaC in colon. Furthermore, we are investigating the importance of ENaC and CAP1/*Prss8* in pathological conditions like inflammatory bowel disease (IBD). Preliminary data showed that *Prss8*-deficiency led to worsening of DSS-induced colitis as compared to their respective controls.

Overall, the present study has shown that under salt restriction, the absence of ENaC in colonic surface epithelium was compensated by the activation of renin-angiotensin-aldosterone (RAAS) system in the kidney. This led to a colon specific pseudohypoaldosteronism type 1 with mineralocorticoid resistance without evidence of impaired potassium retention.

Keywords: serine protease, sodium transport, *Scnn1a*, *Prss8*, sodium and potassium balance, intestinal superficial cells

Résumé

Dans les cellules épithéliales sensibles à l'aldostérone, le canal sodique épithélial (ENaC) joue un rôle critique dans le contrôle de l'équilibre sodique, le volume sanguin, et la pression sanguine. Le rôle d'ENaC est bien caractérisé dans le rein et les poumons, cependant le rôle d'ENaC et son régulateur positif la protéase activatrice de canal 1 (CAP1/*Prss8*) sur le transport sodique dans le côlon reste en grande partie inconnu. Nous avons étudié l'importance d'ENaC et de CAP1/*Prss8* dans le côlon. Les souris déficientes pour la sous-unité αENaC (souris *Scnn1a*^{KO}) dans les cellules superficielles intestinales étaient viables et ne montraient pas de létalité embryonnaire ou postnatale. Sous diète normale (RS) ou pauvre en sodium (LS), la différence de potentiel rectale sensible à l'amiloride (ΔPD_{amil}) était drastiquement diminuée et son rythme circadien atténué. Sous diète normale (RS) ou diète riche en sodium (HS) ou fort chargement de potassium, le sodium et le potassium plasmatique et urinaire n'étaient pas significativement changé. Cependant, sous LS, les souris *Scnn1a*^{KO} perdaient des quantités significativement augmentées de sodium dans leurs fèces, accompagnées par de très hauts taux d'aldostérone plasmatique et une rétention urinaire en sodium augmentée. Les souris déficientes en CAP1/*Prss8* (*Prss8*^{KO}) dans les cellules superficielles intestinales étaient viables et ne montraient pas de létalité embryonnaire ou postnatale. Sous diètes RS et HS cependant, les souris *Prss8*^{KO} montraient une diminution significative du ΔPD_{amil} dans l'après-midi, mais le rythme circadien était maintenu. Sous diète LS, la perte de sodium par les fèces était accompagnée par des niveaux d'aldostérone plasmatiques plus élevés. Par conséquent, nous avons identifié la protéase activatrice de canal CAP1/*Prss8* comme un régulateur important d'ENaC dans le côlon *in vivo*. De plus, nous étudions l'importance d'ENaC et de CAP1/*Prss8* dans les conditions pathologiques comme les maladies inflammatoires chroniques de l'intestin (MICI). Le résultat préliminaire out montre qu'une déficience d'*Prss8* mènait à la détérioration de la colite induite par le DSS comparé aux modèles contrôles respectifs.

En résumé, l'étude a montré que sous restriction de sel, l'absence d'ENaC dans l'épithélium de surface du côlon était compensée par l'activation du système rénine-angiotensine-aldostérone (RAAS) dans le rein. Ceci a mené à un pseudohypoaldostéronisme de type I spécifique au côlon avec résistance aux minéralocorticoïdes sans signe d'altération de rétention de potassium.

Mots clés : protéase à serine, transport de sodium, *Scnn1a*, *Prss8*, équilibre sodique et potassique, cellules intestinales superficielles

List of abbreviations

AQP2: Aquaporin -2 channel

AE: Anion exchanger

ASDN: Aldosterone-sensitive distal nephron

ASIC: Acid-sensitive ion channel

CAP1: Channel activating protease 1

cAMP : Cyclic adenosine monophosphate

CD: Crohn's disease

CFTR: Cystic fibrosis transmembrane conductance regulator

ENaC: Epithelial sodium channel

H&E: Hematoxylin and eosin (staining)

IBD: Inflammatory bowel disease

$I_{SC:}$ Short-circuit current

I_{Na} : Sodium current

KO: Knockout

mCCD: mouse cortical collecting duct

mCNT: mouse connecting tubule

mDCT: mouse distal convoluted tubule

MR: Mineralocorticoid receptor

mRNA: Messenger ribonucleic acid

NCC: Na-Cl cotransporter

Nedd4-2: Neural precursor cell expressed developmentally down-regulated protein 4-2

NHE: Sodium –hydrogen Exchanger

NHERF: Na^+/H^+ exchanger regulatory factor

PCR: Polymerase chain reaction

PHA1: Pseudohypoaldosteronism type 1

pNCC : Phosphorylated Na-Cl cotransporter

qPCR: Quantitative PCR

SGK1: Serum and glucocorticoid-induced kinase 1

TRPV5: Transient receptor potential cation channel subfamily V member 5

UC: Ulcerative colitis

USP2: Ubiquitin specific peptidase 2

1. INTRODUCTION

1.1 The digestive system

The Digestive system is a group of organs and tissues involve in the breaking down of ingested food in the alimentary canal into a form that can be absorbed and assimilated by the tissues of the body (Osunderu AU,2008). The digestive system begins with the mouth and is followed by the pharynx, the esophagus, and the intestine, which is divided into two major sections: the small intestine and the large intestine. The small intestine can be subdivided into the duodenum, the jejunum, and the ileum. The large intestine is mainly comprised of caecum, colon and rectum. The intestinal epithelium is the most vigorously self-renewing tissue of adult mammals (van der Flier and Clevers, 2009).

The prime function of digestive tract is water, electrolyte and nutrient transport. The epithelium lining is in close contact with gastrointestinal lumen that is connected to external environment and is exposed to high bacterial and antigen load. Epithelium has to prevent pathogenic agents within gastrointestinal lumen from gaining access to internal tissues (Shen, 2009). The gastrointestinal tract forms a barrier in order to separate intestinal lumen from underlying tissue and also moving water, electrolytes and nutrient's across the barrier. Epithelial cells of gastrointestinal tract create a selectively permeable barrier that is tightly regulated. Intestinal mucosa also involves in host defense by engaging the mucosal immune system. Complex tissue organization and diverse cellular composition are necessary to face such a broad range of functions (Shen, 2009).

1.1.1 Organization of the gastrointestinal tract wall

The small and large intestine exhibits certain histologic characteristics similarities. The wall of the small intestine and colon is composed of four layers: mucosa which is the innermost layer (or mucous membrane); submucosa which is a layer of connective tissue that's supports the mucosa; muscularis externa (or muscularis propria), and adventitia (or serosa) which is the outermost layer of gastrointestinal tract as shown in **Fig.1A** (Osunderu AU,2008). The mucosa is composed of an innermost layer of epithelial cells, a layer of supporting loose connective tissue directly beneath the epithelium, termed the lamina propria, and a thin layer of smooth muscle cells, the muscularis mucosae, that forms the boundary between the mucosa and the submucosa (**Fig.1B, C)** (Shen, 2009).
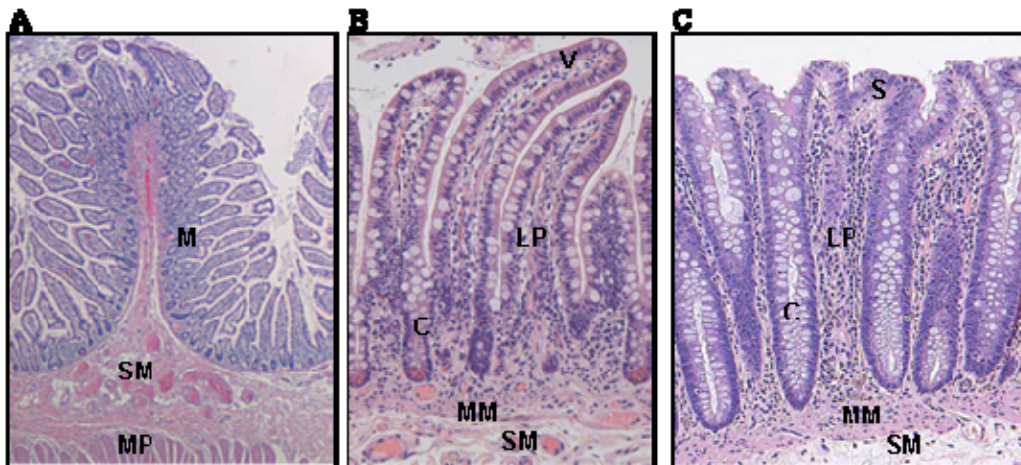
Figure. 1. Structure of Gastrointestinal tract

(**A**)The small intestinal mucosa mucosa (M) and submucosa (SM) are organized to increase the surface area for digestion and absorption. The mucosa is structurally divided into crypts and villi. The inner circular layer is muscularis propria (MP). (**B**) The lamina propria (LP) of small intestine is composed of connective tissue, blood vessels, and immune cells. The muscularis mucosa (MM) separates the mucosa from the submucosa (SM). (**C**) The colonic epithelium form crypts (C) along with flat surface epithelium.

1.1.2 Specialized epithelial cells of the gastrointestinal tract

1.1.2.1 Absorptive enterocytes

Enterocytes, the major cell type in the villus epithelium, are tall columnar cells whose primary function is nutrient absorption (Cheng and Leblond, 1974). At the apical surface, villus enterocytes are covered by a dense brush border composed of microvilli, microscopic extrusions with a length of ~1 mm (**Fig. 2**).
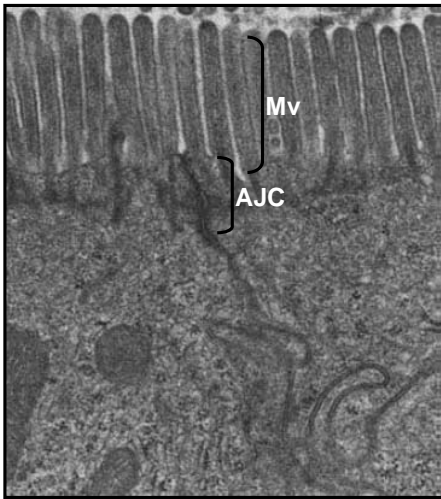
Figure 2. Absorptive enterocytes

This electron micrograph shows the apical portion of absorptive enterocytes. Microvilli (Mv) exist on the apical surface. The apical junctional complex (AJC) is specialized to mediate adhesion between adjacent enterocytes (Shen, 2009).

1.1.2.2 Undifferentiated Crypt Enterocytes

Undifferentiated crypt epithelial cells derived from the epithelial stem cells continue to divide within the crypt region. In contrast to villus absorptive enterocytes, undifferentiated crypt cells have shorter and less microvilli on their apical membranes. Physiologic salt and water secretion from the intestine depends on the activation of Cl^- channels in the apical membrane of epithelial cells lining the crypt, or secretory gland of the intestine (Welsh et al., 1982). These cells, termed "undifferentiated Cl^--secreting crypt cells", express the necessary ion channels, pumps, and cotransporters on their basolateral membranes to mass Cl^- ions inside the cell. Activation of Cl^--channels in the apical membrane allows Cl^- to flow out of the cell

down its electrochemical gradient into the crypt lumen. This ion flux hyperpolarizes the crypt lumen that drives Na^+ and water across inter epithelial tight junctions to produce a secretory response (Lencer et al., 1997).

1.1.2.3 Goblet cells

Goblet cells are mucin-producing cells that present throughout the small intestine and colon (Karam, 1999). The goblet cell morphology involves the mucin granules located below the apical membrane as shown in **Fig.3** (Kim and Ho, 2010). Goblet cells synthesize and secrete high-molecular weight glycoproteins 'mucins'. Upon secretion, it generates protective mucus blanket overlying the epithelial surface. Within the mucus gel, other components, including water, electrolytes, sloughed epithelial cells, and secreted immunoglobulin's, present. This makes a physical and chemical barrier that protects the epithelium from luminal agents such as enteric bacteria, bacterial and environmental toxins, and some dietary components that pose a threat to the mucosa (Kim and Ho, 2010).
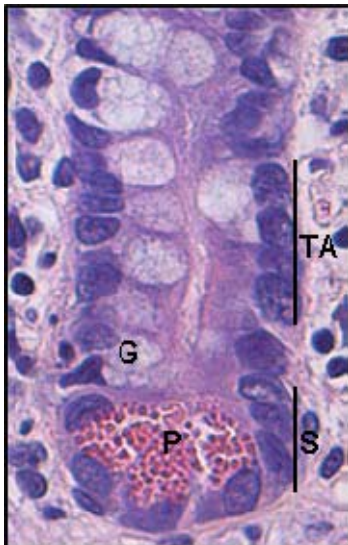
Figure 3. A crypt cell

Paneth cells (P) located at the bottom of the crypts, with prominent eosinophilic granules in the apical cytoplasm. Above the Paneth cells is the stem cell zone (S).The proliferating undifferentiated crypt enterocytes are located within the transit-amplifying zone (TA). Goblet cells (G) also present in the crypts (Shen, 2009).

1.1.2.4 Enteroendocrine Cells

Enteroendocrine cells are narrow at the apical side, and wide at the base, with relatively few microvilli at the apical surface. One of the important features of this cell type is the concentration of secretory granules in the basal end of the cytoplasm, below the nucleus (Schonhoff et al., 2004). The released hormones may function locally as paracrine signals or enter the blood stream to exert systematic effects. Specific functions for each enteroendocrine cell type are not clear, they might play critical role in intestinal function, as neurogenin-3 mutation, a critical transcriptional factor for these cells, leads to complete loss of enteroendocrine cells in human causing congenital malabsorptive diarrhea (Wang et al., 2006).

1.1.2.5 Paneth Cells

Paneth cells are secretory cells that normally present at the crypt base of the small intestine, cecum, and ascending colon as exhibited in **Fig.3**. Their distribution depends on surface expression of ephrin receptor EphB tyrosine kinases and their ephrin B ligands, as genetic deletion of these genes in mice causes Paneth cells to lose their normal localization in the crypt base (Batlle et al., 2002, van Es et al., 2005, Cortina et al., 2007). Paneth cells are pyramid-shaped columnar cells with basally localized nuclei; the apical cytoplasm is filled with eosinophilic and electron dense secretory granules. The exocytic granules contain antimicrobial molecules including lysozyme, phospholipase A, α1-antitrypsin, and antimicrobial peptides such as defensins. With the ability to secrete such a wide array of antibacterial proteins, Paneth cells are thought to be important in innate immunity. When Paneth cells are depleted by specific toxins or genetic manipulation, animals are more susceptible to bacterial infection (Wilson et al., 1999, Sherman et al., 2005).

1.1.3 Maintenance and regulation of the epithelial barrier

The intestinal epithelium is a single layer of cells lining the intestinal lumen and performs mainly 2 critical functions. It acts as a barrier to prevent the passage of harmful intraluminal entities, including foreign antigens, microorganisms, and their toxins (Podolsky, 1999, Blikslager et al., 2007). Second function is to be a selective filter, which allows the translocation of essential dietary nutrients, electrolytes, and water from the intestinal lumen into the blood circulation (Kunzelmann and Mall, 2002, Broer, 2008).

The intestinal epithelium performs selective permeability through transepithelial/ transcellular and paracellular pathways (**Fig.4**) (Tsukita et al., 2001). Transcellular permeability is mediated by solute transport via epithelial cells and regulated by selective transporters for amino acids, electrolytes , short-chain fatty acids, and sugars. The paracellular route is via transport between epithelial cells and is regulated by intercellular complexes present at apical-lateral membrane junction and along the lateral membrane (Groschwitz and Hogan, 2009).
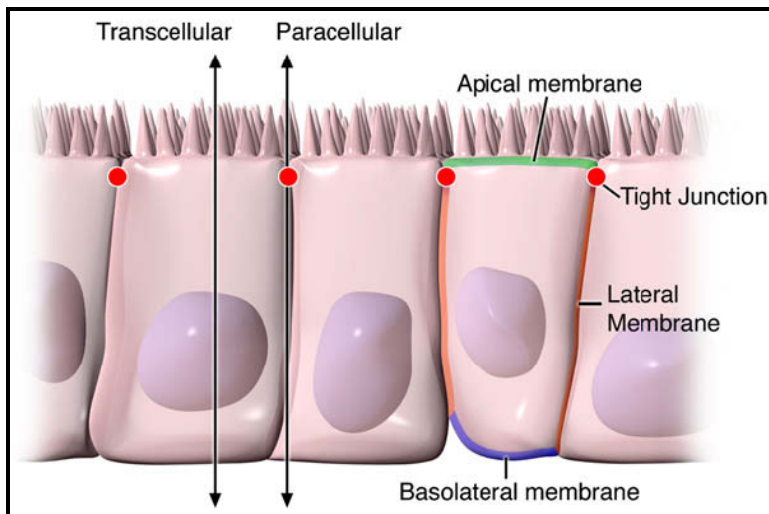
Figure 4. Intestinal epithelial permeability.

Intestinal epithelium makes a selective barrier which is maintained by transcellular and paracellular routes (Groschwitz and Hogan, 2009).

Intestinal epithelial cells are composed of 3 components that can be identified at the ultrastructural level: desmosomes, adherens junctions (AJs), and tight junctions (TJs; **Fig.5**) (Farquhar and Palade, 1963). The AJ and TJ complexes perform important function in the regulation of cellular proliferation, polarization, and differentiation (Tsukita and Furuse, 2000, Cereijido et al., 2004, Groschwitz and Hogan, 2009).
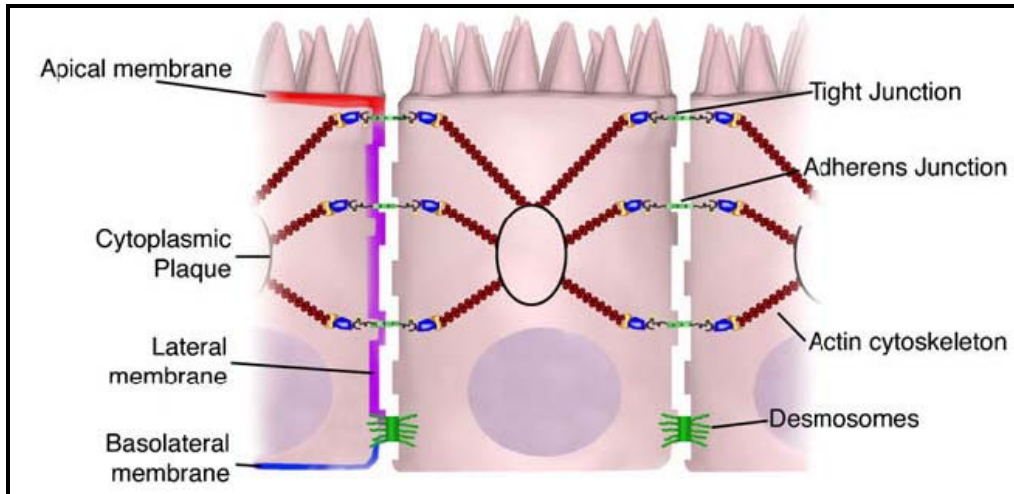
Figure 5. Components of intestinal epithelium.

The intestinal epithelium is made of a single layer of polarized epithelial cells. Desmosomes are located as dense plaques that are connected to keratin filaments. AJs and TJs both made of transcellular proteins connected intracellularly through adaptor proteins to the actin cytoskeleton (Groschwitz and Hogan, 2009).

1.1.4 Electrolyte transport in mammalian colon

The intestine functions as both a secretory and an absorptive organ, where 10 l of fluid enters the small intestine from ingestion and as secretions from a variety of sources, including the salivary glands, stomach, pancreas, and bile ducts as well as the small intestine. Of this 9 l, 7.5 l are mostly absorbed by the epithelial cells of the small intestine, and the remainder is absorbed by the colon. The small remaining volume that is not absorbed (100 to 200 ml) is excreted in feces. Thus, the intestine is capable of transporting very large volumes of fluid and electrolytes. However, these represent net values and do not take into consideration the

constant and dynamic exchange of fluid and electrolytes at the mucosal luminal interface necessary for digestion and physiologic homeostasis (Banks and Farthing, 2002).

The physiologic control of ion transport is complex and involves in relation to architecture of the whole intestine. Mostly secretion occurs through mucosal crypt cells while absorption takes place in the villous cells (Welsh et al., 1982).

1.1.4.1 Colonic electroneutral absorption of NaCl

Bulk transport of NaCl in the colonic epithelium is due to electroneutral absorption by luminal Na^+/H^+ and Cl^-/HCO_3^- exchange. The remaining absorption is electrogenic and is due to absorption via luminal epithelial sodium channel (ENaC) and transcellular/paracellular absorption of Cl^-. The contribution of paracellular Cl^- absorption might be limited by the paracellular shunt resistance, which is roughly 20 times larger than the transepithelial resistance (Gitter et al., 2000).

There is a clear segmental heterogeneity with respect to Na^+ absorption present in proximal and descending distal colon in human and other species. In the proximal colon, Na^+ transport is primarily mediated by an electroneutral process, while Na^+ transport in the descending colon is dominated by electrogenic absorption via amiloride-sensitive Na^+ channels under the influence of aldosterone (Levitan et al., 1962, Clauss et al., 1985, Sandle et al., 1986b). In the absence of steroids, electroneutral absorption is the predominant transport process in both rat proximal and distal colon (Foster et al., 1986, Binder et al., 1987, Foster et al., 1990). There are species differences exist regarding the contribution of electroneutral and electrogenic Na^+ absorption. For instance, electrogenic absorption dominates the rabbit distal colon, while the rat colon is dominated by electroneutral absorption (Potter and Burlingame, 1986). For electroneutral absorption of NaCl, the presence of parallel Na^+/H^+ and Cl^-/HCO_3^- exchangers in luminal brush-border membranes of colonic epithelial cells is required (**Fig. 6**). Na^+/H^+

14

exchangers type 2 and 3 (NHE2 and NHE3) is important for Na^+ absorption from the luminal side of the epithelium (Ikuma et al., 1999). Regulation of NHE2 and NHE3 differ in proximal and distal colon, in as much as expression of both types is upregulated by Na^+ depletion in the proximal colon, but is attenuated in the distal colon (Rajendran and Binder, 1990). The Na^+/H^+ exchange regulatory factor (NHERF) interacts with NHE3 and is required for cAMP-dependent inhibition of NHE3 (Yun et al., 1997, Weinman et al., 2000). Luminal NHE activity is paralleled by luminal Cl^-/OH^- and Cl^-/HCO_3^- exchange, due to the proteins DRA (downregulated in adenoma) and anion exchanger type 1 (AE1) (Schweinfest et al., 1993, Rajendran et al., 2000). Anion exchangers type 1 and 2 (AE1 and AE2) are responsible for basolateral anion exchange (Rajendran and Binder, 1999). The transport of Na^+ and Cl^- is coupled via changes in intracellular pH and Cl^- (Rajendran and Binder, 1990, Rajendran et al., 1995). It is regulated by Na^+ depletion or steroids (Ikuma et al., 1999, Winter et al., 1999).
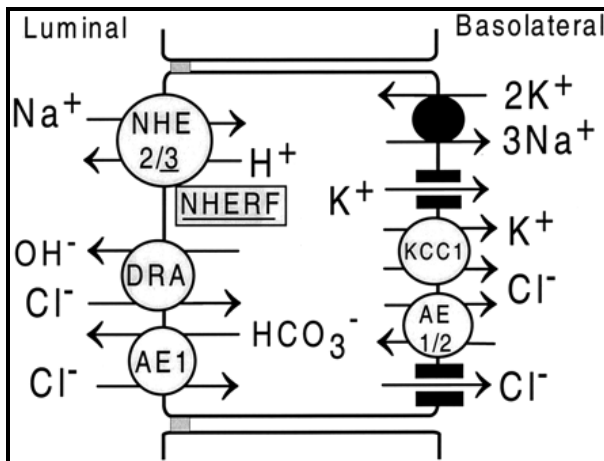
Figure 6. Electroneutral absorption in colon. (Kunzelmann and Mall, 2002).

1.1.4.2 Colonic electrogenic absorption of Na^+

In epithelial cells of distal colon, addition to electroneutral absorption by Na^+/H^+ and Cl^-/HCO_3^-, there is as well an electrogenic uptake of Na^+. The epithelial sodium channel (ENaC) is responsible for electrogenic absorption and is located in the surface membrane of colonic

epithelial cells. ENaC is potently inhibited by amiloride in nanomolar range (Rossier et al., 1994, Renard et al., 1995, Garty and Palmer, 1997). In addition to ENaC, other types of cation channels have been detected in the cecum (Sellin et al., 1988, Sellin and Dubinsky, 1994). Due to the electrochemical gradient for Na^+ and the negative cell membrane voltage, there is a large driving force for luminal Na^+ uptake via ENaC (Dawson, 1991). Absorption of Na^+ is accompanied by the counter ion Cl^-, which is taken up by Cl^- channels, localized in the apical membrane of absorptive epithelial cells shown in **Fig.7** (Mall et al., 1999). Na^+ is absorbed from the luminal side of the epithelium by epithelial Na^+ channels (ENaC). The basolateral Na^+-K^+-ATPase generates the driving force for the luminal Na^+ uptake by lowering intracellular Na^+ concentration. Basolateral cAMP and Ca^{2+}-activated K^+ channels are involved in the recycling pathway for K^+ (Kunzelmann and Mall, 2002). Na^+ uptake cause a large lumen-negative transepithelial voltage which facilitates Cl^- absorption through luminal cystic fibrosis transmembrane conductance regulator (CFTR) and/or other luminal Cl^- channels and eventually a Cl^-conductive paracellular shunt pathway. CFTR is the predominant luminal Cl^- channel in the colonic epithelium. Whole cell patch-clamp experiments and in situ hybridization suggests coexpression of CFTR and ENaC in surface and mid crypt epithelial cells of the rat colon (Trezise and Buchwald, 1991). Na^+ that has been taken up into the cell is pumped out again on the basolateral side of the epithelium by the Na^+, K^+-ATPase. Cl^- that have entered the cytosol via apical Cl^- channels leave the cell via basolateral Cl^- channels or Cl^-/HCO_3^- exchangers (Quinton, 1990). Basolateral KCl cotransporter (KCC1), Cl^- channels, and anion exchangers type 1 or 2 (AE1/2) may transport Cl^- to the blood side of the epithelium. K^+ secretion to the luminal side of the epithelium is driven by electrogenic uptake of Na^+ (Kunzelmann and Mall, 2002).
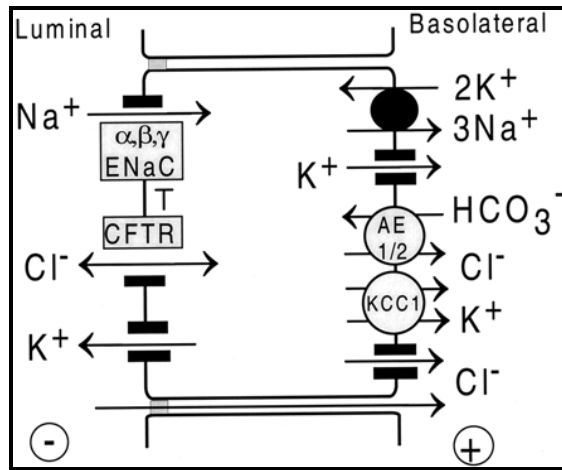
Figure 7. Electrogenic absorption in colon. (Kunzelmann and Mall, 2002).

ENaC expression along the intestine shows a great deal of plasticity. For instance, after proctocolectomy ENaC starts to be expressed in the distal part of the small intestine, i.e., the ileum, thereby unveiling the importance of an electrogenic amiloride-sensitive transport for the final reabsorption of salt and water in this part of the intestine (Koyama et al., 1999). The expression of α, β and γ ENaC is limited to the surface epithelial cells (Duc et al., 1994). Two independent studies revealed that endogenous aldosterone stimulation enhances β and γ ENaC mRNA transcript expression in rat distal colon (Lingueglia et al., 1994, Renard et al., 1995). Based on these results, it was proposed that ENaC activity is regulated by aldosterone-dependent transcriptional control of its β and γ subunits. Furthermore, a time course study of ENaC mRNA transcript expression in rat distal colon showed upregulation of β and γ ENaC mRNA 3 hours following aldosterone administration (Asher et al., 1996). If dietary sodium intake is low and plasma aldosterone levels are high, the distal colon can efficiently absorb dietary sodium against a large concentration gradient (Sandle, 1998, Kunzelmann and Mall, 2002). Enhanced ENaC expression in colon thus contributes to sodium retention observed in mice with Liddle's syndrome (Pradervand et al., 1999, Pradervand et al., 2003) along with increased responsiveness to aldosterone (Bertog et al., 2008). On the other side, down-

regulation of ENaC with reduction in sodium reabsorption in colon may contribute to diarrhea associated with inflammatory bowel disease (Amasheh et al., 2004, Zeissig et al., 2008).

1.1.4.3 Colonic electrolyte secretion

Intestinal secretion is not only important for digestion and absorption but also occurs as a result of pathophysiologic processes. Secretion involves the active transport of chloride and biocarbonate (Banks and Farthing, 2002, Kunzelmann and Mall, 2002). In the absorbing colon, release of K^+ to the luminal side is potential driven and largely maintained by the ENaC. This leads to a luminal K^+ concentration which is above that of plasma. As for the absorption of NaCl, polarized distribution of transport proteins is required for secretory salt transport. Thus secretory epithelial cells contain Cl^- and K^+ channels in their lumen membranes, which allows secretion KCl (Kunzelmann and Mall, 2002). In addition, after secretory stimulation and upon inhibition of absorption, paracellular transport of Na^+ facilitates secretion of NaCl (Schultheiss and Diener, 1997, Mall et al., 2000).

Electrolytes secretion in colon has been identified many years ago (Dawson, 1991) as described in **Fig.8.** Cl^- secretion is activated by cAMP-dependent stimulation of apical CFTR Cl^- channels, which are the prominent Cl^- channels in the native colon (Barrett and Keely, 2000, Greger, 2000). Cl^- secretion is paralleled by secretion of K^+ via luminal K^+ channels (Warth and Bleich, 2000) and Na^+ transport through the paracellular shunt. Cl^- is taken up into the cells by the basolateral Na^+-K^+-$2Cl^-$ cotransporter NKCC1 (Dawson, 1991, Kunzelmann and Mall, 2002). Cl^- transport is maintained by basolateral cAMP-activated KVLQT1/KCNE3 (Lohrmann et al., 1995, Warth et al., 1996), Ca^{2+}-activated SK4 (Bleich et al., 1996, Nielsen et al., 1998) and large-conductance Slo (BK channel) K^+ channels (Warth and Bleich, 2000).
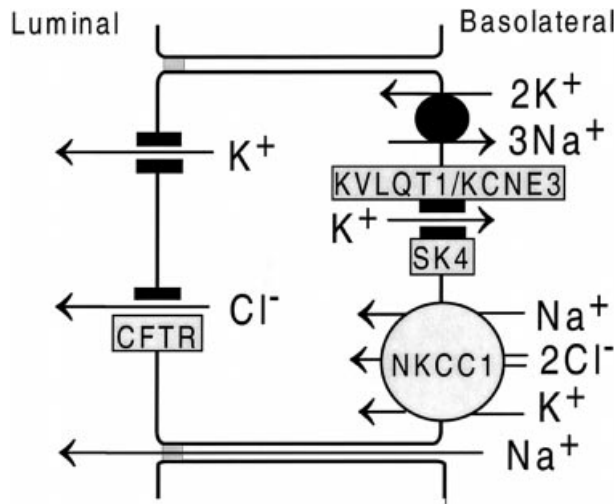
Figure 8.Colonic chloride secretion (Kunzelmann and Mall, 2002)

In parallel to KCl, bicarbonate is also secreted to the luminal side of the epithelium, producing an intestinal juice of slightly alkaline pH. HCO_3^- is secreted by different mechanisms, including electrogenic secretion via luminal CFTR Cl^- channels, a luminal $SCFA^-/HCO_3^-$ exchanger, and the luminal Cl^-/HCO_3^- exchanger DRA (Sullivan and Smith, 1986, Feldman and Stephenson, 1990).

1.1.4.4 Colonic potassium handling

The daily dietary K^+ intake of ~100 mmol is excreted predominantly by the distal tubules of the kidney. About 10% of the ingested K^+ is excreted via the intestine (Agarwal et al., 1994). One important basic aspect of K^+ transport in the colon is its segmental difference. Under normal conditions, the proximal colon performs net K^+ secretion while net K^+ absorption is observed in the distal colon (Sweiry and Binder, 1989, Rechkemmer et al., 1996). The proximal colon does not absorb K^+ actively (Foster et al., 1984). Active K^+ absorption in the distal colon occurs via the transcellular route and involves a primary active K^+ entry step across the apical membrane. In mammalian distal colon, this active transport is conducted by the non-gastric H^+/K^+ ATPase (HKα2) localise in surface cells of the distal colon as shown

in **Fig.9A** (Suzuki and Kaneko, 1989, Jaisser et al., 1993, DuBose et al., 1999). K^+ is initially pumped into the cytosol by the basolateral Na^+/K^+ ATPase or secondarily active via the basolateral secretory $Na^+/2Cl^-/K^+$ co-transporter (NKCC1). In a second step K^+ leaves the cell into the gut lumen via apical K^+ channels (Halm and Dawson, 1984, Sweiry and Binder, 1989).cAMP-mediated colonic K^+ secretion is conducted by the luminal BK channel (**Fig.9B**) (Sorensen and Leipziger, 2009, Sorensen et al., 2010a, Sorensen et al., 2010b).
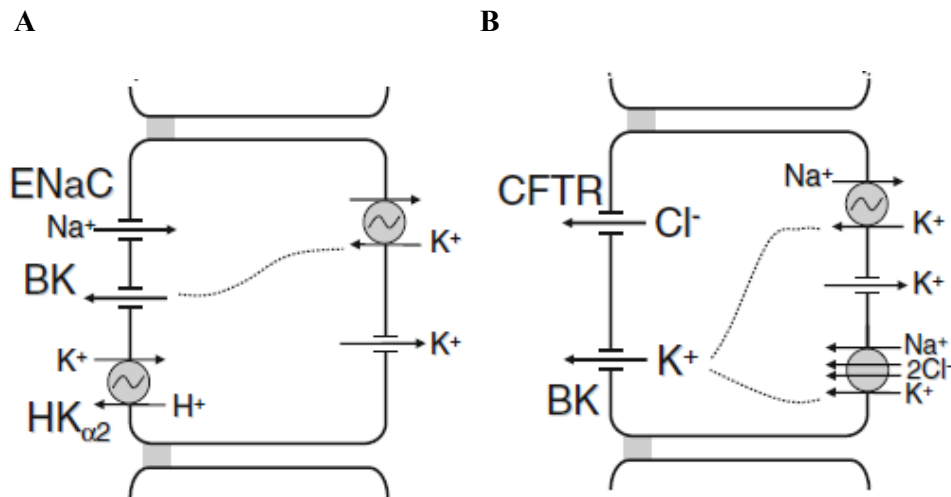
Figure 9: Schematic representation of potassium handling in distal colon (Sorensen et al., 2010b) (A) K^+ absorption in surface enterocytes of mammalian distal colon (B) K^+ secretion in crypt enterocytes of mammalian distal colon.

1.1.4.5 Water transport in colon

Water transport across the intestinal epithelium is a passive process and has been shown to be closely coupled with solute movement (Madara and Marcial, 1984). Although water movement carried out by paracellular or cellular pathway routes still remains controversial and evidence exists to support both pathways (Hasegawa et al., 1992, Loo et al., 1996).

1.2 Defective ion transport under pathological conditions

In parallel with the kidney, the gastrointestinal tract is uniquely positioned, both structurally and functionally, to maintain the electrolyte homeostasis, fluid homeostasis and passive mucosal defense. In an adult human, the gastrointestinal tract handles an average luminal daily load of nine liters of water under normal circumstances and 800mEq of Na^+ originating from ingestion as well as secretory fluids. Small intestine has a substantial capacity to absorb osmolytes and water (Banks and Farthing, 2002) , with nearly 80% of the daily load absorbed and approximately 2 l/day of resulting ileocecal flow. Large intestine has the capacity to absorb 1.5–1.9 l/day, although in pathological states with defective small intestinal absorption, the initiated adaptive mechanisms allow the colon to compensate with absorption rate reaching 5–6 l/day. Exceeding this maximal capacity will result in diarrhea, commonly observed in response to intestinal inflammation such as in chronic inflammatory bowel diseases or secondary to microbial infections (Kiela and Ghishan, 2009).

1.2.1 Secretory diarrhea

Disturbances in colonic electrolyte transport may be either congenital or acquired. Defective luminal Cl^-/ HCO_3^- exchanger DRA and defective Na^+/H^+ exchange leads to chloride ,sodium diarrhea respectively which considered as congenital origin (Hoglund et al., 1996, Muller et al., 2000). Intestinal colonization by pathogenic microorganisms is a major cause for acquired secretory and inflammatory diarrhea. Several species of bacteria induce secretory and inflammatory diarrhea, including *E. coli, Shigella flexneri, Salmonella typhimurium,* and *Vibrio cholerae*. These pathogens causes alteration of ion transport, disruption of tight junctions, and activation of an inflammatory response (Sandle, 2011).

1.2.2 Inflammatory diarrhea

Inflammatory bowel diseases (IBD) consist of 2 common types which include Crohn's disease (CD) and ulcerative colitis (UC) which is mainly characterized by diarrhea. In normal human distal colon and rectum, electrogenic Na^+ absorption (mediated by the epithelial Na^+ channel, ENaC) is the dominant Na^+ absorptive process and accounts for the substantial lumen-negative transmucosal electrical potential difference (PD) (Sandle, 2011). A loss of this PD is the hallmark of mucosal inflammation in active ulcerative colitis (UC), is proportional with impaired electrogenic Na^+ absorption, and reflects marked dysfunction of apically located ENaC, owing to downregulation of its β and γ-subunits by tumour necrosis factor-a (TNF-α) and/or interferon (IFN)-γ (Amasheh et al., 2004, Greig et al., 2004). Reduced colonic Na^+ absorption in UC may also observed due to defective electroneutral NaCl transport as colonic DRA is reduced in UC (Yang et al., 1998) and IFN-γ decreases activity and expression of NHE-3/-2 mRNA and protein rat colon as well as Caco-2 cells (Rocha et al., 2001). Additionally, reduced NHE-3 expression is seen in the IL-2 knockout mouse (Barmeyer et al., 2004). ENaC-mediated electrogenic Na^+ absorption was also markedly impaired in the non-inflamed sigmoid colon of patients with active CD of the terminal ileum (Zeissig et al., 2008). Additionally, reduced colonic ENaC γ-subunit transcription without a change in epithelial barrier function, while TNF-α produced similar changes in rat distal colon (Zeissig et al., 2008).

In a recent report, Sullivan and colleagues (Sullivan et al., 2009) described that in ileal or sigmoid biopsies of a considerable number of patients with active Crohn's disease or ulcerative colitis, there is reduced expression of NHE3, NHERF-1, NHE1, epithelial sodium channel (ENaC), and CLC-5 protein, with the latter suggested to participate in endosomal NHE3 trafficking rather than epithelial Cl^- conductance. These findings were recapitulated in

mouse models of chemically induced colitis, thus further highlighting and explaining the role of altered transepithelial Na^+ and fluid transport in IBD-associated diarrhea. Thus, impaired colonic Na^+ absorption not only contributes significantly to the pathogenesis of diarrhea in UC, but also appears to contribute to diarrhea in CD patients with disease restricted to the small intestine, in whom inflammatory cytokines are present at increased levels, even in histologically normal colon (Zeissig et al., 2008). Severe diarrhea in active and extensive UC often leads to hypokalemia, generally assumed to solely reflect K^+ leakage across the hyperpermeable inflamed colonic epithelium (Sandle et al., 2007). Does colonic ENaC in particular participates in mucosal responses to epithelial damage is largely unknown.

Intestinal inflammation is associated with defects in epithelial barrier function and ion flux, both contributing to impaired fluid homeostasis and diarrhea. The altered or increased permeability leads to increased transport of microbial flora and antigens from the intestinal lumen into the submucosa, which finally leads to inflammation and mucosal injury (Clayburgh et al., 2004). Decreased barrier function is known to be positively correlated with mucosal inflammation in Crohn's disease (Murphy et al., 1989) and ulcerative colitis patients. Structural changes associated with barrier dysfunction are well studied, although regulatory pathways that dynamically control intestinal barrier homeostasis are still less understood. CAP1/*Prss8* was identified as an important factor for maintenance of skin epithelial barrier homeostasis (Leyvraz et al., 2005). Thus, contribution of intestinal CAP1/*Prss8* to development of IBD is still important question to be address.

1.3 Epithelial sodium channel (ENaC)

In most forms of hypertension, increased sodium and water retention is responsible for development of this disease. This was proposed by Guyton years ago (Guyton et al., 1967). In case of hypertension, human mutation has been identified, which causes increase in the

function of epithelial sodium channel leads to sodium retention and elevation in blood pressure (Lifton, 1995). The epithelial sodium channel (ENaC) is the rate-limiting step for sodium absorption across tight epithelia and thus playing a vital role in blood pressure (BP) and blood volume. ENaC subunits were originally identified from rat colon using an expression cloning strategy with mRNA isolated from tissue of animals challenged with a low salt diet (Canessa et al., 1994b). The amiloride sensitive epithelial sodium channel (ENaC) has been predominantly described in the apical plasma membrane of epithelia. There, the ion channel mediates the first step of active sodium reabsorption in the kidney, colon, lung and sweat glands (Bhalla and Hallows, 2008, Schild, 2010).

ENaC belongs to a gene superfamily that involves genes identified from *Caenorhabditis elegans* based on mutations that result in mechanosensation defects (*mec*) or neurodegeneration (*deg*) (Canessa et al., 1993, Huang and Chalfie, 1994, Corey and Garcia-Anoveros, 1996), acid-sensing ion channels (ASIC) (Bassilana et al., 1997, Chen et al., 1998). ENaC is a heteromultimeric protein made of three homologous subunits, α, β and γ, and presents the limiting step of aldosterone-controlled sodium reabsorption (Canessa et al., 1994b). Without the α ENaC subunit, β and γ ENaC subunits are not transported to the membrane and no amiloride-sensitive sodium current is measured *in vitro* (Canessa et al., 1994b) or *in vivo* (Hummler et al., 1996, Rubera et al., 2003). Each subunit of ENaC shares approximately 30 to 40% sequence identity and consists of two transmembrane domain (M1, M2), short intracellular N- and C- termini, and a large extracellular loop. The β and γ subunits each contain a canonical "PY" motif in their COOH-termini (Canessa et al., 1994a) as shown in **Fig.10**. Various biochemical and functional evidence indicate heterotetrameric structure of the channel, likely comprising of 2α, 1β and 1γ subunits (Firsov et al., 1998, Dijkink et al., 2002). However crystal structure of an ASIC channel isoform (ASIC1$_A$) shows

a trimeric oligomerization (Gonzales et al., 2009). This subunit architecture of ENaC needs to be further studied.
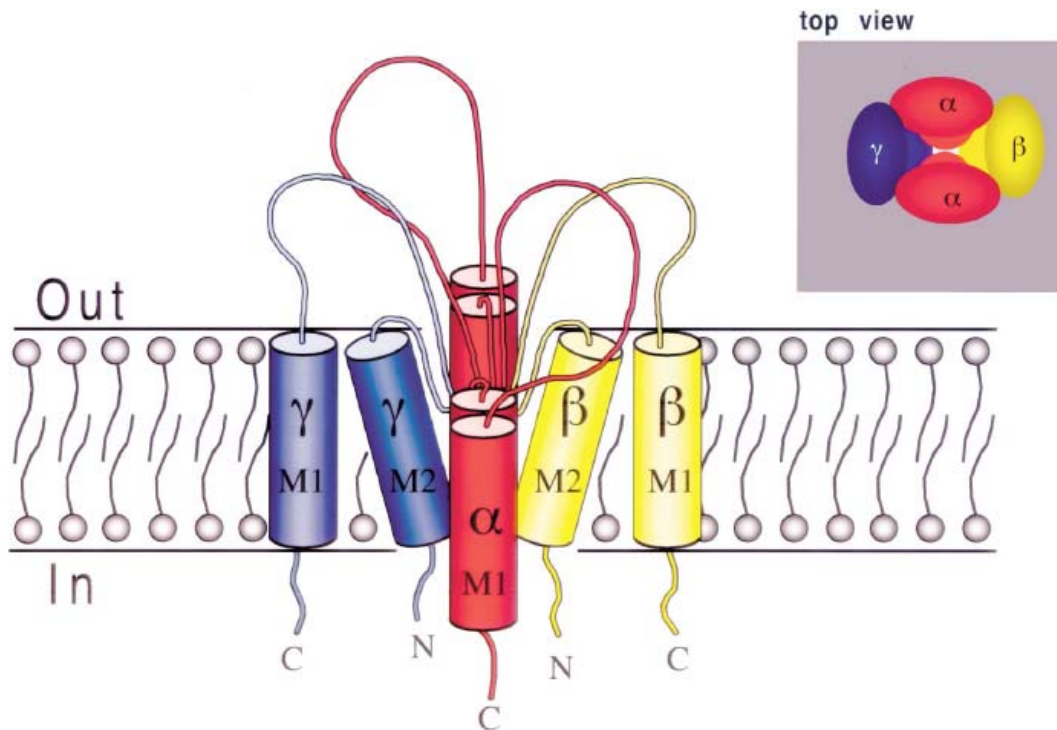
Figure 10. Structure of ENaC (Rossier et al., 2002)

The extracellular loop contains numerous potential N-linked glycosylation sites (Canessa et al., 1994a). Using a site-directed mutagenesis approach, amino acid residues has been identified to be involved in ion permeation and critical for channel block by amiloride. This segment of α, β. γ subunits may form a pore loop structure at the extracellular face of the channel, where amiloride binds within the channel lumen. This shows that amiloride interacts with Na^+ ions at an external Na^+ binding site preventing ion permeation through the channel pore (Schild et al., 1997). The C-terminus of each subunit contains proline-rich domain which is responsible for interactions with regulatory proteins (Grunder et al., 1997). ENaC is a constitutively active channel which is localized at apical membrane and exhibits short half-life of less than 60 mins (Alvarez de la Rosa et al., 2002, Lu et al., 2007). ENaC can be

inhibited by pharmacological blockers like amiloride or triamterene which acts on extracellular side and binds to second transmembrane segment which lines the channel pore (Kellenberger et al., 2003).

1.3.1 Implication of ENaC in human diseases

Liddle's syndrome is characterized by severe hypertension and low plasma potassium concentrations, metabolic alkalosis in combination with low levels of renin and aldosterone (Botero-Velez et al., 1994). This increased blood pressure in Liddle's syndrome can only be reduced under salt restriction and amiloride treatment. In 1994, Shimkets and colleagues (Shimkets et al., 1994), found a mutation in the amiloride-sensitive epithelial Na^+ channel (ENaC) that was present in members of a family afflicted with the genetic disease, Liddle's syndrome (Warnock, 2001, Garovic et al., 2006). The mutation identified is a 45 amino acid deletion in the cytosolic C-terminus of the β ENaC subunit. The mutation is relevantly rare, further more deletions identified in the C-terminus of γ subunit, but not in α subunit. Additionally, missense mutation causing Liddle's syndrome were identified in the both β and γ ENaC that involved the conserved proline-rich motif (Hansson et al., 1995, Schild et al., 1996). The mutation that is responsible for Liddle's syndrome led to an increased channel activity (Schild et al., 1995, Auberson et al., 2003) and open probability (Firsov et al., 1996).

Pseudohypoaldosteronism type 1 (PHA-1) is characterized by severe dehydration, hyponatremia, and hyperkalemia. This disease exhibits two clinical forms (i) an autosomal recessive form (affects several organs, systemic) which affect mainly kidney, colon, salivary gland and sweat ducts (ii) an autosomal dominant form which is restricted to only kidneys. Patients with a systemic form of PHA-1 harbor mutations in α, β and γ ENaC subunits (Chang et al., 1996). This nonsense, frameshift or missense mutations lead to channel 'loss of

function'. The autosomal dominant form of PHA-1 is caused by mutations in mineralocorticoid receptors (Geller et al., 1998).

1.3.2 Physiological role of ENaC (mouse models)

A number of mouse models have been generated in order to study the physiological and pathophysiological role of ENaC in the maintenance of whole body sodium homeostasis and regulation of blood pressure (Schild, 2010). Constitutive deletion of all subunits of ENaC shows the importance of ENaC in the regulation of Na^+ and K^+ balance. The constitutive α knockout mice died soon after birth showing hyperkalemia, metabolic and respiratory acidosis, and pulmonary edema due to impaired lung fluid clearance (Hummler et al., 1996). While, β , γ-deficient mice show a milder lung phenotype, with increased Na^+ excretion, high K^+ retention, and elevated plasma aldosterone levels (Barker et al., 1998, McDonald et al., 1999).

The epithelial Na^+ channel (ENaC) is expressed at the apical plasma membrane in many epithelial tissues throughout the body, including principal cells in the distal nephron of the kidney and epithelial cells in the urinary bladder, lung airway, distal colon, and ducts of salivary and sweat glands (Garty and Palmer, 1997). In the inner ear, ENaC seems to play an important role in controlling ionic composition of the endolymph which is required for mechanotransduction in hair cells (Grunder et al., 2001). In taste buds, a role in salt tasting was discovered (Chandrashekar et al., 2010). Recently, novel role of ENaC has been documented in embryo implantation by triggering prostaglandin E2 release (Ruan et al., 2012).

In order to understand organ-specific role of ENaC in kidney, α ENaC expression was selectively deleted in the CCD segment of the distal nephron, by using gene targeting

approach. These knockout mice did not exhibit any impairment in sodium handling by kidney and also plasma aldosterone levels were maintained. This data indicate that the CCD is dispensible for Na^+ homeostasis (Rubera et al., 2003). In order to investigate the role of α ENaC in CNT, CNT and CCD-specific knockout has been generated and these knockout mice showed lower plasma sodium, increased plasma potassium, higher urinary sodium excretion and increased urine volume. Upon salt restriction, weight loss, increased urinary sodium excretion, and hyperkalemia were observed. Under both diets plasma aldosterone was elevated. This data pinpoint the importance of CNT for sodium and potassium homeostasis (Christensen et al., 2010). Recently, in our laboratory whole nephron-specific αENaC knockout has been generated (Romain Perrier, unpublished data). These knockout mice show severe body weight loss, hyponatremia, life-threatening hyperkalemia, increased urinary sodium excretion. However, the role of the ENaC-mediated Na^+ absorption in the colon in the maintenance of Na^+ balance is a still largely unknown.

1.3.3 Regulation of ENaC by extrinsic and intrinsic factors

In order to detect rapid changes in salt and water absorption and secretion, ENaC is regulated by several extrinsic and intrinsic factors. ENaC activity is ultimately controlled by regulation of channel expression/synthesis, intracellular channel trafficking, and single-channel properties such as open probability (*Po*) (Garty and Palmer, 1997) (Gormley et al., 2003). Open probability of channel is changed by intracellular and extracellular concentrations of Na^+, a decrease in the intracellular pH, an increase in intracellular Ca^{2+} and intracellular oxidative stress (Palmer and Frindt, 1987, Chraibi and Horisberger, 2002, Kellenberger et al., 2005, Anantharam et al., 2006).

ENaC is known to be downregulated by CFTR in Madin-Darby canine kidney (MDCK) cells but also other type of cells (Stutts et al., 1995, Berdiev et al., 2009). In cystic fibrosis,

perturbed ENaC and CFTR regulation leads to an increase in ENaC activity, which causes enhanced mucous viscosity, decreased fluid clearance and bacterial colonization (Rotin, 2000, Zhou et al., 2011). The importance of ENaC in cystic fibrosis by generation of transgenic mice airway-specific overexpressing β ENaC has been studied (Mall et al., 2004, Zhou et al., 2011). Recently, gain-of-function effect of the mutation in β subunit has been studied, which has been identified from a patient with cystic fibrosis-like symptoms, which may contribute to cystic fibrosis pathology by increasing sodium and fluid absorption in the respiratory tract (Rauh et al., 2013).

In general, epithelial sodium transport is regulated by aldosterone (Verrey, 1999, Shigaev et al., 2000), arginine vasopressin (AVP) (Ecelbarger et al., 2001), atrial natriuretic peptide (ANP) (Zeidel et al., 1988), insulin (Marunaka et al., 1992) and endothelin (Gilmore et al., 2001). One of the main determinants of the stability of ENaC at cell surface includes ubiquitylation. Ubiquitylation serves to tag proteins for rapid degradation. It is carried out by the sequential transfer of the 76 amino acid ubiquitin (Ub) from a ubiquitin-activating enzyme (E1), to a ubiquitin-conjugating enzyme (E2) and usually to a ubiquitin protein ligase (E3) such as Nedd4. The E3 enzyme is thus responsible for the attachment of ubiquitin, or multiubiquitin chains, onto lysine residues of target proteins (Rotin et al., 2001). Nedd4 E3 protein-ubiquitin ligases contain 3-4 WW domains responsible for binding to canonical PY motifs at the C-termini of the β and γ subunits of ENaC by the HECT domain of Nedd4-2 (Staub et al., 1997). Nedd4-2 shown to efficiently suppress ENaC activity by ubiquitylation of the active channel complex at cell surface and followed by clathrin-mediated endocytosis and degradation in *Xenopus* oocytes (Kamynina et al., 2001).

Aldosterone is essential to increase the number of active ENaC channel at cell surface (Loffing et al., 2000). Aldosterone induces the phosphatidylinoside 3'-kinase (PI3K)-

dependent kinase SGK1 (serum –and glucocorticoid-regulated kinase 1), a kinase which elevates ENaC level and activity at cell surface in *xenopus* oocytes (Alvarez de la Rosa et al., 1999). Later, mechanism has been revealed, SGK1 was found to phosphorylate Nedd4-2 leading to a decreased interaction and ubiquitylation of ENaC subunits, results in increased ENaC activity at cells surface (Debonneville et al., 2001) (**Fig.11**). In addition, ENaC regulation in CCD cells, Usp-45, a deubiquitinating enzyme, is potently upregulated by aldosterone and reverses the inhibitory effects of Nedd4-2 on ENaC retrieval (Fakitsas et al., 2007).

A further hormone involved in the regulation of ENaC, is vasopressin as shown in **Fig.11**. Vasopressin increases the activity of ENaC in the aldosterone-sensitive distal nephron (ASDN) (Bugaj et al., 2009). Vasopressin binds to the V2 receptors and stimulates the release of cAMP, which increase the number of ENaC channel at cell surface (Canessa and Schafer, 1992, Auberson et al., 2003). cAMP- dependent protein kinase (PKA) has been shown to phosphorylate nedd4-2, same like SGK1 and thereby preventing binding to ENaC (Snyder et al., 2004). PKA has also suggested modulating tyrosine kinase activity to increase apical expression of ENaC (Woollhead and Baines, 2006).
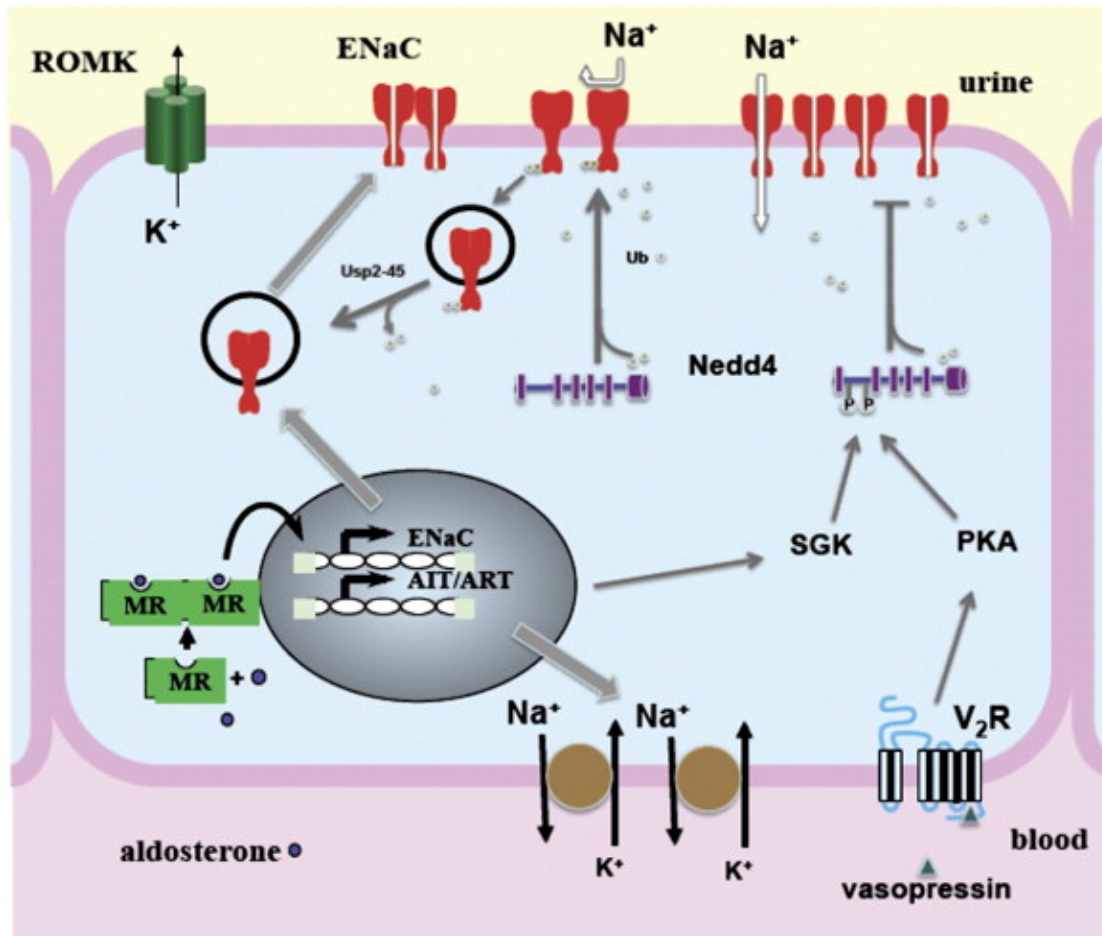
Figure 11. ENaC regulation by aldosterone and vasopressin (Schild, 2010)

After binding of aldosterone to its receptor (MR) and it translocate into the nucleus, where it binds with DNA responsive elements. This causes induction of AIT (aldosterone-induced transcripts) such as ENaC, the Na^+,K^+-ATPase ,SGK1 and ART (aldosterone-repressed transcripts).Vasopressin binds to its receptor V2R, which leads to activation of protein kinase 1 (PKA). Both SGK1 and PKA inactivate Nedd4-2 upon phosphorylation. Deubiquitylation by USP2-4 allows ENaC to recycle for endocytic vesicles back to cell surface (Schild, 2010)

There are some kinases which independently regulate ENaC. The ENaC cell surface expression and Na^+ current is unregulated by IκB kinase when interacts with ENaC in CCD cells (Lebowitz et al., 2004). With No Lysines (WNK1) also alter SGK1 activity results in increased ENaC activity, while Akt which also act similar to SGK1 which disrupts ENaC-Nedd4-2 binding results in stimulation of channel (Lee et al., 2007). The phosphorylation of Nedd4-2 by SGK1 and PKA stabilizes the interaction of Nedd4-2 with 14-3-3 scaffolding

proteins, preventing the Nedd4-2 dependent ubiquitylation of ENaC (Bhalla et al., 2005). AMP-activated kinase (AMPK) which is metabolic sensor can detect easily external stimuli or intracellular energy stores indirectly inhibits ENaC surface expression by increasing interaction between Nedd4-2 and ENaC (Bhalla et al., 2006). While, phosphatidylinositol 3-kinase influences both ENaC trafficking (through SGK1 and/or Akt) and P_o (Pochynyuk et al., 2006). These signaling pathways demonstrate a complex regulatory network that directly and indirectly influences ENaC surface expression and P_o.

Addition to this, a signaling cascade involving Raf 1-MAPK/ERK kinases acts to inhibit the cell surface expression of ENaC by stimulating interaction between Nedd4-2 and ENaC (Nicod et al., 2002, Falin and Cotton, 2007). Glucocorticoid-induced leucine zipper protein (GILZ) prevents activation of Raf1-MAPK/ERK pathway and their inhibitory effects on ENaC (Schild, 2010) .

1.4 Serine proteases

The Serine proteases perform variety of function which includes proteolysis of proteins as e.g., in blood clotting and fibrinolysis, humoral and cellular immunity, embryonic development and neuronal plasticity, extracellular matrix remodeling, hormone maturation, apoptosis, and fertilization. ENaC may be activated through cleavage by intra- and extracellular proteases see for review (Rossier and Stutts, 2009). ENaC-activating proteases belong to the PA (**P**roteases of mixed nucleophile, superfamily **A)** or SB clans of these proteases (Rawlings and Barrett, 1993). ENaC is regulated by some type II transmembrane serine proteases (TTSPs), enterokinase, corin, human airway trypsin-like proteases, the human TMPRSS subfamily, and matriptase (MT-SP1) (Hooper et al., 2001). Furin-like protein convertases that may play a critical role in ENaC activity belong to the SB clan, which also includes subtilisin and kexin (Page and Di Cera, 2008). Soluble proteases that

stimulate ENaC are from the PA clan, family S1, and include trypsin, chymotrypsin, and elastase (Rossier and Stutts, 2009).The mechanism involved in proteolytic regulation of ENaC is still under investigation. However, several putative (known and suspected) cleavage sites in α and γENaC has been identified, but not for β subunit (**Fig.12**) (Rossier and Stutts, 2009).
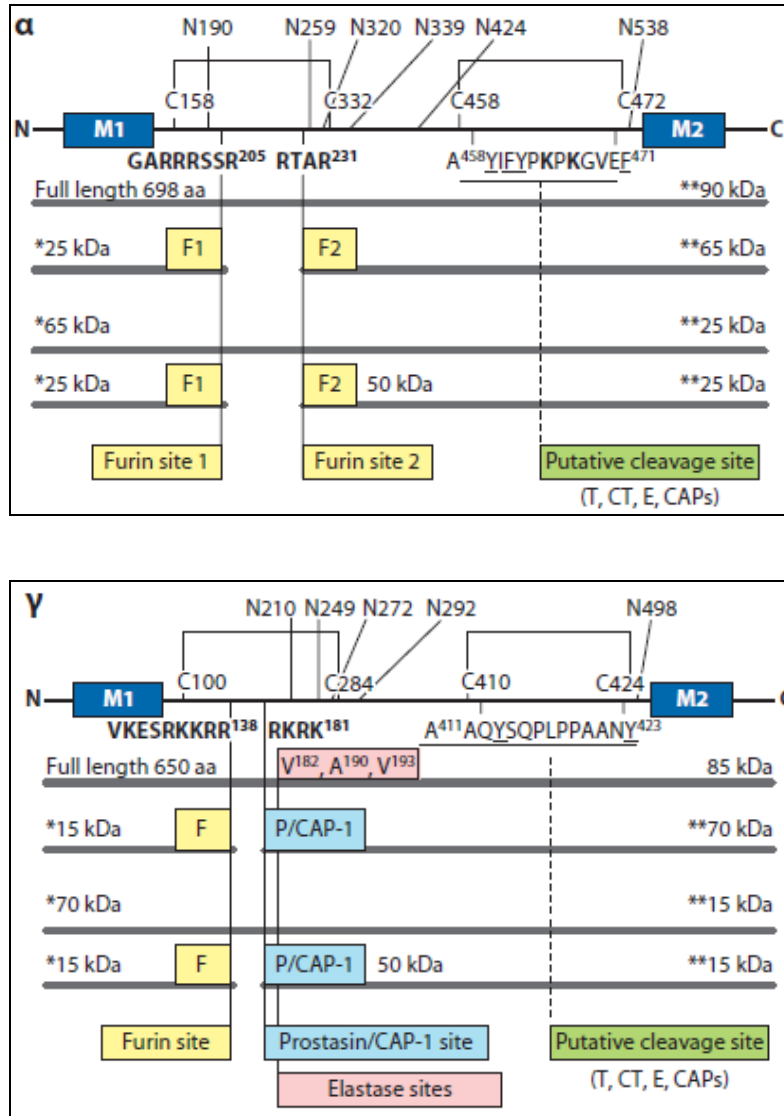
Figure 12. Linear model of ENaC cleavage sites (Rossier and Stutts, 2009)

(***Top***) In the α subunit model, (C158-C332) two furin cleavage sites (F) are identified (*yellow boxes*). Putative trypsin (T), chymotrypsin (CT), elastase (E), or SPs (C458-C472) are indicated (*green box*). (***Bottom***) In the γ subunit model, only one furin cleavage site (F) is observed (C100-C284) (*yellow*). A CAP-1/prostasin cleavage site (*light blue box*) and elastase cleavage sites (*pink box*) are indicated.

Putative trypsin (T), chymotrypsin (CT), elastase (E), or SPs within the second cysteine disulfide bridge (C410-C424) are indicated.

1.4.1 Channel-activating protease 1 (CAP1)/*Prss8*

The first observation that ENaC is regulated by endogenous serine proteases was made using functional complementation assay of α subunit that had been used to clone the β and γ subunits of ENaC (Canessa et al., 1994b). CAP1, also called prostasin was identified, as a factor that augments ENaC currents when coexpressed in oocytes (Vallet et al., 1997, Vallet et al., 1998). CAP-1 is a glycosyl-phosphatidylinositol (GPI)-anchored protein and, expressed to the apical membrane of epithelial cells (Chen et al., 2001). *Xenopus* CAP-1 and mouse CAP-1 are orthologs of human prostasin, purified from seminal fluid (Yu et al., 1994) and cloned from human prostate (Yu et al., 1995). These findings showed a new class of membrane-bound serine proteases and a novel regulatory pathway. Additionally, two additional SPs, mCAP-2 [homolog of human transmembrane protease serine 4 (TMPRSS4)] and mCAP-3 (MT-SP1/ matriptase or epithin), were identified by homology cloning and were found to increase the activity of ENaC coexpressed in *Xenopus* oocytes (Vuagniaux et al., 2002). In order to understand molecular mechanisms behind the regulation of ENaC by CAP1, *Xenopus* oocyte expression system has been used. Cell surface expression of CAP-1 is required for activation of ENaC (Vallet et al., 2002). The triple HDS (Histidine-aspartate-serine) catalytic mutant of mCAP1was still able to fully activate ENaC in the oocyte expression system (Andreasen et al., 2006). CAP1/*Prss8* stimulates ENaC-mediated sodium absorption at the cell surface by rapidly increasing the open probability (Vuagniaux et al., 2000, Vuagniaux et al., 2002), although the mechanism is not completely understood (Kleyman et al., 2009, Rossier and Stutts, 2009).

CAP1/*Prss8* is co-expressed with ENaC in many salt-absorbing tight epithelia, such as distal colon, urinary bladder, and airways (Vuagniaux et al., 2000, Vuagniaux et al., 2002).

CAP1/*Prss8* expression in the epidermis is crucial for the epidermal permeability barrier and is important for postnatal survival (Leyvraz et al., 2005). First *in vivo* evidence suggests that CAP1/*Prss8* is an important and physiologically relevant activator of ENaC came from the study of mice lacking the serine protease CAP1/*Prss8* in the alveolar epithelium unveiling a crucial role for lung fluid balance (Planes et al., 2010). In the colon however, the physiological role of this membrane-serine protease in ENaC activation was hitherto unknown and it was unclear whether it was implicated in regulating colonic ENaC activity.

1.4.2 Furin

The intracellular protease furin is a proprotein convertase that is predominantly found in vesicles of the trans-Golgi network and first evidence of ENaC cleavage has been shown by (Hughey et al., 2003). The α and γ ENaC subunits are cleaved during maturation at consensus sites for furin cleavage. By using furin mutants in α and γ subunits, furin-deficient cells, and furin specific inhibitors, the authors proposed that furin-mediated ENaC cleavage correlates with channel activity (Hughey et al., 2004). Contrary to this finding (Harris et al., 2008) by using labeling of cell surface–expressed proteins of ENaC obtained a correlation of channel cleavage and amiloride-sensitive ENaC-mediated Na^+ transport. The α subunit alone (or in combination with the β and/or γ subunits) was efficiently transported to the cell surface; α ENaC contained in two other subunits appeared at the cell surface as the full-length (95 kDa) molecule and a 65 kDa fragment, whereas αR205A/R231A (furin mutant) ENaC appeared only as full length. I_{Na} of α(furin mutant)$\beta\gamma$ was decreased by 60%. The γ subunit expressed alone did not appear at the cell surface, γ coexpressed with α reached the surface but was not detectably cleaved, and γ in $\alpha\beta\gamma$ complexes appeared mainly as a 76 kDa species in the surface pool. When the γ R138A (furin mutant) was expressed with other subunits, γ ENaC appeared in the cell surface pool as the 93 kDa full-length protein. However, basal I_{Na} was

similar to I_{Na} of αβγ. Thus, furin-mediated cleavage was not essential for participation of α or γ in αβγ heteromers, and basal I_{Na} was reduced by preventing furin-mediated cleavage of the α, but not the γ, subunit (Harris et al., 2008). Although, further studies indirectly supported the importance of the α furin sites in proteolytic regulation of ENaC (Carattino et al., 2006, Sheng et al., 2006, Bruns et al., 2007). (Carattino et al., 2006) showed that ENaC is inhibited by a peptide (26 residue, αAsp-206-Arg-231) derived from proteolytic processing of its α subunit at furin consensus site. In addition to this, later same authors proposed that a eight-residue tract between the α furin sites is a key conserved inhibitory domain that provides epithelial cells with a reserve of inactive channels that can be activated as required by proteases (Carattino et al., 2008). Furthermore, they have described different contribution of cleavage at the α subunit furin to normal activity of ENaC. They proposed that this activation could be resulted partly by relieving the channel of Na^+ self-inhibition (Sheng et al., 2006).

So far, most of work has been done in *Xenopus laevis* oocytes expression system, which itself has some limitations. This expression system does not bear epithelial polarity and is not able to measure transepithelial sodium transport upon hormonal stimulation. It is possible that assembly, plasma membrane targeting may be different in this system and also gene expression of serine protease; serine protease inhibitors are likely to be different than in a renal cell system. In order to address importance of furin-mediated ENaC proteolysis on channel activation, it is important to study this correlationship in native renal cell lines (mCCD, mCNT, mDCT).

2. AIMS OF THE THESIS

Aim of the **first part** of my doctoral study was to investigate whether deficient colonic ENaC activity affects sodium and/or potassium balance, and/or what are the compensatory mechanisms. These compensatory mechanisms could be intrinsically through increased expression of electroneutral sodium/chloride transporters as NHE3 or SLC26 or extrinsically to the colon by activation of the renin-angiotensin-aldosterone system. Furthermore, I have investigated whether ENaC is activated by CAP1 *in vivo* in colon. To achieve that, I have specifically deleted either αENaC/*Scnn1a* or CAP1/*Prss8* in the colonic surface epithelium using transgenic mice expressing Cre driven by the *villin* promoter and measured *in vivo* the electrogenic sodium transport as assessed by amiloride-sensitive rectal potential difference to correlate plasma electrolytes with fecal sodium loss and plasma aldosterone concentrations.

Aim of the **second part** was to understand whether ENaC and /or CAP1/*Prss8*-deficiency predispose mice to dextran sodium sulfate (DSS) - induced colitis. To address this question, I have chemically induced colitis in both mouse models by applying an acute (5%) and chronic (2%) dose of DSS.

Aim of **third part** of my thesis was to understand role of furin consensus site on αENaC subunit on channel activation. To achieve this, we have generated doxycycline-inducible *Scnn1a*-deficient mouse distal convoluted tubule (mDCT), mouse connecting tubule (mCNT) and mouse cortical collecting duct (mCCD) cell lines derived from *Scnn1a*$^{lox/lox}$ /Pax8/LC1 mice. Furthermore, I have investigated consequences αENaC deletion on ENaC-mediated sodium transport in these cells by performing electrophysiological measurements.

3. RESULTS: FIRST PART

Part I – Role of Epithelial sodium channel (ENaC) and its positive regulator, Channel-activating protease 1 (CAP1/*Prss8*) in intestine

Aim of this part was to investigate role of colonic ENaC and CAP1/*Prss8* on sodium and/or potassium balance, and/or what are the compensatory mechanisms. The first of part of results includes the generation and characterization of colon-specific *Scnn1a*^{KO} and *Prss8*^{KO} mice challenged with different salt conditions. For this part, the major experimental part has been performed by me. Roch-Phillipe Charles performed the Western blot analysis on *Prss8*^{KO} mice which corresponds to **Fig.8C**. Chloe Sergi performed Western blot analysis on *Scnn1a*^{KO} mice. Marc Maillard analyzed plasma aldosterone measurements on both KO mouse models.

3.1 Results

3.1.1 Intestine-specific Scnn1a-deficient mice are viable and exhibit normal colon histology

To ablate αENaC expression in intestinal superficial cells, we mated $Scnn1a^{+/-\,;}$ $villin::Cre^{tg/0}$ mice with mice harbouring two floxed αENaC ($Scnn1a^{loxlox}$). Age-matched wild type-like $Scnn1a^{lox/+}$ ($Scnn1a^{Lox}$), heterozygous mutant, $Scnn1a^{lox/-}$ ($Scnn1a^{Het}$), intestine-specific heterozygous mutant, $Scnn1a^{lox/+};villin::Cre^{tg/0}$, ($Scnn1a^{Hetc}$) and intestine-specific αENaC knockout, $Scnn1a^{lox/-},villin::Cre^{tg/0}$, ($Scnn1a^{KO}$) mice were obtained (**Fig. 1A**). Analysis of a total of 252 offspring at weaning showed no deviation from the expected Mendelian distribution ($Scnn1a^{Lox}$, n= 60; $Scnn1a^{Het}$, n= 68; $Scnn1a^{Hetc}$, n= 70; $Scnn1a^{KO}$, n= 54) indicating that αENaC inactivation in intestine superficial cells had no effect on fetal development and postnatal survival. Adult $Scnn1a^{KO}$ mice were viable, showed no increased mortality, and were indistinguishable from the other groups in appearance, growth and body weight (**Table 1**). In the $Scnn1a^{KO}$ mice, intestinal superficial cells lack near 99 % of $Scnn1a$ mRNA transcript expression, while heterozygotes ($Scnn1a^{Het}$) exhibit intermediate (71%) expression levels compared to $Scnn1a^{Lox}$ (left panel, $P<0.05$; **Fig. 1B**). The expressions of β and γENaC mRNA transcripts were higher in $Scnn1a^{KO}$ mice, but this difference did not reach statistical significance (middle and right panel, **Fig. 1B**). The successful deletion of $Scnn1a$ in scraped superficial cells was further confirmed on the protein level (**Fig. 1C and D**). Heterozygotes for the $Scnn1a$ allele ($Scnn1a^{Het}$ and $Scnn1a^{Hetc}$) showed intermediate expression (70% and 50 % of $Scnn1a^{Lox}$), respectively.
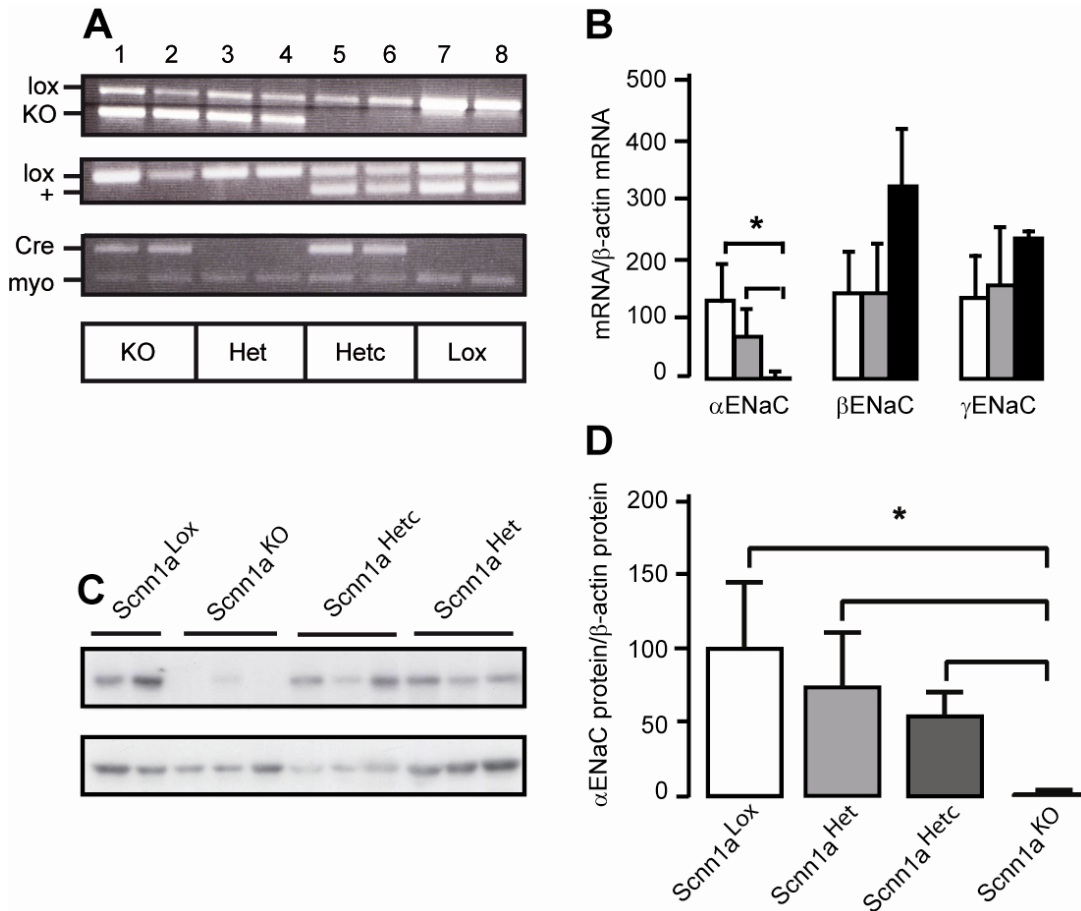
Figure 1. Generation of intestinal superficial cell-specific *Scnn1a*-deficient mice.

DNA, mRNA and proteins samples were analyzed from tissues **(A)** or isolated intestinal superficial cells **(A-D)**. **(A)** PCR analysis on ear biopsies with primers distinguishes between the lox (580 bp) and the KO (360 bp) allele of the *Scnn1a* gene locus (top). In the middle, primers indicated distinguish between *wt* (+; 220 bp), and *lox* (280 bp) allele in experimental *Scnn1a $^{lox/-}$;villin::Cre$^{tg/+}$* (*Scnn1a^{KO}*) and controls, lane 1-2, *Scnn1a$^{lox/-}$* (*Scnn1a^{Het}*); lane 3-4, *Scnn1a $^{lox/+}$;villin::Cre$^{tg/+}$* (*Scnn1a^{Hetc}*); lane 5-6, and *Scnn1a $^{lox/+}$* (*Scnn1a^{Lox}*) ; lane 7-8 littermates. Detection of the *villin::Cre* transgene using Cre-specific primers. Myogenin-specific primers were used as internal control (lower panel). **(B)** Quantification of α, β, γENaC mRNA transcripts by qRT-PCR in colonic scrapped cells from *Scnn1a^{Lox}* (n=5, white), *Scnn1a^{Het}* (n=4, light grey) and *Scnn1a^{KO}* mice (n=4, black column). Results are expressed as the ratio of mRNA/ β-actin mRNA (*, *P*<0.05). **(C)** Representative immunoblot showing the expression of αENaC (upper) and β-actin (lower) protein in scraped colon cells from *Scnn1a^{Lox}*, *Scnn1a^{Het}*, *Scnn1a^{Hetc}* and *Scnn1a^{KO}* mice. **(D)** Quantification of αENaC protein expression levels in scraped colon cells from *Scnn1a^{Lox}* (white), *Scnn1a^{Het}* (light grey), *Scnn1a^{Hetc}* (dark grey) and *Scnn1a^{KO}* (black) mice after analysis with ImageJ software; (n=3 mice per group, *, *P*<0.05). Results are expressed as the ratio of αENaC protein/ β-actin protein. Values are mean ± S.E.M.

Macroscopically, the morphology of the adult distal colon was not different (**Fig.2**). The

colon epithelium and mucin-secreting goblet cells appeared to be normal in knockout mice,

without any effect on the number of crypt cells (not shown). The intestine length-to-body

weight ratio was not different between the $Scnn1a^{Lox}$ (1.97 ±0.05), $Scnn1a^{Het}$ (1.89±0.05) and

$Scnn1a^{KO}$ (1.83±0.06) groups.
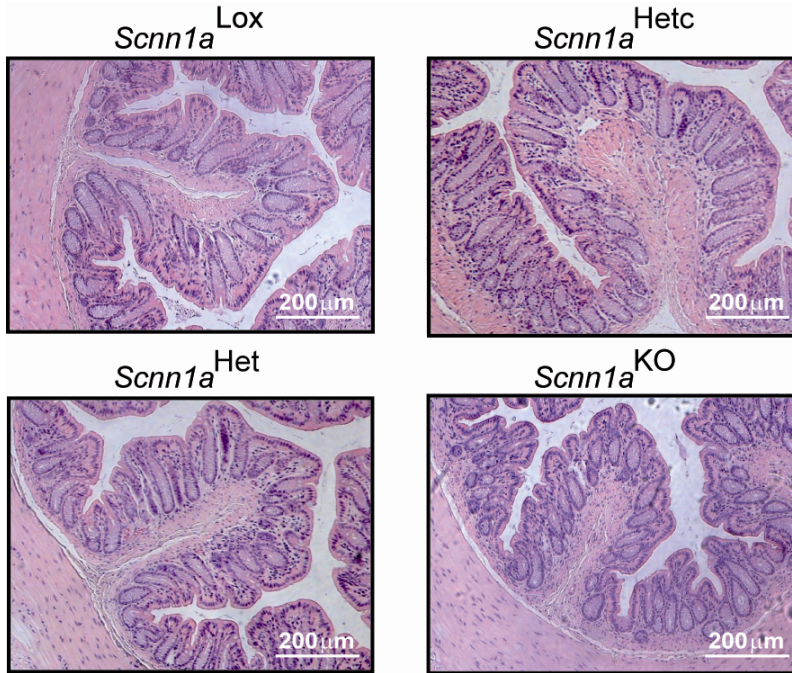
Figure 2. Colon histology in $Scnn1a^{KO}$ mice

Light photomicrographs of representative distal colon sections from age-matched (2 months old) $Scnn1a^{Lox}$, $Scnn1a^{Het}$ and $Scnn1a^{KO}$ littermates (H&E-staining); n=3 animals/genotpye. Scale bar, 200 µm.

3.1.2 Implication of ENaC in intestinal electrogenic sodium transport and sodium balance

In distal colon and rectum, the ENaC-mediated sodium transport is electrogenic and

generates an amiloride-sensitive transepithelial potential difference (ΔPD_{amil}) that can be

conveniently and non-invasively measured *in vivo*. This measurement allowed excluding the

contribution of other ion currents such as electrogenic chloride secretion or potassium

secretion. As previously found, ΔPD_{amil} was mainly due to changes in electrogenic sodium

transport upon various salt sodium diets and followed the RAAS cyclicity (Wang et al.,

2000). Thus, we measured ΔPD_{amil} and switched from HS (**Fig. 3A**), to RS (**Fig. 3B**) and to

LS (**Fig. 3C**) diets induced a progressive increase in plasma aldosterone (**Fig. 4**).
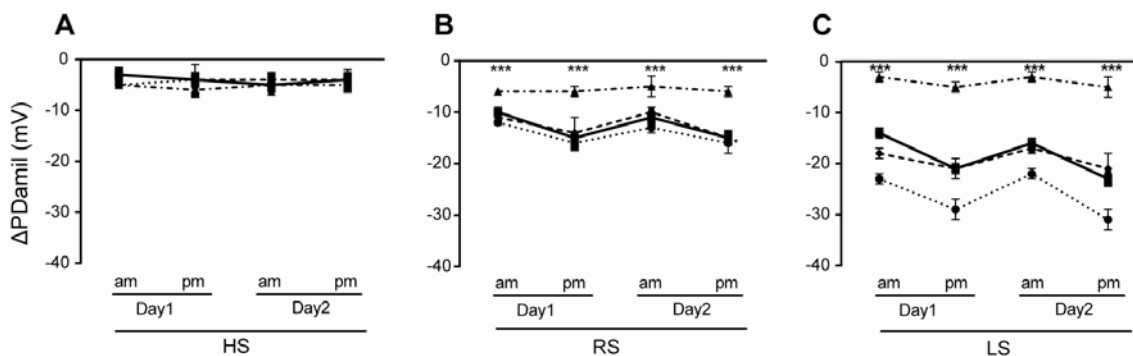
Figure 3. Colonic sodium transport was affected in *Scnn1a*^KO mice

Morning and afternoon measurements of amiloride-sensitive rectal potential difference (ΔPD_{amil}, mV) on 2 consecutive days in *Scnn1a*^Lox mice (n= 7; —), *Scnn1a*^Het (n=7; ---), *Scnn1a*^Hetc (n=7 ; ⋯) and *Scnn1a*^KO, (n=8 ; ·-··-) mice treated with high (HS, **A),** regular (RS, **B)**, or low salt (LS, **C)** diets. ***, $P < 0.001$. Values are mean ± S.E.M.

Upon HS diet, plasma aldosterone (0.1-0.2 nmol/l) (**Fig. 4**) and baseline ΔPD_{amil} (**Fig. 3A**)

were equally low (-5 to -6 mV) and undistinguishable between groups (**Fig. 3A**). Upon RS

diet, plasma aldosterone increased from 0.7 nmol/l in *Scnn1a*^Lox to 1.2 nmol/l in *Scnn1a*^Het

and to 1 nmol/l in *Scnn1a*^Hetc (**Fig. 4**). Now, the 3 genotypes (*Scnn1a*^Lox, *Scnn1a*^Het and

Scnn1a^Hetc) showed a very significant (-10 to -15 mV) increase in ΔPD_{amil} in comparison to

the HS diet. The circadian rhythm expressed as (am/pm) cyclicity was readily observed (**Fig.**

3A, B). The highest plasma aldosterone was observed in the *Scnn1a*^KO group (2.4 nmol/l)

contrasting with the ΔPD_{amil} that remained very low (-6 to -8 mV) and without evidence for

cyclicity (**Fig. 3B, 3**). Upon LS diet, plasma aldosterone increased in all groups to reach high

values in the *Scnn1a*^KO group (8.5 nmol/l; **Fig. 4**). Despite this drastic increase in plasma

aldosterone level, ΔPD_{amil} remained very low (-5 to -6 mV) with blunted cyclicity (**Fig. 3C,**

4). Interestingly, the group carrying one wild type and one floxed allele (*Scnn1a*^Lox) showed a

significantly higher ΔPD_{amil} than the one of the heterozygotes. In all conditions, an amiloride-

insensitive negative PD was observed (between -6 and – 8 mV) (data not shown). The nature of this PD was not examined but might be linked to either electrogenic chloride secretion and/or potassium reabsorption. The data were consistent with the idea that the αENaC subunit in the colon plays a critical role in the amiloride-sensitive electrogenic sodium reabsorption in distal colon and rectum.
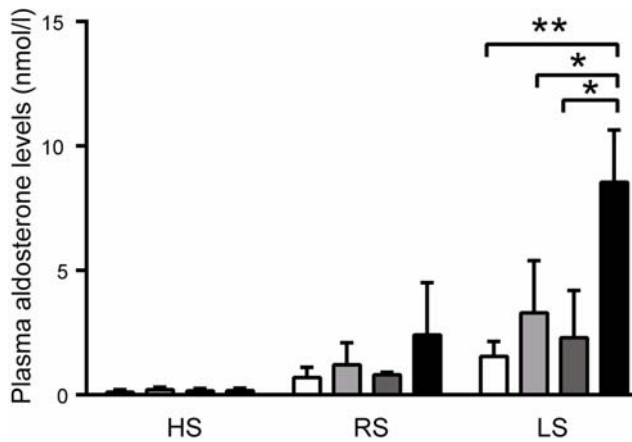
Figure 4. *Scnn1a*^{KO} mice showed elevated plasma aldosterone levels

Plasma aldosterone (nmol/l) concentrations in *Scnn1a*^{Lox} (n= 6; white), *Scnn1a*^{Het} (n=7; light grey), *Scnn1a*^{Hetc} (n=6 ; dark grey) and *Scnn1a*^{KO} (n= 7; black) mice groups were analysed upon various sodium diets. *, $P < 0.05$; **, $P < 0.01$; RS, regular salt; LS, low salt and HS, High salt diet. Values are mean ± S.E.M.

The observed hyperaldosteronism suggested that loss of sodium in the feces could have caused a significant hypovolemia and triggered the activation of the renin-angiotensin-aldosterone system (RAAS). To address this question, we analyzed total sodium and potassium in the feces. We found that upon regular (RS) and low salt (LS) diet, *Scnn1a*^{KO} mice lost significantly more sodium compared with the control groups (RS, $P<0.05$; NS, $P<0.001$). This difference was not observed upon high diet (**Fig. 5A**). Following different diets, fecal potassium was not significantly different amongst the groups (**Fig. 5B**).

Moreover, wet/ dry ratio of feces was similar in all groups ($Scnn1a^{KO}$: 0.32± 0.02, $Scnn1a^{Lox}$:

0.30± 0.02 and $Scnn1a^{Het}$: 0.34± 0.02).
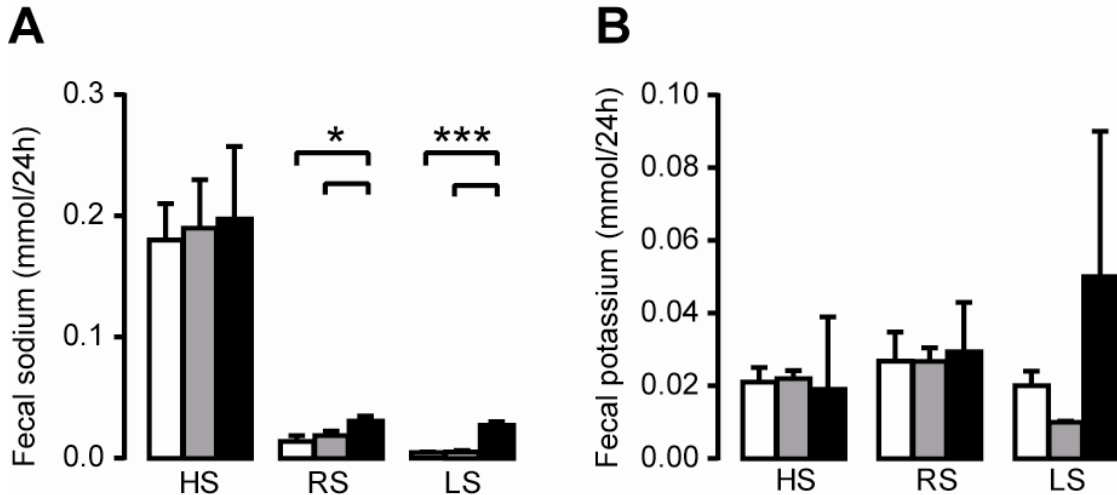
Figure 5. Sodium is lost through feces in $Scnn1a^{KO}$ mice

Measurements of sodium (mmol/24h, **A**) and potassium (mmol/24h, **B**) electrolytes levels in feces from $Scnn1a^{Lox}$ (n=6; white), $Scnn1a^{Het}$ (n=7; light grey) and $Scnn1a^{KO}$ (n=7 ; black) mice upon various sodium diets. Values are mean ± S.E.M; *, $P < 0.05$ ***; $P< 0.001$, $Scnn1a^{KO}$ vs. $Scnn1a^{Lox}$ and $Scnn1a^{Het}$ mice.

In order to understand this compensation from kidney, we have analyzed the expression of

α,β and γENaC mRNA transcriptional expression from kidney extract. αENaC mRNA

expression was decreased in knockout mice as compared to control and heterozygous mutant

($p<0.005$). While expression of β and γENaC did not change between the groups **(Fig.6A).**

The expression of α, β and γENaC did not change at protein level between the groups under

RS diet, but β expression slightly increased under LS diet **(Fig.6 B,F)**. We also analyzed

expression of the sodium transporter in kidney, the NCC and its phosphorylated form P-NCC.

Expression of NCC increased in $Scnn1a^{KO}$, but not P-NCC expression **(Fig.6D, G)**.
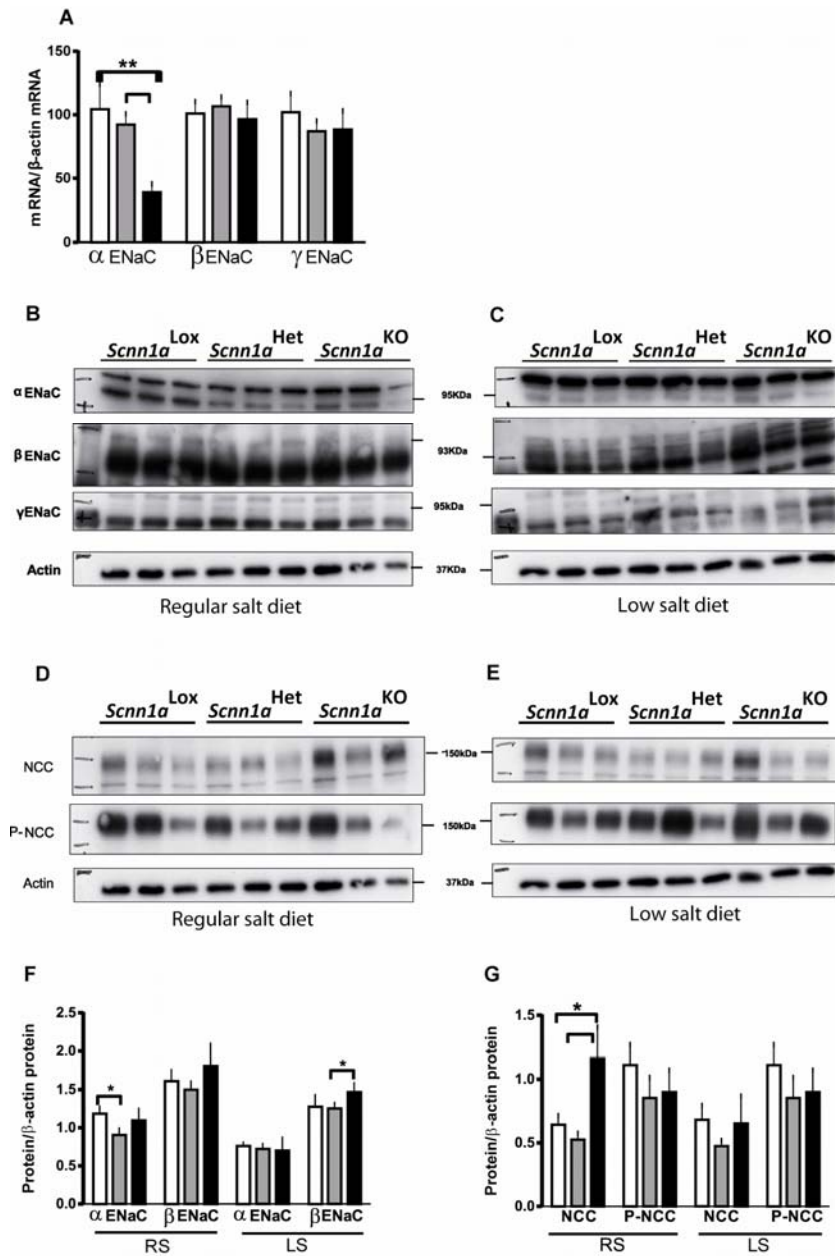
Figure 6: mRNA transcript, protein expression of α, β & γENaC subunit and protein expression of NCC, P-NCC in kidney of *Scnn1a*[KO] mice on regular and low salt diet

(A) Quantification of α, β & γENaC mRNA transcripts by qRT-PCR in kidneys from *Scnn1a*[Lox], *Scnn1a*[Het] and *Scnn1a*[KO] treated with regular salt diet. Results are expressed as the ratio of α/ β /γENaC mRNA/β-actin mRNA (n=5 mice per group); **(B,C)** Representative Western blots showing the expression of α (93 kDa), β (95 kDa), γ (95 kDa) ENaC subunit and actin protein in kidney extracts from *Scnn1a*[Lox], *Scnn1a*[Het] and *Scnn1a*[KO] mice (n=3 per group) under regular (RS) and low salt diet (LS), **(D;E)** Representative Western blot analysis showing the expression of NCC (150 kDa) , P-NCC (150 kDa) and actin protein in kidney extract from *Scnn1a*[Lox], *Scnn1a*[Het] and *Scnn1a*[KO] mice (n=3 per group) under regular (RS) and low salt (LS); **(D)** Quantification of α,β,γENaC subunit and NCC, P-NCC protein expression in pooled *Scnn1a*[Lox], *Scnn1a*[Het] and *Scnn1a*[KO] kidney by using odyssey software. (n=5 mice per group, *: $p<0.05$, **: $p<0.005$).

3.1.3 The kidney compensates the loss of Na$^+$ via feces

Scnn1a^{KO} mice should be able to compensate the fecal sodium loss by an aldosterone-dependent absorption of the distal nephron. Hence, mice were put into metabolic cages and, upon HS, RS and LS diets, food and water intake, feces output, urinary volume, plasma and urinary sodium and potassium were measured (**Table 1**).

Parameters	Regular salt diet			Low salt diet		
	Scnn1a^{Lox}	*Scnn1a*^{Het}	*Scnn1a*^{KO}	*Scnn1a*^{Lox}	*Scnn1a*^{Het}	*Scnn1a*^{KO}
n	7	5	9	5	5	4
BW(g)	25.83±1.5	25.92±0.4	26.75±1	25.50±1.2	24.80±0.2	23.83±0.7
Food intake/body weight ratio	0.13±0.02	0.15±0.0	0.14±0.03	0.12±0.01	0.13±0.0	0.13±0.0
Water intake/body weight ratio	0.16±0.01	0.16±0.03	0.22±0.02	0.16±0.04	0.18±0.01	0.22±0.02
Urine output /body weight ratio	0.05±0.01	0.06±0.01	0.08±0.01	0.06±0.02	0.05±0.01	0.06±0.06
Feces output/body weight ratio	0.02±0.0	0.02±0.01	0.02±0.0	0.02±0.0	0.02±0.0	0.02±0.0
Plasma Na$^+$(mM)	151.6±1.2	149±0.2	161±4.2	148.2±2.2	153±2.4	148±1.07
Plasma K$^+$(mM)	5.2±0.2	4.28±0.2	5.1±0.28	4.23±0.2	4.62±0.2	4.83±0.07

Parameters	High salt diet			High potassium diet (48 hrs)		
	Scnn1a^{Lox}	*Scnn1a*^{Het}	*Scnn1a*^{KO}	*Scnn1a*^{Lox}	*Scnn1a*^{Het}	*Scnn1a*^{KO}
n	4	4	4	4	4	4
BW(g)	25.83±0.6	25.41±0.5	25.13±0.4	26.34±0.3	25.21±0.2	25.23±0.2
Food intake/body weight ratio	0.11±0.02	0.12±0.02	0.11±0.0	0.11±0.03	0.10±0.01	0.11±0.01
Water intake/body weight ratio	0.19±0.01	0.20±0.10	0.21±0.01	0.12±0.03	0.11±0.01	0.12±0.01
Urine output /body weight ratio	1.6±0.01	1.7±0.01	1.75±0.02	0.04±0.03	0.05±0.01	0.04±0.01
Feces output/body weight ratio	0.01±0.0	0.01±0.0	0.01±0.0	0.01±0.0	0.01±0.0	0.01±0.0
Plasma Na$^+$(mM)	154±1.2	152±0.2	157±4.3	159.8±3.1	162±4.2	159.7±2.1
Plasma K$^+$(mM)	5.1±0.29	4.5±0.2	5.1±0.2	4.3±0.1	4.1±0.5	4.4±0.5
Urinary Na$^+$(mM/24h)				0.39±0.03	0.34±0.1	0.37±0.1
Urinary K$^+$(mM/24h)				3.6±1	3.1±1.1	3.6±1.2

Table 1: **Physiological parameters of *Scnn1a*^{KO} mice**

Physiological parameters in *Scnn1a*^{Lox}, *Scnn1a*^{Het} and *Scnn1a*^{KO} mice following different diets. Data are mean ± SEM.

Upon HS diet, cumulative urinary sodium loss was undistinguishable amongst groups (**Fig. 7A**). Under a RS diet, cumulative urinary sodium loss of *Scnn1a*^{KO} mice was significantly reduced with respect to the *Scnn1a*^{Lox}, but not to the *Scnn1a*^{Het} groups (**Fig. 7B**). Upon LS diet, cumulative urinary sodium excretion in the *Scnn1a*^{KO} group was significantly diminished as compared to all groups (**Fig. 7C**; $P<0.05$). Cumulative urinary potassium loss was not different amongst all groups (**Fig. 7D-F**).
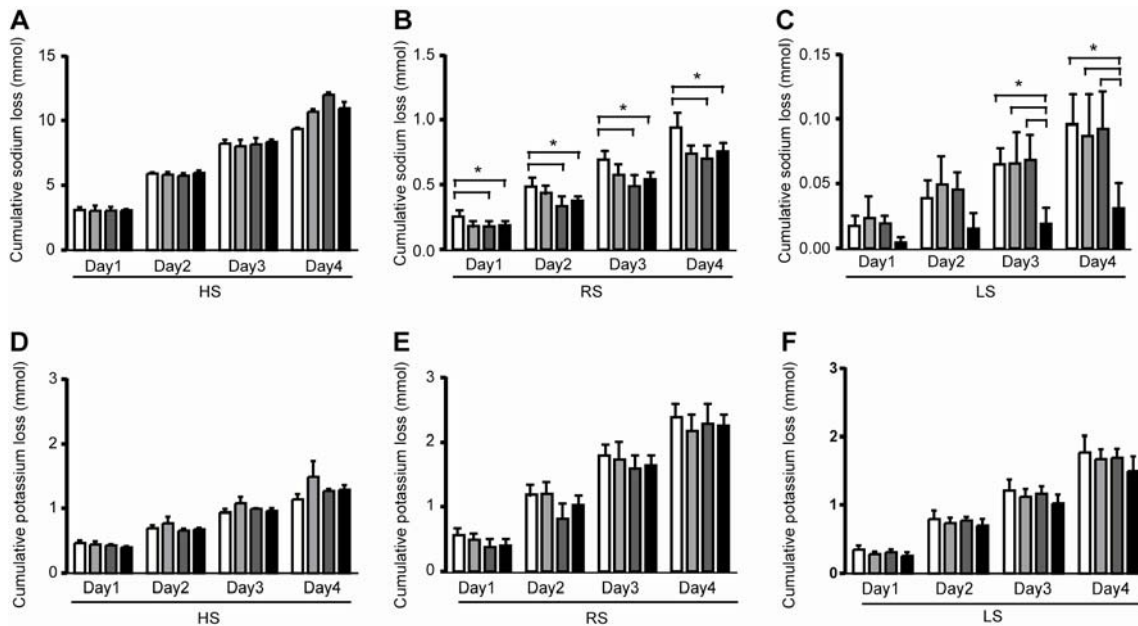
Figure 7. Diet-dependent sodium loss in urine of *Scnn1a*^{KO} mice

Measurement of cumulative urinary sodium **(A- C,** mmol**)** and potassium electrolyte **(D-F,** mmol**)** levels in *Scnn1a*^{Lox} (n=8 ; white), *Scnn1a*^{Het} (n= 7; light grey), *Scnn1a*^{Hetc} (n=8 ; dark grey) and *Scnn1a*^{KO} (n=8 ; black) mice upon High salt (HS; **A)**, regular salt (RS; **B**), and low salt (LS; **C**) diets; *, $P < 0.05$; Values are mean ± S.E.M.

Additionally, when mice were challenged with high potassium (HK, 5%) diet for two consecutive days, no change in plasma and urinary sodium and potassium was observed (**Table. 1**).

3.1.4 CAP1/*Prss8* identified as an in-vivo regulator of ENaC in distal colon

To test the role of CAP1/*Prss8* on ENaC activity in distal colon *in vivo*, we equally used the *villin::Cre* transgenic line. The generation of intestine-specific CAP1/*Prss8*-deficient (*Prss8*^{KO}, *Prss8*^{Δ/lox}; *villin::Cre*^{tg/0},) and wild type-like (*Prss8*^{Lox}) as well as heterozygous (*Prss8*^{Het} and *Prss8*^{Hetc}) mice is shown in **Fig. 8A**. Analysis of a total of 219 offspring at weaning showed no deviation from the Mendelian distribution (*Prss8*^{Lox}, n= 55; *Prss8*^{Het}, n= 55; and *Prss8*^{Hetc}, n= 56) and KO group (*Prss8*^{KO}, n= 53) indicating no impairment of pre-

and postnatal development. In *Prss8*[KO] mice, intestinal superficial cells lacked CAP1/*Prss8*

mRNA transcript expression (<1%) while heterozygotes (*Prss8*[Het]) exhibited intermediate

expression levels compared to *Prss8*[Lox] cells (70%) (**Fig.8B**). The mRNA transcript

expression of CAP2/*Tmprss4* and CAP3/*Prss14* was not altered (**Fig. 8B**). The successful

deletion of CAP1/*Prss8* in scraped intestinal superficial cells was further confirmed on the

protein level (**Fig.8 C-D**). Protein expression levels from heterozygotes (*Prss8*[Het]) were not

different from *Prss8*[Lox] mice (**Fig. 8D**).
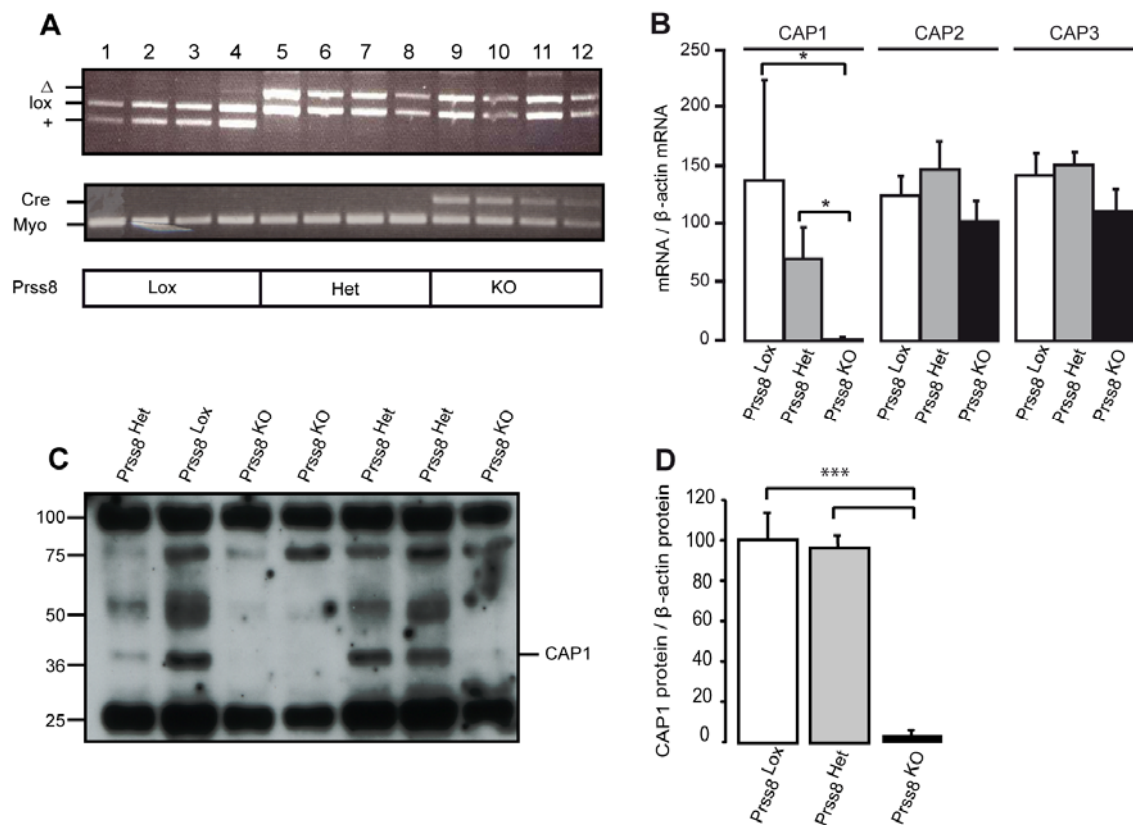
Figure 8. Generation of colon-specific *Prss8*[KO] mice

DNA (ear biopsies), mRNA and proteins samples were analyzed from isolated intestinal superficial
cells as indicated (**A-D**). **(A)** DNA-based PCR analysis on ear biopsies using primers distinguishing
wild-type (+; 379 bp), *lox* (413 bp) and Δ allele (top, 473 bp) in *Prss8*[lox/+](*Prss8*[Lox], lane 1-4),
Prss8[lox/Δ] (*Prss8*[Het], lane 5-8) and *Prss8*[Δ/lox];*villin::Cre*[tg/+](*Prss8*[KO]; lane 9-12) littermates. The
villin::Cre transgene (bottom, 400 bp) and myogenin (internal control) are detected using specific
primers. **(B)** Quantification of CAP1/*Prss8*, *CAP2/Tmprss4* and *CAP3/SP14* mRNA transcripts by
qRT-PCR in pooled scraped colon cells from *Prss8*[Lox] (n=4, white), *Prss8*[Het] (n=5, grey) and *Prss8*[KO]
(n=8, black) mice. Data are expressed as the ratio of mRNA/ β-actin mRNA. *: *P*<0.05). **(C)**
Representative immunoblot showing the expression of CAP1/*Prss8* and β-actin protein in scraped

colon cells from $Prss8^{Lox}$, $Prss8^{Het}$ and knockouts $Prss8^{KO}$. **(D)** Quantification of CAP1/$Prss8$ signals in $Prss8^{Lox}$ (n=4, white), $Prss8^{Het}$ (n=5, grey) and $Prss8^{KO}$ (n=6, black) scraped colon cells analyzed with ImageJ software; (***, $P<0.001$). Results are expressed as the ratio of CAP1/$Prss8$ protein/ β-actin protein. Values are mean ± S.E.M.

$Prss8^{KO}$ mice were not different in body weight, food and water intake, urine or feces output and plasma and urinary sodium and potassium levels compared to the age-matched control ($Prss8^{Lox}$ and $Prss8^{Het}$) groups (**Table. 2**).

Parameters	Regular salt diet			Low salt diet		
	$Prss8^{Lox}$	$Prss8^{Het}$	$Prss8^{KO}$	$Prss8^{Lox}$	$Prss8^{Het}$	$Prss8^{KO}$
n	7	5	9	5	5	4
BW (g)	24.95±0.6	24.12±0.3	25.15±0.4	23.93±0.8	22.30±0.2	22.15±0.4
Food intake/body weight ratio	0.12±0.3	0.13±0.3	0.12±0.9	0.12±0.2	0.13±0.3	0.12±0.3
Water intake/body weight ratio	0.15±0.1	0.15±0.3	0.16±0.2	0.16±0.1	0.16±0.1	0.18±0.1
Urine output /body weight ratio	0.04±1.1	0.05±0.4	0.05±0.3	0.05±0.1	0.05±0.1	0.06±0.3
Feces output/body weight ratio	0.02±0.2	0.01±0.0	0.01±0.0	0.02±0.0	0.01±0.0	0.02±0.0
Plasma Na^+(mM)	154±4.3	155±1.5	152±2.9	138±1.5	142±1.2	135±3.8
Plasma K^+(mM)	4.5±0.1	4.7±0.09	4.8±0.1	4.6±0.2	4.3±0.5	4.4±0.1
Urinary Na^+(mM)	37±1.9	24±1.3	25±8.2	6.6±1.0	6.39±0.34	8.3±0.48
Urinary K^+(mM)	35±1.8	30.2±2.3	30.19±2.4	59±8.1	58±3.23	62±3.05
High salt diet						
n	4	4	4			
BW (g)	21.30±0.6	21.45±0.4	20.12±0.3			
Food intake/body weight ratio	0.12±0.2	0.12±0.2	0.11±0.3			
Water intake/body weight ratio	0.17±0.1	0.18±0.1	0.19±0.1			
Urine output /body weight ratio	1.8±0.1	1.8±0.1	1.85±0.3			
Feces output/body weight ratio	0.01±0.0	0.02±0.0	0.01±0.0			
Plasma Na^+(mM)	147±1.8	143±1.02	142±1.02			
Plasma K^+(mM)	5±0.1	4.8±0.2	5.08±0.1			
Urinary Na^+(mM)	163±10.2	168±14.56	186±11.7			
Urinary K^+(mM)	25.5±3.1	26.34±4.1	26.44±2.8			

Table 2: **Physiological parameters of $Prss8^{KO}$ mice**

Physiological parameters in $Prss8^{Lox}$, $Prss8^{Het}$ and $Prss8^{KO}$ mice following different diets. Data are mean ± SEM.

Colon histology was indistinguishable from the other groups (**Fig. 9A**) without any apparent effect on the number of crypt cells (data not shown). The intestine length-to-body weight

ratio was not different between the wild type like ($Prss8^{Lox}$: 2.04 ±0.14), heterozygotes ($Prss8^{Het}$: 2.16±0.13) and knockout ($Prss8^{KO}$: 1.91±0.1) (P= 0.4). When we monitored the intestinal permeability following fluroscein isothiocyanate dextran supply in blood plasma, we found that, besides a slight increase in knockouts, the intestinal barrier function was not significantly increased (P= 0.09 to $Prss8^{Het}$, and P=0.39 to $Prss8^{Lox}$; **Fig. 9B**).
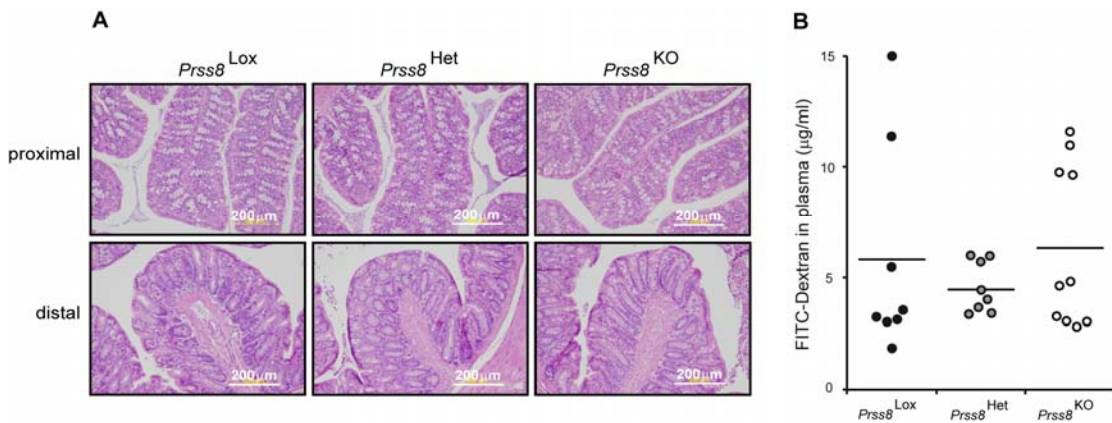
Figure 9. Normal colon histology and intestinal permeability in $Prss8^{KO}$ mice

(A) Representative light photomicrographs of proximal and distal colon sections from $Prss8^{Lox}$, $Prss8^{Het}$ and $Prss8^{KO}$ littermates stained with haematoxylin and eosin; for each genotype, 3 independent animals were analyzed. Scale bar, 200 μm **(B)** Measurement of intestinal permeability in $Prss8^{Lox}$ (n=8, closed circles), $Prss8^{Het}$ (n=8, half-open circles) and $Prss8^{KO}$ (n=10, open circles) mice. Horizontal bar indicates the average.

When mRNA expression levels of ENaC subunits were quantified in distal colon and in the kidney, there was not difference amongst the groups with the exception of βENaC mRNA transcripts, (KO versus Lox and Het, $P<0.05$; **Fig. 10A, B**). Western blot analysis using the anti-αENaC antibody revealed the full-length 93kDa form and its cleaved 30kDa form (**Fig. 10C**). The 95kDa full-length β- and γENaC including the cleaved 75kDa γENaC proteins are equally present in all groups (**Fig. 10 C-F**).
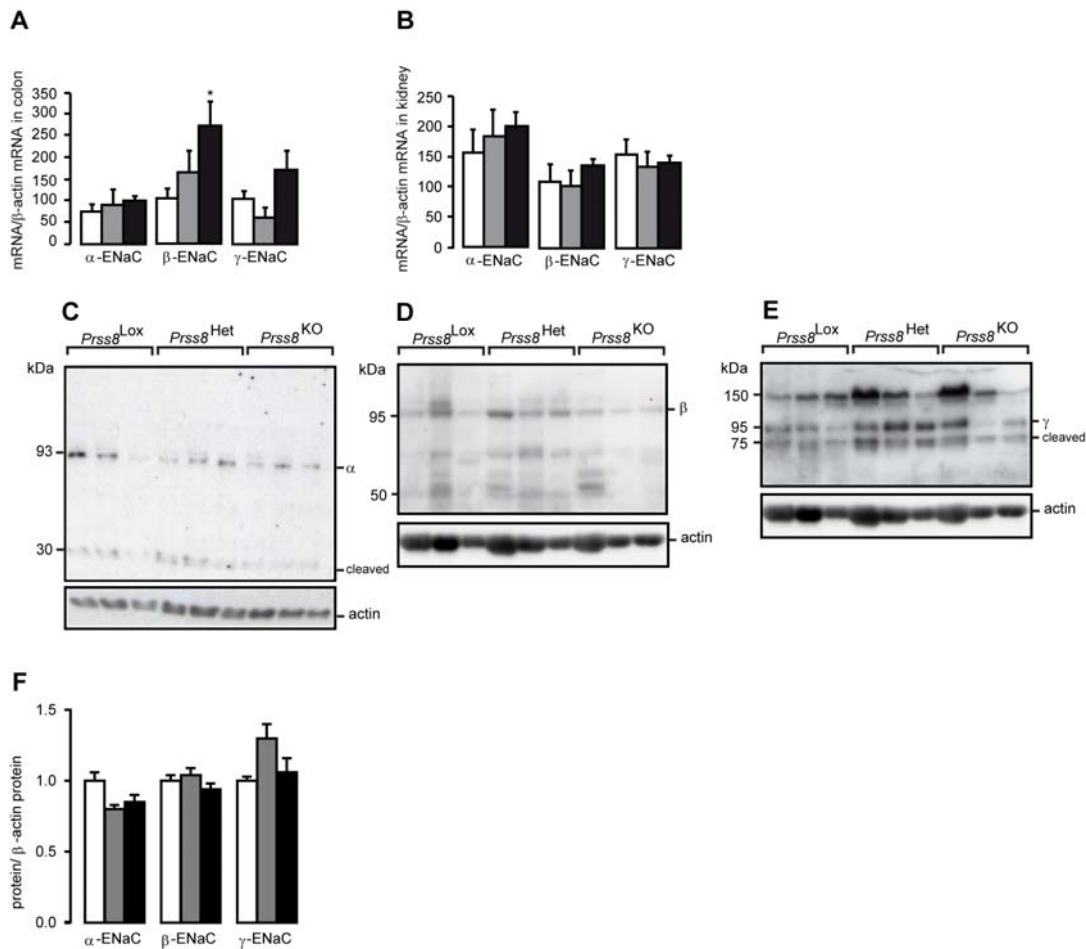
Figure 10. Expression of ENaC subunits in kidney and distal colon of *Prss8*[KO] mice

(**A and B**), Quantification of α (left), β (middle) and γENaC mRNA transcript expression in (**A**) distal colon and (**B**) kidney by quantitative RT-PCR from *Prss8*[Lox] (white), *Prss8*[Het] (grey) and *Prss8*[KO] (black bar) mice. Results are expressed as the ratio of ENaC mRNA subunits to β-actin mRNA (n ≤ 6 mice per group); *, $P < 0.05$. Representative immunoblot showing the expression of alpha (93kDa) (**C**), beta (95kDa) (**D**) and gamma ENaC (95kDa) (**E**) subunit and β-actin protein in scraped colon cells from *Prss8*[Lox], *Prss8*[Het] and knockouts *Prss8*[KO]; (n=3 mice per group). (**F**) Quantification of α,β and γENaC protein in *Prss8*[Lox], *Prss8*[Het] and *Prss8*[KO] colon samples. β-actin expression is shown as loading control; in each experiment, 3 mice were used per group. Values are mean ± S.E.M.

We finally measured ΔPD$_{amil}$ following HS (**Fig. 11A**), RS (**Fig. 11B**) and LS (**Fig. 11C**) diets that induced a progressive increase in plasma aldosterone levels in all groups (**Fig. 11D**). Upon HS diet, baseline ΔPD$_{amil}$ and plasma aldosterone levels (0.1-0.2 nmol/l) were equally low (-8 to -10 mV) and undistinguishable amongst groups (**Fig. 11A, D**). Cyclicity

51

was maintained, although blunted. Upon RS diet, ΔPD_{amil} of $Prss8^{Lox}$ and $Prss8^{Het}$ mice increased markedly (-15 to -25 mV) with respect to HS diet and (am/pm) cyclicity was readily observed (**Fig. 11A, B**). Despite increased (0.5 nmol/l) plasma aldosterone levels, the cyclicity of the $Prss8^{KO}$ group was blunted, mainly due to a significant decrease of ΔPD_{amil} in the afternoon. Upon LS diet, ΔPD_{amil} in $Prss8^{KO}$ remained significantly lower with blunted cyclicity than that of $Prss8^{Lox}$ or $Prss8^{Het}$ mice (**Fig. 11C**), although plasma aldosterone levels reached comparable high and even significant ($p<0.05$) values in the $Prss8^{KO}$ (2.3 nmol/l) when compared with both ($Prss8^{Ctrl}$ and $Prss8^{Het}$) groups together. Interestingly, although, the feces wet/ dry ratio was not altered in the knockout ($Prss8^{KO}$: 0.33± 0.02 versus controls, $Prss8^{Lox}$: 0.31± 0.02 and $Prss8^{Het}$: 0.37± 0.02; P =0.4), sodium was significantly lost in feces from the knockouts (**Fig. 11E**). However, feces potassium levels were not different amongst the genotypes (**Fig. 11F**, $P< 0.05$).
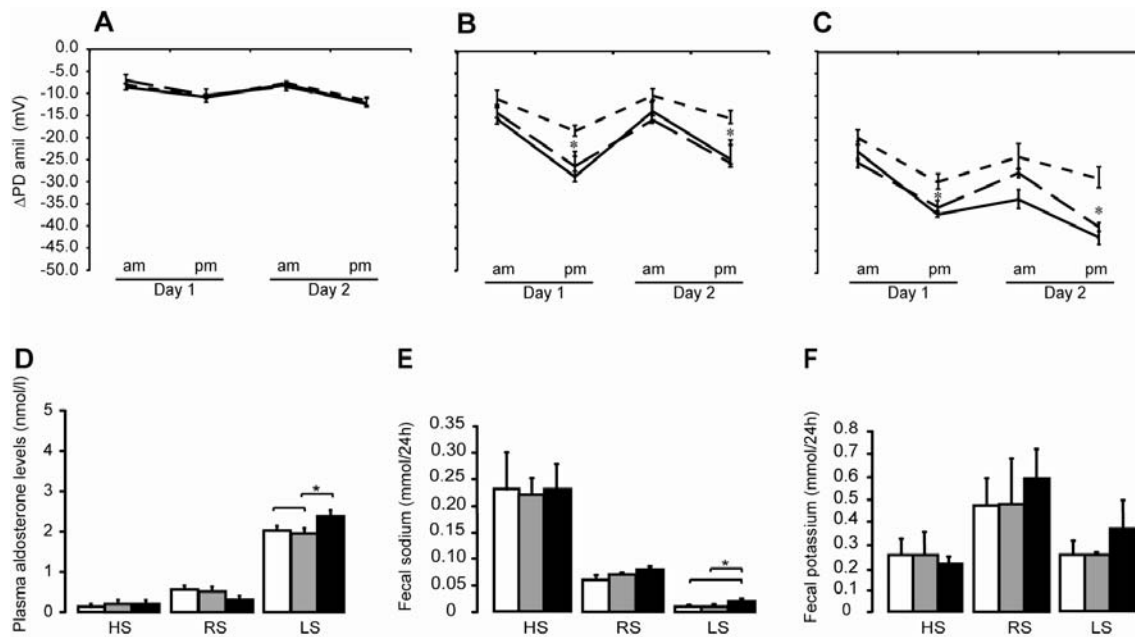
Figure 11. CAP1/*Prss8* is a regulator of ENaC in colon

(A) Morning and afternoon measurements of amiloride-sensitive rectal potential difference (ΔPD_{amil}, mV) on 2 consecutive days in control ($Prss8^{Lox}$ (n= 8; —), $Prss8^{Het}$ (n=7; - - -) and $Prss8^{KO}$ (n= 8; ---) mice treated with High salt (HS, **A**), regular salt (RS, **B**), and low salt (LS, **C**) diet. **(D)** Plasma aldosterone concentrations following various sodium diets (nmol/l). **(E)** Fecal sodium and **(F)** fecal

potassium concentrations (mmol/24h) in *Prss8*^{Lox} (n=5; white), *Prss8*^{Het} (n= 6; grey) and *Prss8*^{KO} (n=6; black) mice following a high-salt (HS), a regular-salt (RS) and low salt (LS) diet; *, *P* < 0.05. Values are mean ± S.E.M.

In summary, our data clearly demonstrated that *in vivo* stimulation of the amiloride-sensitive ENaC-mediated sodium transport was dependent on the expression of the membrane-bound serine protease CAP1/*Prss8*, and more strikingly in the afternoon when the RAAS is maximally activated.

3.2 Conclusion and discussion

ENaC-mediated electrogenic sodium transport is limiting for the final absorption of sodium in distal colon and rectum: evidence for colon-specific haploinsufficiency

In the present study, we studied mice with an efficient deletion of (α)ENaC/*Scnn1a* along the intestine and found a strict gene dosage effect at the mRNA transcript and protein expression level (**Fig. 1**). Electrogenic sodium transport in distal colon was mainly mediated by ENaC even if a low but significant electrogenic transport was measured following amiloride application (**Fig. 3**). Nevertheless, we cannot exclude some residual ENaC activity in some part of the colon due to incomplete recombination or due to expression of β and γENaC subunits. As previously shown in a heterologous expression system, ENaC channels made of $\beta\gamma$ subunits can lead to small (2%) but significant activity (Bonny et al., 1999). This possibility is unlikely in our experimental situation, since even upon a High salt (HS) diet, β and γENaC subunit mRNA transcript expression should be rather repressed when aldosterone is low. Furthermore, NHE3 might be sensitive to high concentrations of amiloride, but its transport is electroneutral and thus undetectable by our PD measurements (**Fig. 3**). Upon RS diet, plasma aldosterone levels increased and both groups of heterozygotes (*Scnn1a*^{Hetc} and *Scnn1a*^{Het}) responded as *Scnn1a*^{Lox} mice, whereas the KO mice remained at a low $\Delta PD_{amil.}$ Under LS diet, a significant dissociation between the two groups of heterozygotes and the floxed (*Scnn1a*^{Lox}) group was observed indicating haploinsufficiency. A distinct phenotype in heterozygous mice with upregulation of AT1 receptors was previously described, although these mice showed an intact capacity to maintain blood pressure and sodium balance under different salt diet (Wang et al., 2001). Since *Scnn1a*^{Hetc} and *Scnn1a*^{Het} mice reacted similarly under any salt diet, this effect of (α)ENaC seemed indeed colon-specific.

Differential activation of RAAS when lowering salt intake: evidence for colon-specific mineralocorticoid resistance

The RAAS is a powerful and sensitive system to vascular resistance, blood volume and blood pressure and highly sensitive to salt intake. In our study, we have varied salt intake from HS to RS (19-fold) and from RS to LS diet with an additional 17-fold decrease in salt intake. As illustrated in the **Fig.12**, the KO showed a drastic aldosterone response with a 14-fold increase in plasma aldosterone (HS to RS) in the *Scnn1a*^{KO} mice (*$P<0.05$) in comparison to a 7-fold increase observed in the other groups (HS to RS, *Scnn1a*^{Lox}, *Scnn1a*^{Het} and *Scnn1a*^{Hetc}). Upon switch from RS to LS, a 2-fold (*Scnn1a*^{Lox}, *Scnn1a*^{Het} and *Scnn1a*^{Hetc}) versus 4-fold (*Scnn1a*^{KO}). On LS diet, knockouts exhibited a 5-fold to the *Scnn1a*^{Lox} and a 3-fold increase in plasma aldosterone to the heterozygotes (*Scnn1a*^{Het} and *Scnn1a*^{Hetc}) (**$P<0.01$). The heterozygotes exhibited an intermediate response.
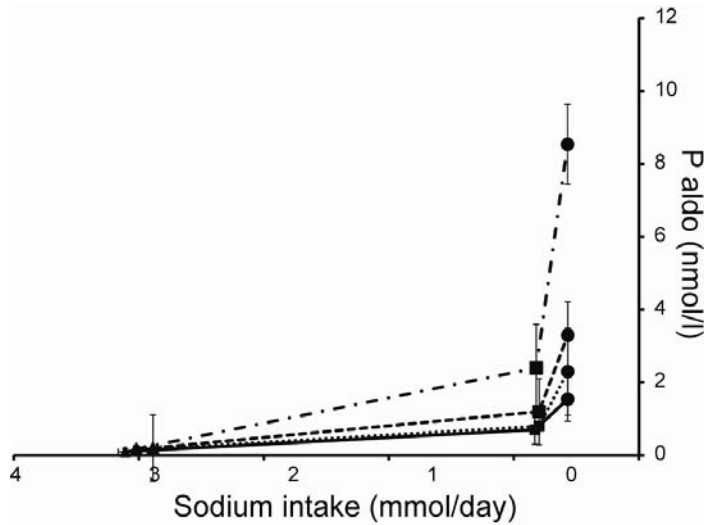
Figure 12. Plasma aldosterone levels in response to salt intake in *Scnn1a*^{KO} mice

Plasma aldosterone values were done from animals maintained on a high (▲), regular (■) or low (●) salt diet. For each genotype, *Scnn1a*^{Lox} mice (n= 6; —), *Scnn1a*^{Het} (n= 7; ---), *Scnn1a*^{Hetc} (n=6; ⋯) and *Scnn1a*^{KO}, (n=7; ·-·-·) animals, the average P$_{Aldo}$ values are plotted against the corresponding average sodium intake values (vertical and horizontal bars indicate S.E.M values).

Absence of ENaC in colon and consequently failure of the colon to absorb sodium against an

electrochemical gradient through ENaC might lead to a colon-specific salt loosing syndrome

accompanied by high aldosterone response. We found a clear correlation between plasma

aldosterone (P_{aldo}) levels and ΔPD_{amil} response, and the KO mice remained unresponsive to

increased P_{aldo} whereas the *Scnn1a*^{Lox} mice were sensitive to changes in P_{aldo}. The response of

the heterozygous mice was intermediate (*P*<0.05; **Fig. 13**).
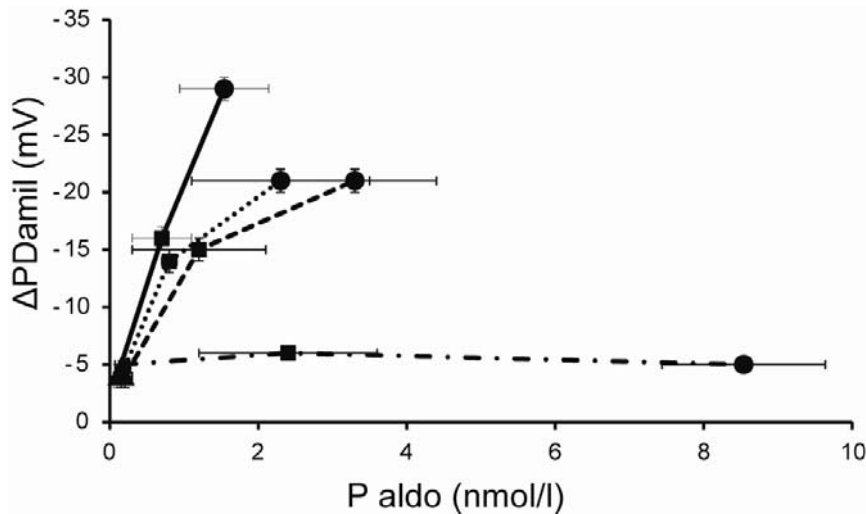
Figure 13. Mineralocorticoid resistance in *Scnn1a*^{KO} mice

ΔPD_{-Amil} and P_{Aldo} values were taken from the experiments summarized in Fig. 2 and 3. For each
genotype (*Scnn1a*^{Lox}(n= 6; —), *Scnn1a*^{Het}(n= 7; ---), *Scnn1a*^{Hetc} (n=6; ⋯) and *Scnn1a*^{KO}(n=7; ·-·-·-),
the average ΔPD_{amil} values are plotted against the corresponding average P_{aldo} values from animals
maintained on a high (▲), regular (■) or low (●) salt diet (vertical and horizontal bars indicate S.E.M.
values). Linear regression of the mean values revealed a significantly (*P* < 0.05) flatter slope in
Scnn1a^{KO} animals compared with the *Scnn1a*^{Lox}, *Scnn1a*^{Het}, *Scnn1a*^{Hetc} mice.

We interpreted these data as indicating a *colon-specific mineralocorticoid resistance* (or

decreased aldosterone responsiveness) that led to a colon-specific PHA-1 phenotype.

Interestingly, a mirrored image of this phenotype was observed in colon of Liddle mice that

harbor a point mutation within the βENaC subunit leading constitutively to hyperactivity of

ENaC. In this model, increased aldosterone responsiveness of the sodium transport was

observed when measured *ex vivo* in colon epithelium using the short circuit current method (Bertog et al., 2008).

Differential effect of colon-specific αENaC knockouts on sodium and potassium balance

The sodium balance was measured under three different salt diets by measuring sodium intake (**Table 1**), fecal sodium (**Fig. 5**) and urinary sodium (**Fig. 7**). The data were summarized in the **Figure 14**. Under HS, there was no significant difference in sodium balance. The total recovery of urinary sodium and fecal sodium accounted for 85 % of the intake. The remaining sodium (sodium gap) might be accounted for either in the transcellular fluid compartment which accounted for about 6 % along the entire length of the intestine and/or into the skin compartment as described by Titze and colleagues (Machnik et al., 2009). Interestingly, the sodium gap decreased under RS (80 to 100% of sodium recovered in urine and feces) and even more under LS (90 to 100% recovery) suggesting that in mice the only route for sodium excretion was the feces and the urine. We found a progressive fecal sodium loss in function of the diet (RS, LS) and according to the genotype. Under LS, the fecal loss of sodium is compensated by a maximal and remarkable retention of sodium in the kidney due to very high P_{aldo} (**Fig. 5**; **Fig. 14**).
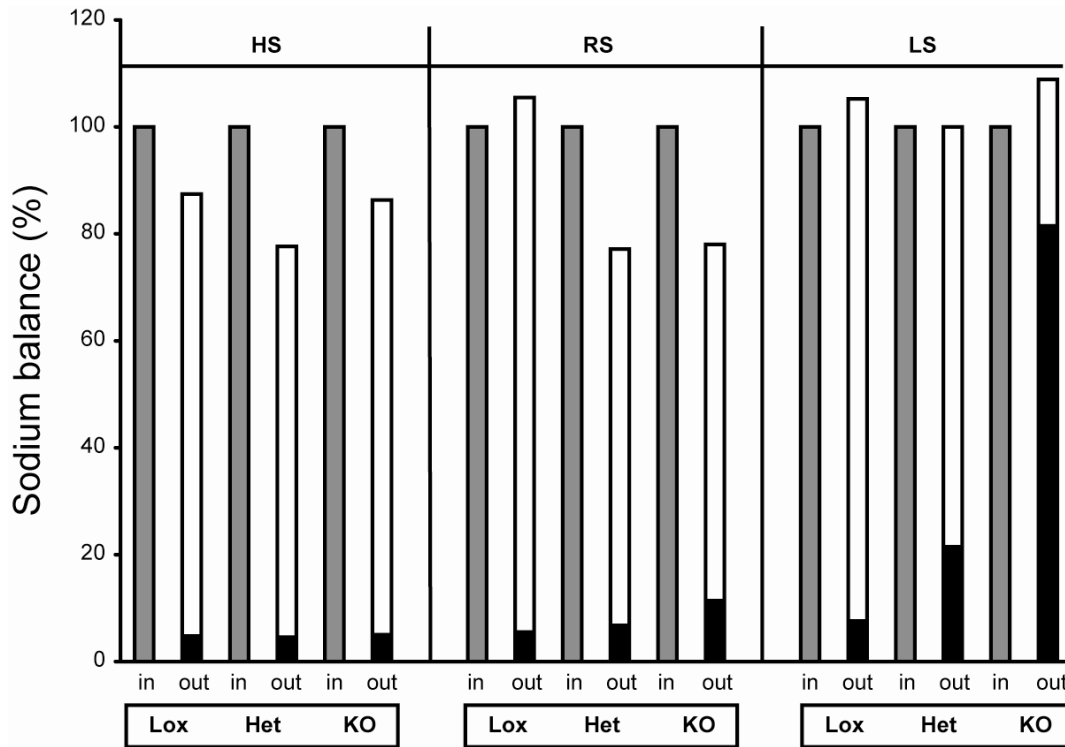
Figure 14. Shifted sodium balance under HS, RS and LS diets in *Scnn1a*^{KO} mice

Sodium balance is considered as ratio between the quantities of sodium output (in urine or in feces) at day 1 normalized by the quantity of sodium intake at day 1. Data were taken from experiments summarized in **Table 1** (food intake), **Fig. 5** (fecal sodium) and **Fig. 7** (urinary sodium). For each of the genotypes (*Scnn1a*^{Lox}, *Scnn1a*^{Het} and *Scnn1a*^{KO}) the average sodium intake via food (grey column) is compared with urinary sodium-output (white column) and fecal sodium output (black column) upon high (HS), regular (RS) or low (LS) salt diet (values indicated in percentage).

We did not have any indication for an effect on potassium balance in the KO mice (**Fig. 5B and 7D-F**). Systemic PHA-1 is characterized by severe renal salt loosing syndrome accompanied by lethal hyperkalemia. Hyperkalemia is explained in large part by the obligatory exchange of potassium against sodium that is directly linked to ENaC activity in the distal nephron and collecting duct and can be either induced pharmacologically by amiloride or through genetic deletion of ENaC activity along the nephron (Rossier et al., 2013). Potassium secretion within ASDN is mainly mediated by ROMK and to a lower extent by BK channels. In surface enterocytes of distal colon, K$^+$ transport is not mediated by ROMK but rather by BK (secretion) and H,K-ATPase (absorption) expressed in the apical

membrane of the epithelia cell (Sorensen et al., 2010b). In crypt enterocytes, K^+ secretion is mediated by apically located BK channels and coupled to chloride secretion mediated by CFTR. In colon, there is thus no direct coupling of ENaC-mediated sodium absorption and potassium secretion. It is proposed that electrogenic sodium reabsorption and potassium secretion are differentially regulated and spatially separated phenomena (Sorensen et al., 2010b). This could explain the absence of impairment of potassium balance in our mouse model.

CAP1 regulates colon ENaC activity by blunting its circadian cyclicity

Previous studies have emphasized the critical importance of CAP1 *in vivo*. CAP1/*Prss8* is required for placental labyrinth maturation and its constitutive knockout led to embryonic lethality highlighting a novel and crucial role for CAP1/*Prss8* in placental development and function (Hummler et al., 2013). Skin-specific deletion of CAP1/*Prss8* led to early postnatal lethality due to a severe impairment of the epidermal barrier function (Leyvraz et al., 2005) Lung alveolar specific deletion of CAP1/*Prss8* led to a severe impairment of alveolar fluid clearance and lung fluid balance (Planes et al., 2010).

In the present study, we provided insight into the distinct and specific role of ENaC regulation in the distal colon. Compared to the ΔPD_{amil} phenotype of the *Scnn1a*^{KO} mice as described above (**Fig. 3 and 4**), the phenotype of the CAP1/*Prss8* deletion in the colon is milder, but consistent with a specific interaction with ENaC activity in the afternoon (**Fig. 11**). In rodents, the circadian rhythm is reversed compared to human, i.e. RAAS is maximally activated during the afternoon. This is precisely the time where a significant interaction between ENaC and CAP1/*Prss8* is observed suggesting that CAP1/*Prss8* is specifically involved in the aldosterone-dependent signaling pathway that is maximally stimulated in the afternoon. Our experimental approach did not allow to prove or disprove a direct interaction

of CAP1/*Prss8* and ENaC leading to the activation of ENaC by cleavage of the γ subunit (Rossier and Stutts, 2009), On the other hand, we cannot rule out or support an indirect mechanism with CAP1/*Prss8* interacting somewhere on the aldosterone signaling pathway. Interestingly, recent analyses in hairless (fr^{CR}) rat and frizzy (*fr/fr*) mice harbouring spontaneous mutations of CAP1/*Prss8* with an estimated low enzymatic activity (Szabo et al., 2012) revealed a significant decreased ΔPD_{amil} although CAP1/*Prss8* mRNA transcript and protein expression levels were not significantly altered (Frateschi et al., 2012).

The intestinal barrier was maintained in **CAP1/Prss8-deficient mice**

We proposed that the channel-activating proteases CAP1/*Prss8*, CAP2/*Tmprss4* and CAP3/*Prss14* are not functionally redundant in the intestine as lack of CAP1/*Prss8* did not result in upregulation of CAP2/Tmprss4 or CAP3/Prss14 (**Fig. 8B**). We previously identified the protease-activated receptor PAR2 as a downstream target of CAP1/*Prss8*, and either knockout or over-expression of the serine protease in the epidermis resulted in postnatal lethality due to severe dehydration through impaired filaggrin processing (Leyvraz et al., 2005) and/or inflammation through increased expression of PAR2 (Frateschi et al., 2012). Surprisingly, in the present study, we did not see an implication of CAP1/*Prss8* in epithelial barrier formation and permeability in the intestine, since CAP1/*Prss8* knockout mice maintained their intestinal barrier (**Fig. 9B**). This was surprising, since epidermis-specific CAP1/*Prss8* knockout mice exhibited a severely impaired epidermal barrier most likely due to defective tight junction function (Leyvraz et al., 2005). In intestinal CAP3/Prss14 (matriptase) knockout mice, Buzza and co-workers suggested, that enhanced expression and incorporation of the permeability associated tight junction protein claudin-2 was causative for the observed intestinal barrier defect (Buzza et al., 2010). This raised again the question whether CAP1/*Prss8* and CAP3/Prss14 were part of the same proteolytic cascade in colon

with CAP1/*Prss8* acting downstream (Netzel-Arnett et al., 2006) or upstream of CAP3/SP14 (Buzza et al., 2013). Since our data did not show an intestinal barrier defect, we could not confirm the presence of either cascade in intestine. Further experiments using genetically-engineered mice will have to elucidate whether the phenotypes of both serine proteases are strongly cell-type and context-dependent.

In conclusion, we demonstrated that in colon of mice lacking ENaC and/or CAP1/*Prss8*, amiloride-sensitive sodium transport is drastically diminished. This leads to increased fecal sodium loss, which is accompanied by mineralocorticoid resistance in ENaC-deficient mice. Since the amount of sodium in the body is the main determinant of extracellular volume, disturbances in sodium balance will lead to clinical situations of volume depletion or overload; the latter will lead to arterial hypertension and heart failure. In CKD, when the ability of the kidneys to excrete sodium decreases, pharmacological inhibition of colonic ENaC may lead to increased intestinal excretion of sodium. This may help to maintain sodium homeostasis in CKD where diuretics have only limited success.

4. RESULTS: SECOND PART

Part II – Role of ENaC and CAP1/*Prss8* in dextran sodium sulfate-induced colitis

Aim of this part of thesis is to understand whether ENaC and /or CAP1/*Prss8*-deficiency predispose mice to dextran sodium sulfate (DSS) - induced colitis or not. This second part resumes results obtained after acute treatment of dextran sodium sulfate (DSS) in *Scnn1a*^{KO} and *Prss8*^{KO} mice which has been described in first part of results. I have performed most of experiments, which includes performing acute DSS treatment on *Scnn1a*^{KO} and *Prss8*^{KO} mice and analysis of these experiments. Paraffin sections and hematoxylin and eosin staining was done by Jean-Christophe Stehle, Pathology platform, UNIL.

4.1 Results

4.1.1 Scnn1a^{KO} and Scnn1a^{Het} mice develops early acute inflammatory DSS-induced colitis

To investigate the functional importance of absent αENaC in colitis, *Scnn1a*^{KO} mice were subjected to acute colitis by using 5 % dextran sodium sulfate (DSS). Oral administration of DSS is injurious to intestinal epithelium and causes an acute colitis that mimics human inflammatory bowel disease (IBD) (Melgar et al., 2005, Melgar et al., 2008). Age matched *Scnn1a*^{KO} and littermate control mice were administered 5% DSS in drinking water for 7 days. *Scnn1a*^{KO} and *Scnn1a*^{Het} mice lost weight more rapidly (significantly) than *Scnn1a*^{Lox} and *Scnn1a*^{Hetc} during first 3 days of treatment, while this loss was more severe in *Scnn1a*^{Het} than in *Scnn1a*^{KO}. Following day 4, all groups lost their body weight equally as shown in **Fig.15**. At the of treatment, the 5th day all groups lost approximately more than 15 % body weight and according to cantonal laboratory animal regulations, I have interrupted the experiment by sacrificing all mice.
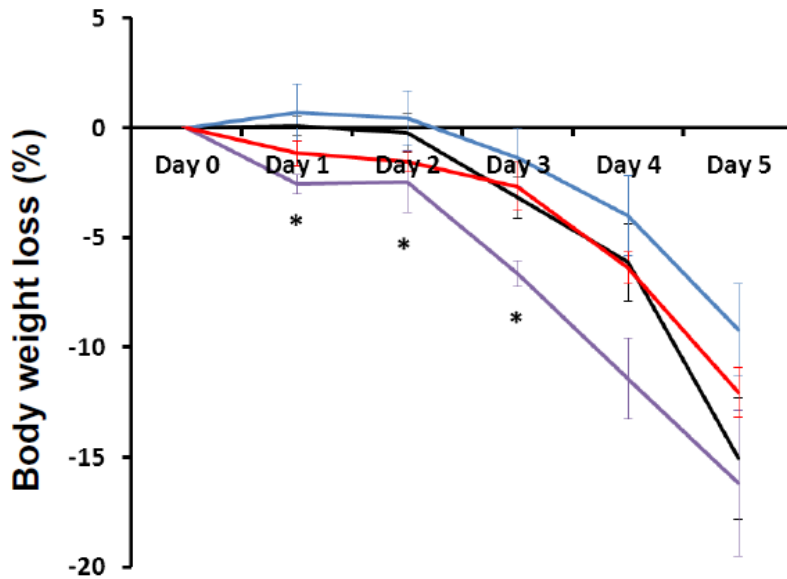
Figure 15. *Scnn1a*^{KO} and *Scnn1a*^{Het} are more susceptible to DSS-induced colitis

Body weight loss (%) relative to Day 0 in *Scnn1a*^{Lox} (black line, n=4), *Scnn1a*^{Het} (purple line, n=4), *Scnn1a*^{Hetc} (blue line, n=4) and *Scnn1a*^{KO} (red line, n=4) during 5 days of the 5% DSS treatment. Values indicated here are Mean ± SEM. *, $P < 0.05$ in *Scnn1a*^{Het} vs *Scnn1a*^{Lox} and *Scnn1a*^{Hetc}.

During 5 days of DSS administration, all groups developed severe diarrhea alongwith blood (diarrhea score 4, as described in methods section) started after day 3 of treatment, while *Scnn1a*^{KO} and *Scnn1a*^{Het} mice started mild diarrhea with blood (diarrhea score 3) just after day 1 of treatment which was confirmed by hemocult test ,while in case of *Scnn1a*^{Lox} and *Scnn1a*^{Hetc}, no diarrhea was observed after day 1 of DSS treatment (**Fig.16**).

$Scnn1a^{Lox}$ $Scnn1a^{Hetc}$ $Scnn1a^{Het}$ $Scnn1a^{KO}$

Figure 16. Fecal hemocult test in DSS-induced *Scnn1a*^{KO} mice
Fecal hemocult test results after Day 1 of DSS treatment in *Scnn1a*^{Lox} (n=4), *Scnn1a*^{Het} (n=4), *Scnn1a*^{Hetc} (n=4) and *Scnn1a*^{KO} (n=4). Presence of blue color on a test field within 30 seconds to 2 minutes corresponds to positive result for occult blood.

However, following 5 days of treatment with DSS, severe substantial microscopic injury was observed in distal colon of all groups as shown in **Fig.17,** characterized by epithelial sloughing, crypt damage and inflammatory infiltration.

$Scnn1a^{Lox}$ $Scnn1a^{Het}$

$Scnn1a^{Hetc}$ $Scnn1a^{KO}$

Figure 17. Colon histology in DSS-induced *Scnn1a*^{KO} mice
Light photomicrographs of representative distal colon sections from age-matched (2 months old) *Scnn1a*^{Lox},*Scnn1a*^{Hetc}, *Scnn1a*^{Het} and *Scnn1a*^{KO} littermates (H&E-staining) after 5 days of DSS treatment; n=4 animals/genotpye. Scale bar, 200 pixel.

Inflammation-induced colonic shortening is monitored as an indicator of crypt damage and severe inflammation as previously described (Netzel-Arnett et al., 2012). In our experiments, there was no siginificant change in colon length of all groups as shown in **Fig.18**.
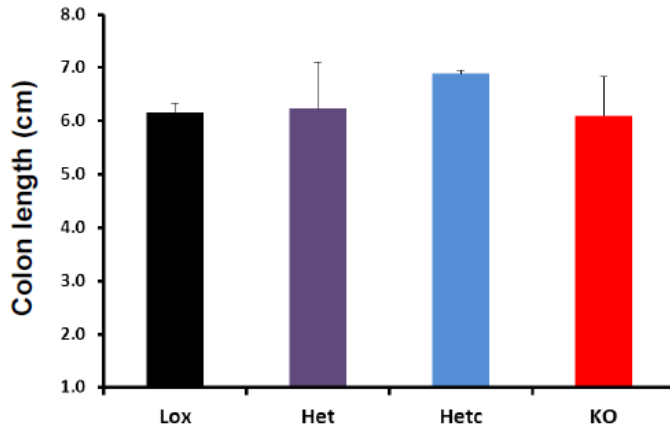
Figure 18. Colon length in in DSS-induced $Scnn1a^{KO}$ mice

Colonic length was measured after 5 days of treatment in $Scnn1a^{Lox}$ (black column, n=4), $Scnn1a^{Het}$ (purple column, n=4), $Scnn1a^{Hetc}$ (blue column, n=4) and $Scnn1a^{KO}$ (red column, n=4). Values here indicated as Mean ± SEM.

Overall, these data suggested that $Scnn1a$-deficiency ($Scnn1a^{KO}$ and $Scnn1a^{Het}$) might lead to worsening of DSS-induced colitis during early days of treatment, but further studies will be needed to confirm this. Although following 3 days of treatment, no difference was observed amongst all groups due to high dose of DSS.

4.1.2 Prss8 deficiency leads to severe inflammatory DSS-induced colitis

To determine the functional importance of $Prss8$ in colitis, $Prss8^{KO}$ mice were subjected to acute colitis by using 5 % dextran sodium sulfate (DSS) as described above. Age-matched $Prss8^{KO}$ and littermate control mice were administered 5% DSS in drinking water for 7 days. During first 3 days, there was no difference in body weight loss in all groups as shown in **Fig.19**. After day 4, $Prss8^{KO}$ and $Prss8^{Het}$ exhibited body weight loss was significantly more

than other groups. By the end of 6 days of treatment, we have lost 2 out 5 *Prss8*^{KO} mice

(40%).
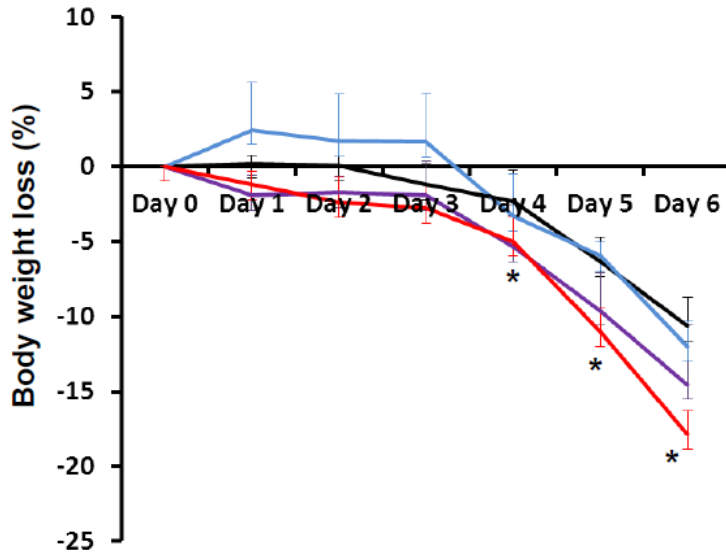
Figure 19. *Prss8*^{KO} mice is more susceptible to DSS-induced colitis

Body weight loss (%) relative to Day 0 in *Prss8*^{Lox} (black line, n=4), *Prss8*^{Het} (purple line, n=4), *Prss8*^{Hetc} (blue line, n=4) and *Prss8*^{KO} (red line, n=5) during 5 days of the 5% DSS treatment. Values indicated here are Mean ± SEM. *, $P < 0.05$ in *Prss8*^{KO} vs *Prss8*^{Lox} and *Prss8*^{Hetc}.

Prss8^{KO} and *Prss8*^{Het} showed diarrhea alongwith blood (diarrhea score around 3) after 1 day

of DSS treatment as shown in **Fig 20**, while other groups alongwith *Prss8*^{KO} started severe

diarrhea alongwith blood (diarrhea score 4) after 3 days.

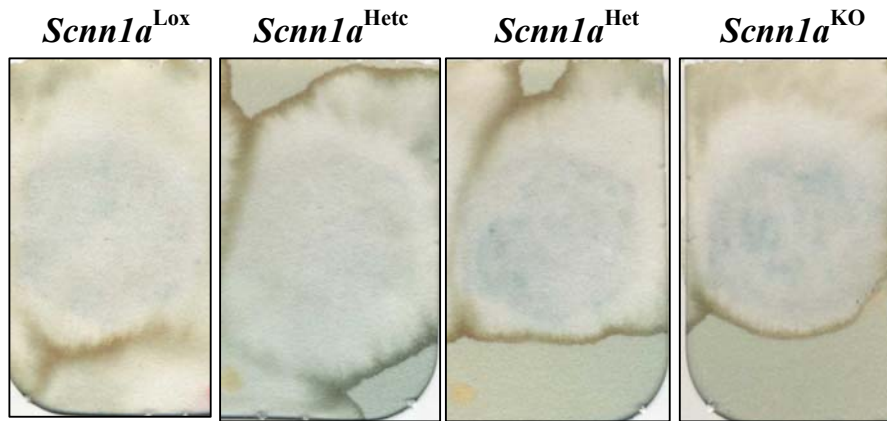$Prss8^{Lox}$ $Prss8^{Hetc}$ $Prss8^{Het}$ $Prss8^{KO}$
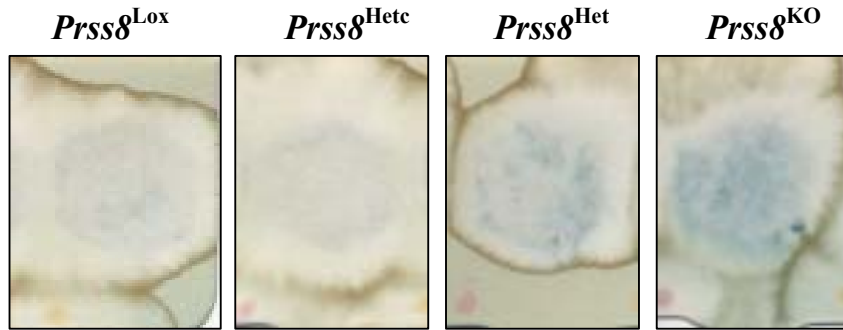
Figure 20. Fecal hemocult test in DSS-induced $Prss8^{KO}$ mice

Fecal hemocult test results after Day 1 of DSS treatment in $Prss8^{Lox}$ (n=4), $Prss8^{Het}$ (n=4), $Prss8^{Hetc}$ (n=4) and $Prss8^{KO}$ (n=4). Presence of blue color on a test field in case of $Prss8^{KO}$ and $Prss8^{Het}$ corresponds to positive result for occult blood.

Following 6 days of treatment with DSS, there was substantial microscopic injury that was severe in distal colon of all groups as shown in **Fig.21,** characterized by epithelial sloughing, crypt damage and inflammatory infiltration which was more severe in $Prss8^{KO}$ colon.

$Prss8^{Lox}$ **$Prss8^{Het}$**

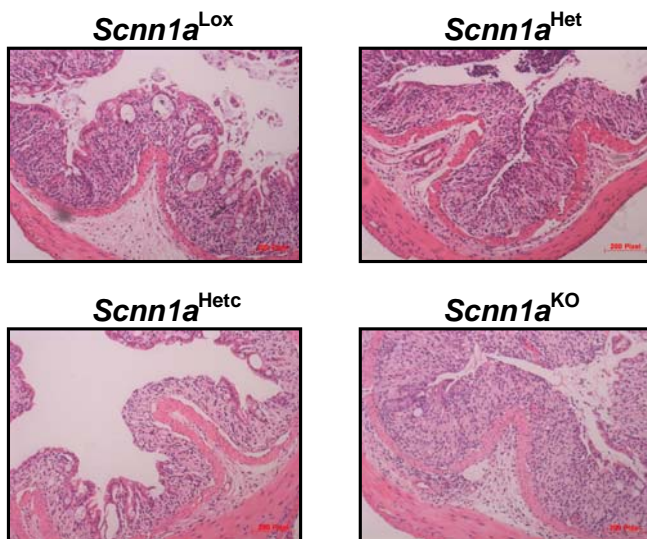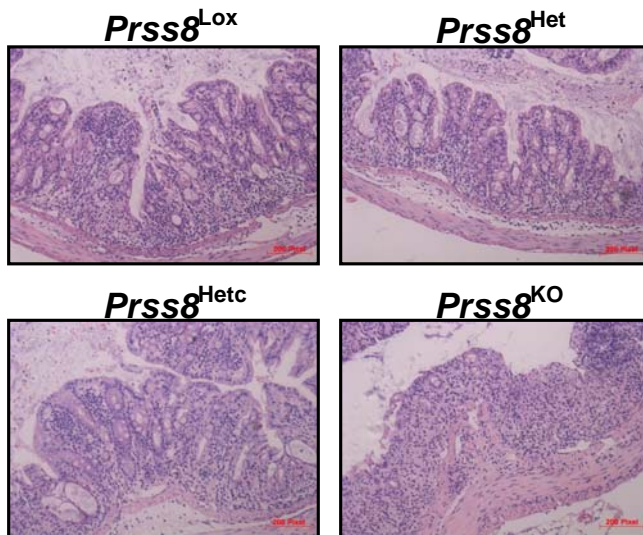**$Prss8^{Hetc}$**   **$Prss8^{KO}$**

Figure 21. Colon histology in DSS-induced $Prss8^{KO}$ mice

Light photomicrographs of representative distal colon sections from age-matched (2 months old) $Prss8^{Lox}$, $Prss8^{Hetc}$, $Prss8^{Het}$ and $Prss8^{KO}$ littermates (H&E-staining); n=4 animals/genotype. Scale bar, 200 pixel.

There was no observed change in colon length in all groups as shown in **Fig.22**.
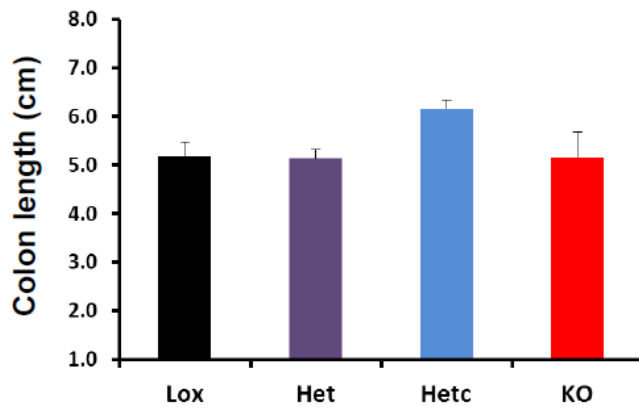
Figure 22.Colon length in in DSS-induced *Prss8*^{KO} mice

Colonic lengths was measured after 5 days of treatment in *Prss8*^{Lox} (black column, n=4), *Prss8*^{Het} (purple column, n=4), *Prss8*^{Hetc} (blue column, n=4) and *Prss8*^{KO} (red column, n=5).Values indicated here are Mean ± SEM.

In the summary, absence of *Prss8* favors a more severe DSS-induced treatment. To better understand role of *Prss8* in colitis, further studies will be required.

4.2 Conclusion, discussion and perspectives

Diarrhea is one of common symptoms of inflammatory bowel diseases (IBD), which occurs approximately 50 % in cases of Crohn's disease (CD), almost in all patients of ulcerative colitis (UC) (Seidler et al., 2006). Diminished or reversed Na^+ reabsorption observed in the colonic mucosa of CD and ulcerative patients (Allan et al., 1975, Hawker et al., 1980) and which can be restored by steroid administration (Sandle et al., 1986a). It has been also demonstrated that combination of epithelial barrier dysfunction and altered electrolyte movement responsible for the changes in net water flux during inflammation-associated diarrhea (Musch et al., 2002, Clayburgh et al., 2006).

Are Scnn1a^{KO} and Scnn1a^{Het} mice more susceptible to DSS-induced epithelial injury?

ENaC is known to be important for renal electrolyte transport, while in intestine our data indicates that loss of colonic ENaC leads to increased fecal sodium loss and increased urinary sodium retention especially under LS diet. ENaC down-regulation and resulting reduced colonic sodium absorption may contribute to diarrhea especially when it is associated with inflammatory bowel disease (Amasheh et al., 2004). In a recent report, (Sullivan et al., 2009) demonstrated that, among other transport-related genes, NHE1,3 (but not NHE2), β-ENaC, Na+/K+-ATPase-α, ClC-5, and NHERF1 were all downregulated in sigmoid mucosal biopsies from most cases of active UC and/or CD compared to controls. While, down regulations of sodium transporters and their regulatory factors has been observed in mice with DSS- and TNBS-induced colitis (Sullivan et al., 2009). They have also concluded here that IBD-associated diarrhea may be due to a coordinated down regulation of multiple Na^+ transporter and related regulatory proteins, including NHE1,3, Na^+, K^+- ATPase, and ENaC, as well as NHERF1,2, and ClC-5, all of which are involved directly or indirectly in intestinal Na^+ absorption. Based on these observations, we hypothesized that in our *Scnn1a*^{KO} mice

which already exhibited abolished ENaC-mediated colonic sodium reabsorption might be more prone to DSS-induced colitis. Our preliminary data indicated that deficiency of ENaC (*Scnn1a*^{KO} and *Scnn1a*^{Het}) led to worsening of DSS-induced colitis. *Scnn1a*^{KO} and *Scnn1a*^{Het} mice exhibited mild diarrhea containing blood 1 day after treatment with DSS. This data indicated that absence of colonic ENaC might leads to worsening of colitis, but further detailed studies are needed.

Another sodium transporter, NHE3-deficient mice exhibit mild chronic diarrhea, distention, and retention of alkaline fluid in all intestinal segments; mild metabolic acidosis; and lower blood pressure (Schultheis et al., 1998). Recently, they have demonstrated that loss of NHE3 activity in NHE3$^{-/-}$ mice results in mild to moderate distal colitis with symptoms, which could be alleviated by broad-spectrum oral antibiotics (Laubitz et al., 2008). Additionally they have studied the effect of NHE3 deficiency on mucosal homeostasis in a well-defined model of dextran sulfate sodium (DSS)-induced mucosal injury (Kiela et al., 2009). These mice also display alterations in epithelial gene and protein expression patterns, which predisposes them to an extremely high susceptibility to DSS, with high and accelerated mortality, even at a very low DSS concentration. Rapid death was observed resulting from a combination of intestinal bleeding, hypovolemic shock, and sepsis. Based on these findings, the first step will be to define the specific role of ENaC during early days of DSS treatment, a 48-hour time point, which may not sufficient to develop any symptoms in WT mice, but results mild bloody diarrhea in *Scnn1a*^{KO} mice. To achieve this, I will start DSS treatment and terminate treatment after day 1 and look for hematologic parameters and morphology of colon. Moreover, NHE3$^{-/-}$ did not show any alteration in intestinal permeability in untreated

condition indicating existence of a compensatory mechanism, which may be sufficient to mitigate the mucosal permeability in the absence of epithelial injury, while upon DSS-treatment leads to a dramatic increase intestinal permeability in terms of increased FITC-

dextran (Kiela et al., 2009). Although, we have not checked intestinal permeability in $Scnn1a^{KO}$ mice. Next step will be to check intestinal permeability with and without DSS treatment as Amasheh and colleagues (Amasheh et al., 2009) showed that aldosterone stimulates Na^+ transport via ENaC not only by increased transcellular absorption, but in parallel also by tightening the paracellular pathway against immediate back-leakage of freshly absorbed Na^+ by upregulating claudin-8. 3 Days after treatment, no obvious changes were detected within groups due to high dose of DSS. To understand role of ENaC more precisely, I like to induce colitis in mice with 2% DSS for consecutive 7 days and on day 8 to tap water alone. The mice will be allowed to recover until day 14, since DSS-induced colitis is a reversible condition.

Does Prss8 play a protective role in DSS-induced colitis?

Compromised epithelial barrier function is known to be important pathophysiologic basis for IBD. The altered or increased permeability leads to increased transport of microbial flora and antigens from the intestinal lumen into the submucosa, which finally leads to inflammation and mucosal injury (Clayburgh et al., 2004). Decreased barrier function is known to be positively correlated with mucosal inflammation in Crohn's disease (Murphy et al., 1989) and ulcerative colitis patients. While increased epithelial permeability precedes clinical relapse (Wyatt et al., 1993, Tibble et al., 2000). In fact, the first degree relatives of CD patients which are more prone to risk of this disease often have increased intestinal permeability (Hollander et al., 1986). In case of mouse models for IBD, exhibited increased epithelial paracellular permeability which can precede chronic mucosal inflammation (Olson et al., 2006) and also altered epithelial barrier function has been associated with colitis (Resta-Lenert et al., 2005). Structural changes associated with barrier dysfunction are well studied, although regulatory pathways that dynamically control intestinal barrier homeostasis are still less understood.

CAP1/*Prss8* was identified as an important factor for maintenance of skin epithelial barrier homeostasis. Skin-specific CAP1/*Prss8* KO mice died within 60 h after birth. They exhibited a lower body weight, impaired skin barrier function and transepidermal water loss measurements leading to rapid, fatal dehydration.CAP1/*Prss8*-deficient skin disturbs stratum corneum lipid composition, corneocyte morphogenesis, the processing of profilaggrin and absence of occludin, a tight junction protein. Therefore CAP1/*Prss8* expression in the epidermis is crucial for the epidermal permeability barrier and is important for postnatal survival (Leyvraz et al., 2005). Other members of the CAPs family, CAP3/matriptase has shown to have protective function against chemically induced colitis (i.e. DSS) and it also promotes intestinal barrier recovery (Netzel-Arnett et al., 2012). Considering the importance of intestinal epithelial barrier function in etiology of IBD, link between CAP1/*Prss8* and barrier function, we have decided to investigate the role of CAP1/*Prss8* in IBD. CAP1/*Prss8*-deficient mice exhibits severe DSS-induced colitis and at day 6 of 5% DSS treatment only 60% of the *Prss8*^{KO} survived. *Prss8*^{Het} mice also exhibit similar phenotype like *Prss8*^{KO} mice. Our result indicates the protective role of CAP1/*Prss8* in DSS-induced colitis, although further studies will be needed. The first step will be to define the specific role of CAP1/*Prss8* during a 48-hour of DSS treatment, which may not sufficient to develop any symptoms in WT mice, but results mild bloody diarrhea in *Prss8*^{KO} mice. We have checked intestinal permeability, which is slightly but not significantly increased in *Prss8*^{KO} mice as shown in **Fig.9B,** but might be altered during pathological conditions like colitis**.** To check this, I will start DSS treatment and terminate treatment after day 1 and look for hematologic parameters, intestinal permeability and morphology of colon. The second step will be to induce colitis in mice with 2% DSS for 7 days and on day 8 switch to tap water only and the mice allowed recovering until day 14. With this protocol, it will be possible to understand whether CAP1/*Prss8* -deficient mice able to recover.

Overall, we will understand role of ENaC and CAP1/*Prss8* in pathological conditions like inflammatory bowel diseases (IBD). Especially for CAP1/*Prss8*, a better understanding of the role of this protease in controlling mucosal integrity by regulating permeability of intestinal barrier function will be important to develop CAP1/*Prss8*-based therapeutic strategies for preventing or altering natural progression of IBD.

5. RESULTS: THIRD PART

Part III - Implication of ENaC cleavage at the furin site on channel activity

Aim of this part of thesis is to understand the role of furin cleavage site which is present on αENaC/*Scnn1a* subunit on channel activation. We have generated and characterized mDCT (distal convoluted tubule), mCNT (connecting tubule) and mCCD (cortical collecting duct) cell lines from microdissecting different parts of distal nephron from *Scnn1a*$^{lox/lox}$/Pax8/LC1 mice (doxycycline inducible renal tubule-specific *Scnn1a*^{KO}, generated by Romain Perrier). This part describes the generation and characterization of doxycycline-inducible *Scnn1a* - deficient mDCT, mCNT and mCCD cell lines. Transfection of *Scnn1a*-deficient mCCD cells with *Scnn1a* tagged with a triple HA epitope at its C-terminus by using electroporation and lipofectamine. Micro-dissection has been done by Nicole Fowler-Jaeger and establishment of primary cell lines by Hanspeter Gaeggeler. For this part, I have characterized these cells and also performed electrophysiological measurements.

5.1 Results

Characterization of the microdissected mDCT, mCNT and mCCD cells from doxycycline inducible renal tubule-specific Scnn1aKO (Scnn1alox/lox/Pax8/LC1)

5.1.1 mRNA transcript expression of gene markers in primary cultures of non-induced Scnn1a$^{lox/lox}$/Pax8/LC1 mDCT, mCNT and mCCD cells

Mouse distal convoluted tubule (mDCT), mouse connecting tubule (mCNT) and mouse cortical collecting duct (mCCD) cells were generated from non-

induced *Scnn1a*$^{lox/lox}$/Pax8/LC1 mice and exhibited presence of following gene markers as shown in **Fig.23.** mDCT cells (clone 5) showed presence of *Scnn1a*, calcium channel (TRPV5), mineralocorticoid receptor (MR), Na^{+}Cl^{-} cotransporter (NCC) minimal upon AVP treatment as compared to non-treated cells. While mCNT showed specific expression of *Scnn1a*, TRPV5, MR, water channel (AQP2). The mCCD (clone 1) cells also exhibits presence of *Scnn1a*, TRPV5, MR, AQP2 like mCNT cells. Thus these results demonstrated that confluent cultured mDCT, CNT, CCD cells conserved the expected mRNA expression of wild-type αENaC.

A
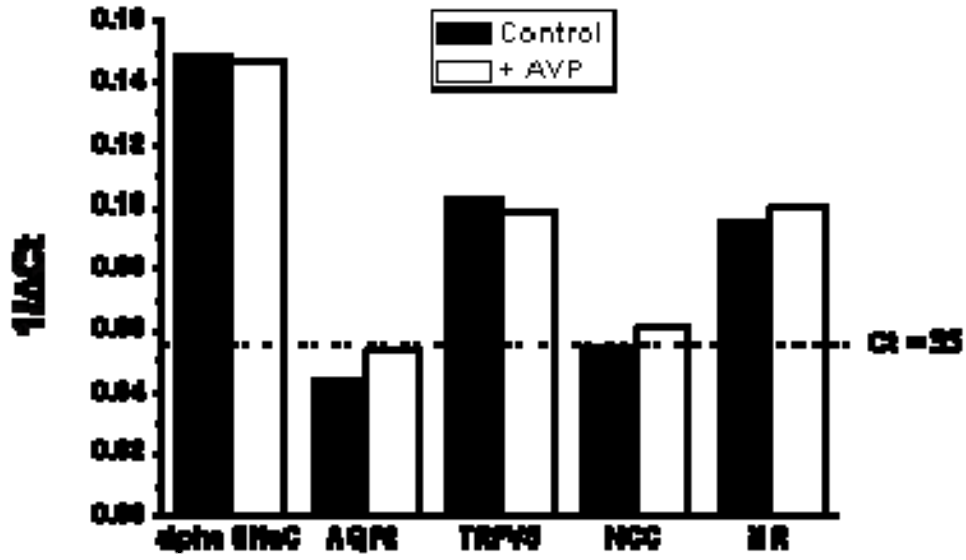
B
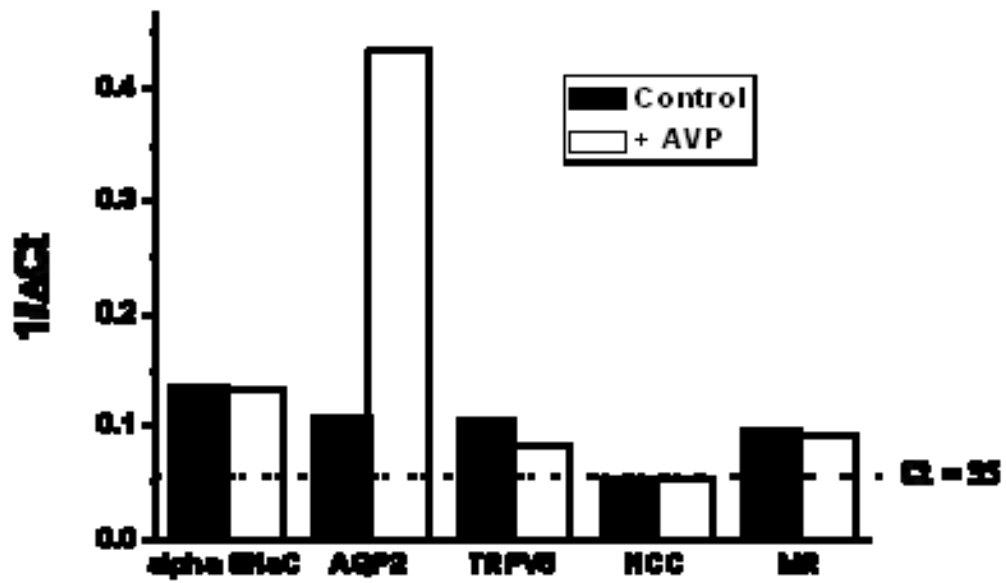
C
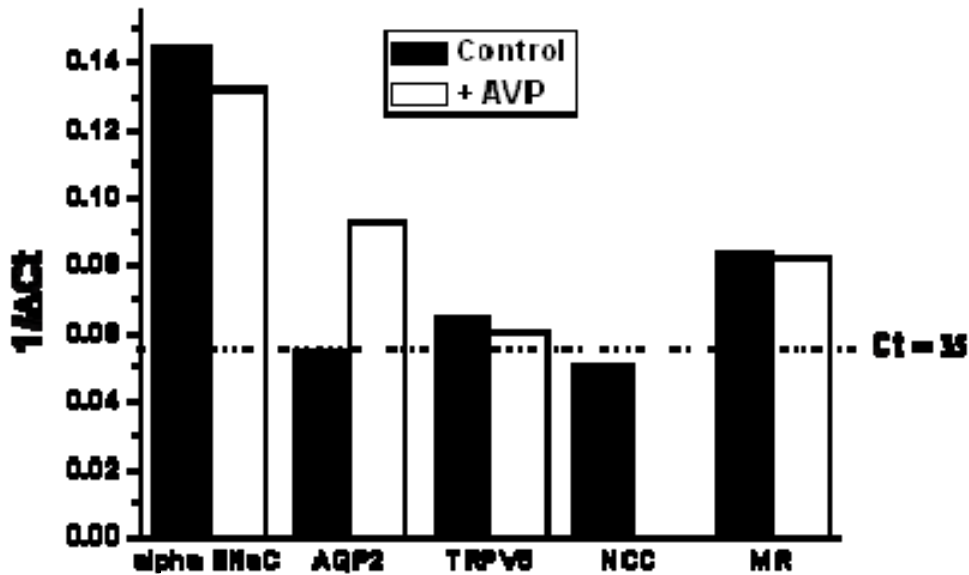
Figure 23. Presence of gene markers

Quantification of αENaC, AQP2, TRPV5, NCC and MR mRNA transcript expression in **(A)** mDCT , **(B)** mCNT and **(C)** mCCD cells by quantitative RT-PCR in control (black column) and AVP-treated (white column) non-induced *Scnn1a*$^{lox/lox}$/Pax8/LC1 cells. Results are expressed as the inverse of ΔCt (n = 3 filters).

5.1.2 Na$^+$ transport in primary cultures of doxycycline-inducible mDCT, mCNT and mCCD

-specific Scnn1a-deficient cells

The transport of Na$^+$ was estimated by measuring the short-circuit current (I$_{sc}$) on confluent

cultures of DCT (clone 5), CNT and CCD (clone 1) grown on Transwell filters. As shown in

Fig.24A, the control (*Scnn1a*$^{lox/lox}$/Pax8/LC1) mDCT cells exhibited a baseline short-circuit

current at approximately 50 µA/cm^2, which remained stable following 8h incubation. Upon

maximal stimulation by aldosterone (300 nM), the short-circuit current increased rapidly to

reach a maximum after 3 to 4h (75 $\mu A/cm^2$). While upon doxycycline treatment short-circuit current was significantly abolished (nearly 1 $\mu A/cm^2$), even after aldosterone stimulation, After 8h of incubation, amiloride treatment led to abolishment of I_{sc} indicating origin of current was ENaC-mediated. In control mCCD (*Scnn1a*$^{lox/lox}$/Pax8/LC1) cells, baseline short-circuit current was observed at approximately 17 $\mu A/cm^2$, maintained stable till 8h (**Fig.24C**). Upon aldosterone induction, the short-circuit current increased rapidly to reach a maximal value after 3 to 6-h (25 $\mu A/cm^2$). In doxycycline treated group, short-circuit current was significantly abolished (2 $\mu A/cm^2$), it did not change after aldosterone stimulation. Finally the control mCNT (*Scnn1a*$^{lox/lox}$/Pax8/LC1) cells exhibited a baseline short-circuit current at approximately 20 $\mu A/cm^2$ for doxycycline-treated or non-treated cells. Aldosterone treatment led to increase short-circuit current of 50 $\mu A/cm^2$ irrespective of doxycycline treatment (**Fig. 24B**).

A
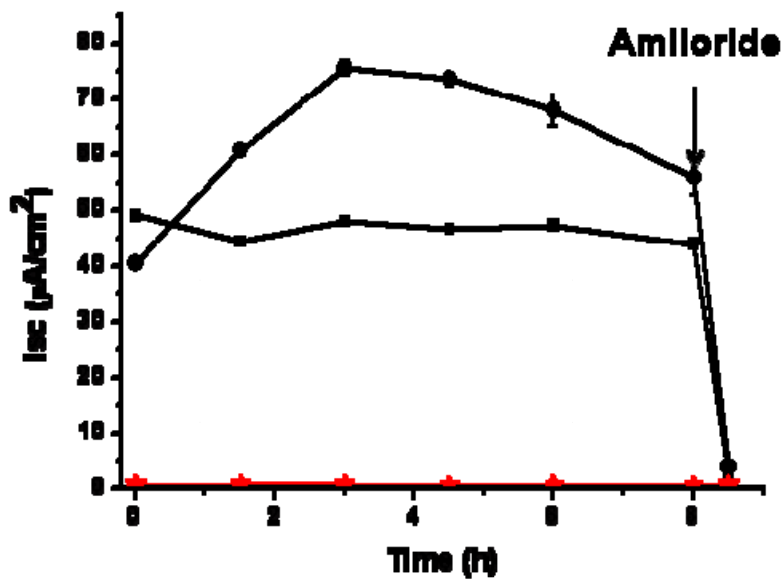
B
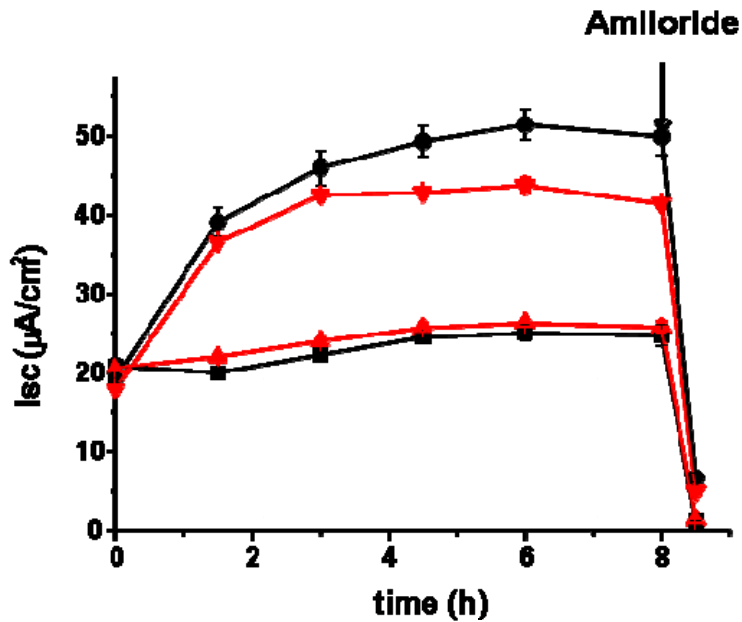
C
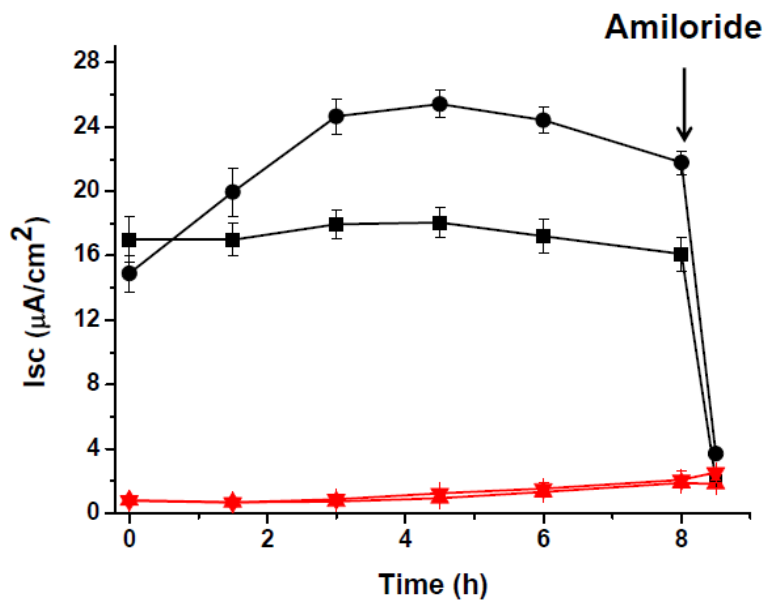
Figure 24. Sodium transport in primary cell culture upon doxycycline treatment

I_{sc} was measured in control (—■—) and doxycycline treated (—▲—) cells without aldosterone and in control (—●—) and doxycycline treated (—▼—) after basal and apical additions of 300 nM of aldosterone for 8 hours at 37^0C in **(A)** mDCT , **(B)** mCNT and **(C)** mCCD cells. At the end of experiments, amiloride (10^{-5}M) has been added .Values are means ± SEM from 12 independent filters for each group. ***$P < 0.001$ versus control (+/- aldosterone).

These results indicated that ENaC-mediated sodium transport was totally abolished in mDCT and mCCD cells upon doxycycline treatment. This was also confirmed by complete absence of αENaC mRNA transcripts expression (**Fig.25**).

In case of mCNT cells, ENaC-mediated sodium transport was detected after doxycycline treatment, which was comparable to non-treated cells. It was also confirmed by intact αENaC mRNA expression (**Fig.25**). This intact ENaC expression as well as ENaC-mediated sodium transport likely to be due to incomplete recombination upon doxycycline treatment.
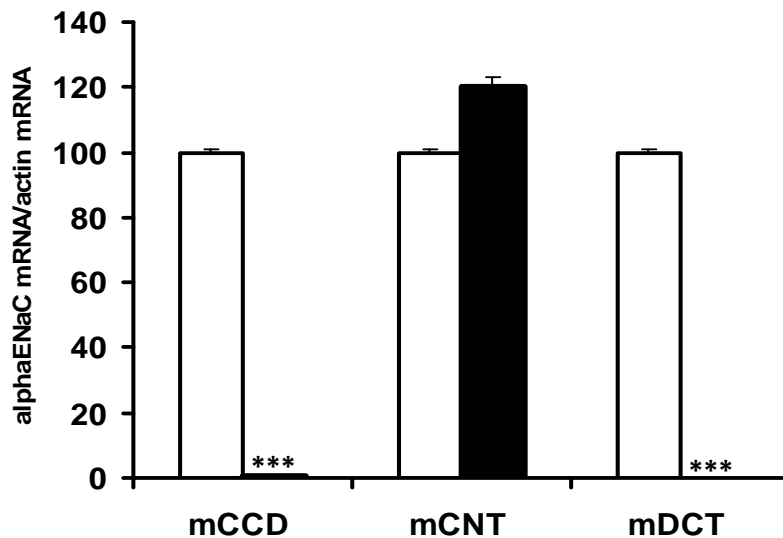
Figure.25 Generation of *Scnn1a* -deficient mDCT, mCNT and mCCD cells

Quantification of *Scnn1a* mRNA transcript expression in mCCD, mCNT and mDCT cells by quantitative RT-PCR in control (white column) and doxycycline-treated (black column) cells.
Results are expressed as the ratio of ENaC mRNA subunits to β-actin mRNA (n = 6 filters per group); ***, $P < 0.001$.

5.1.3 Transfection of Scnn1a-deficient mCCD cells

After generation and characterization of *Scnn1a*-deficient mCCD cells, we would like to further understand the role of the furin consensus site on *Scnn1a* for channel activation. To

achieve this, the first step was to standardize the transfection protocol for mCCD cells. We have stably transfected *Scnn1a*-deficient mCCD cells with αENaC-tagged (triple HA epitope at its C-terminus) (Staub et al., 1996) under the control of a glucocorticoid-inducible promoter (Hirt et al., 1992) by using electroporation and lipofectamine. Transfected cells with lipofectamin exhibited comparable expression of αENaC at mRNA levels as control cells (non -induced). Cells which were transfected by electroporation exhibits 15 % of αENaC mRNA expression as compared to control cells (non -induced) (**Fig. 26**).
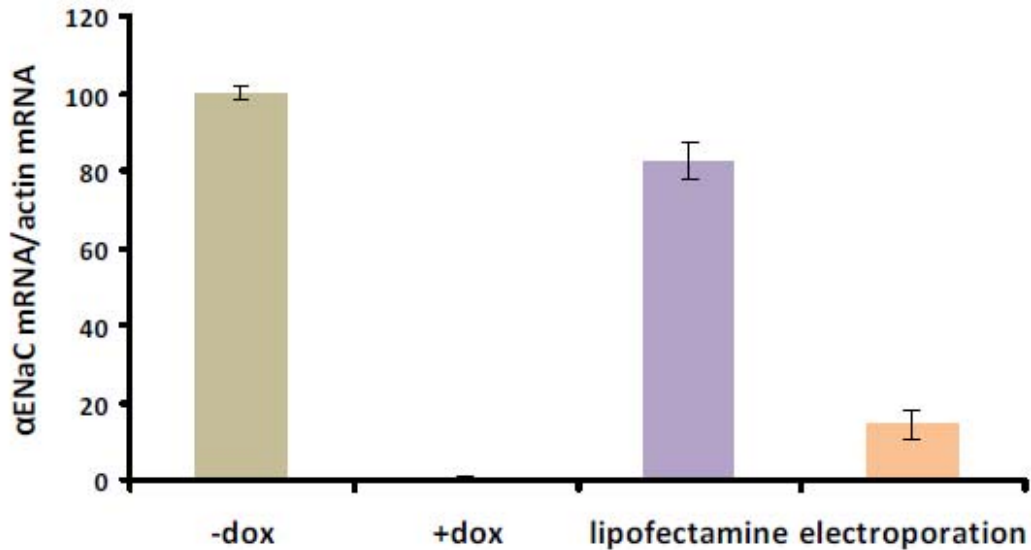
Figure 26. Quantification of αENaC mRNA transcript expression in *Scnn1a*[lox/lox]/Pax8/LC1 mCCD cells without doxycycline (yellow column), cells with doxycycline (black column), cells with doxycycline + transfected with αENaC[wt] by lipofectamine (purple column) and cells with doxycycline + transfected with αENaC[wt] by electroporation (orange column). Results are expressed as the ratio of αENaC mRNA subunits to β-actin mRNA (n = 3 filters per group).

Transfection efficiency was also assessed at the protein level as shown in **Fig.27**.Cells transfected by lipofectamine exhibited comparable levels of αENaC as compared to control cells (non-treated), while by electroporation shows low levels of αENaC as compared to

control cells. These results indicated that mCCD cells can be efficiently transfected by using

lipofectamine.
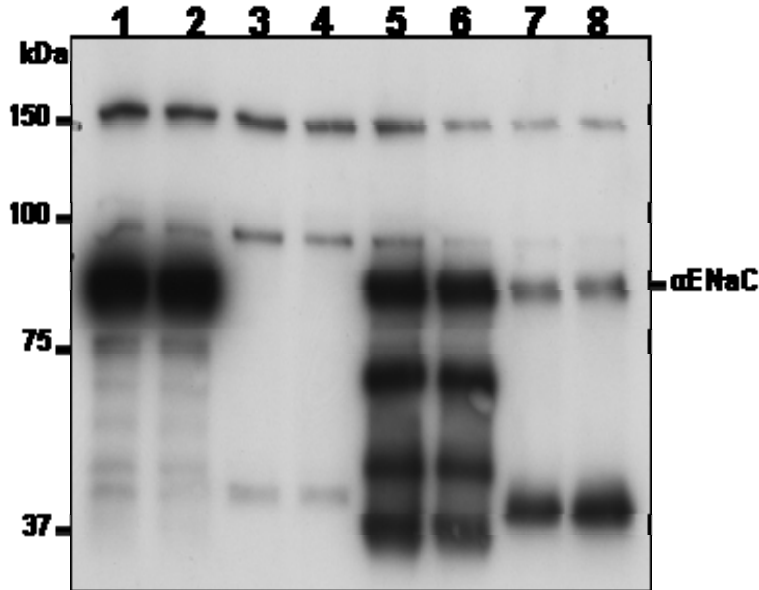
Figure 27. Representative Western blot analysis showing the expression of alphaENaC (95kDa) in *Scnn1a*[lox/lox]/Pax8/LC1 mCCD cells without doxycycline (lane 1-2), doxycycline treated (lane 3-4), cells with doxycycline + transfected with αENaC[wt] by lipofectamine (lane 5-6) and cells with doxycycline + transfected with αENaC[wt] by electroporation (lane 7-8).

The electrophysiology experiments were performed by measuring transport of Na^+ as

measured as the short-circuit current (I_{sc}) in these stably transfected cells as shown in **Fig.28**.

The control (*Scnn1a*[lox/lox]/Pax8/LC1) mCCD cells without doxycycline treatment, exhibited a

baseline short-circuit current at approximately 25 $\mu A/cm^2$, which remained stable following

5-h incubation. While upon doxycycline treatment short-circuits current was significantly

abolished (nearly 1 $\mu A/cm^2$). *Scnn1a*[lox/lox]/Pax8/LC1 treated with doxycycline and stably

transfected with αENaC[wt] by lipofectamine showed moderate baseline short-circuit current at

approximately 4 $\mu A/cm^2$ and thus rescued about 15-20 % Na^+ transport as compared to

control cells. Upon electroporation, baseline short-circuit current at approximately 1 $\mu A/cm^2$

was measured. At the end of experiment, amiloride treatment led to abolishment of I_{Na} indicating origin of current was ENaC-mediated. These data indicated efficiency of lipofectamine mediated transfection over electroporation. This has been confirmed by electrophysiology data as well as αENaC mRNA transcripts (**Fig.26)** and αENaC protein levels (**Fig.27).**
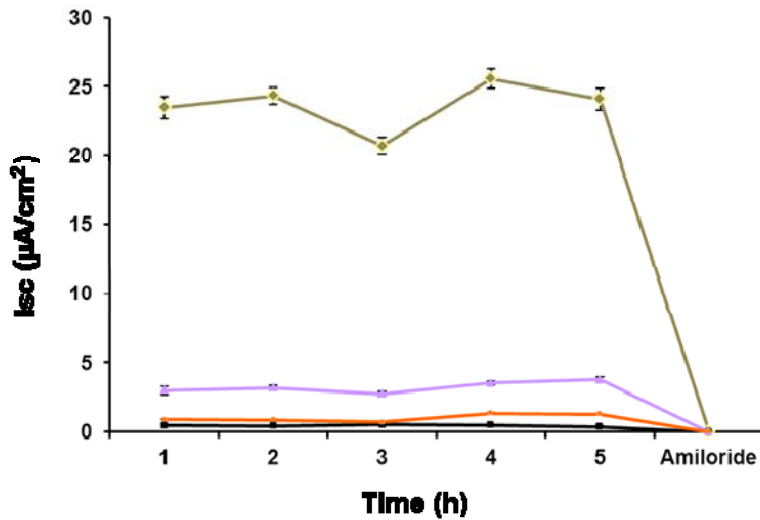
Figure 28. Sodium transport in *Scnn1a*$^{lox/lox}$/Pax8/LC1 mCCD cells

I_{sc} was measured in *Scnn1a*$^{lox/lox}$/Pax8/LC1 mCCD cells without doxycycline (yellow line), doxycycline treated (black line), cells with doxycycline + transfected with αENaC by lipofectamine (purple line) and cells with doxycycline + transfected with αENaC by electroporation (orange line) for 5 hours at 37°C. At the end of each experiment, amiloride (10^{-5}M) has been added. Values are means ± SEM from 6 independent filters for each group.

In summary, we have generated and characterized doxycycline-inducible mDCT, mCNT and mCCD -specific *Scnn1a*-deficient cells. Later, we have also standardized transfection protocol for mCCD cells. ENaC-mediated sodium transport was totally abolished in mDCT and mCCD cells upon doxycycline treatment. mCNT cells upon doxycycline treatment showed intact ENaC-mediated sodium transport and *Scnn1a* /αENaC expression likely to be due to incomplete recombination. Furthermore, this data indicated efficiency of lipofectamine

mediated transfection over electroporation. Transfection by lipofectamine efficiently rescued ENaC-mediated sodium transport. Future experiments will be needed in order to better understand role of furin cleavage site on αENaC for channel activation.

5.2 Conclusion, discussion and perspectives

ENaC is preferentially assembled as heteromeric αβγ complexes. By using *Xenopus* oocytes expression system, it has been possible to quantitate the number of channel expressed at cell surface and to measure amiloride-sensitive current generated by ENaC at cell surface (Grunder et al., 1997). Maximal ENaC activity was measured when all subunits were co-injected together (Firsov et al., 1996). When the α subunit is injected alone, only 1or 2 % of maximal activity observed. When αβ or αγ are co-injected, 5-15% of maximal activity was recorded. The β or γ subunit alone did not lead to any channel activity (Bonny et al., 1999). These data indicated that α subunit has an essential chaperone role, bringing β and γ subunits to plasma membrane. Relevant to this finding, our data of doxycycline-inducible mDCT and mCCD -specific *Scnn1a*-deficient cells proved the importance of α subunit in channel activation as shown in **Fig.24**. Although, ENaC expression as well as ENaC-mediated sodium transport was observed in mCNT cells most likely indicates incomplete recombination upon doxycycline treatment.

ENaC activity is regulated by proteases which have been demonstrated previously. ENaC-activating proteases belong to the PA or SB clans of evolutionally related serine proteases (Rawlings and Barrett, 1993). Extracellular trypsin has been shown to increase channel activity (Chraibi et al., 1998, Vuagniaux et al., 2000, Bridges et al., 2001, Donaldson et al., 2002, Caldwell et al., 2004). Extracellular trypsin activates near-silent ENaC channels by dramatically increasing their Po (Caldwell et al., 2005). A family of membrane bound channel-activating serine proteases referred as CAPs, have been identified, which includes CAP1 (prostasin), CAP2 and CAP3 (matriptase) on the basis of their ability to activate ENaC (Vuagniaux et al., 2002). The mechanism by which ENaC can be activated by serine proteases is not clearly understood.

To understand whether proteolysis of ENaC subunits or cleavage of regulatory protein is responsible for the activation of ENaC, Hughey and colleagues (Hughey et al., 2003) showed that when tagged subunits were expressed alone in Chinese hamster ovary or Madin-Darby canine kidney type 1 epithelia, the α(95kDa), β(96kDa), and γ(93kDa) subunits produced a singly band on SDS gel by immunoblotting. While, co-expression of αβγ ENaC subunits revealed a second band for each subunit (65 kDa for α, 110kDa for β, 75 kDa for γ). They showed that the smaller size of processed α and γ subunits was consistent with proteolytic cleavage. This was the first direct evidence of ENaC cleavage. This group later subsequently showed importance of furin in ENaC proteolytic processing (Hughey et al., 2004). They demonstrated that the α and γ ENaC subunits may be cleaved during maturation at consensus sites for furin cleavage. Using site-specific mutagenesis of the key P1 arginine in the R-X-X-R (P1) furin sequences in the α and γ subunits, ENaC expression in furin-deficient cells, and by using furin specific inhibitors, the authors proposed that ENaC cleavage was correlated with channel activity. In order to better understand, whether this processing occur endogenously or at plasma membrane, a direct experimental approach has been used by Harris and colleagues to make correlation between endogenous proteolytic cleavage of surface-expressed ENaC and its activation in the same. (Harris et al., 2008) co-injected the subunits in all combinations and measured I_{Na}, the size of ENaC subunits expressed at the cell surface or in intracellular pool. They have demonstrated that furin-mediated cleavage was not essential for participation of α or γ in αβγ heteromers, and basal I_{Na} was reduced by preventing furin-mediated cleavage of the α, but not the γ, subunit. The correlation between furin-mediated cleavage and ENaC activation was not observed. These results are on contrary to previous findings, but it is possible that cleavage at furin site might be a necessary step required for a second cleavage by endogenous or exogenous proteases. It is also important to

87

understand whether this furin-mediated cleavage is a cause or consequence for ENaC activation.

All these experiments have been done in *Xenopus* oocytes expression system. To better understand role of furin consensus site on ENaC for channel activation, it will be important to check this hypothesis in native renal cells like e.g. aldosterone-sensitive distal nephron cell lines. To address this question, we have generated *Scnn1a*^{lox/lox}/Pax8/LC1 mDCT, mCNT and mCCD which are sensitive to aldosterone stimulation as shown in **Fig.24** and exhibited corresponding gene marker for corresponding segment of distal nephron (**Fig.23**).Upon doxycycline-induction these cells leads to deletion of *Scnn1a* in mDCT and mCCD cells (**Fig.24 A,C**).We have stably transfected these *Scnn1a*-deficient mCCD cells with αENaC by using lipofectamine ,which leads to recovery of 15-20 % ENaC activity as compared to maximal activity as shown in **Fig.28**.This established *Scnn1a*-deficient mCCD cells will allow us to investigate role of furin cleavage site for channel activation.

After the generation and characterization of doxycycline-inducible αENaC-deficient mDCT, and mCCD cell lines, next step will be to generate an αENaC wild-type and an αENaC mutated construct at furin cleavage site (R205A/R231A) by DNA-based site-directed mutagenesis. After generation of these plasmids, next step will be to stably transfect αENaC-deficient mCCD cells with αENaC^wt and αENaC^furin mutant (R205A/R231A) plasmid. After generation of these stably transfected cells, we will characterize αENaC^wt and αENaC^furin mutant (R205A/R231A) transfected cells. We will test whether by mutating furin cleavage site on αENaC subunit has any impact on ENaC-mediated transport by performing short-circuit current measurements with/without aldosterone stimulation on above mentioned transfected cells. Finally with this experimental setup, we would like to also address whether this proteolytic activation of ENaC by furin occurs at cell surface or intracellularly by

performing immunoblotting. Overall, this project will be able to reveal relationship between

cleavage of ENaC at the furin site and channel activity on native renal cells.

6. FINAL CONCLUSIONS

The data presented in first part of the thesis showed the role of colonic ENaC and CAP1/*Prss8* in sodium and potassium balance. The deletion of ENaC and/or CAP1/*Prss8* led to diminished amiloride-sensitive sodium transport. I have identified for the first time CAP1/Prss8 as a regulator of ENaC in colon *in vivo*. Abolished ENaC-mediated transport in colon led to increased fecal sodium loss, which is accompanied by mineralocorticoid resistance in ENaC-deficient mice. In patients with PHA-1 mutations, this might become pathophysiologically relevant and aggravate sodium loss especially under salt deprivation. This first part of thesis provided a better understanding of the electrogenic sodium transport in colon and to dissect aldosterone-dependent and –independent mechanisms.

In the second part, preliminary study had been conducted in order to understand the importance of ENaC and CAP1/*Prss8* in pathological conditions like Inflammatory Bowel Diseases (IBD). Both KO models had been exposed to dextran sodium sulfate (DSS) to chemically induce acute colitis and to investigate whether deficiency of ENaC /*Prss8* predisposed mice to inflammatory bowel disease or not. Preliminary data indicated that *Prss8*-deficiency led to worsening of DSS-induces colitis as compared to their respective controls. Further studies will be conducted to confirm the data and also these findings will be helpful to prevent or alter progression of IBD.

In the third part, doxycycline-inducible mDCT, mCNT and mCCD -specific *Scnn1a*-deficient cells had been generated and characterized. ENaC-mediated sodium transport was totally abolished in mDCT and mCCD cells upon doxycycline treatment. *Scnn1a*-deficient mCCD cells have been transfected by $\alpha ENaC^{wt}$ plasmid which led to rescue of 15-20% of ENaC activity (sodium transport). Future experiments have to be conducted here in order to understand role of furin cleavage site on αENaC for channel activation by using this established *Scnn1a*-deficient mCCD cell lines.

7. MATERIALS AND METHODS

In-vivo part

Intestine-specific *Scnn1a*-deficient mice

Intestine-specific αENaC (*Scnn1a*) knockout mice were generated by interbreeding *Villin::Cre* transgenic mice (el Marjou et al., 2004) kindly provided by Louvard, Paris, which were heterozygous mutant for the αENaC (Hummler et al., 1996) knockout allele with mice homozygous for the respective conditional alleles *Scnn1a$^{loxlo\,x}$*(Hummler et al., 2002).

For intestine-specific αENaC KO, we have mated *Scnn1a$^{+/-}$* ; *villin::Cre$^{tg/0}$* mice with mice harbouring two floxed αENaC (*Scnn1a^{loxlox}*). Age-matched wild type-like *Scnn1a$^{lox/+}$*(*Scnn1a^{Lox}*), heterozygous mutant, *Scnn1a$^{lox/-}$* (*Scnn1a^{Het}*), intestine-specific heterozygous mutant, *Scnn1a$^{lox/+}$*;*villin::Cre$^{tg/0}$*, (*Scnn1a^{Hetc}*) and intestine-specific αENaC knockout, *Scnn1a$^{lox/-}$*,villin::Cre$^{tg/0}$, (*Scnn1a^{KO}*) mice were obtained. In **Table.3**, the obtained genotypes together with the abbreviations that I used throughout the text.

Breeding	*Scnn1a$^{+/-}$* ; villin::Cre$^{tg/0}$ × *Scnn1a^{loxlox}*			
Obtained Genotypes	*Scnn1a$^{lox/+}$*	*Scnn1a$^{lox/-}$*	*Scnn1a$^{lox/+}$*; villin::Cre$^{tg/0}$	*Scnn1a$^{lox/}$*; villin::Cre$^{tg/0}$
Common Nomenclature	*Scnn1a^{Lox}*	*Scnn1a^{Het}*	*Scnn1a^{Hetc}*	*Scnn1a^{KO}*

Table 3. Obtained genotypes for Intestine-specific *Scnn1a*-deficient mice

Intestine-specific CAP1/^{Prss8}-deficient mice

Intestine-specific *Cre* transgenic mice (el Marjou et al., 2004) which were heterozygous mutant for the CAP1/*Prss8* (Leyvraz et al., 2005) knockout allele with mice homozygous for the respective conditional alleles CAP1/*Prss8*$^{lox/lox}$ *(Rubera et al., 2002)*.

For intestine-specific CAP1/*Prss8* KO, we have mated *Prss8*$^{\Delta/+}$; *villin::Cre*$^{tg/0}$ mice with mice harboring two floxed CAP1/*Prss8* (*Prss8*^{loxlox}). Age-matched control CAP1/*Prss8*$^{lox/+}$ (*Prss8*^{Lox}), heterozygous mutant, CAP1/*Prss8*$^{lox/\Delta}$ (*Prss8*^{Het}), intestine-specific heterozygous mutant, CAP1/*Prss8*$^{lox/+}$;villin::Cre$^{tg/0}$, (*Prss8*^{Hetc}) and intestine-specific CAP1/*Prss8* knockout, CAP1/*Prss8*$^{lox/\Delta}$,villin::Cre$^{tg/0}$, (*Prss8*^{KO}) mice were obtained. In **Table.4**,the obtained genotypes together with the abbreviations that I used throughout the text.

Breeding	*Prss8*$^{\Delta/+}$;villin::Cre$^{tg/0}$ × *Prss8*^{loxlox}			
Obtained Genotypes	CAP1/*Prss8*$^{lox/+}$	CAP1/*Prss8*$^{lox/\Delta}$	CAP1/*Prss8*$^{lox/+}$; villin::Cre$^{tg/0}$	CAP1/*Prss8*$^{lox/\Delta}$; villin::Cre$^{tg/0}$
Common Nomenclature	*Prss8*^{Lox}	*Prss8*^{Het}	*Prss8*^{Hetc}	*Prss8*^{KO}

Table 4. Obtained genotypes for Intestine-specific *Prss8*-deficient mice

All animal work was conducted according to Swiss federal guidelines. All mice were kept in the animal facility under cantonal/swiss animal care regulations. They were housed in individual ventilated cages at 23±1 °C with a 12-h light/dark cycle. All animals were supplied with food and water ad libitum. If not otherwise indicated, 6-12 weeks old age-matched male and female αENaC and CAP1/*Prss8* control and experimental (knockout) mice (homozygous for Ren-1^c) were fed for at least 3 weeks with regular (RS, 0.17% Na$^+$), high-salt (HS, 3.2% Na$^+$) or low-salt (LS, 0.01% Na$^+$) diet. All diets were obtained from ssniff Spezialdiäten GmbH, Soest, Germany.

Genotyping

Genotyping by PCR was performed using the following primers as indicated in **Table 5**:

Target genes	Primer sequence
CAP1/*Prss8*$^{+/lox/\Delta}$	*Prss8-1* sense, (5′-GCAGTTGTAAGCTGTCATGTG-3′)
	Prss8- 2 sense,(5′ CAGCAGCTGAGGTACCACT 3′)
	Prss8 3 antisense, (5′ CCAGGAAGCATAGGTAGAAG 3′)
αENaC$^{+/-}$	αENaC$^{+/-}$-1 antisense, (5′TTAAGGGTGCACACAGTGACGGC3′)
	αENaC$^{+/-}$-2 antisense, (5′ TTTGTCACGTCCTGCACGACGCG3′)
	αENaC$^{+/-}$-3 sense (5′AACTCCAGAAGGTCAGCTGGCTC3′)
αENaC$^{+/lox/\Delta}$	αENaC$^{lox/+}$-1 sense (5′ CTCAATCAGAAGGACCCTGG3′)
	αENaC$^{lox/+}$-2 sense (5′ GTCACTGTGTGCACCCTTAA3′)
	αENaC$^{lox/+}$-3 antisense (5′ GCAAAAGATCTTATCCACC3′)
Villin::Cre transgene	*Villin::Cre* sense (5′ CCTGGAAAATGCTTCTGTCCG-3′)
	Villin::Cre antisense (5′CAGGGTGTTATAAGCAATCCC3′)
Myogenin-specific primers	sense, (5′ TTACGTCCTCGTGGACAGC-3′)
	antisense, (5′-TGGGCTGGGTGTTAGTCTTA-3′)

Table 5.Primers sequences for PCR-based genotyping

If not otherwise stated, 35 cycles were run, each consisting of 1 min at 94°C, 56°C (58°C for ENaC) and 72^{0}C.

Quantitative RT-PCR analysis on distal colon and kidney samples

Total RNA was prepared from freshly isolated mouse colon superficial cells and whole kidney using the RNeasy extraction kit (Qiagen, Hilden, Germany). The RNA (1µg/sample) was reverse-transcribed at 37^{0}C for 1h using superscript II RNAse H-reverse-transcriptase (Invitrogen, Basel, Switzerland) and oligo-dT(20) primers (Invitrogen). The products were

then diluted ten times before proceeding with the real-time PCR reaction. Real-time PCRs were performed by Taqman® PCR with the Applied Biosystems 7500 (Foster City, CA, USA). The primers and probes mix 20X (Mm00504792 m1 for mCAP1 and 4352341E for β-actin) were purchased with the Universal Taqman mix 2X and used according to the manufacturer instructions (Applied Bio systems, Foster City, CA, USA). Quantification of fluorescence was performed with the $\Delta\Delta C_T$ normalized to β-actin. Each measurement was performed in duplicate. Further following primers have been used as indicated in **Table 6**:

Target genes	Primer sequence
Scnn1a	FOR, 5' GCACCCTTAATCCTTACAGATACACTG 3'
	REV, 5'CAAAAAGCGTCTGTTCCGTG-3'
	Probe 5'-FAM-AGAGGATCTGGAAGAGCTGGACCGCA-BHQ1-3'
Scnn1b	FOR, 5'GGGTGCTGGTGGACAAGC 3'
	REV, 5' ATGTGGTCTTGGAAACAGGAATG-3'
	Probe, 5'-FAM-CAGTCCCTGCACCATGAACGGCT-BHQ1-3'
Scnn1g	FOR, 5'-AACCTTACAGCCAGTGCACAGA-3'
	REV, 5'-TTGGAAGCATGAGTAAAGGCAG-3'
	Probe, 5'-FAM-AGCGATGTGCCCGTCACAAACATCT-BHQ1-3'
Prss8	FOR,5'-CCCATCTGCCTCCCTGC-3'
	REV, 5'-CCATCCCGTGACAGTACAGTGA-3'
	Probe, 5'-FAM CCAATGCCTCCTTTCCCAACGGC-BHQ1-3'
Prss14	FOR, 5' GAAGCTTTGATGTCGCTCCC-3'
	REV, 5'-GGAGGGTGAGAAGGTGCCA-3'
	Probe, 5'-FAM- CCACGCTGTGGTGCGGCTG-BHQ-1-3'

Tmprss4	FOR, 5'AGTAGGCATCGTGAGCTGGG-3'
	REV, 5'-GGACGGCAGCGTTACATCTC-3'
	Probe, 5'-FAM-ATGGATGCGGCGGCCCAA-BHQ1-3'
β-actin	FOR, 5'-AGGTCATCACTATTGGCAACGA-3'
	REV, 5'CACTTCATGATGGAATTGAATGTAGTT-3'
	Probe, 5'TGCCACAGGATTCCATACCCAAGAAGG-3'

Table 6.Primers sequences for Q-PCR

Western blot analysis of distal colon and kidney samples

Animals (n= 3-4 months old) were kept under a RS diet or LS diet for 2 weeks. Colon and kidney were freshly isolated and snap frozen in liquid nitrogen. Proteins were extracted by homogenization using polytron and by sonication with an IKA sonicator in 8M urea buffer, then incubated 30' on ice and centrifuged for 30' at 4 °C at 14000 rpm. The supernatant was taken and centrifuged again for 10' at 4 °C at 14000 rpm. The supernatant was used to detect the protein concentration with a BCA protein kit (PIERCE, Rockford, IL, USA). Samples of protein extracts were separated by SDS-PAGE on 10% acrylamide gels, electrically transferred to polyscreen polyvinylidene difluoride (PVDF) transfer membrane (Perkin Elmer, Boston, USA) and subsequently probed for CAP1/*Prss8*, *Scnn1a* (αENaC), *Scnn1b* (ßENaC), *Scnn1g* (γENaC), NCC, P-NCC and β-actin by using primary rabbit antibodies *Scnn1a*, 1:500 (Sorensen et al., 2013); Scnn1b and Scnn1g, 1:1000 (Wagner et al., 2008); CAP1, 1:1000 (Planes et al., 2005); NCC,1:200 and P-NCC,1:700 (Ronzaud et al., 2013); β-actin, 1:1000 (Sigma) and anti-rabbit IgG secondary antibody (1:10000, Amersham Pharmacia Biotech, UK). The signal was developed with ECL+ system (Amersham, Hyperfilm™ ECL, Burkinghampshire, UK). Quantification of protein level was obtained using NIH image software.

Histological analysis of proximal and distal colon

Colons were fixed in 4% paraformaldehyde overnight and subjected to paraffin embedding and sectioning (4μm sections). These were stained with haematoxylin and eosin and were examined by light microscopy using an Axioplan microscope (Carl Zeiss Microimaging, Inc. Oberkochen/Jena, Germany) and images were acquired with a high sensibility digital color camera (Carl Zeiss Microimaging, Inc.).

Determination of intestine structural and functional parameters

Determination of length-to-body weight: Length of intestine (cm) was individually measured and normalized to its body weight from 3-months-old mice. Results were determined as mean ± SEM.

Feces wet-to-dry weight and electrolyte measurements: feces samples were collected from age-matched 3 months old control (n=6), heterozygote mutant (n=6) and knockout (n=7) mice that were kept under regular salt diet in metabolic cages for 4 consecutive days. Wet-to-dry weight was determined by determining the wet weight feces samples collected within 24 hours, dried at $80^{\circ}C$ for further 24 hours for desiccation and weighed again to calculate the wet-to-dry feces ratio as described (Frateschi et al., 2012). Sodium and potassium fecal electrolytes were determined from samples as described (Meneton et al., 1998). Briefly, the feces were collected over two consecutive days, weighed and resuspended overnight into 0.75N nitric acid at $4^{\circ}C$. After centrifugation an aliquot of supernatant was measured for Na^+ and K^+ content with a flame photometer (Instrumentation Laboratory 943 Electrolyte Analyzer, UK).

Intestinal permeability assay: In vivo intestinal permeability was determined as described previously (List et al., 2009). Briefly, mice were kept under regular salt diet and gavaged with 10 ml/kg of a solution of 22 mg/ml fluorescein isothiocyanate (FITC) - dextran (4 kDa, Sigma, St. Louis, MO, USA) in PBS, pH 7.4. Three hours following gavage, plasma was

96

collected at the end of the experiment, centrifuged at 3000 rpm for 20 min. at $4^{°}$C. Following a 1:1 dilution in PBS, the concentration of fluorescein was determined using a 96-plate reader with an excitation wavelength at 485nm and an emission wavelength at 535 nm using serially diluted samples of the tracer as a standard.

Metabolic cage studies

6-12 weeks old age-matched control and knockout mice were individually placed in metabolic cages (Tecniplast, Buguggiate, Italy) for 5 consecutive days to measure urine and feces output. Food and water intake was daily measured. For the entire experiment, mice had free access to food and water. During experimental days, urine and feces were collected. Sodium intake was measured as sodium (mmol) intake per day in percentage of total food intake. Sodium output was measured as urinary sodium (mmol) and fecal sodium (mmol) excretion per day in percentage of total food intake.

High-Potassium Diet

Experimental mice and control mice were placed in individual metabolic cages and fed a standard diet for 2 consecutive days (0.95% potassium). This was followed by 2 days on 5% potassium in drinking water (the potassium was added as KCl). During the experiment, the animals had free access to food and water. During experimental days, urine was collected. Blood and urine were collected 2 days after the experiment.

Analyses of urinary electrolytes and blood plasma analysis

Twenty four hour urine samples were collected in metabolic cages. Blood samples were collected at the end of the experiment. Urine and plasma electrolytes were analyzed using an Instrumentation Laboratory 943 Electrolyte Analyzer (UK).

Blood collection for aldosterone measurements

Control and knockout mice (8-12 weeks old) were kept in standard cages with free access to food and water and fed with RS, LS or HS diets for 12 consecutive days. At the end of the experiment, blood samples were collected. Plasma aldosterone levels were measured according to standard procedures using a radioimmunoassay (RIA) (Coat-A-Count RIA kit, Siemens Medical Solutions Diagnostics, Ballerup, Denmark) (Christensen et al., 2010). Samples with values > 1200 pg/ml were further diluted using a serum pool with a low aldosterone concentration (<50 pg/ml).At the end, aldosterone concentration unit has been changed from pg/ml to nMol/l.

Amiloride-sensitive rectal transepithelial potential difference measurements

Mice were fed a low salt diet (LS) and high salt diet (HS) during 3 weeks. Amiloride-sensitive transepithelial rectal PD measurements were performed as previously described (Wang et al., 2000, Frateschi et al., 2012). Briefly, rectal potential difference (PD) and amiloride-sensitive rectal PD were measured in the morning (10 am to noon) and in the afternoon (4 pm to 6 pm) on two days of the same week. The rectal PD was monitored continuously by a VCC600 electrometer (Physiologic instruments, San Diego, CA, USA) connected to a chart recorder. After stabilization of rectal PD (approx. 1 min), 0.05 ml saline solution was injected through the first barrel as a control manoeuvre and the PD was recorded for another 30 seconds. A similar volume of saline solution containing 25 μmol/l amiloride was injected through the second barrel of the pipette and the PD was recorded for 1 min. The potential difference was recorded before and after the addition of amiloride as amiloride-sensitive PD.

Dextran sodium sulfate (2 %) – chronic protocol

Chronic colitis was induced in above mentioned *Scnn1a*[KO], *Prss8*[KO] mouse models along with their respective controls (8-12 weeks old) as described (Netzel-Arnett et al., 2012). It was induced by using 2% (m/v) of Dextran sodium sulfate (Mol.wt. 36000-50000, MP Biologicals, LLC, Illkirch Cedex, France) dissolved in drinking water ad libitum for 7 days, followed by recovery with normal drinking water for up to 8 days. During these 15 days period, body weight, diarrhea, and occult blood in stool (Guaiac test, HEMDETECT, DIPROmed GmbH, Weigelsdorf, Austria) were determined daily. This Hemdetect test is based on guaiac method for detecting occult blood in feces qualitatively. Diarrhea scores were : 0,no diarrhea; 1,mild diarrhea; 2,severe diarrhea; 3,mild diarrhea with blood; 4,severe diarrhea with blood. At the end of treatment, animals were anesthetized by using isoflurane gas and sacrificed by cervical dislocation. Colon length and histology analyzed at the end of experiment.

Dextran sodium sulfate (5 %) – acute Protocol

Acute colitis was induced in above mentioned *Scnn1a*[KO], *Prss8*[KO] mouse models alongwith their respective controls (8-12 weeks old) as described previously (Cooper et al., 1993, Hashimoto et al., 2012). Colitis was induced by using 5% (w/v) of Dextran sodium sulfate dissolved in drinking water ad libitum for the experimental days 1-7. DSS solutions were made fresh every day2. During 7 days of treatment, body weight, diarrhea, and occult blood in stool (Guaiac test, HEMDETECT, DIPROmed GmbH, Weigelsdorf, Austria) were determined daily. At the end of treatment, animals were anesthetized by using isoflurane gas and sacrificed by cervical dislocation. Colon length and histology was analysed at the end of experiment.

In-vitro part

Primary cultures of doxycycline-inducible $Scnn1a^{lox/lox}$/Pax8/LC1 mDCT, mCNT and mCCD cells

Experiments were performed on confluent primary cultures of DCT, CNT and CCD microdissected from kidneys of $Scnn1a^{lox/lox}$/Pax8/LC1 mice. Inducible renal tubule-specific *Scnn1a* knockout mice were generated by combined use of Tet-On and Cre-loxP systems in our laboratory by Romain Perrier (Perrier et al., manuscript in preparation). Pax8-rtTA transgenic mice, which express the reverse tetracycline-dependent transactivator (rtTA) in all proximal and distal tubules, and the entire collecting duct system of both embryonic and adult kidneys were bred with TRE-LC1 transgenic mice, which express the Cre recombinase under the control of a rtTA-response element (Traykova-Brauch et al., 2008). Double transgenic Pax8-rtTA/TRE-LC1 mice (Pax8/LC1), which allow doxycycline (a tetracycline analog)-inducible renal tubule-specific Cre-mediated recombination, were bred with mice homozygous for the *Sccn1a* floxed allele (Hummler et al., 1996) to obtain double transgenic $Scnn1a^{fl/fl}$/Pax8/LC1 mutants ($Scnn1a^{Pax8/LC1}$).

Confluent primary cultures of DCT, CNT and CCD microdissected were grown in growth medium, according to the previously described method (Pradervand et al., 2003, Gaeggeler et al., 2005). DCT, CNT and CCD fragments of nephron tubules (0.5 to 1 mm long) from the kidneys of 5- to 8 week-old-mice were microdissected under sterile conditions in defined medium (DMEM: Ham's F12 [1:1 vol/vol], 60 nM sodium selenate, 5 μg/ml transferrin, 2 mM glutamine, 50 nM dexamethasone, 1 nM triiodothyronine, 10 ng/ml epidermal growth factor, 5 μg/ml insulin, 2% decomplemented calf serum FCS, 20 mM HEPES, pH 7.4], supplemented with 0.1% (wt/vol) collagenase. Isolated CCD were pooled (8 to 10 fragments), rinsed in fresh DM medium, seeded on Transwell filters (0.4 μm pore size, 0.33 cm^2 diameter; Corning Costar Corp., Cambridge, MA) and grown in DM at 37°C in 5% CO_2-

95% air atmosphere. The medium was changed every 1 d after the fifth day of culture, and the experiments were carried out 1 week after seeding on confluent cells having developed high transepithelial electrical resistance ($>900 \ \Omega \cdot cm^2$).

Materials- Electrophysiology experiments

DMEM/Ham's F_{12} (1:1 vol/vol) was from Life Technologies Invitrogen (Switzerland). (^{3}H) aldosterone, and (^{3}H) dexamethasone were from Amersham Bioscience (Otelfingen, Switzerland). Hormones and reagents were from Sigma (St. Louis, MO). Aldosterone was 10 mM stock solution in 100% DMSO. Stock solutions are diluted to their final concentrations in DMEM. FCS was from Fisher Scientific (Wohlen, Switzerland). FCS was always selected after growth and electrophysiological screening (responses to aldosterone and vasopressin) of eight to 10 different batches of sera provided by different companies. Only approximately 20% of the sera tested were found to be able to sustain growth and full differentiation. Tissue culture treated Transwell (0.4 μM pore size, 4.5 cm^2 diameter) were from Corning Costar Corp. (Cambridge, MA). Collagen was prepared from rat tails kept in 70% ethanol as previously described (Gaeggeler et al., 2005). Filter cups (Transwell Costar 3412 [4.7 cm^2] or 3119 [44 cm^2]) were coated by adding 0.5 ml (or 3 ml, respectively) of collagen solution, and excess solution was removed until a thin layer of approximately 10 μl/cm^2 was obtained. Collagen then was polymerized for 2 h at room temperature adding 250 μl of NH$_3$ (28%) in empty spaces between wells. After NH$_3$ was removed, filters were preincubated with growth medium (1.5 ml apical and 2.5 ml basolateral) for 24 h, and seeding was performed using fresh medium.

Quantitative RT-PCR analysis on DCT, CNT and CCD

Total RNA was extracted from confluent cells that were seeded on filters by RNeasy extraction kit (Qiagen, Hilden, Germany). The RNA (1μg/sample) was reverse-transcribed

and real-time PCRs were performed by Taqman® PCR with the Applied Biosystems 7500 (Foster City, CA, USA) as mentioned in the beginning of Methods section. Further following primers have been used as indicated in **Table 7**:

Target genes	Assay ID(Applied Biosystems)/primer, probe sequence
Scnn1a	FOR, 5' GCACCCTTAATCCTTACAGATACACTG 3'
	REV, 5'CAAAAAGCGTCTGTTCCGTG-3'
	Probe 5'-FAM-AGAGGATCTGGAAGAGCTGGACCGCA-BHQ1-3'
AQP2	*Mm00437575_m1*
NCC	*Mm00490213_m1*
TRPV5	*Mm01166037_m1*
MR	*Mm01241596_m1*

Table 7.Primers sequences for Q-PCR

Cell protein extraction and Western blot analysis

Cell extracts were prepared in lysis buffer containing 50 mM HEPES, pH 7.4, 150 mM NaCl, 1 mM EGTA, pH 8.0, 10% glycerol, 1% Triton X-100, 1.2 mg/ml NEM, and complete protease inhibitor cocktail (1 tablet/.20 ml; Roche). Before use 1 mM DTT, 100 mM sodium fluoride, and 10 mM disodium pyrophosphate were added to the lysis buffer. After centrifugation for 20 min at 20,000 g and 4°C, supernatants were collected and assayed for total protein as described previously (Faresse et al., 2010). For western blot analysis, same protocol has been used as described in in *vivo* part of thesis.

Culture Media

Growth medium was DMEM supplemented with insulin (0.87 μM), human apotransferrin (5

μg/ml), EGF (10 ng/ml), T3 (1 nM) dexamethasone (50 nM), penicillin (100 μ/ml),

streptomycin (130 μg/ml), and 2% FCS. Filter cup medium was DMEM supplemented with 3

nM dexamethasone.

DNA constructs and stable transfection of induced *Scnn1a*^{lox/lox}/Pax8/LC1 mCCD cells

with αENaC

αENaC constructs were based on rat ENaC. Dexamethasone-inducible plkneo-αENaC-(HA)3

was described previously and has a G418 resistance gene (Hirt et al., 1992, Staub et al.,

1996) by using electroporation and lipofectamine. Cells were maintained in DMEM, 10%

FBS, G418 (Chemie Brunschwig AG, Basel, Switzerland; 0.25 mg/ml). These cells were

transfected with Lipofectamine according the manufacturer's protocol (Invitrogen). While for

electroporating cells protocol was used as described previously (Mordasini et al., 2005, Leroy

et al., 2009). Briefly, 4×10^6 cells, along with 1 ml of culture medium supplemented with

10% serum and 1.25% DMSO and 8 μl of plasmid constructs, then transferred to

electroporation cuvettes (Gene Pulser cuvette 0.4 cm; Bio-Rad, Hercules, CA), electroporated

(300 mV, 960 pF, pulse duration 22 to 24 ns in mCCD$_{cl1}$ cells) using a Bio-Rad Gene Pulser.

Cells were seeded on permeable filters at a density of 500,000 cells per well, allowed to

recover for 24 h in culture medium containing 10% serum, and then were maintained in

serum and hormone-free medium for another 48 h.

Electrophysiological Studies

Confluent cells that were seeded and grown in growth medium on collagen-coated Transwells

for 5 d then were grown (and/or Doxycycline (10 μg/ml, Sigma Aldrich, France)) for another

5 d in filter cup medium and then overnight in DMEM before measuring sodium transport

response to aldosterone (apical and basolateral side of filter). Short-circuit current (I_{sc} in $\mu A/cm^2$) was measured by clamping transepithelial potential difference (P_D in mV) to 0 for 10 s, and transepithelial electrical resistance (Ohm/cm^2) was recorded under sterile condition using a homemade voltage clamp apparatus.

Statistical analysis

Results are presented as mean ± SEM. Throughout the study, and if not otherwise stated, data were analyzed by one-way ANOVA. Unpaired t test was used for the comparison between 2 groups (Fig. 7B). $P < 0.05$ was considered statistically significant.

ANNEX

Contribution for papers:

1. Renal tubular NEDD4-2 deficiency causes NCC-mediated salt-dependent hypertension.

Ronzaud C, Loffing-Cueni D, Hausel P, Debonneville A, **Malsure SR**, Fowler-Jaeger N, Boase NA, Perrier R, Maillard M, Yang B, Stokes JB, Koesters R, Kumar S, Hummler E, Loffing J, Staub O.

J Clin Invest. 2013 Feb 1; 123(2):657-65.

Contributions: I have performed perfusion of kidney and microdissection of several parts of nephron which has been used for RealTime PCR and Western blot analysis in Fig.1 (B-D) ,Fig.3 (D-I) and Fig.6.

2. Mutations of the serine protease CAP1/Prss8 lead to reduced embryonic viability, skin defects, and decreased ENaC activity.

Frateschi S, Keppner A, **Malsure S**, Iwaszkiewicz J, Sergi C, Merillat AM, Fowler-Jaeger N, Randrianarison N, Planès C, Hummler E.

Am J Pathol. 2012 Aug; 181(2):605-15.

Contributions: I have performed functional analysis as amiloride-sensitive rectal potential difference measurements in colon of Frizzy mice and hairless rat model which contribute to Fig.6.

3. **Sodium and potassium balance depends on αENaC expression in connecting tubule.**

Christensen BM, Perrier R, Wang Q, Zuber AM, Maillard M, Mordasini D, **Malsure S**, Ronzaud C, Stehle JC, Rossier BC, Hummler E.

J Am Soc Nephrol. 2010 Nov; 21(11):1942-51.

Contributions: I have performed perfusion of kidney and microdissection of several parts of nephron which has been used for Western blot analysis in Fig.1 and Fig.2.

Research article

Renal tubular NEDD4-2 deficiency causes NCC-mediated salt-dependent hypertension

Caroline Ronzaud,[1] Dominique Loffing-Cueni,[2] Pierrette Hausel,[1] Anne Debonneville,[1] Sumedha Ram Malsure,[1] Nicole Fowler-Jaeger,[1] Natasha A. Boase,[3] Romain Perrier,[1] Marc Maillard,[4] Baoli Yang,[5] John B. Stokes,[6] Robert Koesters,[7] Sharad Kumar,[3] Edith Hummler,[1] Johannes Loffing,[2] and Olivier Staub[1]

[1]Department of Pharmacology and Toxicology, University of Lausanne, Lausanne, Switzerland. [2]Institute of Anatomy, University of Zurich, Zurich, Switzerland. [3]Department of Hematology, Centre for Cancer Biology, Adelaide, Australia. [4]Nephrology Department, Centre Hospitalier Universitaire Vaudois (CHUV), Lausanne, Switzerland. [5]Department of Obstetrics and Gynecology, University of Iowa, Iowa City, Iowa, USA. [6]Department of Internal Medicine, University of Iowa, and VA Medical Center, Iowa City, Iowa, USA. [7]INSERM UMRS 702, UPMC, Tenon Hospital, Paris, France.

The E3 ubiquitin ligase NEDD4-2 (encoded by the *Nedd4L* gene) regulates the amiloride-sensitive epithelial Na$^+$ channel (ENaC/SCNN1) to mediate Na$^+$ homeostasis. Mutations in the human β/γENaC subunits that block NEDD4-2 binding or constitutive ablation of exons 6–8 of *Nedd4L* in mice both result in salt-sensitive hypertension and elevated ENaC activity (Liddle syndrome). To determine the role of renal tubular NEDD4-2 in adult mice, we generated tetracycline-inducible, nephron-specific *Nedd4L* KO mice. Under standard and high-Na$^+$ diets, conditional KO mice displayed decreased plasma aldosterone but normal Na$^+$/K$^+$ balance. Under a high-Na$^+$ diet, KO mice exhibited hypercalciuria and increased blood pressure, which were reversed by thiazide treatment. Protein expression of βENaC, γENaC, the renal outer medullary K$^+$ channel (ROMK), and total and phosphorylated thiazide-sensitive Na$^+$Cl$^-$ cotransporter (NCC) levels were increased in KO kidneys. Unexpectedly, *Scnn1a* mRNA, which encodes the αENaC subunit, was reduced and proteolytic cleavage of αENaC decreased. Taken together, these results demonstrate that loss of NEDD4-2 in adult renal tubules causes a new form of mild, salt-sensitive hypertension without hyperkalemia that is characterized by upregulation of NCC, elevation of β/γENaC, but not αENaC, and a normal Na$^+$/K$^+$ balance maintained by downregulation of ENaC activity and upregulation of ROMK.

Introduction

Hypertension is a major risk factor for stroke, myocardial infarction, and heart and kidney failure. The postmacula densa segments of the nephron, namely the distal convoluted tubule (DCT), the connecting tube (CNT) and the collecting duct (CD), control Na$^+$ and K$^+$ balance and thus extracellular volume and blood pressure. Na$^+$ reabsorption occurs in the DCT by electroneutral cotransport via the thiazide-sensitive Na$^+$Cl$^-$ cotransporter (NCC) and in the late portion of the DCT (DCT2), CNT, and CD by electrogenic Na$^+$ reabsorption through the amiloride-sensitive epithelial Na$^+$ channel (ENaC) (1). ENaC provides the driving force for K$^+$ secretion via the renal outer medullary K$^+$ channel (ROMK) (2).

The significance of these 3 renal segments for controlling Na$^+$ balance and blood pressure is underscored by genetic diseases affecting ENaC and NCC. Gain-of-function mutations within *SCNN1* cause Liddle syndrome, which is characterized by increased ENaC activity, and result in salt retention and hypertension (3). Such mutations in β- and γENaC lead to inactivation of the PY motif that interacts with WW domains of the ubiquitin-protein ligase NEDD4-2 (encoded by the *Nedd4L* gene), which ubiquitylates and degrades the channel (4–8). With increased aldosterone secretion, serum- and glucocorticoid-regulated kinase 1 (SGK1) interferes with ENaC ubiquitylation by NEDD4-2 (9). In addition, ENaC has been shown to

be activated by proteolytic cleavage of the α and γ subunits that reflects ENaC activation and leads to channel with a higher open probability (10–12). Moreover, the α subunit is needed to bring β- and γENaC to the apical membrane, making functional channels (13–15).

The activity of NCC plays a major role in Na$^+$ balance and blood pressure regulation. Thiazide diuretics, which inhibit NCC and lower blood pressure, and genetic mutations that suppress or heighten NCC function cause hypotension or hypertension, respectively (16). NCC is also a downstream molecular target of the with-no-lysine WNK1/WNK4 kinases (17, 18), the kelch-like KLHL3/Cullin 3 (CUL3) ubiquitin-protein ligase complex (19, 20), and the SGK1 kinase (21). Mutations in human proteins lead to overactive NCC and cause pseudohypoaldosteronism type II (PHAII) (19, 20, 22), characterized by hyperkalemia, hypertension, hypercalciuria, and metabolic acidosis that can be treated by thiazides (23). Very recently, we have shown both in vitro and in vivo that Nedd4-2 is involved in NCC regulation (24).

Generation of constitutive *Nedd4L* KO mice, by removing exons 6 to 8 of the *Nedd4L* gene (*Nedd4L-Δ6-8* KO mice), demonstrated the importance of NEDD4-2 in the control of ENaC activity and blood pressure (25). Indeed, these mice displayed impaired Na$^+$ excretion and hypertension, apparently mediated by ENaC overactivity (25). No effect on NCC was observed. To determine the role of renal NEDD4-2 in controlling Na$^+$ balance and blood pressure during adulthood and to dissect the mechanisms behind this regulation, we developed inducible renal tubule–specific *Nedd4L*$^{flox/flox}$/*Pax8-rTA/LC1* KO mice (*Nedd4L*$^{Pax8/LC1}$). Here, we show that loss of *Nedd4L* in adult renal tubules leads to some
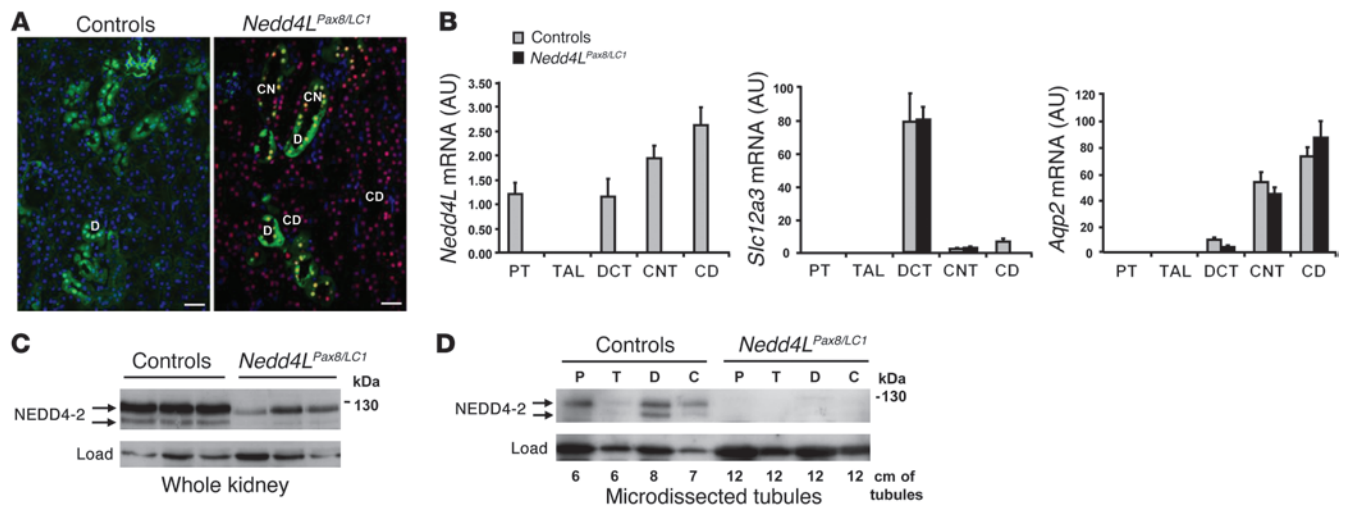
Figure 1

Generation of inducible renal tubule–specific *Nedd4L* KO mice. *Nedd4L$^{flox/flox}$/Pax8-rTA/LC1* KO mice and control littermates (*Nedd4L^{Pax8}* or *Nedd4L^{LC1}*) were obtained and treated with doxycycline as described previously (24) to induce *Nedd4L* ablation in renal tubular cells. (**A**) Immunofluorescence for CRE and calbindin CaBP28 on kidney sections from control (left panel) and induced *Nedd4L$^{Pax8/LC1}$* KO (right panel). CRE recombinase is expressed in all renal tubules in induced KO mice, including CaBP28-positive DCT/CNT cells (CRE: red; CaBP28: green; DAPI: blue). Scale bars: ~50 μm. C, CNT; D, DCT. (**B**) Quantitative real-time PCR analysis for *Nedd4L*, *Slc12a3* (encoding NCC), and aquaporin 2 (*Aqp2*) mRNA on microdissected renal tubules normalized to *Gapdh*: *Nedd4L* mRNA is not detected in *Nedd4L$^{Pax8/LC1}$* KO, and *Slc12a3* mRNA levels are unchanged (n = 4 per group, 8 days of high-Na$^+$ diet). *Slc12a3* was used as DCT marker and *Aqp2* as CNT/CD marker. (**C** and **D**) Analysis of NEDD4-2 protein expression by Western blot in whole kidney lysates (**C**) and microdissected tubules (**D**). The lower NEDD4-2 expression observed in KO whole-kidney lysates is absent in microdissected tubules (n = 3 mice per genotype). Load: unspecific band used as loading control. C, CNT/CD; P, PT; T, TAL.

features of salt-sensitive PHAII with overactive NCC, leading to increased blood pressure and hypercalciuria. Interestingly, compensation by increased ROMK abundance and downregulation of ENaC activity allows the maintenance of a normal Na$^+$/K$^+$ balance.

Results

Generation of inducible renal tubule–specific Nedd4L KO mice. Germline deletion of exons 6 to 8 of the *Nedd4L* gene in mice leads to ENaC overactivation and hypertension (25). To determine the role of renal NEDD4-2 in regulating Na$^+$ balance and blood pressure in adult mice, we generated inducible renal tubule–specific *Nedd4L* KO mice using the same floxed allele used previously (25) and a combination of the inducible Tet-On and Cre-loxP systems, as previously described (24). Double-transgenic *Nedd4L$^{flox/flox}$/Pax8-rTA/LC1* (*Nedd4L$^{Pax8/LC1}$*) conditional KO mice and single-transgenic *Nedd4L$^{flox/flox}$/Pax8-rTA* (*Nedd4L^{Pax8}*) or *Nedd4L$^{flox/flox}$/LC1* (*Nedd4L^{LC1}*) control littermates were treated with doxycycline as described previously (24). Immunofluorescence analysis showed that Cre recombinase is expressed in every tubular cell along the renal tubules of doxycycline-treated KO, but not in the blood vessels (Figure 1A). Consistent with previous report (26), *Nedd4L* mRNA could be detected in the proximal tubule (PT), DCT, CNT, and CD in microdissected tubules of control mice, but not in KO (Figure 1B). Western blot on total kidney lysates revealed a decrease of the 130-kDa NEDD4-2 protein in doxycycline-treated KO mice (Figure 1C). Using several antibodies against NEDD4-2, we observed that the remaining band at 130 kDa was consistently present at low levels in the KO mice (Supplemental Figure 1; supplemental material available online with this article;

doi:10.1172/JCI61110DS1). However, this band was completely lost when Western blots were performed on microdissected tubules (Figure 1D). These data indicate that the lower expression of NEDD4-2 observed on whole kidney extracts of KO mice corresponds to NEDD4-2 expressed in nontubular cells that were not targeted using the Pax8-rTA/LC1 system. Moreover, no additional truncated NEDD4-2 protein could be detected with the existing NEDD4-2 antibodies in the KO. As it was previously reported that the Pax8-rTA/LC1-mediated recombination system was leaky in some hepatocytes (27), we performed PCR to check the presence of recombination in liver and observed a weak band corresponding to the *Nedd4L* null allele in the KO (Supplemental Figure 2A). However, immunoblotting on whole KO liver showed normal NEDD4-2 protein expression in the KO (Supplemental Figure 2B). NEDD4-1 protein, closely related to NEDD4-2 (28), was not upregulated in the *Nedd4L$^{Pax8/LC1}$* KO mice, indicating that there is no compensation by this paralogue (Supplemental Figure 3).

Nedd4L$^{Pax8/LC1}$ KO mice show normal urine and plasma Na$^+$ and K$^+$ levels. Control and KO mice were fed with a standard or high-Na$^+$ diet and placed in metabolic cages to analyze Na$^+$/K$^+$ balance. Plasma aldosterone levels were strongly decreased in the KO mice under both diets, suggesting increased Na$^+$ retention (Figure 2A). However, KO did not show any change in plasma Na$^+$ and K$^+$ concentrations (Table 1). Moreover, after a change from standard to high-Na$^+$ diet, KO mice showed a tendency to retain Na$^+$ compared with controls, but this was not statistically significant (Supplemental Figure 4). These data indicate either that the *Nedd4L$^{Pax8/LC1}$* KO mice are able to maintain a normal Na$^+$/K$^+$ balance or that they have a modest Na$^+$ retention that could not be detected by measuring urinary Na$^+$ excretion. Interestingly, when fed with a high-Na$^+$
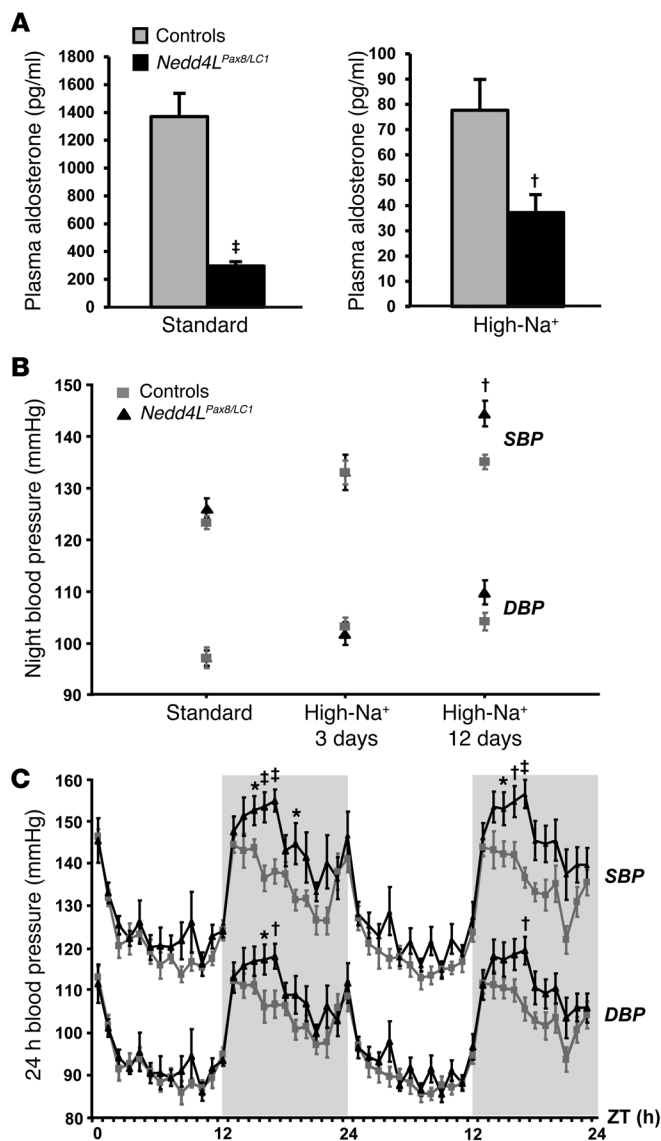
Figure 2

Inducible *Nedd4L*$^{Pax8/LC1}$ KO mice show decreased plasma aldosterone and salt-sensitive blood pressure increase. (**A**) Plasma aldosterone levels were decreased in induced *Nedd4L*$^{Pax8/LC1}$ KO ($n = 7–10$) compared with controls ($n = 6–9$) under both standard and high-Na$^+$ diets. (**B**) Graphs represent SBP and DBP 12-hour night averages measured by telemetry in controls ($n = 8$) and *Nedd4L*$^{Pax8/LC1}$ KO ($n = 6$) under standard diet and after 3 and 12 days of high-Na$^+$ diet. (**C**) SBP and DBP 24-hour profiles (day, white zone; night, gray zone) in controls (gray curve) and *Nedd4L*$^{Pax8/LC1}$ KO (black curve) after 12 days of high-Na$^+$ diet. ZT, Zeitgeber time (ZT0 or ZT24, light on; ZT12, light off). *$P < 0.05$, †$P < 0.01$, ‡$P < 0.005$, KO versus controls.

both β- and γENaC are strongly increased in *Nedd4L*$^{Pax8/LC1}$ KO renal tubules (Figure 3, B and C, and Supplemental Figure 5). However, the cellular localization of both subunits was mainly cytoplasmic. Interestingly, αENaC expression was not increased in KO mice and seen predominantly at intracellular sites (Figure 3A and Supplemental Figure 5). Consistently, *Scnn1a* mRNA levels were lower in microdissected tubules of KO mice that paralleled the decreased plasma aldosterone levels observed in these mice (Figure 3D). On the other hand, *Scnn1b* and *Scnn1g* mRNA expression was unchanged (Figure 3, E and F). It is known that proteolytic cleavage of the α and γ subunits is involved in ENaC activation (10, 12, 29). We therefore analyzed by immunoblotting whether loss of NEDD4-2 would affect ENaC cleavage. *Nedd4L*$^{Pax8/LC1}$ KO mice showed a strong increase in the 90-kDa band for βENaC (Figure 3H). The same was observed for γENaC, but no 70-kDa cleaved form could be detected (Figure 3H). For αENaC, there was no change in the expression of the 90-kDa uncleaved band (quantification of blots from 3 independent experiments: controls: 1.00 ± 0.22, $n = 16$; KO: 0.94 ± 0.18, $n = 17$; $P = 0.818$), but the 30-kDa cleaved band was decreased in the KO (controls: 1.00 ± 0.20, $n = 16$; KO: 0.48 ± 0.13, $n = 17$; $P = 0.044$) (Figure 3G). When aldosterone was administered to the *Nedd4L*$^{Pax8/LC1}$ KO mice using osmotic minipumps, both uncleaved and cleaved forms of αENaC expression increased and achieved comparable levels to those in the controls (Figure 3I). These results indicate that the downregulation of the αENaC proteolytic cleavage is due to decreased aldosterone. Taken together, our data suggest that ENaC activity is downregulated in *Nedd4L*$^{Pax8/LC1}$ KO mice.

Loss of renal tubule NEDD4-2 in adult mice leads to overactive NCC. We have recently showed that NEDD4-2 is involved in the regulation of NCC at the posttranslational level (24). Here, we confirm, by using immunofluorescence, that loss of NEDD4-2 leads to increased NCC protein abundance (Figure 4A) without any change of *Slc12a3* mRNA expression in microdissected renal tubules (Figure 1B). NCC immunostaining was hardly visible in control mice fed a high-Na$^+$ diet, while an immunofluorescent signal was easily detectable in the KO mice. Immunoblotting data indicated that the elevated NCC phosphorylation at T53, T58, and S71, known to be involved in the activation of the cotransporter, followed the increased NCC protein abundance in KO (ref. 30 and Figure 4, B and C). To confirm our observation, we looked at NCC expression in kidneys from P19 *Nedd4L*-Δ15-16 KO mice generated by Boase et al. (31) and observed an increase of expression and phosphorylation of the cotransporter also in these mice (Supplemental Figure 6). Thus, we confirm that loss of NEDD4-2 leads to increased NCC. PHAII patients and mouse models with overactive NCC dis-

diet, KO mice displayed increased water consumption, elevated urine output, and diluted urine (Table 1), as previously observed in constitutive *Nedd4L*-Δ6-8 KO mice (25).

Loss of renal tubule NEDD4-2 in adult mice leads to salt-sensitive blood pressure increase. Systolic and diastolic arterial blood pressures (SBP and DBP) were measured by telemetry for 3 consecutive 24-hour periods upon standard and high-Na$^+$ diets. No significant difference between *Nedd4L*$^{Pax8/LC1}$ KO and control littermates was observed under standard diet (Figure 2B). However, following 12 days of high-Na$^+$ diet, the difference between controls and KO reached 10 mmHg for the SBP during the active night period (Figure 2, B and C). These data indicate that renal tubule NEDD4-2 in adult mice is important for maintaining normal blood pressure under high-salt intake.

Nedd4L inactivation in adult renal tubules leads to increased β- and γENaC protein expression, but reduced αENaC proteolysis. Because NEDD4-2 has been shown to participate in the degradation of ENaC, it was expected that *Nedd4L* inactivation would result in more ENaC expression. Immunofluorescence showed that

Table 1

Urine and plasma electrolytes in controls and inducible $Nedd4L^{Pax8/LC1}$ KO mice under standard and high-Na$^+$ diet (8 days)

	Standard diet		High-Na$^+$ diet	
	Controls	$Nedd4L^{Pax8/LC1}$	Controls	$Nedd4L^{Pax8/LC1}$
Food intake (g/g BW/24 h)	0.13 ± 0.00 (7)	0.15 ± 0.01 (4)	0.18 ± 0.01 (18)	0.17 ± 0.01 (15)
Water intake (ml/g BW/24 h)	0.31 ± 0.04 (7)	0.36 ± 0.03 (4)	0.32 ± 0.01 (21)	0.39 ± 0.02[B] (15)
Urine				
Urine volume (ml/24 h)	0.13 ± 0.01 (7)	0.14 ± 0.02 (4)	0.13 ± 0.01 (21)	0.17 ± 0.01[A] (15)
Osmolality (mmol/g H$_2$O)	ND	ND	2541 ± 204 (10)	1791 ± 72[A] (9)
Na$^+$ excretion (μmol/24 h)	150 ± 15.8 (7)	187 ± 9.84 (4)	1375 ± 204 (10)	1352 ± 154 (14)
Na$^+$/Cr (10^3)	0.03 ± 0.00 (7)	0.05 ± 0.01 (4)	0.59 ± 0.06 (7)	0.55 ± 0.08 (4)
K$^+$ excretion (μmol/24 h)	520 ± 51.8 (7)	609 ± 71.7 (4)	428 ± 29.4 (21)	438 ± 30.2 (14)
K$^+$/Cr (10^3)	0.10 ± 0.01 (7)	0.16 ± 0.02 (4)	0.14 ± 0.01 (7)	0.13 ± 0.02 (4)
Na$^+$/K$^+$	0.27 ± 0.02 (7)	0.32 ± 0.03 (4)	3.07 ± 0.18 (18)	3.25 ± 0.35 (15)
GFR (ml/g BW/24 h)	14.3 ± 2.69 (7)	17.6 ± 3.30 (4)	12.9 ± 3.10 (8)	11.1 ± 0.87 (6)
pH	6.08 ± 0.04 (7)	6.17 ± 0.00 (4)	5.81 ± 0.20 (4)	5.91 ± 0.21 (6)
Plasma				
Na$^+$ (mM)	150 ± 1.26 (7)	147 ± 1.35 (4)	151 ± 1.14 (15)	151 ± 1.43 (11)
K$^+$ (mM)	5.35 ± 0.29 (7)	6.19 ± 1.12 (4)	4.71 ± 0.19 (10)	4.72 ± 0.19 (10)
Blood pH	ND	ND	7.55 ± 0.04 (5)	7.58 ± 0.04 (7)

Values are given as average ± SEM. Number of mice indicated in parentheses. Cr, creatinine. [A]$P < 0.05$, [B]$P < 0.005$, KO versus controls.

play hypercalciuria that can be treated by thiazides, whereas hypocalciuria is observed in *Slc12a3* KO mice (32). NCC activity is thus correlated with renal Ca^{2+} excretion. Based on this observation, we measured the urinary Ca^{2+} and found that the *Nedd4L$^{Pax8/LC1}$* KO excrete more Ca^{2+} under a high-Na$^+$ diet. Interestingly, thiazide treatment markedly reduced the elevated Ca^{2+} excretion in the KO, similar to what occurs in PHAII patients (Figure 4D). In addition, thiazide, but not amiloride, decreased the difference in blood pressure between controls and KO during the active night period (Figure 4E). Taken together, these data suggest that loss of NEDD4-2 in renal tubules in adult mice leads to increased NCC activity.
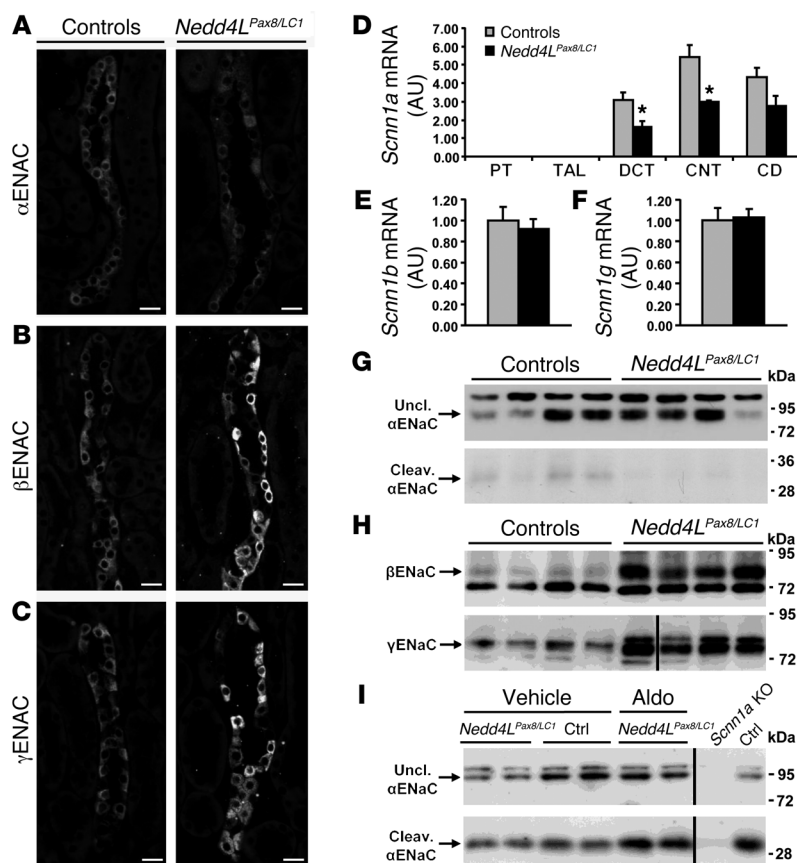
Nedd4L$^{Pax8/LC1}$ KO mice have increased ROMK abundance. Increased NCC activity has been shown to be linked with K$^+$ retention (33, 34). Therefore, the absence of hyperkalemia in *Nedd4L$^{Pax8/LC1}$* KO mice was unexpected, as they do also show decreased ENaC activity and plasma aldosterone that should decrease the electrochemical driving force for K$^+$ excretion via apical K$^+$ channels such as ROMK in the ENaC-expressing cells. We therefore analyzed the abundance and subcellular localization of ROMK in control and KO mice. Interestingly, immunofluorescence showed a strong increase in ROMK protein abundance and apical localization in the DCT and CNT of *Nedd4L$^{Pax8/LC1}$* KO (Figure 5A) and in CD and thick ascending limb (TAL) (Figure 5A). *Kcnj1* mRNA expression levels (Figure 5B) were not different between controls and KO, indicating that loss of NEDD4-2 affects ROMK expression at the posttranslational level.

Nedd4L ablation in renal tubules during embryonic development results in a phenotype similar to that seen when the deletion occurs at adult age. Because the total *Nedd4L-Δ6-8* KO mice showed no change in plasma aldosterone under standard and high-Na$^+$ diets, increase in αENaC expression, and no alteration of NCC abundance (25), we hypothesized that the time of *Nedd4L* deletion may account for the differences with the *Nedd4L$^{Pax8/LC1}$* KO mice. We treated the pregnant mothers of *Nedd4L$^{Pax8/LC1}$* KO mice and control littermates with doxycycline during gestation to induce deletion during

embryonic development, as previously reported (27). We observed that the constitutive *Nedd4L* ablation in renal tubules had effects on NCC and α-, β- and γENaC expression (Figure 6, A–C) similar to those seen when the deletion was induced during adulthood. Moreover, the constitutive *Nedd4L$^{Pax8/LC1}$* KO mice showed decreased plasma aldosterone (Figure 6D) and hypercalciuria (Table 2). These data suggest that the differences in phenotype between the *Nedd4L$^{Pax8/LC1}$* KO mice and the total *Nedd4L-Δ6-8* KO mice are most likely not due to early developmental adaptation, but rather to nonrenal NEDD4-2 or to the differences in genetic background between these mouse models.

Discussion

Mutations in human β- and γENaC leading to inactivation of the PY motif that interacts with NEDD4-2 WW domains cause Liddle syndrome, characterized by increased ENaC activity, salt retention, and hypertension (3). Surprisingly, constitutive deletion of exons 6 to 8 of the *Nedd4L* gene in the mouse results in amiloride-sensitive salt-induced hypertension, but no sign of volume expansion or impaired Na$^+$/K$^+$ balance (25). These observations raise the question on the role of renal NEDD4-2 in controlling ENaC and blood pressure. To address this issue, we generated inducible renal tubule–specific *Nedd4L* KO (*Nedd4L$^{Pax8/LC1}$*) mice. No *Nedd4L* mRNA corresponding to the deleted region as well as no protein product could be detected in microdissected renal tubules of *Nedd4L$^{Pax8/LC1}$* KO mice, suggesting that *Nedd4L* is efficiently deleted in the targeted renal tubular cells. Recently, another constitutive *Nedd4L* KO mouse model was generated by constitutively deleting exons 15 and 16 of the *Nedd4L* gene (*Nedd4L-Δ15-16* KO mice) (31). Such deletion led to a perinatal lethal lung phenotype in contrast to the *Nedd4L-Δ6-8* KO model. Boase et al. provided evidence that production of a partial NEDD4-2 protein product in the lungs of the *Nedd4L-Δ6-8* KO may be the reason for the differences between the 2 models (31). Such truncated NEDD4-2 protein product was not detected in kidneys of our *Nedd4L$^{Pax8/LC1}$* KO mice.
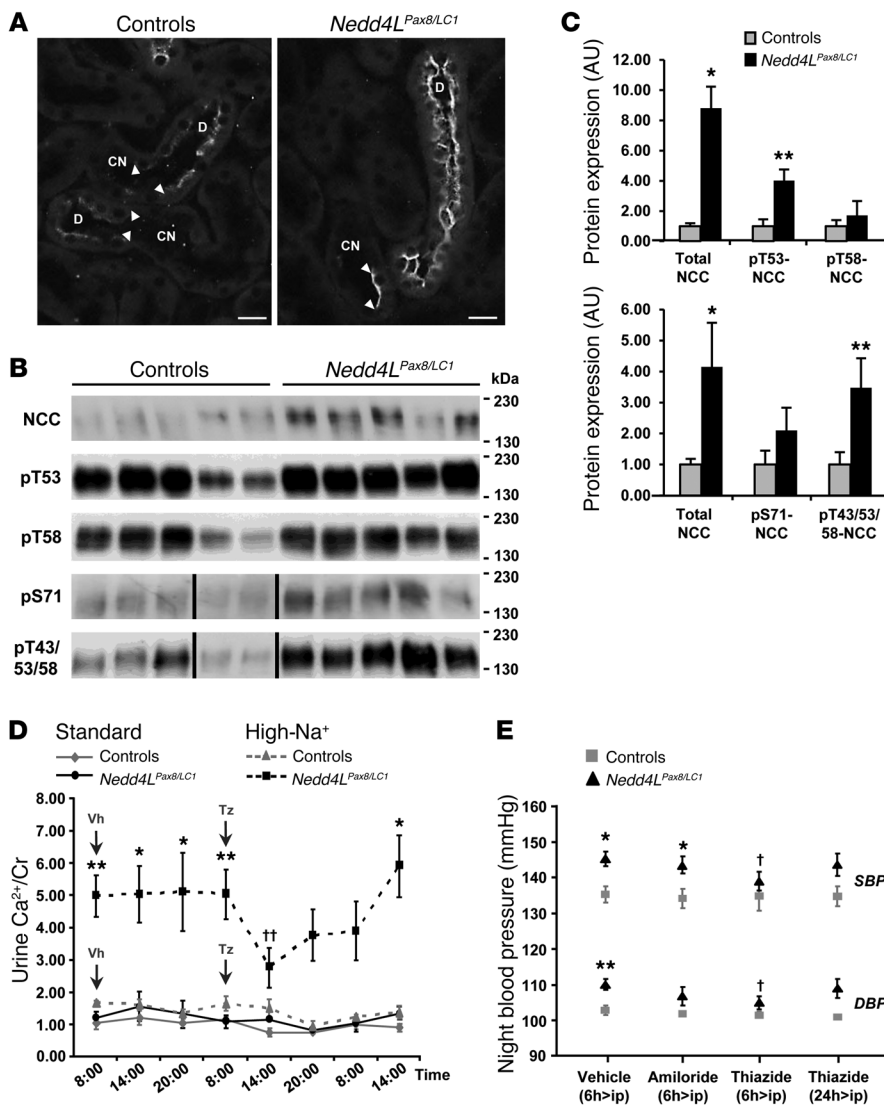
Figure 3

Nedd4L[Pax8/LC1] KO mice have increased β- and γENaC abundance, but not αENaC. (**A**–**C**) Immunostaining for α- (**A**), β- (**B**), and γENaC (**C**) on kidney cryosections of control and KO mice under high-Na⁺ diet. Cytoplasmic β- and γENaC abundance is increased in CD of KO, whereas αENaC is decreased. Scale bars: ~20 μm. (**D**) TaqMan analysis of *Scnn1a* mRNA on microdissected renal tubules shows downregulation in KO (*n* = 4 per group). (**E** and **F**) TaqMan analysis for *Scnn1b* (**E**) and *Scnn1g* (**F**) mRNA on whole kidney (*n* = 6 per genotype). mRNA expression was normalized to *Gapdh* mRNA levels and expressed relative to control values. (**G** and **H**) Representative Western blots for α-, β-, and γENaC: the cleaved 30-kDa αENaC band was decreased in *Nedd4L*[Pax8/LC1] KO mice (**G**), whereas β- and γENaC expression were elevated (**H**). For γENaC, lanes were run on the same gel but were noncontiguous, as indicated by the vertical black line. (**I**) Aldosterone infusion in *Nedd4L*[Pax8/LC1] KO mice results in increased αENaC protein (uncleaved and cleaved form) expression, suggesting that the reduced expression observed in the KO is due to the decreased plasma aldosterone. Kidney extract from *Scnn1a* KO mice was used as negative control. Lanes that were run on the same gel but were noncontiguous are indicated with the vertical black lines. *$P < 0.05$, KO versus controls. Ctrl, control mice.

Surprisingly, despite the increase in NCC, and β- and γENaC protein levels and the decreased circulating aldosterone, suggesting Na⁺ retention and confirming our previous report (24), *Nedd4L*[Pax8/LC1] KO mice showed normal urine and plasma Na⁺ and K⁺ levels. NCC has been reported to be activated by increasing its cell-surface expression and phosphorylation state, mainly via the WNK-SPAK/OSR1 pathway (17, 35). We found that NCC abundance was increased in *Nedd4L*[Pax8/LC1] KO mice and is accompanied by a proportional increase in phosphorylation of T53, T58, and S71 (30, 35). We also observed that *Nedd4L*[Pax8/LC1] KO mice have salt-sensitive blood pressure increase and hypercalciuria that could both be corrected by thiazides, corroborating the assumption that the increased NCC is functional. Of interest, thiazides did not completely correct the high blood pressure, suggesting that mechanisms other than NCC activation are likely to contribute. Interestingly, β- and γENaC abundance were increased in the *Nedd4L*[Pax8/LC1] KO mice, but their cellular localization was mainly intracellular, and γENaC appeared to be in its uncleaved form. Unexpectedly, *Scnn1a* mRNA expression and proteolytic cleavage of the subunit were decreased in the *Nedd4L*[Pax8/LC1] KO mice, suggesting ENaC downregulation. Moreover, amiloride treatment of *Nedd4L*[Pax8/LC1] KO mice did not decrease the high blood pressure, indicating that ENaC is not involved in the hypertensive phenotype. Interestingly, the ENaC downregulation observed in the *Nedd4L*[Pax8/LC1] KO mice paralleled the decreased plasma aldosterone and could be rescued by administrating aldosterone to the KO mice. These data confirm (a) the crucial role of aldosterone in controlling αENaC expression in the kidney (36), and (b)

the importance of αENaC for apical trafficking of the 2 other ENaC subunits (37). To our knowledge, this is the first in vivo study showing differential regulation between the upregulation of β/γENaC (a likely result of the lack of ubiquitylation) and the downregulation of proteolytic activation of αENaC due to decreased aldosterone. Interestingly, no human mutation in the gene encoding αENaC (*Scnn1a*) has been reported to cause Liddle syndrome. Taken together, these results give new insights about how the different mechanisms involved in ENaC regulation can interact and compensate each other if one is impaired. However, our results stand in contrast with the phenotype of Liddle syndrome, where ENaC activity is increased despite the low circulating aldosterone levels (38). It is likely that deletion of *Nedd4L* affects other factors, such as NCC upregulation and consequent compensatory pathways, or other factors involved in controlling ENaC activity or trafficking (39). Because modifications in the abundance of individual renal Na⁺ transporters often result in compensatory changes in the expression levels of other Na⁺ transporters to maintain Na⁺ balance (40), we propose that NEDD4-2 deficiency leads to increased NCC-mediated Na⁺ reabsorption, which is compensated by decreased ENaC activity. Consistent with our hypothesis, KO mice for the kidney-specific *KS-Wnk1* isoform, in which NCC is strongly upregulated, present a very similar phenotype with downregulation of the 3 ENaC subunits (41). Of interest, the phenotype of the *Nedd4L*[Pax8/LC1] KO mice is the mirror image of the *Slc12a3* KO, which show increased plasma aldosterone, decreased calciuria, and upregulation of ENaC activity in CD (28).

research article

Figure 4

NCC is overactivated in *Nedd4L*[Pax8/LC1] KO mice. (**A**) Immunofluorescence for NCC on kidney sections of control and KO mice under high-Na⁺ diet. NCC expression is increased in DCT of KO. Scale bars: ~20 μm. (**B**) Western blot analysis for total NCC and phosphorylated pT53-, pT58-, pS71-, and pT43/53/58-NCC. A representative blot on 5 controls and 5 KO is shown. For pS71-NCC and pT43/53/58-NCC, lanes that were run on the same gel but noncontiguous are indicated with a vertical black line. (**C**) Graphs show quantification of Western blots for phosphorylated NCC and the corresponding total NCC from 2 independent experiments (pT53-NCC and pT58-NCC: $n = 5$ per genotype; pS71-NCC and p43/53/58-NCC: $n = 11$ per genotype). Protein expression was normalized to the amount of β-actin or β-tubulin and expressed relative to control values. (**D**) Urine Ca^{2+} measurement in control and KO mice under high-Na⁺ diet (10 days). *Nedd4L*[Pax8/LC1] KO are hypercalciuric as shown by the 3-fold increased urine Ca^{2+}/creatinine (Cr) ratio, which can be corrected by thiazide ($n = 4$ per group). Vh, vehicle; Tz, thiazide. (**E**) Plot showing telemetric measurement on controls versus KO under high-Na⁺ diet. The increased SBP and DBP observed in KO after 5 weeks of high-Na⁺ diet can be prevented by thiazide, but not by amiloride ($n = 4$ per group). $*P < 0.05$, $**P < 0.01$, KO versus controls. $†P < 0.05$, $††P < 0.01$, thiazide versus vehicle.

Our results in the *Nedd4L*[Pax8/LC1] KO mice are however different to what was observed in the total *Nedd4L-Δ6-8* KO mice, in which NCC was unchanged and all 3 ENaC subunits were increased (25). One substantial difference between the 2 models is the plasma aldosterone that is much higher in the total *Nedd4L-Δ6-8* KO mice and could be attributed to the systemic effects. This difference in plasma aldosterone could explain many of the changes, especially with regard to ENaC. Compensatory mechanisms that could occur during development in the total *Nedd4L-Δ6-8* KO mice may also explain the difference with our inducible system. However, when we induced the renal *Nedd4L* deletion during embryonic development, we obtained a phenotype similar to that in the postnatal deletion of renal *Nedd4L*, with decreased plasma aldosterone, increased NCC, and decreased αENaC proteolysis. Therefore, the differences with the total *Nedd4L-Δ6-8* KO model could rather be due to variations in genetic background or to loss of nontubular NEDD4-2 function. Indeed, Van Huysse et al. recently demonstrated that the salt-induced elevated blood pressure in the *Nedd4L-Δ6-8* KO mouse model depends critically on ENaC overexpression in the brain (42).

Interestingly, despite the strong increase in renal NCC expression levels, the *Nedd4L*[Pax8/LC1] KO mice displayed some but not all the features characteristic of PHAII. The role of NCC overactivation in developing PHAII has been highlighted by human mutations and animal models. Wilson et al. first identified mutations in the *WNK1* and *WNK4* genes in some patients with PHAII (22). The PHAII-*Wnk4*[Q562E] transgenic mouse model developed by Lalioti et al. exhibits increased NCC and PHAII features that could be abolished by crossing these mice with *Slc12a3* KO mice (33). Yang et al. generated mice with 1 normal copy of *Wnk4* and 1 mutant *Wnk4*[D561A] (34). These mice displayed increased phosphorylation and expression of NCC as well as hypertension and hyperkalemia that could be treated with thiazide. However, there is now increasing evidence that overactive NCC alone is not sufficient to lead to PHAII and that the deregulation of other channels or transporters might be required. As mentioned above, *KS-Wnk1* KO mice, with strong increase in NCC and decreased ENaC, showed only few of the PHAII features (41). In addition, a recent study of NCC overexpression in mice showed no effect on blood pressure, plasma, or urine electrolyte and urinary Ca^{2+} (43). One of the PHAII features that is missing
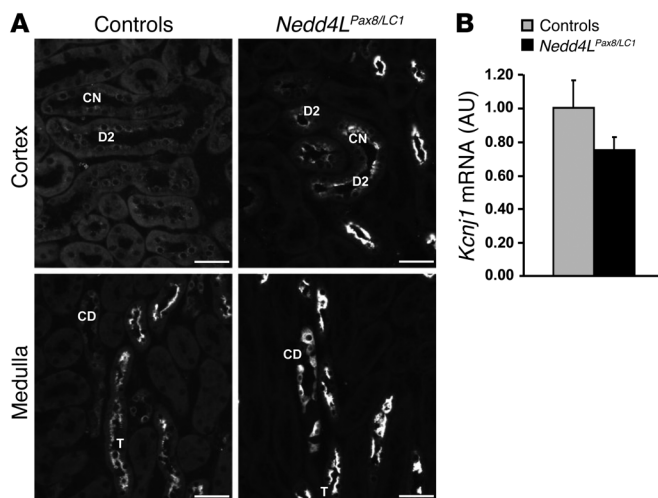
Figure 5

Nedd4L^{Pax8/LC1} KO mice have increased ROMK abundance. (**A**) Immunofluorescence for ROMK on kidney sections from control and KO mice fed with high-Na$^+$ diet (10 days) shows increase in the channel in DCT2 (D2), CNT (CN), CD and TAL (T) in KO. Scale bars: ~40 μm. (**B**) TaqMan analysis showed that *Kcnj1* mRNA levels are not changed between controls and KO mice on whole kidney.

control of NCC surface expression (51). Finally, our data suggest that under high-Na$^+$ intake, NEDD4-2 is not crucial for regulating renal ENaC, as the low plasma aldosterone leading to decreased αENaC proteolytic cleavage is probably sufficient to counterbalance the increased β- and γENaC abundance in the *Nedd4L^{Pax8/LC1}* KO mice and thus to compensate for the increased NCC activity and maintain normal Na$^+$/K$^+$ balance. Why other pathways known to regulate NCC, such WNK-SPAK/OSR1, do not compensate for the increased NCC activity resulting from the lack of NEDD4-2 represents an important question for further investigation.

Methods

Generation and induction of renal tubule–specific Nedd4L KO mice. Inducible renal tubule–specific *Nedd4L^{flox/flox}/Pax8-rTA/LC1* KO (*Nedd4L^{Pax8/LC1}*) mice were generated as described previously (24). Genotyping and recombination of PCR were performed as described in Supplemental Methods. Three- to 4-week-old KO and single transgenic homozygous *Nedd4L^{Pax8}* or *Nedd4L^{LC1}* littermates (controls) were treated with doxycycline (2 mg/ml in 2% sucrose in drinking water) for 11 days. All experiments were started 1 day after the end of the induction, if not stated otherwise. To delete *Nedd4L* during embryonic development, pregnant females were treated with doxycycline as described above during the breeding and gestation periods, and resulting pups were treated until weaning. Induced mice were fed a standard (0.18% Na$^+$; Sniff) or high-Na$^+$ diet (>3.2% Na$^+$) for 8 days and placed in metabolic cages to measure BW, water, and food consumption and to collect urine for 24 hours. For thiazide treatment, mice were injected i.p. at Zeitgeber time ZT2 (2 hours after light on) with vehicle or thiazide (20 mg/kg BW) and urine was collected 6, 12, 24, and 30 hours after injection. Creatinine and Ca^{2+} were measured by the Laboratory of Clinical Chemistry at the Lausanne Hospital (CHUV) using a Modular

in the *Nedd4L^{Pax8/LC1}* KO mice is the hyperkalemia. Several lines of evidence have shown that NCC is important for K$^+$ conservation, as Gitelman patients (44) and *Slc12a3* KO mice exhibit hypokalemia (45) and hyperkalemia is observed in PHAII patients (33, 34). The increased ROMK abundance observed in the *Nedd4L^{Pax8/LC1}* KO mice, which could result from the lack of NEDD4-2–mediated ubiquitylation (46), may lead to higher K$^+$ excretion, as it has been reported for the *KS-Wnk1* KO mice (41). Another possibility could be that the *Nedd4L^{Pax8/LC1}* KO mice have some residual ENaC activity sufficient for excreting enough K$^+$ to maintain a normal kalemia. Whether some ENaC-independent K$^+$ secretion occurs in the *Nedd4L^{Pax8/LC1}* KO mice remains to be addressed.

In conclusion, we provide evidence that inactivation of *Nedd4L* exons 6 to 8 in renal tubules of adult mice does not lead to a Liddle syndrome phenotype associated with elevated ENaC activity, but rather causes a salt-sensitive PHAII-like syndrome with NCC upregulation, increased blood pressure, and hypercalciuria. Based on these results, NEDD4-2 appears to primarily target NCC and might thus be an attractive target to treat hypertension, avoiding the most severe side effect of thiazides, namely hypokalemia. Moreover, there is an interesting clinical association of hypercalciuria with hypertension and an increased risk of nephrolithiasis in hypertension (47–50). Defects in NEDD4-2 could therefore underlie these associations, and its study could lead to important mechanistic insights. The recent discoveries that mutations in *KLHL3* and *CUL3* (part of a ubiquitin-protein ligase complex) lead to PHAII demonstrate the importance of the ubiquitylation process in the control of NCC activation. In addition, Khan et al. very recently demonstrated that NCC ubiquitylation is regulated by phosphorylation of the cotransporter and may contribute to the

Figure 6

Nedd4L ablation in renal tubules during embryonic development results in phenotype similar to that seen when the deletion occurs at adult age. Mice were treated with doxycycline during embryonic development to induce *Nedd4L* ablation early on. (**A**–**C**) Western blot analysis on 5-week-old control and KO mice showed increased NCC (**A**), β-, and γENaC (**C**) expression, and decreased cleaved αENaC under high-Na$^+$ diet (10 days) (**B**). (**D**) Plasma aldosterone levels were decreased in KO (*n* = 7) compared with control mice (*n* = 7) under standard diet. *P < 0.05, KO versus controls.

Table 2

Urine and plasma electrolytes in controls and constitutive *Nedd4L$^{Pax8/LC1}$* KO mice under high-Na$^+$ diet (8 days)

	Controls	*Nedd4L$^{Pax8/LC1}$*
Food intake (g/g BW/24 h)	0.20 ± 0.01 (9)	0.20 ± 0.01 (7)
Water intake (ml/g BW/24 h)	0.61 ± 0.06 (9)	0.67 ± 0.05 (6)
Urine		
Urine volume (ml/g BW/24 h)	0.23 ± 0.03 (9)	0.30 ± 0.02^A (7)
Ca^{2+} excretion (μmol/24 h)	13.5 ± 3.88 (9)	44.3 ± 7.16^B (7)
Ca^{2+}/Cr (10^3)	2.84 ± 0.52 (9)	7.50 ± 0.98^B (9)
Na$^+$ excretion (μmol/24 h)	2192 ± 232 (9)	2249 ± 279 (7)
Na$^+$/Cr (10^3)	0.66 ± 0.04 (9)	0.61 ± 0.06 (7)
K$^+$ excretion (μmol/24 h)	538 ± 40.0 (9)	639 ± 42.0 (7)
K$^+$/Cr (10^3)	0.16 ± 0.01 (9)	0.17 ± 0.01 (7)
Na$^+$/K$^+$	4.02 ± 0.20 (9)	3.49 ± 0.30 (7)
GFR (ml/g BW/24 h)	15.9 ± 1.38 (8)	15.6 ± 1.40 (5)
Plasma		
Na$^+$ (mM)	151 ± 0.47 (9)	152 ± 0.81 (7)
K$^+$ (mM)	4.20 ± 0.16 (9)	4.16 ± 0.20 (7)

Values are given as average ± SEM. Number of mice indicated in parentheses. ^AP < 0.05, ^BP < 0.005, KO versus controls.

Analytics System (Roche Diagnostics). Mice were anesthetized by isoflurane inhalation for blood collection by retroorbital plexus puncture and sacrificed by cervical dislocation for tissue collection.

Inducible renal tubule–specific Scnn1a KO mice. Scnn1a$^{flox/flox}$/Pax8-rTA/LC1 KO mice were generated and induced as described above for the *Nedd4L$^{Pax8/LC1}$* KO mice, but using Scnn1a$^{flox/flox}$ mice (52).

Microdissection of mouse renal tubules. Kidneys were perfused and microdissected as described previously (53). For each tubular segment (PT, TAL, DCT, or CNT/CD), tubules microdissected from 3 mice were pooled together with equal tubular length (controls: 6–8 cm; KO: 12 cm to be sure not to miss any weak signal in comparison with controls).

Real-time quantitative PCR. Total RNA was isolated from kidney using the RNAquous Kit (Ambion) (1 μg) or from renal tubules microdissected as described in (53) using the RNeasy MicroKit (QIAGEN). RNA was reverse-transcribed and used for real-time quantitative PCR as described (24). Information about TaqMan Gene Expression Assays (Applied Biosystems) and primer/probe sequences are given in Supplemental Table 1. Regarding *Nedd4L*, the probe and primers were chosen to be located in the exon 6 to 8 region that was deleted in the KO mice after doxycycline treatment.

Measurement of urine and plasma metabolites and aldosterone. Urinary and plasma Na$^+$ and K$^+$ were measured using a flame photometer (Cole-Palmer Instrument), and urine osmolality with an Advanced 2020 osmometer (Advanced Instruments). Glomerular filtration rate (GFR) was estimated based on creatinine clearance. Plasma aldosterone levels were measured as described (24).

Telemetry. Experiments were performed on 1.5-month-old male controls and induced KO as described (41). Mice were fed a standard diet for 7 days, a low-Na$^+$ diet (<0.01% Na$^+$; Sniff) for 7 days, and then a high-Na$^+$ diet for up to 5 weeks. After a 10-day recovery period, cardiovascular parameters were recorded 9 seconds every minute for 24 hours in a light/dark-cycle (ZT0-ZT12/ZT12-ZT24). For thiazide and amiloride experiments, mice were injected i.p. with either vehicle, thiazide (20 mg/kg BW), or amiloride (5 mg/kg BW) at ZT11 and blood pressure was measured during the active night period between 2 hours (ZT13) and 9 hours (ZT20) after injection.

Aldosterone treatment. The ALZET 1003D osmotic mini-pumps (preloaded with vehicle or aldosterone to get a dose of 150 μg/kg BW/d for 3 days) were implanted s.c. Mice were kept on a low-Na$^+$ diet, from the implantation day until sacrifice, to avoid aldosterone escape.

Immunoblotting. Frozen tissues were homogenized and protein extracted as described (24). Anti–α-, –β-, and –γENaC were used as described (14). Kidneys from inducible renal tubule–specific *Scnn1a* KO mice were used as controls for the ENaC-specific bands. For analysis of protein expression in *Nedd4L* total KO mice, kidneys from P19 *Nedd4L-Δ15-16* total KO mice (31) were used. NEDD4-2 was detected using an anti–NEDD4-2 generated in the laboratory of S. Kumar and diluted 1/1000 (31) or with other antibodies directed against different regions of NEDD4-2 and described in Supplemental Methods. NEDD4-1 was detected as described in Supplemental Methods. NCC was detected with an anti-NCC antibody (Chemicon). For anti-phosphorylated pT53-NCC and pT58-NCC, peptide-synthesis, immunizations of rabbits, and antibody purifications were custom-made by Pineda Antibody Services. Phospho-antibodies were preincubated with the corresponding non–phospho-peptides and diluted 1/5000. Anti-phosphorylated pS71-NCC and anti-pT43/53/58-NCC were provided by D. Alessi (MRC Protein Phosphorylation Unit, University of Dundee, Dundee, United Kingdom) and preincubated with the corresponding non–phospho-peptide (35, 54). Anti–β-actin or anti–β-tubulin antibody (Sigma-Aldrich) was used as loading control. For protein analysis on microdissected renal tubules, Western blots were performed as described (53) using the NEDD4-2 antibody previously described (31).

Immunofluorescence. Kidneys were processed and cryosections incubated with antibodies against CRE, α-, β-, γENaC, NCC, and ROMK1,2 as described (15, 55).

Statistics. All values are presented as mean ± SEM. The data were analyzed using unpaired 2-tailed Student's *t* test, KO versus controls. For thiazide and amiloride injection, a paired *t* test was used, diuretic injected versus vehicle injected. A *P* value of less than 0.05 was considered significant.

Study approval. All experimental procedures were approved by the Swiss Federal Veterinary Office and carried out in accordance with the local animal welfare act.

Address correspondence to: Oliver Staub, Department of Pharmacology and Toxicology, University of Lausanne, Rue du Bugnon 27, 1005 Lausanne, Switzerland. Phone: 41.21.692.5407; Fax: 41.21.692.5355; E-mail: olivier.staub@unil.ch. Or to: Johannes Loffing, Institute of Anatomy, University of Zurich, Winterthurerstrasse 190, 8057 Zurich, Switzerland. Phone: 41.44.635.5320; Fax: 41.44.635.5702; E-mail: johannes.loffing@anatom.uzh.ch.

1. Reilly RF, Ellison DH. Mammalian distal tubule: physiology, pathophysiology, and molecular anatomy. *Physiol Rev*. 2000;80(1):277–313.

2. Giebisch G. Renal potassium transport: mechanisms and regulation. *Am J Physiol*. 1998;274(5 pt 2):F817–F833.

3. Shimkets RA, et al. Liddle's syndrome: heritable human hypertension caused by mutations in the β subunit of the epithelial sodium channel. *Cell*. 1994;79(3):407–414.

4. Snyder PM, Steines JC, Olson DR. Relative contribution of Nedd4 and Nedd4-2 to ENaC regulation in epithelia determined by RNA interference. *J Biol Chem*. 2004;279(6):5042–5046.

5. Staub O, et al. WW domains of Nedd4 bind to the proline-rich PY motifs in the epithelial Na^+ channel deleted in Liddle's syndrome. *EMBO J*. 1996;15(10):2371–2380.

6. Kamynina E, Debonneville C, Bens M, Vandewalle A, Staub O. A novel mouse Nedd4 protein suppresses the activity of the epithelial Na^+ channel. *FASEB J*. 2001;15(1):204–214.

7. Abriel H, et al. Defective regulation of the epithelial Na^+ channel (ENaC) by Nedd4 in Liddle's syndrome. *J Clin Invest*. 1999;103(5):667–673.

8. Harvey KF, Dinudom A, Cook DI, Kumar S. The Nedd4-like protein KIAA0439 is a potential regulator of the epithelial sodium channel. *J Biol Chem*. 2001;276(11):8597–8601.

9. Debonneville C, et al. Phosphorylation of Nedd4-2 by Sgk1 regulates epithelial Na(+) channel cell surface expression. *EMBO J*. 2001;20(24):7052–7059.

10. Hughey RP, et al. Maturation of the epithelial Na+ channel involves proteolytic processing of the α- and γ-subunits. *J Biol Chem*. 2003;278(39):37073–37082.

11. Masilamani S, Kim G-H, Mitchell C, Wade JB, Knepper MA. Aldosterone-mediated regulation of ENaC α, β, and γ subunit proteins in rat kidney. *J Clin Invest*. 1999;104(7):R19–R23.

12. Rossier BC, Stutts MJ. Activation of the epithelial sodium channel (ENaC) by serine proteases. *Annu Rev Physiol*. 2009;71:361–379.

13. Canessa CM, et al. Amiloride-sensitive epithelial Na^+ channel is made of three homologous subunits. *Nature*. 1994;367(6462):463–467.

14. Rubera I, et al. Collecting duct-specific gene inactivation of αENaC in the mouse kidney does not impair sodium and potassium balance. *J Clin Invest*. 2003;112(4):554–565.

15. Ronzaud C, et al. Impairment of sodium balance in mice deficient in renal principal cell mineralocorticoid receptor. *J Am Soc Nephrol*. 2007;18(6):1679–1687.

16. Gamba G. Molecular physiology and pathophysiology of electroneutral cation-chloride cotransporters. *Physiol Rev*. 2005;85(2):423–493.

17. Wilson FH, et al. Molecular pathogenesis of inherited hypertension with hyperkalemia: the Na-Cl cotransporter is inhibited by wild-type but not mutant WNK4. *Proc Natl Acad Sci U S A*. 2003;100(2):680–684.

18. Yang CL, Angell J, Mitchell R, Ellison DH. WNK kinases regulate thiazide-sensitive Na-Cl cotransport. *J Clin Invest*. 2003;111(7):1039–1045.

19. Louis-Dit-Picard H, et al. KLHL3 mutations cause familial hyperkalemic hypertension by impairing ion transport in the distal nephron. *Nat Genet*. 2012;44(4):456–460.

20. Boyden LM, et al. Mutations in kelch-like 3 and cullin 3 cause hypertension and electrolyte abnormalities. *Nature*. 2012;482(7383):98–102.

21. Faresse N, et al. Inducible kidney-specific Sgk1 knockout mice show a salt-losing phenotype. *Am J Physiol Renal Physiol*. 2012;302(8):F977–F985.

22. Wilson FH, et al. Human hypertension caused by mutations in WNK kinases. *Science*. 2001;293(5532):1107–1112.

23. Mayan H, Vered I, Mouallem M, Tzadok-Witkon M, Pauzner R, Farfel Z. Pseudohypoaldosteronism type II: marked sensitivity to thiazides, hypercalciuria, normomagnesemia, and low bone mineral density. *J Clin Endocrinol Metab*. 2002;87(7):3248–3254.

24. Arroyo JP, et al. Nedd4-2 Modulates Renal Na+-Cl-Cotransporter via the Aldosterone-SGK1-Nedd4-2 Pathway. *J Am Soc Nephrol*. 2011;22(9):1707–1719.

25. Shi PP, et al. Salt-sensitive hypertension and cardiac hypertrophy in mice deficient in the ubiquitin ligase Nedd4-2. *Am J Physiol Renal Physiol*. 2008;295(2):F462–F470.

26. Loffing-Cueni D, et al. Dietary sodium intake regulates the ubiquitin-protein ligase nedd4-2 in the renal collecting system. *J Am Soc Nephrol*. 2006;17(5):1264–1274.

27. Traykova-Brauch M, et al. An efficient and versatile system for acute and chronic modulation of renal tubular function in transgenic mice. *Nat Med*. 2008;14(9):979–984.

28. Kamynina E, Tauxe C, Staub O. Differential characteristics of two human Nedd4 proteins with respect to epithelial Na^+ channel regulation. *Am J Physiol*. 2001;281:F469–F477.

29. Ruffieux-Daidie D, Poirot O, Boulkroun S, Verrey F, Kellenberger S, Staub O. Deubiquitylation regulates activation and proteolytic cleavage of ENaC. *J Am Soc Nephrol*. 2008;19(11):2170–2180.

30. Pacheco-Alvarez D, et al. The Na+:Cl- cotransporter is activated and phosphorylated at the amino-terminal domain upon intracellular chloride depletion. *J Biol Chem*. 2006;Na(39):28755–28763.

31. Boase NA, et al. Respiratory distress and perinatal lethality in Nedd4-2-deficient mice. *Nat Commun*. 2011;2:287.

32. Loffing J, et al. Altered renal distal tubule structure and renal Na(+) and Ca(2+) handling in a mouse model for Gitelman's syndrome. *J Am Soc Nephrol*. 2004;15(9):2276–2288.

33. Lalioti MD, et al. Wnk4 controls blood pressure and potassium homeostasis via regulation of mass and activity of the distal convoluted tubule. *Nat Genet*. 2006;38(10):1124–1132.

34. Yang SS, et al. Molecular pathogenesis of pseudohypoaldosteronism type II: generation and analysis of a Wnk4(D561A/+) knockin mouse model. *Cell Metab*. 2007;5(5):331–344.

35. Richardson C, et al. Activation of the thiazide-sensitive Na+-Cl- cotransporter by the WNK-regulated kinases SPAK and OSR1. *J Cell Sci*. 2008;121(pt 5):675–684.

36. Asher C, Wald H, Rossier BC, Garty H. Aldosterone-induced increase in the abundance of Na+ channel subunits. *Am J Physiol*. 1996;271(2 pt 1):C605–C611.

37. Rubera I, et al. Collecting duct-specific gene inactivation of alphaENaC in the mouse kidney does not impair sodium and potassium balance. *J Clin Invest*. 2003;112(4):554–565.

38. Pradervand S, et al. Dysfunction of the epithelial sodium channel expressed in the kidney of a mouse model for Liddle syndrome. *J Am Soc Nephrol*. 2003;14(9):2219–2228.

39. Staub O, Rotin D. Role of ubiquitylation in cellular membrane transport. *Physiol Rev*. 2006;86(2):669–707.

40. Brooks HL, et al. Profiling of renal tubule Na+ transporter abundances in NHE3 and NCC null mice using targeted proteomics. *J Physiol*. 2001;530(pt 3):359–366.

41. Hadchouel J, et al. Decreased ENaC expression compensates the increased NCC activity following inactivation of the kidney-specific isoform of WNK1 and prevents hypertension. *Proc Natl Acad Sci U S A*. 2010;107(42):18109–18114.

42. Van Huysse JW, Amin MS, Yang B, Leenen FH. Salt-induced hypertension in a mouse model of liddle syndrome is mediated by epithelial sodium channels in the brain. *Hypertension*. 2012;60(3):691–696.

43. McCormick JA, Nelson JH, Yang CL, Curry JN, Ellison DH. Overexpression of the sodium chloride cotransporter is not sufficient to cause familial hyperkalemic hypertension. *Hypertension*. 2011;58(5):888–894.

44. Simon DB, et al. Gitelman's variant of Bartter's syndrome, inherited hypokalaemic alkalosis, is caused by mutations in the thiazide-sensitive Na-Cl cotransporter. *Nat Genet*. 1996;12(1):24–30.

45. Morris RG, Hoorn EJ, Knepper MA. Hypokalemia in a mouse model of Gitelman's syndrome. *Am J Physiol Renal Physiol*. 2006;290(6):F1416–F1420.

46. Lin DH, et al. POSH stimulates the ubiquitination and the clathrin-independent endocytosis of ROMK1 channels. *J Biol Chem*. 2009;284(43):29614–29624.

47. Khan SR. Is oxidative stress, a link between nephrolithiasis and obesity, hypertension, diabetes, chronic kidney disease, metabolic syndrome? *Urol Res*. 2012;40(2):95–112.

48. Cupisti A. Update on nephrolithiasis: beyond symptomatic urinary tract obstruction. *J Nephrol*. 2011;18:S25–S29.

49. Reilly RF, Peixoto AJ, Desir GV. The evidence-based use of thiazide diuretics in hypertension and nephrolithiasis. *Clin J Am Soc Nephrol*. 2010;5(10):1893–1903.

50. Obligado SH, Goldfarb DS. The association of nephrolithiasis with hypertension and obesity: a review. *Am J Hypertens*. 2008;21(3):257–264.

51. Hossain Khan MZ, et al. Phosphorylation of Na-Cl cotransporter by OSR1 and SPAK kinases regulates its ubiquitination. *Biochem Biophys Res Commun*. 2012;425(2):456–461.

52. Hummler E, et al. Early death due to defective neonatal lung liquid clearance in alpha-ENaC-deficient mice. *Nat Genet*. 1996;12(3):325–328.

53. Christensen BM, et al. Sodium and potassium balance depends on alphaENaC expression in connecting tubule. *J Am Soc Nephrol*. 2010;21(11):1942–1951.

54. Rafiqi FH, et al. Role of the WNK-activated SPAK kinase in regulating blood pressure. *EMBO Mol Med*. 2010;2(2):63–75.

55. Wagner CA, et al. Mouse model of type II Bartter's syndrome. II. Altered expression of renal sodium- and water-transporting proteins. *Am J Physiol Renal Physiol*. 2008;294:F1373–F1380.

Molecular Pathogenesis of Genetic and Inherited Diseases

Mutations of the Serine Protease *CAP1/Prss8* Lead to Reduced Embryonic Viability, Skin Defects, and Decreased ENaC Activity

Simona Frateschi,* Anna Keppner,*
Sumedha Malsure,* Justyna Iwaszkiewicz,[†]
Chloé Sergi,* Anne-Marie Merillat,*
Nicole Fowler-Jaeger,* Nadia Randrianarison,[‡]
Carole Planès,[‡] and Edith Hummler*

From the Department of Pharmacology and Toxicology* and the Protein Modeling Facility,[†] University of Lausanne, Lausanne, Switzerland; and Equipe d'Accueil EA 2363 Cellular and Functional Responses to Hypoxia,[‡] UFR Health, Medicine and Human Biology - Bobigny, Paris University 13, Paris, France

CAP1/Prss8 is a membrane-bound serine protease involved in the regulation of several different effectors, such as the epithelial sodium channel ENaC, the protease-activated receptor PAR2, the tight junction proteins, and the profilaggrin polypeptide. Recently, the V170D and the G54-P57 deletion mutations within the *CAP1/Prss8* gene, identified in mouse frizzy (*fr*) and rat hairless (*fr^{CR}*) animals, respectively, have been proposed to be responsible for their skin phenotypes. In the present study, we analyzed those mutations, revealing a change in the protein structure, a modification of the glycosylation state, and an overall reduction in the activation of ENaC of the two mutant proteins. *In vivo* analyses demonstrated that both *fr* and *fr^{CR}* mutant animals present analogous reduction of embryonic viability, similar histologic aberrations at the level of the skin, and a significant decrease in the activity of ENaC in the distal colon compared with their control littermates. Hairless rats additionally had dehydration defects in skin and intestine and significant reduction in the body weight. In conclusion, we provided molecular and functional evidence that *CAP1/Prss8* mutations are accountable for the defects in *fr* and *fr^{CR}* animals, and we furthermore demonstrate a decreased function of the CAP1/Prss8 mutant proteins. Therefore, *fr* and *fr^{CR}* animals are suitable models to investigate the consequences of CAP1/Prss8 action on its target proteins in the whole organism. *(Am J Pathol 2012, 181:605–615; http://dx.doi.org/10.1016/j.ajpath.2012.05.007)*

Proteolytic enzymes and their inhibitors count for >2% of the known proteome, and a crucial role of these proteins in tissue homeostasis, diseases, and development has been demonstrated.[1–4]

CAP1/Prss8 (also known as prostasin) is a glycosyl-phosphatidylinositol membrane-anchored serine protease expressed in the epithelium of various organs, such as prostate, kidney, lung, colon, and skin.[5–7] CAP1/Prss8 was the first of several membrane-tethered serine proteases found to activate the amiloride-sensitive epithelial sodium channel ENaC in a kidney epithelial cell line, and for this reason it was named channel-activating protease 1 (CAP1).[8,9] These findings predicted that CAP1/Prss8 has an important role in regulating the epithelial sodium transport *in vivo*,[10] and ENaC currents became a suitable way to monitor CAP1/Prss8 activity.

CAP1/Prss8 has also been demonstrated to play essential functions in the physiopathology of lung and skin. *CAP1/Prss8* inactivation addressed to the alveolar epithelium decreased ENaC-mediated alveolar sodium transport and increased alveolar lining fluid volume in an experimental model of acute volume overload.[6] The lack of *CAP1/Prss8* in the skin caused early postnatal mortality because of severe skin dehydration defects, altered the processing of profilaggrin and generating defective tight junctions.[7] On the other hand, *CAP1/Prss8* overexpression in the skin severely impaired the epidermal barrier function and provoked ichthyosis and inflammation. Those pathologic features were completely negated when superposed on a protease-activated receptor 2 (*PAR2*) knockout background, placing PAR2 as a downstream effector of CAP1/Prss8.[1] PAR2 is a G-protein–coupled receptor also involved in neural tube closure, and it can be activated by local proteases as CAP1/Prss8 for regulating epithelial integrity.[11] Moreover, *CAP1/Prss8*

was found to be down-regulated in hormone refractory prostate cancers, gastric cancer, and breast cancer[12–14] and up-regulated in epithelial ovarian cancer,[15] suggesting an additional role of CAP1/Prss8 in tumor invasion. Thus, CAP1/Prss8 emerged as involved in various different processes that range from organ integrity to disease.

Recently, Spacek and colleagues[16] located the genetic defects in the spontaneous mouse frizzy (*fr*) and rat hairless (*fr*[CR]) models on the *CAP1/Prss8* gene.[16] Mice carrying the *fr* mutation in homozygosity display a nearly normal, wavy coat and distinctly curly vibrissae that are apparent after birth and persist throughout life.[17] The Charles River *fr*[CR] rat is one of the autosomal recessive hypotrichotic models actively studied in pharmacologic and dermatologic research, and it is characterized by almost complete baldness.[18] Spacek and coworkers demonstrated that the *fr* mutation consists of a T to A transversion in the *CAP1/Prss8* gene that results in a valine to aspartate substitution at residue 170. The assignment of *fr* mutation on the *CAP1/Prss8* gene was supported by complementation test that indicated the failure of the knockout allele (Δ) of *CAP1/Prss8*[19] to complement the *fr* defect in compound heterozygotes (*fr/Δ*). In addition, sequence analysis of CAP1/Prss8 coding regions in *fr*[CR] rat identified a 12-bp deletion in the third exon, leading to G54-P57 ablation in the CAP1/Prss8 protein, which indicated that *fr* and *fr*[CR] mutations may indeed be orthologues,[16] as already suggested by previous studies.[20] Therefore, the V170D missense and G54-P57 deletion mutations in the *CAP1/Prss8* gene have been proposed as the molecular bases for the *fr* and *fr*[CR] variants, respectively.

Aiming to investigate whether these genetic data could be supported by molecular and functional evidence, we analyzed the consequences of those mutations and performed *in silico*, *in vitro,* and *in vivo* experiments. V170D and G54-P57 deletion mutations changed CAP1/Prss8 protein structure and reduced ENaC activation in the *Xenopus laevis* oocyte cell system. Inheritance, histologic, and functional studies of *fr/fr* mice, *fr/Δ* mice, and *fr*[CR]/*fr*[CR] rats compared with littermate control groups, unveiled very similar features among these variants, defined by reduced embryonic viability, skin abnormalities, and decreased ENaC activity in the distal colon. Therefore, we could demonstrate, at the molecular and functional level, that the *fr* and *fr*[CR] phenotypes are caused by V170D and G54-P57 deletion mutations in the *CAP1/Prss8* gene. Finally, *fr* and *fr*[CR] animals emerged as suitable models for CAP1/Prss8 reduced function in the whole organism.

Materials and Methods

Homology Modeling, in Silico Alanine Scanning, and Amino Acid Alignment

Mouse CAP1/Prss8 45–290 sequence fragment obtained from the CAP1/Prss8 entry Q9ESD1 at the UniProt knowledgebase[21] was a target sequence for homology modeling of murine CAP1/Prss8 structure. As a template, the crystal structure of human homologous protein available in the protein structures database under the 3DFJ code was used.[22] The alignment between the two sequences was built using the Modeller 9v5 program (*http://salilab.org/modeller/download_installation.html*).[23] An 80% sequence identity between the target and the template sequence in the calculated alignment implies a good reliability of the final model. The standard modeling procedure using spatial restraints derived from the alignment was performed with the Modeler 9v5 program. The 100 models were constructed, and their ANOLEA scores[24] were calculated. The model with the best overall ANOLEA score was chosen for further studies. The quality of the model was checked with the PROCHECK software (*http://www.ebi.ac.uk/thornton-srv/software/PROCHECK*) and PDBsum software (*http://www.ebi.ac.uk/thornton-srv/databases/pdbsum/Generate.html*). Noteworthy, no residues were appearing in the disallowed regions of Ramachandran plot, and 91.1% of residues appeared in the most favored regions of the plot, indicating the good quality of the structure. The FoldX program (*http://foldx.crg.es*)[25] was used to perform a computational alanine scan by mutating selected residues to an alanine and estimating the change in the protein stability. Amino acid alignment was performed by using the clustalw2 program (*http://www.ebi.ac.uk/Tools/msa/clustalw2*; EMBL-EBI Wellcome Trust Genome Campus Hinxton, Cambridgeshire, UK).

Construct Preparation, Xenopus Oocyte Injections, Electrophysiologic Measurements, and HEK-293 Cell Transfections

The T to A transversion that results in a valine to aspartate substitution at residue 170 and the 5′-GGTCAGTG-GCCC-3′ deletion that results in G54-P57 ablation in the transcribed protein were each inserted into the mouse *CAP1/Prss8* coding sequence (GenBank GenInfo Identifier 19111159) and introduced in the pSDeasy expression vector, a modified pSD5 vector,[26] for *in vitro* transcription. SP6 RNA polymerase (Promega, Madison, WI) was used for cRNA synthesis.

Expression studies performed in *X. laevis* oocytes (African Xenopus Facility, Noordhoek, South Africa) in stage V/VI have been previously described.[27] A total of 0.25 ng of each cRNA encoding the three rat ENaC subunits in the presence or absence of 2 ng of wild-type (WT) or mutant CAP1/Prss8 cRNA in a total volume of 50 nL was injected into oocytes. Oocytes were incubated in modified Barth saline solution. Twenty-four hours after cRNA injection, electrophysiologic measurements were performed using the two-electrode voltage clamp technique. The amiloride-sensitive current was measured in the presence of 120 mmol/L Na$^+$ in frog Ringer with and without 5 μmol/L amiloride and without 20 mg/mL of trypsin at a holding potential of -80 mV.

WT and mutant mouse *CAP1/Prss8* coding sequences were inserted in the pRK5 expression vector for HEK-293 cells transfection. HEK-293 were cultured in Dulbecco's modified Eagle's medium (DMEM) supplemented with 10% fetal calf serum and 100 μg/mL gentamicin and

transfected at 50% to 60% confluence in 100-mm dishes using the calcium-phosphate method. After transfection, cells were grown for 48 hours in DMEM supplemented with 10% fetal calf serum before harvesting. The total amount of transfected DNA was 12 μg per 100-mm dish.

Western Blot and Pulse-Chase Experiments

Xenopus oocytes were homogenized in 1% Triton X-100, 20 mmol/L Tris-HCl, pH 7.6, and 100 mmol/L NaCl. Lysates were centrifuged at 13,000 × g for 10 minutes at 4°C. HEK-293 cells were lysed using 1 mL of lysis buffer per dish of 1% Triton buffer (20 mmol/L Tris-HCl, pH 7.4, 150 mmol/L NaCl, 1% Triton X-100, 100 mmol/L each leupeptin, pepstatin, and aprotinin, 10 mmol/L phenyl-methylsulfonyl fluoride). HEK-293 cells lysates were incubated 1 hour at 4°C on a rotating wheel. The solubilized material was centrifuged at 10,000 × g for 30 minutes at 4°C, and the supernatants were collected. Animal tissues were lysed in 1 mL of radioimmunoprecipitation assay buffer (50 mmol/L Tris-HCl, pH 7.2, 150 mmol/L NaCl, 1% NP-40, 0.1% SDS, 0.5% sodium deoxycholate, 100 mmol/L each leupeptin, pepstatin, and aprotinin, 10 mmol/L phenylmethylsulfonyl fluoride). Lysates were centrifuged at 13,000 × g for 15 minutes at 4°C, and the supernatants were collected. For SDS-PAGE, samples were loaded and separated on a 10% polyacrylamide gel. Western blot analysis was performed using rabbit anti-mouse antibodies to CAP1/Prss8.[28] Signals were revealed using anti-rabbit IgG from goat (1:10,000; GE Healthcare, Glattbrugg, Switzerland) as secondary antibody and the SuperSignal West Dura detection system (Pierce, Rockford, IL).

To study CAP1/Prss8 protein expression, cRNA-injected oocytes were incubated in modified Barth's solution (MBS) containing 0.7 to 1 mCi/mL [35S]methionine (NEG772007MC; Perkin Elmer, Schwerzenbach, Switzerland) for 6 hours and subjected to 4- and 16-hour chase periods in MBS containing 10 mmol/L unlabeled methionine. After the pulse-chase periods, protein extracts were prepared and subjected to nondenaturing immune-precipitations.[29] After overnight incubation at 4°C with CAP1/Prss8 antibody, the immune complexes were recovered on protein A Sepharose beads (GE Healthcare, Waukesha, WI) and washed several times with MBS containing unlabeled methionine. Immunoprecipitates were resolved by SDS-PAGE (10% polyacrylamide) gels.

Isolation of Rat AECs

The procedure of rat alveolar epithelial cell (AEC) isolation accorded with legislation currently in force in France and Switzerland and animal welfare guidelines (Ministère Français de la Pêche et de l'Agriculture, agreement 5669). The AECs were isolated from adult WT, heterozygous, and homozygous mutant rats by elastase digestion of lung tissue followed by sequential filtration and differential adherence on bacteriologic dishes as previously described.[28] Cell purity was >80%, and cell viability >95%.

Preparation of AEC Protein Extracts and Western Blotting Procedure

Freshly isolated rat AECs were resuspended in 30 μL of ice-cold lysis buffer containing 150 mmol/L NaCl, 50 mmol/L Tris-HCl, pH 7.6, 1% Triton X-100, 0.1% SDS, and protease inhibitors and kept on ice for 1 hour. Cell lysates were then centrifuged at 15,000 × g for 15 minutes at 4°C, and samples of the supernatants were immediately frozen before use. For Western blotting, samples of protein extracts (40 μg total protein) in one volume of sample buffer (containing 13.8% sucrose, 9.6% SDS, 4.2% β-mercaptoethanol, and 0.0126% bromophenol blue in water) were resolved through 10% acrylamide gels, electroblotted, electrically transferred to polyvinylidene difluoride membranes, and subsequently probed for CAP1 protein detection. The goat anti-rabbit IgG secondary antibody (Santa Cruz Biotechnology, Santa Cruz, CA) was used at dilution 1:3000, and the signal was developed with the Western Blotting Luminol Reagent (Santa Cruz Biotechnology).

Animal Genotyping and Stool Assay

The genotype of fr mouse and fr^{CR} rat animal models (kindly provided by Dr. Thomas R. King; Biomolecular Sciences, Central Connecticut State University, New Britain, CT) was assessed as formerly described.[16] We previously reported the generation and genotyping of the engineered null allele (Δ) of CAP1/Prss8.[19] Experimental procedures and animal maintenance followed federal guidelines and were approved by local authorities. All animals were housed in a temperature- and humidity-controlled room with an automatic 12-hour light/dark cycle and had free access to food and tap water.

Fecal hydration was assessed as follows: freshly evacuated stools were collected in the morning and weighed before and after at least 2 hours of dehydration performed by using the SpeedVac. Values are expressed as means ± SEM of the difference in weight.

RNA Extraction and Quantitative RT-PCR

Cells and organs were homogenized using tissue lyser (Qiagen, Valencia, CA), and RNA was extracted with the Qiagen RNeasy Mini kit (Basel, Switzerland) following the manufacturer's instructions. A total of 1 μg of RNA was reverse-transcribed using M-MLV Reverse Transcriptase RNase H Minus Point Mutant (Promega AG, Dübendorf, Switzerland). Real-time PCR was performed by TaqMan PCR using Applied Biosystems 7500 (Carlsbad, CA). Each measurement was taken in duplicate. Quantification of fluorescence was normalized to β-actin. Primer and probe sequences have been previously described.[1]

Immunofluorescence and Histologic Analysis

Cells and organs were embedded into paraffin. Slides were incubated in xylene for at least 4 hours and rinsed with decreasing concentrations of ethanol. Antigen retrieval was performed for 10 minutes in TEG buffer. Slides

were washed in 50 mmol/L NH_4Cl in PBS for 30 minutes and blocked by 1% bovine serum albumin, 0.2% gelatin, and 0.05% saponin in PBS at room temperature for 10 minutes three times. Primary antibody was diluted in 0.1% BSA, 0.3% Triton X-100 in PBS, overnight at 4°C. Affinity-purified CAP1/Prss8 rabbit anti-mouse antiserum[28] was diluted 1:200. Slides were rinsed three times for 10 minutes in PBS containing 0.1% bovine serum albumin, 0.2% gelatin, and 0.05% saponin at room temperature, and the secondary antibody (Alexa Fluor 488 diluted 1:5000; Invitrogen, Grand Island, NY) was diluted in 0.1% bovine serum albumin and 0.3% Triton X-100 in PBS. Staining was visualized using an LSM confocal microscope (LSM 510 Meta, Carl Zeiss MicroImaging Inc., Jena, Germany).

For H&E staining, the paraffin was removed and the slides rehydrated 2 times in xylol for 5 minutes, 2 times in 100% ethanol for 1 minute, in 95% ethanol for 1 minute, and finally with tap water. Slides were incubated in staining glychemalun solution (0.013 mol/L Hematein, Gurr #34036; 0.3133 mol/L potassium alum, Merck #1047; 30% glycerol; 1% acetic acid, Merck #1.00063) for 4 minutes, tap water, 1% acid alcohol for 3 seconds, tap water, water for 15 seconds plus a few drops of NH_3, tap water, 0.2% erythrosine solution (0.0023 mol/L erythrosin, Merck #15936; 0.1% formaldehyde, Merck #4003) for 30 seconds, and finally tap water. Slides were then dehydrated by following steps from 70% ethanol to xylol and mounted (Eukitt, Hatfield, PA). Pictures were taken using an Axion HRC (Carl Zeiss MicroImaging Inc.).

Measurement of TEWL and Rectal Transepithelial PD

The rate of transepithelial water loss (TEWL) from the ventral aspect of the skin of preshaved, anesthetized animals was measured using a Tewameter TM210 (Courage and Khazaka, Koln, Germany). The mean ± SEM results are given.

Rectal potential difference (PD) and amiloride-sensitive rectal PD were measured in the morning (10 AM to noon) and in the afternoon (4 PM to 6 PM) of two different days of the same week. Animals were anesthetized with an i.p. injection of 75 mg/g body weight of Ketalar (Park-Davis, Baar, Switzerland) and 2.3 mg/g body weight of Rompun (Bayer, Leverkusen, Germany) and placed on a heated table. A winged needle filled with isotonic saline was placed in the subcutaneous tissue of the back. A double-barreled pipette was prepared from borosilicate glass capillaries (1.0 mm OD/0.5 mm ID; Hilgerberg, Malsfeld, Germany) and pulled to an approximate 0.2-mm tip diameter. The first barrel was filled with isotonic saline buffered with 10 mmol/L Na^+-HEPES (pH 7.2), and the second barrel was filled with the same solution containing 25 mmol/L amiloride. The tip of the double-barreled pipette was placed in the rectum approximately 3 to 5 mm from the skin margin. The electrical PD was measured between the first barrel and the subcutaneous needle, both connected to Ag/AgCl electrodes by means of plastic tubes filled with 3 mmol/L KCl in 2% agar. The rectal PD was monitored continuously by

a VCC600 electrometer (Physiological Instruments, San Diego, CA) connected to a chart recorder. After stabilization of the rectal PD for approximately 1 minute, 0.05 mL of saline solution was injected through the first barrel as a control maneuver, and the PD was recorded for another 30-second period. A similar volume of saline solution containing 25 mmol/L amiloride was injected through the second barrel of the pipette, and the PD was recorded for another 1 minute. The amiloride-sensitive PD was calculated as the difference between the PD recorded before and after the addition of amiloride.

Results

Reduced ENaC Activation of V170D and G54-P57 CAP1/Prss8 Deletion Mutant Proteins

Taking advantage of the *in silico* protein modeling technique, we built the homology model of the mouse CAP1/Prss8 (Figure 1A), using as a template the crystal structure–based homology model of human CAP1/Prss8.[30] V170 belongs to one of the β strands in the inside of the protein and is located in a hydrophobic environment. V170 makes hydrophobic contacts with the methyl groups of V256 and L191. The alanine scanning for V170 resulted in 2.4 Kcal loss of energy upon mutation to Ala. G54-P57 residues (Gly-Gln-Trp-Pro) in CAP1/Prss8 are found on the external surface of the molecule and therefore are solvent exposed. This fragment, which is deleted in the fr^{CR}/fr^{CR} mutant rats, contains the structurally important Trp56, leading to 4.5-Kcal loss in stability when mutated to Ala. Multiple sequence alignments illustrated that the mutated residues are conserved among different species (Figure 1B).

To investigate the consequences of the V170D and G54-P57 deletion mutations on *CAP1/Prss8* expression and function, we introduced V170D and G54-P57 deletion mutations in the mouse *CAP1/Prss8*, inserted the cDNA sequences in the pSDeasy expression vector for *in vitro* transcription,[26] and co-injected CAP1/Prss8 and ENaC cRNA in the *Xenopus* oocytes. CAP1/Prss8 cRNA stability was estimated by real-time PCR, and no remarkable difference in the level of each V170D and G54-P57 deletion mutant versus WT *CAP1/Prss8* was observed (data not shown). CAP1/Prss8 immunostaining was detected at the plasma membrane in oocytes that were injected with WT CAP1/Prss8, and equal results were obtained with V170D and G54-P57 deletion CAP1/Prss8 mutants (Figure 2A). Western blot analysis against CAP1/Prss8 evidenced the presence of two bands, of 37 and 40 kDa, that might correspond to two different glycosylation states of the protein and showed that the two mutant proteins can be translated as well as the WT (Figure 2B). Glycosylation of CAP1/Prss8 was assessed by treatment of oocyte extracts with the deglycosylating enzyme PNGase F that revealed the presence of a nonglycosylated (n) native form upon deglycosylation treatment. Thus, the two bands of 37 and 40 kDa most likely correspond to the core-glycosylated form (c), which is typical of newly synthesized proteins, and the fully glycosylated
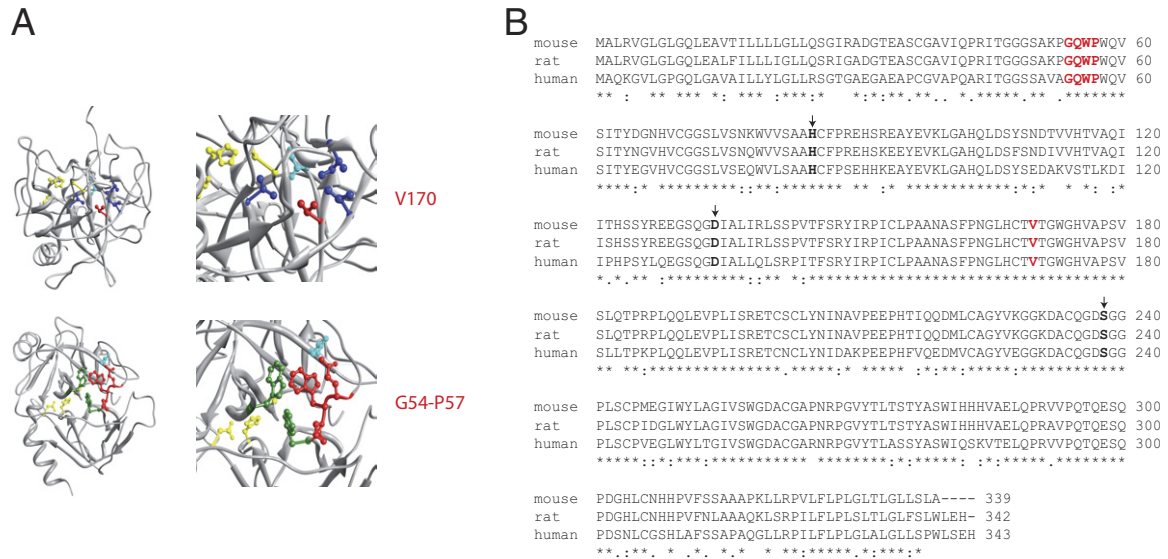
A

B

```
mouse  MALRVGLGLGQLEAVTILLLLGLLQSGIRADGTEASCGAVIQPRITGGGSAKPGQWPWQV 60
rat    MALRVGLGLGQLEALFILLLIGLLQSRIGADGTEASCGAVIQPRITGGGSAKPGQWPWQV 60
human  MAQKGVLGPGQLGAVAILLYLGLLRSGTGAEGAEAPCGVAPQARITGGSSAVAGQWPWQV 60
       **  :  ** *** *: *** :***:.*   *.*:**.**.. *.*****.** .*******

mouse  SITYDGNHVCGGSLVSNKWVVSAAHCFPREHSREAYEVKLGAHQLDSYSNDTVVHTVAQI 120
rat    SITYNGVHVCGGSLVSNQWVVSAAHCFPREHSKEEYEVKLGAHQLDSFSNDIVVHTVAQI 120
human  SITYEGVHVCGGSLVSEQWVLSAAHCFPSEHHKEAYEVKLGAHQLDSYSEDAKVSTLKDI 120
       ****:* ********:.::**:******* **  :* *********:**.*:*  * *: :*

mouse  ITHSSYREEGSQGDIALIRLSSPVTFSRYIRPICLPAANASFPNGLHCTVTGWGHVAPSV 180
rat    ISHSSYREEGSQGDIALIRLSSPVTFSRYIRPICLPAANASFPNGLHCTVTGWGHVAPSV 180
human  IPHPSYLQEGSQGDIALLQLSRPITFSRYIRPICLPAANASFPNGLHCTVTGWGHVAPSV 180
       *.*.** :********:.:** *:************************************

mouse  SLQTPRPLQQLEVPLISRETCSCLYNINAVPEEPHTIQQDMLCAGYVKGGKDACQGDSGG 240
rat    SLQTPRPLQQLEVPLISRETCSCLYNINAVPEEPHTIQQDMLCAGYVKGGKDACQGDSGG 240
human  SLLTPKPLQQLEVPLISRETCNCLYNIDAKPEEPHFVQEDMVCAGYVEGGKDACQGDSGG 240
       ** **:***********:****.*****:*  *****.:*:**:*****:***********

mouse  PLSCPMEGIWYLAGIVSWGDACGAPNRPGVYTLTSTYASWIHHHVAELQPRVVPQTQESQ 300
rat    PLSCPIDGLWYLAGIVSWGDACGAPNRPGVYTLTSTYASWIHHHVAELQPRAVPQTQESQ 300
human  PLSCPVEGLWYLTGIVSWGDACGARNRPGVYTLASSYASWIQSKVTELQPRVVPQTQESQ 300
       *****::*:.***.*********** ********:*:*****: :*:*****.********

mouse  PDGHLCNHHPVFSSAAAPKLLRPVLFLPLGLTLGLLSLA---- 339
rat    PDGHLCNHHPVFNLAAAQKLSRPILFLPLSLTLGLFSLWLEH- 342
human  PDSNLCGSHLAFSSAPAQGLLRPILFLPLGLALGLLSPWLSEH 343
       **.:**. * .*. *.* * **:*****.*:****.
```

Figure 1. A: Homology model of the mouse CAP1/Prss8 tertiary protein structure constructed on the crystal structure–based homology model of the human CAP1/Prss8. Val170 residue, mutated into Asp in the *fr* mouse variant (**upper panels**, entire and zoomed view), and the Gly54-Gln-Trp-Pro57 fragment, deleted in the *fr*[CR] rat variant (**lower panels**, entire and zoomed view), are highlighted in red. The residues of the serine protease active site, Asp134, His85, and Ser238, are represented in yellow. The hydrophobic environment of Val170 consists of Ile45, Leu191, and Val256 shown in dark blue and Asp237 in cyan. Gly54-Pro57 interacts with adjacent residues: Trp triad formed by Trp 56 (red) and Trp58 and Trp250 (in dark green), Gln190 (in cyan) side chain forming hydrogen bond with Trp56, and hydrogen bond formed by Gln55 and Lys52 backbone. **B:** Amino acid alignment of the full-length protein of mouse (GenInfo Identifier: 19111160), rat (GenInfo Identifier: 20301968), and human (GenInfo Identifier: 4506153) CAP1/Prss8 performed using the ClustalW2 multiple sequence alignment program (*http://www.ebi.ac.uk/Tools/msa/clustalw2*). Mouse and rat share 92% of CAP1/Prss8 sequence identity, mouse and human 77%, and rat and human 75%. The amino acids of the catalytic triad (His, Asp, Ser) are indicated by **arrows** and bold text. The four residues deleted in the *fr*[CR] rat (Gly, Gln, Trp, Pro) and the Val170 substituted with Asp in the *fr* mouse variants are indicated in red and result conserved among these species. **Asterisks** indicate identical amino acid residues, and double dots and dots indicate amino acids with similar and less similar side chain proprieties, respectively.

form (f) characteristic of mature proteins, respectively (Figure 2C). Analogous results were obtained in transfected HEK-293 cells (Figure 2D).

To gain further insight not only into the production but also into the degradation of WT and mutant proteins, we performed pulse-chase experiments by pulsing radioactively the oocytes during 6 hours (P) and chasing them during 4 (C1) and 16 (C2) hours in unlabeled media. WT CAP1/Prss8 protein production was evident after 6 hours of pulse, and protein degradation was observed already after the first chase period. Similar results were obtained for the two mutant proteins. However, CAP1/Prss8 V170D and G54-P57 deletion mutants showed different glycosylation states compared with the WT CAP1/Prss8, evidencing an increased fully glycosylated state of the G54-P57 deletion mutant versus an increased core-glycosylated state of the V170D mutant (Figure 2E).

Co-expression of WT CAP1/Prss8 with ENaC leads to a significant increase in the amiloride-sensitive sodium current in the *Xenopus* oocyte cell system[31]; hence, ENaC current is considered an appropriate parameter to monitor CAP1/Prss8 activity. Trypsin can activate near-silent ENaC channels by significantly increasing its open probability, indicating maximal ENaC activity of the cells.[32] Co-injection of WT CAP1/Prss8 and ENaC revealed a 3.7-fold significant increase in the amiloride-sensitive sodium current relative to trypsin compared with oocytes that were injected with ENaC alone. In contrast, when either CAP1/Prss8 V170D or G54-P57 deletion mutant was co-expressed with ENaC, the ability of CAP1/Prss8 to increase ENaC-mediated currents was significantly re-

duced, leading to a 2.8- and 2.1-fold increase relative to trypsin, respectively (Figure 2F).

Reduced Viability and Similar Hair Phenotype in fr *Mouse and* fr[CR] *Rat Models*

To study the consequences of CAP1/Prss8 V170D and G54-P57 deletion mutations and to investigate whether they might be responsible for the phenotypes observed in the *fr* mouse and *fr*[CR] rat models, we performed inheritance, histopathologic, molecular, and functional analyses of *fr/fr*, *fr/Δ*, and *fr*[CR]/*fr*[CR] versus control littermates.

Each *fr/fr* and *fr/Δ* mouse variant presented reduced prenatal viability, deriving from crosses of *fr/+* x *fr/Δ*, yielding only approximately 16% *fr/fr* and 13% *fr/Δ* mutant offspring, respectively, rather than the expected 25%. *fr*[CR]/+ x *fr*[CR]/+ rat crosses generated 10% *fr*[CR]/*fr*[CR] mutants instead of the expected 25%. A total of 83% of the *fr*[CR]/*fr*[CR] rats resulted in males (Tables 1 and 2).

The *fr/fr*, *fr/Δ*, and *fr*[CR]/*fr*[CR] animals were distinguishable from their siblings as soon as the hair started to grow. Compared with WT controls, *fr/fr* mice manifested curly whiskers and a wavy coat. The phenotype of *fr/Δ* animals was more severe, showing curly whiskers accompanied by less and shorter hair. *fr*[CR]/*fr*[CR] rats were almost completely bald. These data are in accordance with previous observations.[16,20]

No histopathologic aberrations were observed in the lung, kidney, and distal colon. In contrast, *fr/fr* and *fr/Δ* mice and *fr*[CR]/*fr*[CR] rats presented hair bulbs deeply
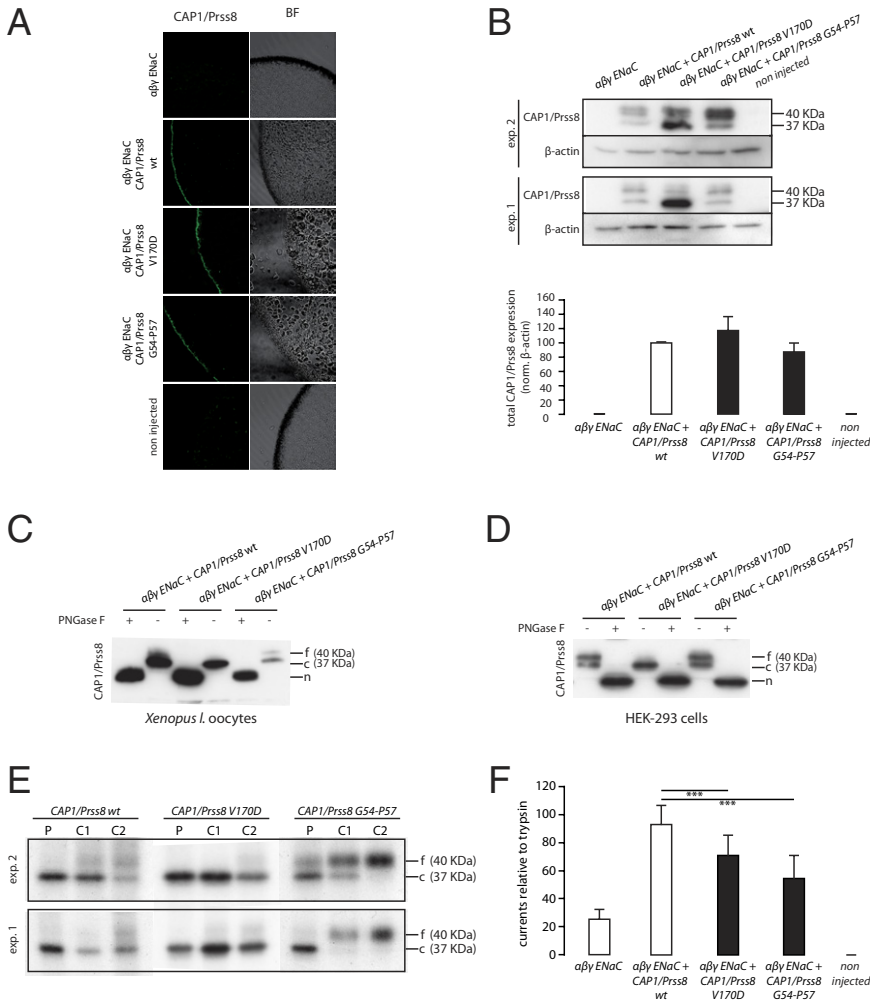
Figure 2. A: CAP1/Prss8 immunofluorescence (green) performed in *Xenopus* oocytes injected with ENaC and CAP1/Prss8 WT, V170D, and G54-P57 deletion mutant cRNA. BF, bright field. **B:** Oocytes were injected as indicated, and Western blot analyses were performed on cell lysates using CAP1/Prss8 and β-actin antibodies. Two representative experiments (exp. 1 and exp. 2) are shown, and quantification relative to β-actin was performed on a total of four independent experiments, each consisting of at least five oocytes injected per condition. **C:** Oocytes were injected as in B, and protein extracts were treated (+) or not (−) with PNGase F to deglycosylate the proteins and then subjected to Western blot analysis using CAP1/Prss8 antibody. f, fully glycosylated; c, core glycosylated; n, nonglycosylated. **D:** HEK-293 cells were transfected as indicated, and protein extracts were treated (+) or not (−) with PNGase F to deglycosylate the proteins and then subjected to Western blot analysis using CAP1/Prss8 antibody. This figure is representative of three independent experiments. **E:** Oocytes were injected as indicated and subjected to 6-hour pulse (P), 4-hour chase period (C1), and 16-hour chase period (C2). After the pulse-chase periods, protein extracts were prepared and subjected to nondenaturing immune precipitations using CAP1/Prss8 antibody. Two experiments (exp. 1 and exp. 2) are shown and are representative of three independent experiments, each consisting of 15 oocytes injected per condition. **F:** Amiloride-sensitive sodium currents from four independent experiments pulled together, each consisting of at least five oocytes measured per condition before and after trypsin perfusion. The currents measured before the perfusion of the oocytes with trypsin were normalized to currents measured after trypsin perfusion. ***$P < 0.001$.

positioned in the lower dermis. In addition, fr^{CR}/fr^{CR} skin exhibited hyperplasic epidermis and hyperkeratosis, as well as swelled and more abundant sebaceous glands. Beside these structural and morphologic defects, no signs of inflammation, such as cellular infiltrations, were detectable in *fr/fr*, *fr/Δ*, and fr^{CR}/fr^{CR} mutant skin (Figure 3).

Aiming to investigate CAP1/Prss8 expression at the transcriptional level, we performed quantitative real-time PCR analyses on skin, lung, kidney, and colon extracts of *fr/fr* and *fr/Δ* mutant mice and control littermates. For all analyzed organs, mice carrying *Δ/+* alleles presented a significant (50%) reduction in the expression of *CAP1/Prss8* when compared with WT animals, as it might be predicted from the absence of one *CAP1/Prss8* allele. Decreased *CAP1/Prss8* expression was detected also in *fr/Δ* heterozygous animals, but it was significant only in the kidney. CAP1/Prss8 mRNA levels in *fr/fr* mutants

Table 1. Inheritance of the *fr* and Δ Mutations

Breeding pair	*fr* and Δ genotype				
	+/+	*fr/+*	Δ/+	*fr/Δ*	*fr/fr*
fr/+ x Δ/+ (n = 111)					
No. of animals	42	32	30	7	
Observed, %	38	29	27	6	
Expected, %	25	25	25	25	
χ^2 test	21.3 ($P < 0.001$)				
fr/Δ x *fr/+* (n = 95)					
No. of mutations		40	28	12	15
Observed, %		42	29	13	16
Expected, %		25	25	25	25
χ^2 test	22.0 ($P < 0.01$)				

Table 2. Inheritance of the fr^{CR} Mutations

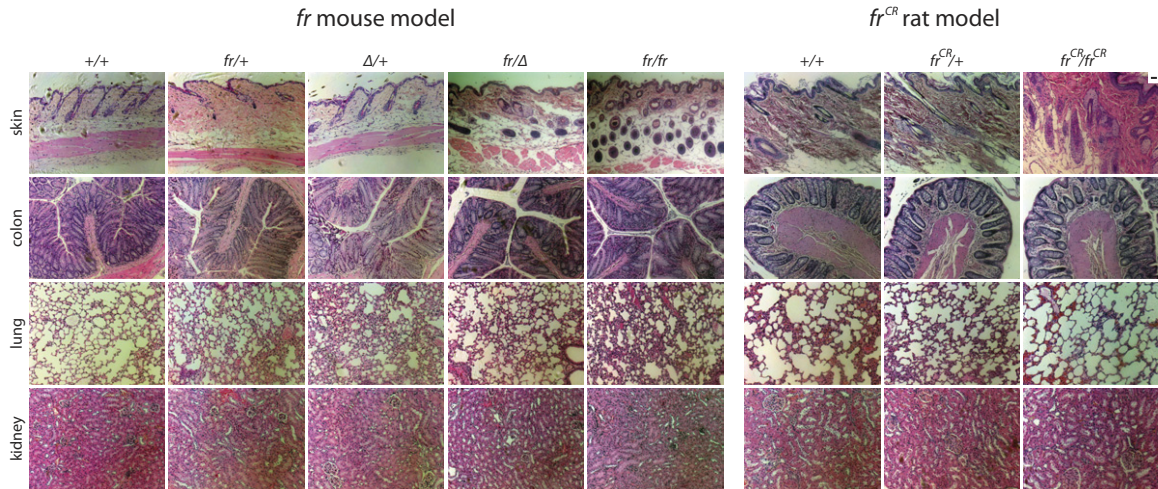| Breeding pair	fr^{CR} genotype		
	+/+	$fr^{CR}/+$	fr^{CR}/fr^{CR}
$fr^{CR}/+$ x $fr^{CR}/+$ (n = 60)			
No. of animals	12	42	6
Observed, %	20	70	10
Expected, %	25	50	25
χ^2 test	18.0 ($P < 0.01$)		
$fr^{CR}/+$ x fr^{CR}/fr^{CR} (n = 50)			
No. of mutations		32	18
Observed, %		64	36
Expected, %		50	50
χ^2 test	7.8 ($P < 0.01$)		

Figure 3. H&E staining of skin, colon, lung, and intestine in *fr* mouse (+/+, *fr/+*, Δ/+, *fr/Δ*, *fr/fr*) and *fr^CR* rat (+/+, *fr^CR/+*, *fr^CR/fr^CR*) variants, performed in young-adult animals. Scale bar = 20 µm.

did not differ from that of WT animals (Figure 4A). Analogous analyses in the skin of *fr^CR/fr^CR* mutant rats compared with WTs revealed a significant twofold increase in the mRNA expression of *CAP1/Prss8*. In contrast, *CAP1/Prss8* was significantly reduced in the distal colon (Figure 4B), whereas no significant changes were observed among the different genotypes in lung and kidney.

Finally, we performed Western blot analyses using CAP1/Prss8 antibody on kidney, lung, and AEC extracts from *fr* mice and *fr^CR* rats, respectively. CAP1/Prss8 detection in *fr/Δ* and *fr/fr* mice evidenced a preferential core-glycosylated state of the mutant protein compared with the WT (Figure 4C). CAP1/Prss8 detection in *fr^CR/fr^CR* rats evidenced a preferential fully glycosylated state compared with controls (Figure 4D). These data are entirely in accordance with the results obtained *in vitro*.

Reduced Body Weight and Dehydration Defects in fr^CR/fr^CR Rats

fr/fr and *fr/Δ* mouse mutants did not present differences in body weight compared with controls (Figure 5A). *fr^CR/fr^CR* rats appeared smaller and exhibited a significantly lower body weight compared with WT and heterozygous littermates (Figure 5B). To investigate whether the macroscopical and histologic defects in *fr/fr*, *fr/Δ*, and *fr^CR/fr^CR* mutants were accompanied by functional abnormalities of the skin and to explore the ability of this organ to protect the body against excessive dehydration, we measured the TEWL. *fr/fr* and *fr/Δ* mouse mutants did not differ from controls with respect to the TEWL (Figure 5C). In contrast, *fr^CR/fr^CR* rats exhibited a significant increase in the TEWL, suggesting that the skin barrier is compromised in these animals (Figure 5D). Moreover, *fr^CR/fr^CR* rats presented diarrhea accompanied by increased stool hydration (Figure 5, E and F).

Significantly Decreased ENaC Activity in the Distal Colon of fr/fr, fr/Δ, and fr^CR/fr^CR Animals

CAP1/Prss8 can increase ENaC-mediated sodium currents.[6,31] To investigate the effect of *CAP1/Prss8* V170D and G54-P57 deletion mutations on ENaC activity *in vivo*, the amiloride-sensitive rectal PD was measured in the distal aspect of the colon of both *fr* mouse and *fr^CR* rat animal models. Because amiloride is a specific and potent inhibitor of ENaC,[33] the amiloride-sensitive PD is an indirect indicator of ENaC function. Rectal PD in rodents follows circadian variation, reflecting differential metabolic activity of the animals during the day.[34] We therefore performed *in vivo* measurements in the morning and afternoon of two different days. Δ/+ and *fr/+* heterozygotes did not manifest differences compared with the WTs. *fr/fr* and *fr/Δ* mice revealed a significant decrease in the amiloride-sensitive PD, reflecting a significantly reduced ENaC activity in the distal aspect of the colon (Figure 6A). Just as *fr/fr* and *fr/Δ* mice did, *fr^CR/fr^CR* rats demonstrated a significant less negative PD. Surprisingly, *fr^CR/+* heterozygous rats had a reduced PD only in the morning, whereas in the afternoon the values were not different from WTs (Figure 6B).

Discussion

We examined whether the spontaneous V170D and G54-P57 deletion mutations within the *CAP1/Prss8* gene of *fr* mice and *fr^CR* rats, respectively, may cause their skin phenotypes and have additional consequences on the homeostasis of various organs where CAP1/Prss8 is expressed. *In silico* experiments indicated that the mutation V170D may alter CAP1/Prss8 protein structure because of unfavorable interactions of hydrophobic side chains with polar Asp, and, most likely, the change of V170 to Asp would lead a more severe modification of the three-dimensional configuration than the 2.4-Kcal loss of energy upon mutation to Ala. G54-P57 residues in CAP1/
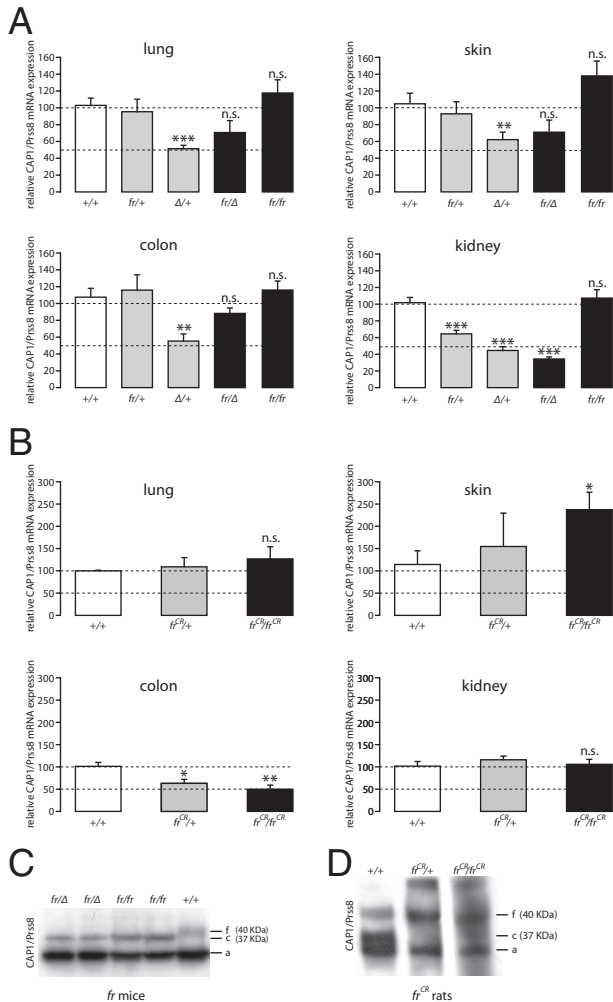
ern blot analyses and pulse-chase experiments revealed a differential glycosylation state of the two mutant proteins compared with the WT CAP1/Prss8, evidencing a preferential core glycosylated state of the V170D mutant versus a preferential fully glycosylated state of the G54-P57 deletion mutant, indicating an increased retention of the V170D mutant in the endoplasmic reticulum and enhanced intracellular transport of the G54-P57 deletion mutant. In addition to the changes in the glycosylation state, pulse-chase experiments demonstrated that the degradation and thus the stability of the mutant proteins do not change compared with the WT. However, a significant amount of energy lost upon mutation of V170 and W56 to Ala is found by *in silico* alanine scanning. This loss of energy might modify the three-dimensional conformation of the mutant proteins that may be responsible of a differential glycosylation state and eventually reduce their activity.

To determine the role of *CAP1/Prss8* in the different tissues, we previously deleted the mouse *CAP1/Prss8* gene locus, located on chromosome 7, in a temporally and/or tissue-specific manner[19] and revealed crucial roles for this serine protease at least in the skin and lung.[7,6,1] *fr/fr* mice, *fr/Δ* mice, and *fr^CR/fr^CR* rats displayed a significant reduction in the embryonic viability compared with the expected mendelian inheritance, coinciding with the prenatal lethality of the *CAP1/Prss8* knockout
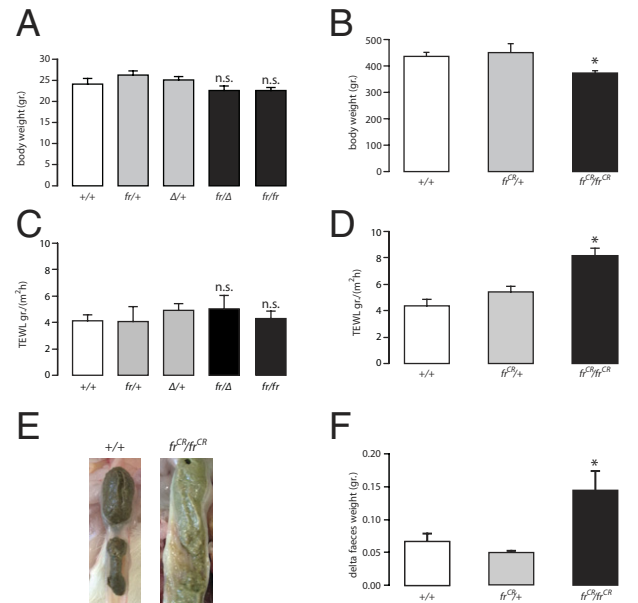
Figure 4. A: *CAP1/Prss8* mRNA levels, relative to β-actin, investigated by quantitative real-time PCR in the lung, skin, colon, and kidney of *fr* mice (+/+ *n* = 10; *fr/+ n* = 6; Δ/+ *n* = 8; *fr/Δ n* = 4; *fr/fr n* = 9 number of analyzed animals). **B:** *CAP1/Prss8* mRNA levels, relative to β-actin, investigated by quantitative real-time PCR, in the lung, skin, colon, and kidney of *fr^CR* rats (+/+ *n* = 4; *fr^CR/+ n* = 4; *fr^CR/fr^CR n* = 4 number of analyzed animals). **P < 0.05, **P < 0.01, ***P < 0.001*. **C:** Western blot analysis performed on kidney extracts from *fr* mice using CAP1/Prss8 antibody. f, fully glycosylated; c, core glycosylated; a, aspecific band. Analogous results were obtained from lung extracts. Three animals per genotype were analyzed. **D:** Western blot analysis using CAP1/Prss8 antibody performed on lung AECs isolated from *fr^CR* rats. Two animals per genotype were analyzed.

Prss8 resulted in solvent exposed, and their deletion could have a considerable impact on folding and architecture of the protein. These alterations of the protein structure may modify the interaction of CAP1/Prss8 with its effectors. We and other researchers have demonstrated that CAP1/Prss8 can increase the activity of the epithelial sodium channel ENaC in various expression systems[8,31,35]; therefore, CAP1/Prss8 activity can be evaluated by measuring ENaC currents. When we injected CAP1/Prss8 V170D and G54-P57 deletion mutants in the *Xenopus* oocytes, we observed that these mutations do not prevent the expression of the protein at the plasma membrane and their capability to activate the channel when co-expressed. However, the ability of CAP1/Prss8 V170D and G54-P57 deletion mutants to stimulate ENaC appeared significantly decreased. West-

Figure 5. A: Body weight measurements expressed in grams of *fr* mice (+/+ *n* = 12; *fr/+ n* = 15; Δ/+ *n* = 23; *fr/Δ n* = 13; *fr/fr n* = 22 number of analyzed animals), performed in young adult animals. n.s., nonsignificant. **B:** Body weight measurements expressed in grams of *fr^CR* rats (+/+ *n* = 8; *fr^CR/+ n* = 8; *fr^CR/fr^CR n* = 10; ****P < 0.001*, male rats only), performed in young adult animals. Same results were obtained for female rats (+/+ 283 ± 6.2 *n* = 6; *fr^CR/+* 296 ± 6.6 *n* = 7; *fr^CR/fr^CR* 259 ± 12.1 *n* = 4; *P < 0.05*). **C:** TEWL measurements of *fr* mice (+/+ *n* = 10; *fr/+ n* = 10; Δ/+ *n* = 5; *fr/fr n* = 9) expressed in grams on square meters per hour. **D:** TEWL measurements of *fr^CR* rats (+/+ *n* = 4; *fr^CR/+ n* = 4; *fr^CR/fr^CR n* = 4; **P < 0.05*) expressed in grams on square meters per hour. **E:** Representative pictures of the intestinal content of *fr^CR/fr^CR* and WT rats clearly show an increased liquid content in the stools of the *fr^CR/fr^CR* mutants. **F:** Feces water content, assessed as difference between freshly collected and completely dehydrated stools (+/+ *n* = 6; *fr^CR/+ n* = 3; *fr^CR/fr^CR n* = 7; **P < 0.05*).
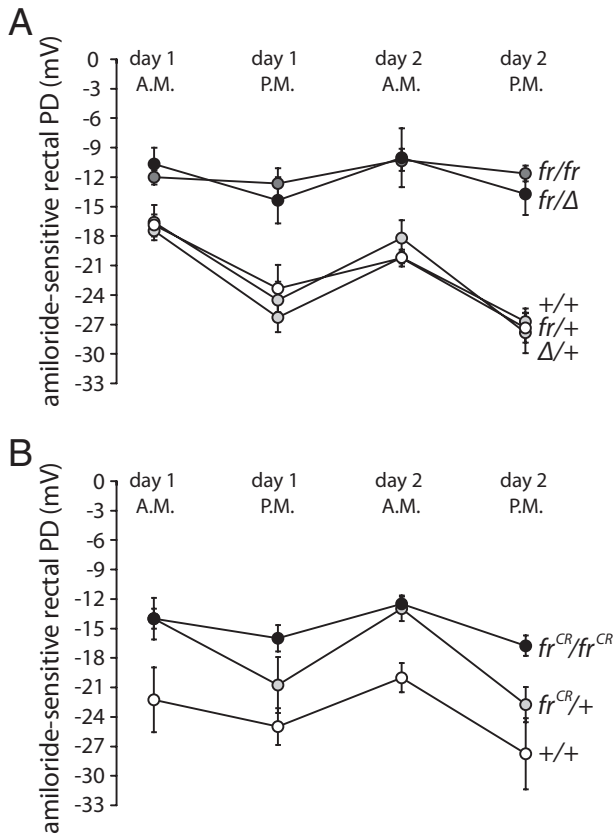
Figure 6. A: Amiloride-sensitive rectal PD, reflecting ENaC activity and expressed in millivolts, measured in the distal colon of *fr* mice (+/+, *n* = 12; *fr*/+ *n* = 12; Δ/+ *n* = 13; *fr*/Δ *n* = 10; *fr*/*fr* *n* = 10) (+/+ versus *fr*/*fr*, *P* < 0.05; +/+ versus *fr*/Δ, *P* < 0.01). **B:** Amiloride-sensitive rectal PD, reflecting ENaC activity and expressed in millivolts, measured in the distal colon of *fr^CR* rats (+/+ *n* = 4; *fr^CR*/+ *n* = 4; *fr^CR*/*fr^CR* *n* = 4). Measurements were performed both in the morning and in the afternoon of two different days (day 1 and day 2) (+/+ versus *fr^CR*/*fr^CR*, *P* < 0.05).

mice and strongly indicating a pleiotropic role of CAP1/ Prss8 in embryonic development. Of interest, similar histopathologic alterations occurred in the skin of *fr*/*fr*, *fr*/Δ, and *fr^CR*/*fr^CR* animals, denoting that both mouse and rat skin structure is sensitive to *CAP1/Prss8* mutations and altered function. Skin anomalies in frizzy and hairless animals did not appear to be accompanied by inflammation; thus, these defects might originate during embryonic development and hair morphogenesis. Interestingly, *fr^CR*/*fr^CR* rats exhibited, in addition to alopecia and hyperkeratosis, an increase in the size and number of sebaceous glands. Sebum is a mixture of lipids[36] that coat the fur as a hydrophobic protection against dehydration and for heat insulation,[37] and *fr^CR*/*fr^CR* animals may compensate their excess in loss of water through the skin by increasing the production of sebum.

The *fr* mutation first appeared in 1949 at the Jackson Laboratory and was identified in 1951 by Falconer and Snell[38] on a mixed genetic background that included the genetically linked recessive visible markers pink-eyed dilution (p), chinchilla (Tyr^ch), and shaker-1 (Myo7a). We consider unlikely that those or other additional mutations in *fr*/*fr* animals could contribute to the phenotype because the same phenotype is maintained or even enhanced in the *fr*/Δ animals and absent in the heterozygotes. In contrast, we cannot exclude the implications of additional recessive mutations on the phenotype of *fr^CR*/ *fr^CR* rats, and a complementation test could solve this issue, but so far CAP1/Prss8 knockout alleles in rats are not available. Additional mutations in *fr^CR*/*fr^CR* animals could be responsible for the baldness and permeability defects observed in the skin and intestine of mutant rats but not in *fr*/*fr* and *fr*/Δ mice. Alternatively, baldness and permeability defects in *fr^CR*/*fr^CR* rats could be the result of more severe consequences generated by the *CAP1/Prss8* G54-P57 deletion mutation compared with the *CAP1/Prss8* V170D mutation or might be species dependent.

Although decreased in the distal colon, *CAP1/Prss8* transcription levels increased in the skin of *fr^CR*/*fr^CR* rats, and a tendency for CAP1/Prss8 mRNA levels to augment could also be noticed in *fr*/Δ mice, not only in the skin but also in the colon and lung. These data reveal a different transcriptional regulation of mutated CAP1/Prss8 in different organs and a transcriptional up-regulation of mutated *CAP1/Prss8* in *fr*/Δ mice that might be due to compensatory effects.

Dehydration defects, caused by either skin or intestine anomalies, are often accompanied by body weight loss.[39,40] Both skin-specific *CAP1/Prss8* knockout and *CAP1/Prss8* overexpressing mice presented increased skin dehydration accompanied by loss in body weight,[7,1] and the tight junction functionality was defective in the skin-specific *CAP1/Prss8* knockouts.[7] Similarly, *fr^CR*/*fr^CR* rats showed significant reduction in body weight and manifested increased loss of water through the skin and intestine, evidencing epidermal permeability barrier defects that might be due to an effect of mutant *CAP1/Prss8* on tight junctions and/or on sodium and therefore water reabsorption. ENaC activity was significantly reduced in the distal colon of mutant mice and rats, and this decrease occurred at the same extent as that observed in intestine-specific *CAP1/Prss8* knockout mice (data not shown). These data indicate that *fr*/*fr* and *fr*/Δ animals exhibit the same reduction in the basal activity of ENaC as that of *CAP1/Prss8* loss-of-function mutants.

The three subunits of ENaC are expressed by surface epithelial cells of the distal colon,[41] and several serine proteases that activate ENaC *in vitro* are also expressed in the gastrointestinal tract, with a tissue distribution broader than that of ENaC. CAP1/Prss8 is present in the stomach and colon in rats and in the stomach, small intestine, and distal colon in mice.[35,31] The activity of ENaC depends on more than one serine protease, and we have previously shown that the serine protease CAP3/ matriptase is able to increase ENaC currents from sixfold to 10-fold.[31] It is noteworthy that both skin-specific deletion of *CAP1/Prss8* and complete abrogation of *CAP3/ matriptase* in mice caused leaky skin barrier[42,7] and that intestine-specific deletion of *CAP3/matriptase* provoked colon enlargement, persistent diarrhea, and increased intestinal paracellular permeability.[43] Moreover, CAP1/ Prss8 and CAP3/matriptase are constitutively co-localized in most epithelia[44] and have been proposed to be involved in the same proteolytic cascade.[11,45] Thus, it is

presumable that CAP1/Prss8 and CAP3/Tmprss14 cooperate to maintain the homeostasis of different organs.

In conclusion, the present study shows that both *fr* mouse and *fr^CR* rat models share similar features, such as reduced embryonic viability, abnormal allocation of hair follicles in the dermis, and reduced amiloride-sensitive sodium current in the distal colon. Together these data support that *fr* and *fr^CR* are mutant alleles of the *CAP1/Prss8* gene. *fr* and *fr^CR* therefore appear as suitable models for *CAP1/Prss8* decreased function in the whole organism, and the consequences of mutated *CAP1/Prss8* on its effectors and related pathways will be the object of further research.

Acknowledgments

References

1. Frateschi S, Camerer E, Crisante G, Rieser S, Membrez M, Charles RP, Beermann F, Stehle JC, Breiden B, Sandhoff K, Rotman S, Haftek M, Wilson A, Ryser S, Steinhoff M, Coughlin SR, Hummler E: PAR2 absence completely rescues inflammation and ichthyosis caused by altered CAP1/Prss8 expression in mouse skin. Nature Commun 2011, 2:161

2. Puente XS, Sanchez LM, Overall CM, Lopez-Otin C: Human and mouse proteases: a comparative genomic approach. Nature Rev 2003, 4:544–558

3. Puente XS, Sanchez LM, Gutierrez-Fernandez A, Velasco G, Lopez-Otin C: A genomic view of the complexity of mammalian proteolytic systems. Biochem Soc Trans 2005, 33:331–334

4. Rawlings ND, Morton FR, Kok CY, Kong J, Barrett AJ: MEROPS: the peptidase database. Nucleic Acids Res 2008, 36:D320–325

5. Verghese GM, Tong ZY, Bhagwandin V, Caughey GH: Mouse prostasin gene structure, promoter analysis, and restricted expression in lung and kidney. Am J Respir Cell Mol Biol 2004, 30:519–529

6. Planes C, Randrianarison NH, Charles RP, Frateschi S, Cluzeaud F, Vuagniaux G, Soler P, Clerici C, Rossier BC, Hummler E: ENaC-mediated alveolar fluid clearance and lung fluid balance depend on the channel-activating protease 1. EMBO Mol Med 2009, 2:26–37

7. Leyvraz C, Charles RP, Rubera I, Guitard M, Rotman S, Breiden B, Sandhoff K, Hummler E: The epidermal barrier function is dependent on the serine protease CAP1/Prss8. J Cell Biol 2005, 170:487–496

8. Vallet V, Chraibi A, Gaeggeler HP, Horisberger JD, Rossier BC: An epithelial serine protease activates the amiloride-sensitive sodium channel. Nature 1997, 389:607–610

9. Vuagniaux G, Vallet V, Jaeger NF, Hummler E, Rossier BC: Synergistic activation of ENaC by three membrane-bound channel-activating serine proteases (mCAP1, mCAP2, and mCAP3) and serum- and glucocorticoid-regulated kinase (Sgk1) in Xenopus oocytes. J Gen Physiol 2002, 120:191–201

10. Narikiyo T, Kitamura K, Adachi M, Miyoshi T, Iwashita K, Shiraishi N, Nonoguchi H, Chen LM, Chai KX, Chao J, Tomita K: Regulation of prostasin by aldosterone in the kidney. J Clin Invest 2002, 109:401–408

11. Camerer E, Barker A, Duong DN, Ganesan R, Kataoka H, Cornelissen I, Darragh MR, Hussain A, Zheng YW, Srinivasan Y, Brown C, Xu SM, Regard JB, Lin CY, Craik CS, Kirchhofer D, Coughlin SR: Local protease signaling contributes to neural tube closure in the mouse embryo. Dev Cell 2010, 18:25–38

12. Takahashi SS, Inaguma S, Ikeda Y, Cho Y-M, Hayashi N, Inoue T, Sugimura Y, Nishiyama N, Fujita T, Chao J, Ushijima T, Shirai T: Down-regulated expression of prostasin in high-grade and hormone-refractory human prostate cancers. Prostate 2003, 54:187–193

13. Chen LM, Chai KX: Prostasin serine protease inhibits breast cancer invasiveness and is transcriptionally regulated by promoter DNA methylation. Int J Cancer 2002, 97:323–329

14. Sakashita K, Mimori K, Tanaka F, Tahara K, Inoue H, Sawada T, Ohira M, Hirakawa K, Mori M: Clinical significance of low expression of Prostasin mRNA in human gastric cancer. J Surg Oncol 2008, 98:559–564

15. Mok SC, Chao J, Skates S, Wong K-k, Yiu GK, Muto MG, Berkowitz RS, Cramer DW: Prostasin, a potential serum marker for ovarian cancer: identification through microarray technology. J Natl Cancer Inst 2001, 93:1458–1464

16. Spacek DV, Perez AF, Ferranti KM, Wu LK, Moy DM, Magnan DR, King TR: The mouse frizzy (fr) and rat 'hairless' (frCR) mutations are natural variants of protease serine S1 family member 8 (Prss8). Exp Dermatol 2010, 19:527–532

17. Paul EL, Badal R, Thompson DS, Magnan DR, Soucy FM, Khan IM, Haughton RA, King TR: The mouse frizzy mutation (fr) maps between D7Csu5 and D7Mit165. Exp Dermatol 2008, 17:640–644

18. Panteleyev AA, Christiano AM: The Charles River "hairless" rat mutation is distinct from the hairless mouse alleles. Comp Med 2001, 51:49–55

19. Rubera I, Meier E, Vuagniaux G, Merillat AM, Beermann F, Rossier BC, Hummler E: A conditional allele at the mouse channel activating protease 1 (Prss8) gene locus. Genesis 2002, 32:173–176

20. Ahearn K, Akkouris G, Berry PR, Chrissluis RR, Crooks IM, Dull AK, Grable S, Jeruzal J, Lanza J, Lavoie C, Maloney RA, Pitruzzello M, Sharma R, Stoklasek TA, Tweeddale J, King TR: The Charles River "hairless" rat mutation maps to chromosome 1: allelic with fuzzy and a likely orthologue of mouse frizzy. J Hered 2002, 93:210–213

21. Hinz U: From protein sequences to 3D-structures and beyond: the example of the UniProt knowledgebase. Cell Mol Life Sci 2010, 67:1049–1064

22. Rickert KW, Kelley P, Byrne NJ, Diehl RE, Hall DL, Montalvo AM, Reid JC, Shipman JM, Thomas BW, Munshi SK, Darke PL, Su HP: Structure of human prostasin, a target for the regulation of hypertension. J Biol Chem 2008, 283:34864–34872

23. Eswar N, Webb B, Marti-Renom MA, Madhusudhan MS, Eramian D, Shen MY, Pieper U, Sali A: Comparative protein structure modeling using MODELLER. Curr Protoc Protein Sci 2007, Chapter 2:Unit 2.9

24. Melo F, Feytmans E: Assessing protein structures with a non-local atomic interaction energy. J Mol Biol 1998, 277:1141–1152

25. Schymkowitz J, Borg J, Stricher F, Nys R, Rousseau F, Serrano L: The FoldX web server: an online force field. Nucleic Acids Res 2005, 33:W382–W388

26. Puoti A, May A, Rossier BC, Horisberger JD: Novel isoforms of the beta and gamma subunits of the Xenopus epithelial Na channel provide information about the amiloride binding site and extracellular sodium sensing. Proc Natl Acad Sci U S A 1997, 94:5949–5954

27. Geering K, Theulaz I, Verrey F, Hauptle MT, Rossier BC: A role for the beta-subunit in the expression of functional Na+-K+-ATPase in Xenopus oocytes. Am J Physiol 1989, 257:C851–C858

28. Planes C, Leyvraz C, Uchida T, Angelova MA, Vuagniaux G, Hummler E, Matthay M, Clerici C, Rossier B: In vitro and in vivo regulation of transepithelial lung alveolar sodium transport by serine proteases. Am J Physiol Lung Cell Mol Physiol 2005, 288:L1099–L1109

29. Geering K, Beggah A, Good P, Girardet S, Roy S, Schaer D, Jaunin P: Oligomerization and maturation of Na,K-ATPase: functional interaction of the cytoplasmic NH2 terminus of the beta subunit with the alpha subunit. J Cell Biol 1996, 133:1193–1204

30. Spraggon G, Hornsby M, Shipway A, Tully DC, Bursulaya B, Danahay H, Harris JL, Lesley SA: Active site conformational changes of prostasin provide a new mechanism of protease regulation by divalent cations. Protein Sci 2009, 18:1081–1094

31. Vuagniaux G, Vallet V, Jaeger NF, Pfister C, Bens M, Farman N, Courtois-Coutry N, Vandewalle A, Rossier BC, Hummler E: Activation of the amiloride-sensitive epithelial sodium channel by the serine protease mCAP1 expressed in a mouse cortical collecting duct cell line. J Am Soc Nephrol 2000, 11:828–834

32. Caldwell RA, Boucher RC, Stutts MJ: Serine protease activation of near-silent epithelial Na+ channels. Am J Physiol Cell Physiol 2004, 286:C190–C194

33. Loffing J, Kaissling B: Sodium and calcium transport pathways along the mammalian distal nephron: from rabbit to human. Am J Physiol Renal Physiol 2003, 284:F628–F643

34. Wang Q, Horisberger JD, Maillard M, Brunner HR, Rossier BC, Burnier M: Salt- and angiotensin II-dependent variations in amiloride-sensitive rectal potential difference in mice. Clin Exp Pharmacol Physiol 2000, 27:60–66

35. Adachi M, Kitamura K, Miyoshi T, Narikiyo T, Iwashita K, Shiraishi N, Nonoguchi H, Tomita K: Activation of epithelial sodium channels by prostasin in *Xenopus* oocytes. J Am Soc Nephrol 2001, 12: 1114–1121

36. Nikkari T: Comparative chemistry of sebum. J Invest Dermatol 1974, 62:257–267

37. Strauss JS, Pochi PE, Downing DT: The sebaceous glands: twenty-five years of progress. J Invest Dermatol 1976, 67:90–97

38. Falconer DS, Snell GD: Two new hair mutants, rough and frizzy in the house mouse. J Hered. 1952, pp. 53–57

39. Herrmann T, van der Hoeven F, Grone HJ, Stewart AF, Langbein L, Kaiser I, Liebisch G, Gosch I, Buchkremer F, Drobnik W, Schmitz G, Stremmel W: Mice with targeted disruption of the fatty acid transport protein 4 (Fatp 4. Slc27a4) gene show features of lethal restrictive dermopathy. J Cell Biol 2003, 161:1105–1115

40. Koletzko S, Osterrieder S: Acute infectious diarrhea in children. Dtsch Arztebl Int 2009, 106:539–547; quiz 548

41. Canessa CM, Merillat AM, Rossier BC: Membrane topology of the epithelial sodium channel in intact cells. Am J Physiol 1994, 267:C1682–C1690

42. List K, Haudenschild CC, Szabo R, Chen W, Wahl SM, Swaim W, Engelholm LH, Behrendt N, Bugge TH: Matriptase/MT-SP1 is required for postnatal survival, epidermal barrier function, hair follicle development, and thymic homeostasis. Oncogene 2002, 21:3765–3779

43. List K, Kosa P, Szabo R, Bey AL, Wang CB, Molinolo A, Bugge TH: Epithelial integrity is maintained by a matriptase-dependent proteolytic pathway. Am J Pathol 2009, 175:1453–1463

44. List K, Hobson JP, Molinolo A, Bugge TH: Co-localization of the channel activating protease prostasin/(CAP1/PRSS8) with its candidate activator, matriptase. J Cell Physiol 2007, 213:237–245

45. Netzel-Arnett S, Currie BM, Szabo R, Lin C-Y, Chen L-M, Chai KX, Antalis TM, Bugge TH, List K: Evidence for a matriptase-prostasin proteolytic cascade regulating terminal epidermal differentiation. J Biol Chem 2006, 281:32941–32945

Sodium and Potassium Balance Depends on αENaC Expression in Connecting Tubule

Birgitte Mønster Christensen,* Romain Perrier,* Qing Wang,† Annie Mercier Zuber,*
Marc Maillard,† David Mordasini,† Sumedha Malsure,* Caroline Ronzaud,‡
Jean-Christophe Stehle,§ Bernard C. Rossier,* and Edith Hummler*

Departments of *Pharmacology and Toxicology and §Pathology, University of Lausanne, Lausanne, Switzerland;
†Service of Nephrology, Lausanne University Hospital, Lausanne, Switzerland; and ‡German Cancer Research
Center, Heidelberg, Germany

ABSTRACT

Mutations in α, β, or γ subunits of the epithelial sodium channel (ENaC) can downregulate ENaC activity and cause a severe salt-losing syndrome with hyperkalemia and metabolic acidosis, designated pseudohypoaldosteronism type 1 in humans. In contrast, mice with selective inactivation of αENaC in the collecting duct (CD) maintain sodium and potassium balance, suggesting that the late distal convoluted tubule (DCT2) and/or the connecting tubule (CNT) participates in sodium homeostasis. To investigate the relative importance of ENaC-mediated sodium absorption in the CNT, we used Cre-lox technology to generate mice lacking αENaC in the aquaporin 2–expressing CNT and CD. Western blot analysis of microdissected cortical CD (CCD) and CNT revealed absence of αENaC in the CCD and weak αENaC expression in the CNT. These mice exhibited a significantly higher urinary sodium excretion, a lower urine osmolality, and an increased urine volume compared with control mice. Furthermore, serum sodium was lower and potassium levels were higher in the genetically modified mice. With dietary sodium restriction, these mice experienced significant weight loss, increased urinary sodium excretion, and hyperkalemia. Plasma aldosterone levels were significantly elevated under both standard and sodium-restricted diets. In summary, αENaC expression within the CNT/CD is crucial for sodium and potassium homeostasis and causes signs and symptoms of pseudohypoaldosteronism type 1 if missing.

Sodium reabsorption in the kidney is essential for maintaining fluid and electrolyte homeostasis as well as regulation of blood pressure (BP). Renal sodium reabsorption is under tight control of aldosterone in the late distal convoluted tubule (DCT2), the connecting tubule (CNT), and the collecting duct (CD).[1] Sodium enters the aldosterone-sensitive epithelial cell through the epithelial sodium channel (ENaC) at the apical plasma membrane, and sodium is extruded to the interstitial fluid *via* the basolateral Na^+-K^+-ATPase in exchange for potassium. In the DCT2, sodium is also absorbed through the thiazide-sensitive NaCl co-transporter (TSC).[2] The critical role of ENaC in sodium homeostasis has been emphasized by identification of gain-of-function mutations in the C-terminus of the β or the γ subunit in patients with Liddle syndrome, a severe form of hypertension caused by sodium retention.[3,4]

Pseudohypoaldosteronism type 1 (PHA-1), conversely, is a severe salt-wasting syndrome

characterized by urinary loss of sodium and reduced potassium excretion despite elevated levels of aldosterone. In humans, a life-threatening form of the disease is inherited as an autosomal recessive trait and is caused by loss-of-function mutations in any of the three ENaC subunits.[5] Clinical symptoms of the disease are weight loss and dehydration, hypovolemia and hypotension, hyponatremia, hyperkalemia, and metabolic acidosis accompanied by elevated plasma aldosterone levels.[6] Complete knockout (KO) of each of the ENaC subunits resulted in an early and lethal PHA-1 phenotype.[7–9] Previously, a CD-specific conditional KO for αENaC was generated, and, surprising, these mice were able to maintain water, sodium, and potassium balance even after 1 week of salt restriction, 23 hours of water deprivation, or 4 days of potassium

Figure 1. Loss of αENaC expression in CD and partial loss in CNT of CNT/CD-specific KO mice. (A and B) Western blot of microdissected CNT and CCD from CD-specific KO mice and their corresponding controls (A) and from the CNT/CD-specific KO mice and littermate controls (B). Anti-αENaC antibody recognizes a band at approximately 95 kD corresponding to full-length αENaC and a band just above 26 kD that may correspond to a cleaved fragment of αENaC (arrowheads*). Some unspecific bands are also observed (arrowheads). The blots are reprobed with anti-actin antibody to examine the amount of protein loaded on the gels.

loading.[10] In this study, we investigated the implication of the CNT and CD for the ENaC-mediated sodium reabsorption using mice that express the Cre recombinase from the Aqp2 promoter (Aqp2::iCre) and conditional alleles of αENaC (Scnn1a^loxlox).[11,12] Aquaporin 2 (AQP2) is a water channel expressed along the CNT and CD.[13,14] Our data indicate that αENaC expression within the CNT is important for sodium and potassium balance.

RESULTS

Inactivation of αENaC in the CD and the CNT

KO and control mice were born consistent with Mendelian inheritance (Scnn1a^lox/− /Aqp2::iCre 25.9%, Scnn1a^lox/+ /Aqp2::iCre 29.4%, Scnn1a^lox/+ 21.8%, and Scnn1a^lox/− 22.8%; n = 197). To verify the deletion of αENaC expression in these CNT/CD-specific KO mice (Scnn1a^lox/− /Aqp2::iCre), we dissected the CNT and the CCD and analyzed these by Western blot (Figure 1). The previously described CD-specific KO mice (Scnn1a^lox/lox /HoxB7::Cre) were used as positive (and negative) control.[10] In the CNT and the CCD of all control groups, a band at approximately 95 kD corresponding to full-length αENaC protein was observed (Figure 1A, lanes 1 and 2, and B, lanes 1 and 2 and lanes 5 and 6). This band was absent in the CCD of the CD-specific KO mice (Figure 1A, lane 4)[10] and in the CCD of the CNT/CD-specific KO mice (Figure 1B, lanes 4 and 8). We observed a faint band corresponding to full-length αENaC protein in the CNT of the CNT/CD-specific KO mice (Figure 1B, lanes 3 and 7), suggesting that the inactivation of αENaC in the CNT was not complete. We further observed a band just above 26 kD in the CNT of the CD-specific KO mice (Figure 1A, lane 3) and in the CNT of the control littermates
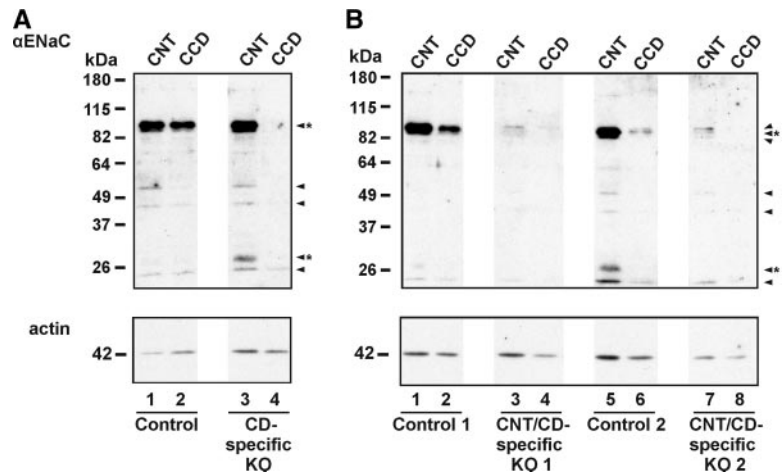
of the CNT/CD-specific KO mice (Figure 1B, lanes 1 and 5) that most likely corresponds to a cleavage product of the α subunit.[15,16] It was not observed in the CNT of the CNT/CD-specific KO mice (Figure 1B, lanes 3 and 7).

Western blots of microdissected tubules from sodium-restricted CNT/CD-specific KO mice and littermate control mice showed that the approximately 95 kD band corresponding to full-length αENaC protein was absent in the CCD of the CNT/CD-specific KO mice (Figure 2). In the CNT of the CNT/CD-specific KO mice, this band was weakly expressed or absent (Figure 2). Thus, on a standard or salt-restricted diet (Figures 1 and 2), αENaC protein is barely detectable in the CNT and not detected in the CCD of KO mice.

To investigate further the recombination efficiency, we performed immunohistochemistry on kidneys from sodium-deprived CNT/CD-specific KO mice and control mice. Double labeling showed almost complete co-localization of AQP2 and Cre recombinase in the principal cells along the CD (Figure 3A). Cellular counting in the CCD revealed that 96% of the AQP2-positive cells showed co-staining with the Cre recombinase. In the CNT, cellular counting showed that approximately 70% of AQP2-positive cells were co-labeled with Cre recombinase (Figure 3B). Double labeling of Cre recombinase and H⁺-ATPase (marker for intercalated cells) revealed no Cre expression in the intercalated cells (Figure 3C).

Within the CNT, immunolabeling was performed with antibodies recognizing αENAC, AQP2, and TSC. The anti-TSC antibody was used as a marker of the DCT.[2] In control mice, αENaC was expressed along the early and late CNT (Figure 3, D through F). The early CNT, which was identified at the transition from the TSC-positive DCT to the TSC-negative CNT, contained none or only a few AQP2-positive cells in both con-
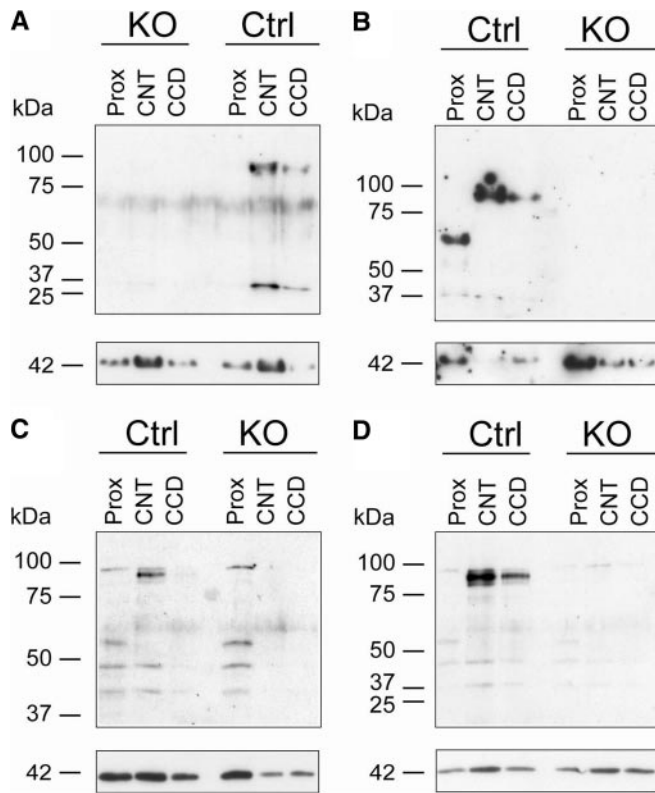
Figure 2. Sodium-restricted CNT/CD-specific KO mice show near-loss of αENaC protein expression in CNT. (A through D) Western blots of microdissected proximal tubules (Prox), CNT, and CCD from four different KO and control mice that are subjected to sodium-deficient diet. Anti-αENaC antibody recognizes a band at approximately 95 kD corresponding to full-length αENaC (top blots). The blots are reprobed with anti-actin antibody (bottom blots).

trol and KO mice (Figure 3, D through I). Consistent with this, αENaC was also detected in such tubules, which were both AQP2 and TSC negative and likely represent early parts of the CNT with undetectable AQP2 expression. In KO mice, αENaC was partly absent in the CNT (Figure 3, G through I) with some expression remaining in both late and early CNT. Approximately 70% of all early CNT cells (both CNT and intercalated cells) in the control were αENaC positive, in comparison with only 50% in the KO situation. In the late CNT, the percentage of αENaC-positive CNT cells (control 63%, KO 18%; identified as TSC negative and AQP2 positive) was reduced by approximately 70% in the KO. In summary, the CNT/CD-specific αENaC KO mice have reduced numbers of αENaC-expressing cells in both the late and early CNT, with a more severe reduction (up to 70%) in the late CNT, and corresponding to an increase in AQP2-expressing cells in the late CNT.

CNT/CD-Specific αENaC KO Mice Exhibit a PHA-1 Phenotype under Standard Salt Diet

Following a standard salt diet, mice did not exhibit reduced body weight. In contrary, the urinary sodium excretion was

significantly higher in the KO mice ($P < 0.05$; Table 1), whereas the urinary potassium excretion was unchanged. Food and, thus, sodium intake were not altered (Table 1). The increased urine excretion ($P < 0.01$; Table 1) was accompanied by lower urinary osmolality ($P < 0.01$; Table 1) and higher water intake ($P < 0.05$; Table 1). The CNT/CD-specific αENaC KO mice presented with significantly lower serum sodium concentrations ($P < 0.05$; Table 1) and hyperkalemia revealed by significantly higher blood potassium concentrations ($P < 0.05$; Table 1). Plasma aldosterone was measured in CNT/CD-specific αENaC KO and control mice that were homozygous for a specific renin allele ($Ren\text{-}2^{-/-}$),[17] and the CNT/CD-specific αENaC KO mice presented with significantly higher plasma aldosterone levels ($P < 0.05$; Table 2). BP was slightly reduced in the KO mice, without any significant difference (Table 1). No significant changes were observed in the heart rate (HR; Table 1).

Sodium-Deficient Diet Induces Severe Renal Sodium Loss

The CNT/CD-specific αENaC KO and control mice were challenged with a sodium-deficient diet for 4 consecutive days. Already after 1 day, the KO mice lost significant body weight, whereas the control mice kept or even gained body weight ($P < 0.001$; Figure 4A). No difference was observed in food intake (KO [$n = 8$] 0.15 ± 0.01 versus control [$n = 10$] 0.14 ± 0.01 g/g body wt), and loss of body weight was paralleled by a severe urinary sodium loss (Figure 4B). The cumulative sodium balance showed that the control mice were able to retain their sodium, whereas the KO mice continued to excrete sodium (KO 0.25 ± 0.014 mmol; control 0.07 ± 0.005 mmol; $P < 0.001$, day 4; Figure 4B). After 1 day of sodium-deficient diet, the urinary potassium excretion was significantly increased in the KO mice ($P < 0.05$), a difference that vanished during the subsequent days (Figure 4C). The KO mice continued to have a significant higher urinary excretion during the first 3 days on the sodium-deficient diet (Figure 5A). The urine osmolality was significantly lower in the KO mice on the sodium-deficient diet ($P < 0.001$, day 4; Figure 5B). Water intake was not different (Figure 5C). After 4 days, a significant increase was found in blood potassium levels (KO [$n = 8$] 6.4 ± 0.2 versus control [$n = 10$] 5.8 ± 0.2 mM; $P < 0.05$, day 4) and plasma aldosterone levels ($P < 0.01$; Table 2).

When the mice were followed for a period of 15 days upon salt-deprivation in standard cages, the KO mice lost weight continuously. The weight loss reached more than 10% of their initial weight ($P < 0.001$; Figure 6). Moreover, plasma aldosterone levels were significantly elevated ($P < 0.001$; Table 2).

CNT/CD-Specific αENaC KO Mice Are not Able to Eliminate a Potassium Load

The ability of the KO mice to eliminate a potassium load was tested by challenging the animals with a diet containing 5% potassium for 2 consecutive days. The KO mice had a significant lower urinary potassium excretion ($P < 0.01$, day 2; Figure 7A) and significantly higher levels of potassium in the
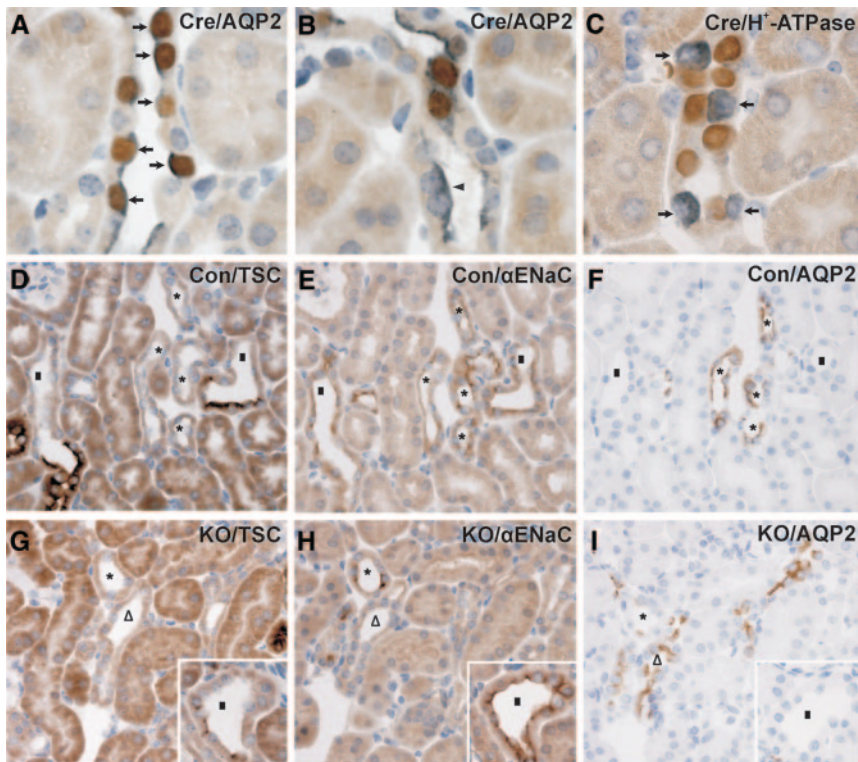
Figure 3. Residual expression of αENaC in CNT of CNT/CD-specific KO mice. (A through I) Immunohistochemistry using whole kidney sections from sodium-restricted control (D through F) and KO mice (A through C and G through I). (A and B) Double labeling of whole kidney sections from a KO mouse is performed with polyclonal primary antibodies that recognize Cre recombinase (brown) and AQP2 (gray-blue). Along the CD, nuclear Cre recombinase staining is observed in AQP2-expressing cells (A, arrows). Within the CNT, some AQP2-expressing cells are negative for Cre recombinase (arrowhead, B). (C) Double labeling with primary antibodies recognizing Cre recombinase (brown) and H$^+$-ATPase (gray-blue) shows no co-localization of the two proteins (arrows). (D through I) Serial kidney sections from a control mouse (D through F) and KO mouse (G through I) incubated with anti-TSC antibody (D and G), anti-αENaC antibody (E and H), and anti-AQP2 antibody (F and I). In control mice, αENaC labeling is observed in the CNT (AQP2 positive and TSC negative, D through F, *) including the early CNT, which is identified adjacent to the transition from the TSC-positive DCT to the TSC-negative CNT (D through F, ■). In the KO mice, αENaC is absent from part of the CNT (G through I, △) but present in other parts (G through I, *), including the early CNT (G through I, inset, ■).

blood ($P < 0.05$; Table 3), whereas the serum sodium concentration was significantly reduced ($P < 0.05$; Table 3). After 1 day of a high-potassium diet, urinary sodium excretion was not affected but was significantly reduced after day 2 ($P < 0.05$, day 2; Figure 7B). Fractional excretion of sodium FE(Na$^+$) was not different (Table 3), but KO mice showed significantly lower urinary chloride excretion (KO [$n = 11$] 1.1 ± 0.2 *versus* control [$n = 11$] 2.5 ± 0.4 mmol; $P < 0.05$, day 2), whereas no difference in serum chloride concentration was observed (Table 3). The concentration of bicarbonate was significantly lower in the KO mice (Table 3), indicating metabolic acidosis. Serum osmolality (Table 3), urine osmolality (KO [$n = 11$] 1198 ± 54 mmol/kg H$_2$O; control [$n = 11$] 1306 ± 62 mmol/kg H$_2$O), urine output (KO [$n = 11$] 0.14 ± 0.03 ml/g

body wt per 24 hours; control [$n = 11$] 0.21 ± 0.04 ml/g body wt per 24 hours), and water intake (KO [$n = 11$] 0.28 ± 0.05 ml/g body wt per 24 hours; control [$n = 11$] 0.37 ± 0.04 ml/g body wt per 24 hours) did not reveal significant differences after 2 days of a high-potassium diet.

DISCUSSION

Constitutive KO of either β or γENaC causes an early lethal phenotype as a result of disturbances in the electrolyte balance.[7,9] αENaC deficiency also induces death shortly after birth, with a lung, skin, and kidney phenotype.[8,18] Mice in which αENaC is deleted specifically in the CD are viable and do not show disturbances in sodium and potassium balance even when subjected to challenging diets.[10] This suggested that the CNT is important in controlling ENaC-mediated sodium reabsorption in the kidney. To investigate this further, we generated mice in which the αENaC gene was deleted in the CD and partly in the CNT. These mice are viable until adulthood and exhibit normal BP, although they show increased urinary sodium excretion, urine output, and plasma aldosterone, leading to hyponatremia and hyperkalemia under standard diet. After sodium restriction, the mice develop a severe salt-losing phenotype and show a continuous life-threatening reduction of body weight.

Partial Inactivation of αENaC in the CNT Is Sufficient to Induce a Severe Salt-Losing Syndrome

Whereas αENaC was deleted efficiently in the CCD principal cells, approximately 30% of the late CNT cells are not targeted and still express αENaC protein. This may explain the remaining αENaC expression in microdissected CNT of some animals under normal and sodium-deprived diet. Similar to our findings, CNT/CD-specific mineralocorticoid receptor (MR) KO mice (using the same Aqp2::iCre transgene) showed complete deletion of MR in the CD, whereas deletion of the MR protein in the early and late CNT was equally partial, thus following the AQP2 expression pattern in these segments.[11]

The absence of AQP2 expression in the early CNT is therefore consistent with previous observations. In vasopressin-deficient Brattleboro rats, the initial portion of the CNT lacks detectable levels of AQP2, whereas long-term

Table 1. Urinary and blood parameters from mice kept on a standard-salt diet

Parameter	KO	Control
Body weight (g)		
females	21.30 ± 0.66 ($n = 13$)	22.10 ± 0.65 ($n = 24$)
males	27.70 ± 0.89 ($n = 13$)	28.20 ± 1.08 ($n = 15$)
Food intake (g/g body wt per 24 h)	0.13 ± 0.01 ($n = 8$)	0.12 ± 0.01 ($n = 10$)
Na^+ intake (mmol/24 h)	0.27 ± 0.03 ($n = 8$)	0.26 ± 0.03 ($n = 10$)
Urinary Na^+ (mmol/24 h)	0.23 ± 0.01 ($n = 31$)[a]	0.19 ± 0.01 ($n = 46$)
Urinary Na^+ (mM)	136 ± 11 ($n = 31$)	155 ± 7 ($n = 46$)
Urinary K^+ (mmol/24 h)	0.33 ± 0.04 ($n = 31$)	0.28 ± 0.03 ($n = 46$)
Urinary K^+ (mM)	213 ± 38 ($n = 31$)	242 ± 23 ($n = 46$)
Urinary osm (mosm/kgH_2O)	1809 ± 119 ($n = 26$)[b]	2442 ± 133 ($n = 39$)
Urine output (ml/g body wt per 24 h)	0.085 ± 0.008 ($n = 31$)[b]	0.055 ± 0.004 ($n = 46$)
Water intake (ml/g body wt per 24 h)	0.25 ± 0.03 ($n = 31$)[a]	0.16 ± 0.01 ($n = 46$)
Serum osm (mosm/kgH_2O)	309 ± 4 ($n = 5$)	313 ± 34 ($n = 6$)
Serum Na^+ (mM)	145.8 ± 1.0 ($n = 5$)[a]	149.8 ± 1.1 ($n = 6$)
Plasma/serum K^+ (mM)	6.3 ± 0.2 ($n = 10$)[a]	5.6 ± 0.1 ($n = 16$)
Mean BP (mmHg)	127 ± 2 ($n = 13$)	135 ± 3 ($n = 19$)
Mean HR (beats/min)	632 ± 18 ($n = 13$)	630 ± 13 ($n = 19$)

Data are means ± SEM.
[a]$P < 0.05$.
[b]$P < 0.01$.

Table 2. Plasma aldosterone (pg/ml) in mice kept on a standard-salt diet or a sodium-deficient diet

Diet	KO	Control
Standard diet ($Ren-2^{-/-}$ gene mice)	1915 ± 396 ($n = 5$)[a]	381 ± 55 ($n = 8$)
Sodium-deficient diet, 4 days ($Ren-2^{-/-}$ gene mice)	3085 ± 400 ($n = 4$)[b]	1064 ± 213 ($n = 6$)
Sodium-deficient diet, 15 days ($Ren-2^{+/-}$ gene mice)	20,984 ± 2775 ($n = 7$)[c]	1218 ± 304 ($n = 7$)

Data are means ± SEM.
[a]$P < 0.05$.
[b]$P < 0.01$.
[c]$P < 0.001$.

vasopressin treatment induced its expression throughout the CNT.[19] Moreover, in *TRPV5::EGFP* transgenic mice, some tubule segments were enhanced green fluorescent protein and calbindin positive but negative for AQP2 and TSC, thus likely representing early CNT.[20]

We observed that the Cre recombinase protein was expressed along the CD, consistent with CNT/CD-specific MR KO mice.[11] Immunohistochemistry also showed that αENaC was not expressed anymore in the early part of the CCD in the CNT/CD-specific αENaC KO mice (Supplemental Figure 1).

The CNT Is Critical for the ENaC-Mediated Sodium Reabsorption

The increased urinary sodium excretion, hyponatremia, and hyperkalemia observed in the KO mice indicate impaired sodium reabsorption in the CNT and are therefore consistent with the absence of ENaC in this segment. Moreover, the KO mice exhibited decreased urine osmolality and increased urine output/water intake. The changes in water balance could be explained by a reduced renal urine-con-

centrating ability, leading to increased urine output and causing increased water intake. The renal effect can be due to impaired ENaC-mediated sodium reabsorption in the CNT and CD, which leads to a reduced driving force for osmotic reabsorption of water in these segments. Apparently, the urine-concentrating ability would be affected only when both the CNT and the CD are targeted because no change in water balance was seen in the CD-specific αENaC KO mice.[10] An impaired urine-concentrating ability was previously described in aldosterone synthase–deficient mice.[21] The changes in water balance could also be due to the activation of the renin-angiotensin-aldosterone system as shown by elevated plasma aldosterone concentrations, which could lead to a stimulation of thirst and result in increased water intake and subsequently increased urine output.

It was previously shown that CD-specific αENaC KO mice do not exhibit a phenotype even after challenging diets.[10] In contrast, we observed that sodium restriction caused a continuous loss of body weight and sodium in the KO mice. The body weight of the KO mice did not stabilize after 15 days of sodium restriction. A similar weight loss in response to a low-sodium diet was reported in transgenic mice expressing low levels of βENaC.[22] Moreover, the severe salt loss in humans with the recessive form of PHA-1 does not improve with age.[6] The CNT/CD-specific αENaC KO mice were hyperkalemic in contrast to the CD-specific αENaC KO mice. Both CNT/CD-specific and CD-specific αENaC KO mice decreased their urine osmolality upon sodium restriction, but only the CNT/CD-specific αENaC KO mice exhibited a significant lower urine osmolality compared with their littermate controls. Challenging the CD-specific αENaC KO mice with a potassium-rich diet for 4 days resulted in increased sodium and potassium in both plasma and urine but not different from the control.[10] In contrast, the CNT/CD-specific αENaC KO mice were not able to excrete a potassium load, as shown by significantly higher potassium concentration in blood and decreased urinary potassium excretion. The potassium-loaded CNT/CD-specific αENaC KO mice also showed indications of metabolic acidosis. Thus, in contrast to CD-specific αENaC KO mice, the CNT/CD-specific αENaC KO mice exhibited symptoms of PHA-1, supporting that the CNT is critical for the ENaC-mediated sodium reabsorption. This is consistent with previous suggestions that the late DCT and CNT, rather than the CD, are the main regulators of ENaC-mediated sodium
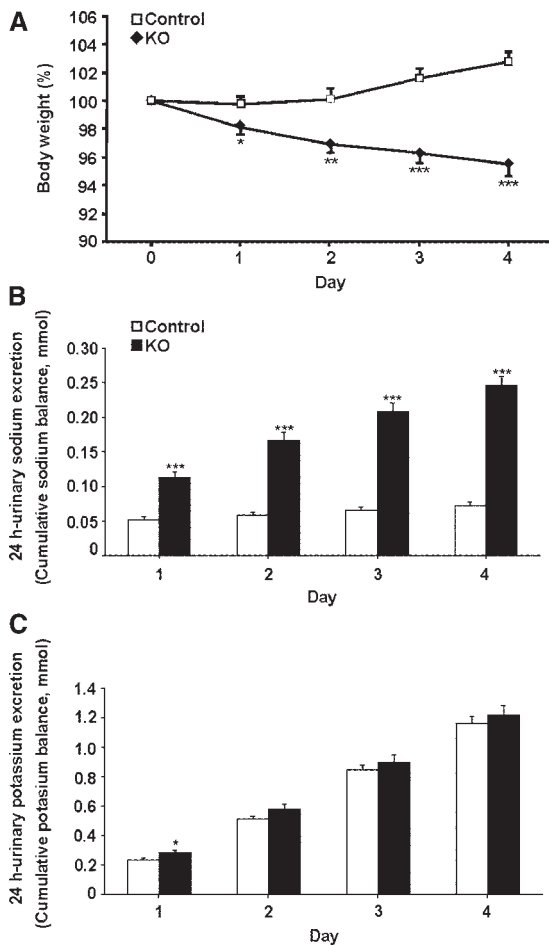
Figure 4. Loss of body weight and sodium in sodium-deprived CNT/CD-specific KO mice. (A) KO (n = 18) and control mice (n = 23) are subjected to a sodium-deficient diet for 4 days, and body weight is measured daily. Body weight is presented as percentage of the initial weight. (B and C) Cumulative sodium (B) and potassium (C) balance in KO mice (n = 18, ■) and control mice (n = 23, □) subjected to a sodium-deficient diet for up to 4 days. *P < 0.05; **P < 0.01; ***P < 0.001.

Figure 5. Increased urine output and reduced osmolality in sodium-deprived CNT/CD-specific KO mice. (A through C) Urine excretion (A), urine osmolality (B), and water intake (C) are measured daily in KO mice (n = 18, ■) and control mice (n = 23, □) subjected to a sodium-deficient diet for up to 4 days. *P < 0.05; **P < 0.01; ***P < 0.001.

and potassium homeostasis.[23,24] The majority (90%) of the sodium delivered to aldosterone-sensitive distal segments is reabsorbed in the CNT and DCT.[25] Moreover, the CNT exhibit a higher ENaC activity compared with the CD of aldosterone-infused rats.[26] The apical ENaC expression has also been shown to be more pronounced in the CNT compared with the CD in mice on a moderately low-sodium diet (0.05%).[27] That a partial gene deletion in the CNT was sufficient to induce a severe salt-losing syndrome also shows that the functional reserve in the CNT is limited because the remaining αENaC-positive CNT cells were unable to compensate fully for the loss of αENaC in the other cells.

CNT/CD-Specific Deletion of αENaC Is More Severe than Inactivation of the MR in the Same Segments

The actions of aldosterone are mediated through the MR. After binding of aldosterone to the MR, the hormone is translocated
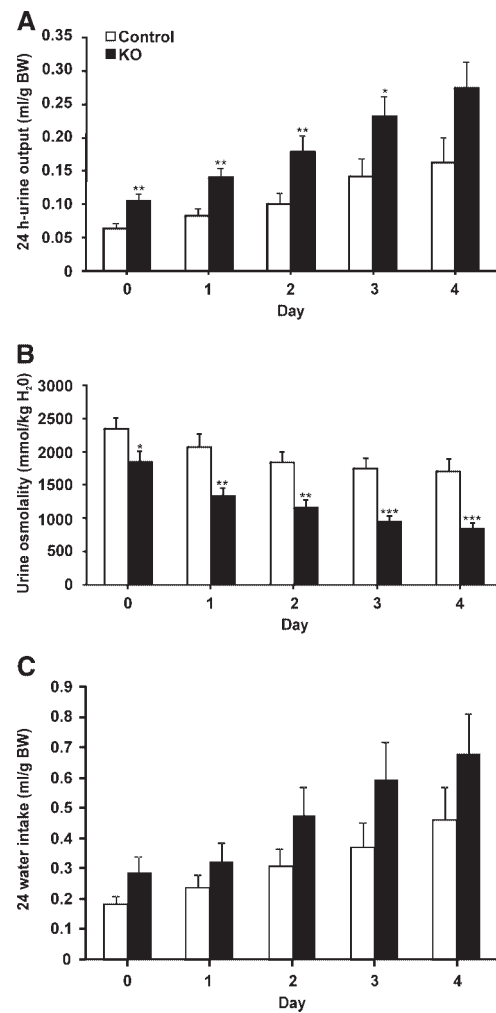
to the nucleus, where it controls the transcription of ENaC and other genes. In contrast to the CNT/CD-specific αENaC KO mice, no disturbance in electrolyte and water balance was observed in CNT/CD-specific MR KO mice subjected to a normal-salt diet.[11] Thus, partial deletion of αENaC in the CNT induces a more severe phenotype than inactivation of MR in the same segments. This may not be surprising because the MR protein is an upstream effector on sodium absorption compared with ENaC as an effector. Upon sodium restriction, the CNT/CD-specific MR KO mice also showed loss of body weight, increased sodium and urinary excretion, and significantly higher plasma aldosterone levels,[11] similar to CNT/CD-specific αENaC KO mice.

In summary, gradual gene deletion in the CNT was sufficient to induce a severe salt-losing syndrome, confirming that the CNT is crucial for maintaining sodium and potassium balance.
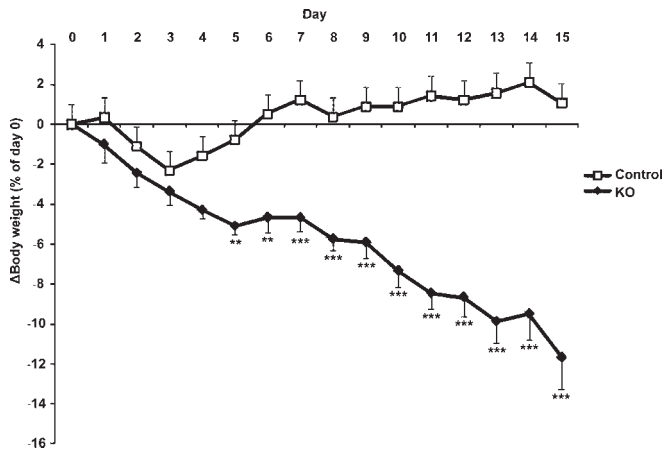
Figure 6. Continuous loss of body weight in sodium-deprived CNT/CD-specific KO mice. KO ($n = 7$) and control mice ($n = 7$) are subjected to a sodium-deficient diet for 15 days in standard cages. Body weight is measured daily and is presented as percentage of the initial body weight (at day 0; **$P < 0.01$, ***$P < 0.001$).

CONCISE METHODS

Generation of Transgenic Mice

To inactivate the *Scnn1a* gene in the CNT cells, we used mice expressing Cre recombinase under the control of the regulatory elements of the mouse *Aqp2* gene[11] and *Scnn1a*^{loxlox} conditional

Figure 7. Retention of potassium in CNT/CD-specific KO mice upon potassium loading. KO mice ($n = 11$) and control mice ($n = 11$) are subjected to a high-potassium diet for 2 days. (A and B) Urinary potassium excretion (A) and urinary sodium excretion (B) are measured daily. *$P < 0.05$; **$P < 0.01$.

KO mice and the *Scnn1a*$^{+/-}$ mice.[8,12] CNT/CD-specific αENaC KO mice (*Scnn1a*$^{lox/-}$/*Aqp2::iCre*; KO group) and heterozygous (*Scnn1a*$^{lox/+}$/±*Aqp2::iCre* and *Scnn1a*$^{lox/-}$; control group) littermates were obtained by interbreeding *Scnn1a*$^{+/-}$/*Aqp2::iCre* mice with *Scnn1a*^{loxlox} mice. Genotyping of the mice was performed by PCR analysis of tail biopsies described previously.[12] To genotype *Scnn1a*$^{+/-}$ and *Aqp2::iCre* mice, the following primers were used: *Scnn1a*$^{+/-}$: primer #1: 5′-TTAAGGGTGCACACAGTGACGGC-3′, #2: 5′-TTTGTCACGTCCTGCACGACGCG-3′, and #3: 5′-AACTCCAGAAGGTCAGCTGGCTC-3′, and *Aqp2::iCre*: #4: 5′-AAGTGCCCACAGTCTAGCCTCT-3′, #5: 5′-CCTGTTGT-TCAGCTTGCACCAG-3′, and #6: 5′-GGAGAACGCTATG-GACCGGAGT-3′.

Microdissection of Nephron Segments

Microdissection of kidneys was performed from KO mice ($n = 2$) and control littermates (*Scnn1a*$^{lox/+}$ and *Scnn1a*$^{lox/+}$/*Aqp2::iCre*; $n = 2$, approximately 3 months of age). As additional controls, we included CD-specific KO mice (*Scnn1a*^{loxlox}/*HoxB7::iCre*; $n = 2$) and their littermate controls (*Scnn1a*^{loxlox}; $n = 2$, approximately 11 months of age).[10] Microdissection was also performed on kidneys from KO mice ($n = 4$) and control littermates (*Scnn1a*$^{lox/+}$; $n = 4$, 2 to 2.5 months of age) that were subjected to a sodium-deficient diet in standard cages for 6 to 17 days. The experiment was performed four times and each time with one KO mouse and one control mouse in parallel. The kidney was perfused with DMEM/F-12 (1:1; 21041 medium; Invitrogen) completed with 40 μg/ml liberase blendzyme TM 2 or 30 μg/ml blendzyme (Roche Applied Science). Thin pyramids cut along the corticomedullary axis were incubated at 37 or 30°C for 40 minutes in the perfusion medium. The action of enzyme was stopped by washing the pyramids with ice-cold DMEM/F-12 (1:1) without blendzyme. Then, the medulla was removed under microscope and the CNT and CCD were microdissected in ice-cold DMEM/F-12 (1:1) without blendzyme. Pools of 10 to 20 microdissected tubules in 5 μl of DMEM/F12 (1:1) were then transferred to 5 μl of 2× concentrated protein sample buffer (9.6% [wt/vol] SDS, 13.8% [wt/vol] sucrose, 0.026% [wt/vol] bromphenol blue, and 4.2% [vol/vol] β-mercaptoethanol).
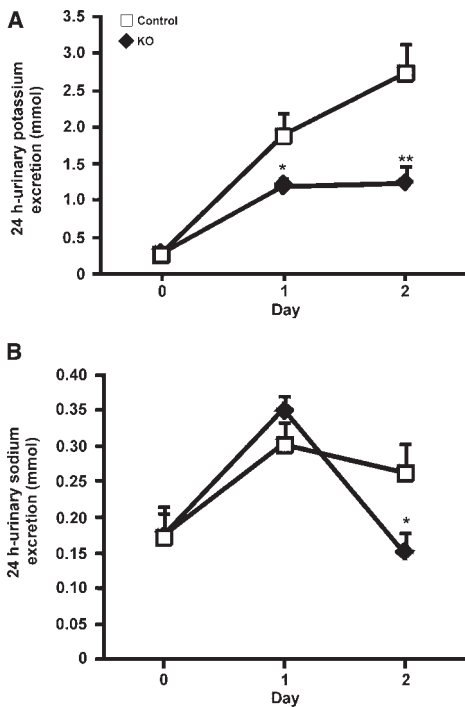
Western Blot Analysis of Microdissected Nephron Segments

Samples were heated at 95°C for 5 minutes and loaded and electrophoresed on an 8% SDS-PAGE. Proteins were then transferred to Protran nitrocellulose membrane (Schleicher & Schuell) or Amersham Hybond-ECL nitrocellulose membrane (Amersham), and Western blots were performed according to standard procedures. The membrane was first probed with affinity-purified αENaC antibody (1:100, 1:500, or 1:2000 dilution[10]); after stripping, anti-actin antibody (1:200 dilution; Sigma) was used. Blots were revealed with SuperSignal reagent (Pierce) or Amersham ECL Western blotting Detection Reagents (Amersham).

Immunohistochemistry

Kidneys from mice that were sodium-restricted for 4 consecutive days (*Scnn1a*$^{lox/-}$/*Aqp2::iCre* [$n = 2$] and *Scnn1a*$^{lox/+}$/*Aqp2::iCre* [$n = 3$]) were fixed by intravascular perfusion of 3% paraformaldehyde and subjected to paraffin embedding and sectioning (2-μm-thick sections).

Table 3. Functional data from mice subjected to a high-potassium diet for 48 hours

Parameter	KO	Control
Serum Na^+ (mM)	147.6 ± 1.4 ($n = 8$)[a]	151.5 ± 0.7 ($n = 11$)
Serum K^+ (mM)	7.7 ± 0.8 ($n = 9$)[a]	5.2 ± 0.2 ($n = 11$)
Serum HCO_3^- (mM)	12.8 ± 1.1 ($n = 7$)[b]	18.3 ± 0.5 ($n = 10$)
Serum osm (mosm/kgH_2O)	329.0 ± 4.7 ($n = 8$)	325.0 ± 1.5 ($n = 9$)
Serum creatinine (mM)	19.1 ± 2.3 ($n = 7$)[a]	12.1 ± 1.5 ($n = 10$)
Serum Cl^- (mM)	114.4 ± 1.4 ($n = 7$)	114.8 ± 0.7 ($n = 10$)
FE(Na^+) (%)	0.27 ± 0.05 ($n = 7$)	0.25 ± 0.02 ($n = 10$)

Data are means $\pm$ SEM.
[a]$P < 0.05$.
[b]$P < 0.001$.

Double Labeling

Double-labeling experiments were performed using (*1*) rabbit polyclonal Cre recombinase antibody (1:8000 dilution; Covance) and biotinylated rabbit polyclonal AQP2 antibody (7661AP; 1:250 dilution) and (*2*) Cre recombinase antibody (1:8000 dilution) and biotinylated rabbit polyclonal H^+-ATPase antibody (H7659AP; 1:100 dilution[28]). Sections were incubated overnight at 4°C with Cre antibody before undergoing incubation with horseradish peroxidase–conjugated goat anti-rabbit secondary antibody and visualization by 3,3′-diaminobenzidine (brown color). Sections were then incubated in 3.5% H_2O_2 in methanol to remove any remaining peroxidase from the first staining. After blocking for endogenous biotin (Biotin Blocking System; DakoCytomation), sections were then incubated overnight at 4°C with either biotinylated AQP2 or H^+-ATPase antibodies. Labeling was visualized by use of Strepavidin horseradish peroxidase (Sigma) and Vector SG substrate (blue-gray color; Vector Laboratories).

Single Labeling of Serial Kidney Sections

Serial paraffin sections were incubated with (*1*) rabbit polyclonal αENaC antibody (1:800 dilution[10]), rabbit polyclonal AQP2 antibody (1:3000 dilution), and mouse monoclonal Calbindin D-28K antibody (1:20,000 dilution; Research Diagnostics) and (*2*) rabbit polyclonal TSC antibody (1:1000 dilution[29]), rabbit polyclonal αENaC antibody (1:800 dilution[10]), and rabbit polyclonal AQP2 antibody (1:3000 dilution). Labeling was visualized by use of peroxidase-conjugated secondary antibody and 3,3′-diaminobenzidine. Sections were counterstained with hematoxylin. Light microscopy was carried out using a Leica DMRE microscope.

Quantification of αENaC-Positive Cells in the CNT

Cell counting was performed on kidney sections from *Scnn1a$^{lox/-}$*/ *Aqp2::iCre* mice and *Scnn1a$^{lox/+}$/Aqp2::iCre* mice that were labeled with rabbit polyclonal αENaC antibodies and peroxidase-conjugated secondary antibodies. Counting was performed on electronic images taken with a $\times 25$ objective. The number of αENaC-positive (labeled) and αENaC-negative (unlabeled) cells with a distinct nucleus was counted in the early CNT, adjacent to the transition from DCT to CNT (the transition was identified on serial sections labeled with TSC antibodies). The total number of cells counted was 65 in the *Scnn1a$^{lox/-}$/Aqp2::iCre* mice ($n = 2$) and 81 in the *Scnn1a$^{lox/+}$/Aqp2::iCre* mice ($n = 2$). Cellular counting was also performed in the late CNT (tubules were identified on serial sections labeled with AQP2 and TSC antibodies). The number of cells counted was 330 in the

Scnn1a$^{lox/-}$/Aqp2::iCre mice ($n = 2$) and 339 in the *Scnn1a$^{lox/+}$/Aqp2::iCre* mice ($n = 3$). The fraction of ENaC-positive cells was calculated from the number of positive cells divided by the total number of cells counted for each animal.

Quantification of Cre Recombinase–Positive Cells in the CCD and the CNT

The cellular counting was performed on kidney sections from *Scnn1a$^{lox/-}$/Aqp2::iCre* mice and *Scnn1a$^{lox/+}$/Aqp2::iCre* mice that were double labeled with rabbit polyclonal Cre recombinase antibody and biotinylated rabbit polyclonal AQP2 antibody. Counting was performed on electronic images taken with a $\times 63$ objective. The number of AQP2-positive/Cre recombinase–positive and AQP2-positive/Cre recombinase–negative cells with a distinct nucleus was counted in the CCD (313 cells, $n = 5$ mice) and in the CNT (465 cells, $n = 5$ mice). The fraction of Cre recombinase–positive cells was calculated from the number of AQP2-positive/Cre recombinase–positive cells divided by the total number of AQP2-positive cells counted for each animal.

Experimental Protocols

Sodium-Deficient Diet in Metabolic Cages

For each metabolic cage study, experimental mice and controls from the same litter were used. Six- to 12-week-old mice were placed in individual metabolic cages (Tecniplast, Buguggiate, Italy) and fed a standard-salt diet (0.23% sodium; Institut National de la Recherche Agronomique, Unité de Préparation des Aliments Expérimentaux, Jouy en Josas, France) for 2 days, followed by 4 consecutive days on a sodium-deficient diet (0% sodium; Institut National de la Recherche Agronomique, Unité de Préparation des Aliments Expérimentaux). During the experiment, the animals had free access to food and water. The diet was given as a mixture of food in gelatin and water (100 g food/60 ml water). Blood was collected from the tail vein of conscious mice at the end of the diet. The experiment was also performed with 8- to 12-week-old mice fed a standard-salt diet (0.17% sodium, given as powder food; Ssniff Spezialdiäten GmbH, Soest, Germany) for 2 days followed by 3 days on a sodium-deficient diet (<0.01% sodium; Ssniff Spezialdiäten GmbH).

Sodium-Deficient Diet in Standard Cages

Experimental ($n = 7$) and control littermate mice ($n = 7$, 8 to 12 weeks old) were fed a standard-salt diet (0.17% sodium; Ssniff Spezialdiäten GmbH), and the body weight was measured at day 0 to determine the reference weight. Then, mice were fed a sodium-deficient diet (<0.01% sodium; Ssniff Spezialdiäten GmbH) with free access to water, and their body weight was monitored daily (at the same time) for 15 consecutive days.

Blood Collection for Aldosterone Measurements

Control and *Scnn1a$^{lox/lox}$/Aqp2::iCre* (KO) mice (8 to 12 weeks old) that were homozygous for a specific renin allele (*Ren-2$^{-/-}$*) were kept in standard cages with free access to food and water. Thirteen mice (eight control and five experimental) were fed a standard-salt diet

(0.17% sodium; Ssniff Spezialdiäten GmbH) and 10 mice (six control and four KO) were fed a sodium-deficient diet (<0.01% sodium; Ssniff Spezialdiäten GmbH) for 4 consecutive days. At the end of experiment, blood samples were collected after decapitation. Plasma aldosterone levels were measured according to standard procedures using a RIA (Coat-A-Count RIA kit; Siemens Medical Solutions Diagnostics, Ballerup, Denmark). Mouse samples with values >1200 pg/ml were further diluted using a serum pool with a low aldosterone concentration (<50 pg/ml).

High-Potassium Diet

Data from two separate experiments were pooled. In the first series of experiments, mice were 4 months old; in the second series, mice were 2.5 to 12 months old. Experimental mice ($n = 5$ for first experiment; $n = 6$ for second experiment) and control mice ($n = 6$ for first experiment; $n = 5$ for second experiment) were placed in individual metabolic cages and fed a standard diet for 2 consecutive days (0.59% potassium in the first experiment and 0.95% potassium in the second experiment). This was followed by 2 days on a 5% potassium diet (the potassium was added as KCl). During the experiment, the animals had free access to food and water. The diets were given as a mixture of food in gelatin and water (100 g food/60 ml water). After the diet, blood was collected from the eye.

Urine and Serum/Plasma Analysis

Urine and serum/plasma osmolarity as well as sodium, potassium, chloride, creatinine, and bicarbonate composition were analyzed at the Laboratoire Central de Chimie Clinique (Centre Hospitalier Universitaire Vaudoise, Lausanne, Switzerland). The potassium values were corrected for the degree of hemolysis.

BP Measurements

The BP and HR were measured in KO ($n = 13$) and control mice ($n = 19$). The mice were kept on a normal-salt diet containing 0.23% of sodium with free access to tap water and were analyzed at the age of 4 to 6 months. BP and HR were recorded intra-arterially using a computerized data-acquisition system (Notocord Systems SA, Croissy, France).[17] Briefly, for placement of the intra-arterial catheter, a mouse was anesthetized *via* inhalation of 1 to 2% halothane with oxygen. The right carotid artery was exposed for a length of approximately 4 mm. A silicone/PE10 catheter filled with 0.9% NaCl solution containing heparin (300 IU/ml) was inserted into the artery. After ligation, the catheter was subcutaneously tunneled to exit at the back of the neck and fixed with a piece of scotch tape and dental cement. The mouse was allowed 3 to 4 hours to recover from the anesthesia and placed in a Plexiglas tube for partial restriction of its movements. Thirty minutes later, the arterial line was connected to a pressure transducer; BP and HR were then monitored every 20 seconds for 15 to 20 minutes using the Notocord computerized data-acquisition system at a sampling rate of 500 Hz. Once BP measurement was completed, blood was sampled from the arterial catheter for analysis of serum sodium and potassium concentrations.

Statistical Analysis

Results are presented as mean ± SEM. Data were analyzed by one-way ANOVA and unpaired *t* test. $P < 0.05$ was considered statistically significant.

DISCLOSURES
None.

REFERENCES

1. Verrey F, Hummler E, Schild L, Rossier BC: Mineralocorticoid action in the aldosterone-sensitive distal nephron. In: *The Kidney Physiology and Pathophysiology*, 4th Ed., edited by Alpern RJ, Hebert SC, Academic Press, 2008, pp 889–924
2. Loffing J, Loffing-Cueni D, Valderrabano V, Klausli L, Hebert SC, Rossier BC, Hoenderop JG, Bindels RJ, Kaissling B: Distribution of transcellular calcium and sodium transport pathways along mouse distal nephron. *Am J Physiol Renal Physiol* 281: F1021–F1027, 2001
3. Shimkets RA, Warnock DG, Bositis CM, Nelson-Williams C, Hansson JH, Schambelan M, Gill JR Jr, Ulick S, Milora RV, Findling JW: Liddle's syndrome: Heritable human hypertension caused by mutations in the beta subunit of the epithelial sodium channel. *Cell* 79: 407–414, 1994
4. Hansson JH, Nelson-Williams C, Suzuki H, Schild L, Shimkets R, Lu Y, Canessa C, Iwasaki T, Rossier B, Lifton RP: Hypertension caused by a truncated epithelial sodium channel gamma subunit: Genetic heterogeneity of Liddle syndrome. *Nat Genet* 11: 76–82, 1995
5. Chang SS, Grunder S, Hanukoglu A, Rosler A, Mathew PM, Hanukoglu I, Schild L, Lu Y, Shimkets RA, Nelson-Williams C, Rossier BC, Lifton RP: Mutations in subunits of the epithelial sodium channel cause salt wasting with hyperkalaemic acidosis, pseudohypoaldosteronism type 1. *Nat Genet* 12: 248–253, 1996
6. Kuhnle U: Pseudohypoaldosteronism: mutation found, problem solved? *Mol Cell Endocrinol* 133: 77–80, 1997
7. Barker PM, Nguyen MS, Gatzy JT, Grubb B, Norman H, Hummler E, Rossier B, Boucher RC, Koller B: Role of gammaENaC subunit in lung liquid clearance and electrolyte balance in newborn mice: Insights into perinatal adaptation and pseudohypoaldosteronism. *J Clin Invest* 102: 1634–1640, 1998
8. Hummler E, Barker P, Gatzy J, Beermann F, Verdumo C, Schmidt A, Boucher R, Rossier BC: Early death due to defective neonatal lung

liquid clearance in alpha-ENaC-deficient mice. *Nat Genet* 12: 325–328, 1996

9. McDonald FJ, Yang B, Hrstka RF, Drummond HA, Tarr DE, McCray PB Jr, Stokes JB, Welsh MJ, Williamson RA: Disruption of the beta subunit of the epithelial Na+ channel in mice: Hyperkalemia and neonatal death associated with a pseudohypoaldosteronism phenotype. *Proc Natl Acad Sci U S A* 96: 1727–1731, 1999

10. Rubera I, Loffing J, Palmer LG, Frindt G, Fowler-Jaeger N, Sauter D, Carroll T, McMahon A, Hummler E, Rossier BC: Collecting duct-specific gene inactivation of alphaENaC in the mouse kidney does not impair sodium and potassium balance. *J Clin Invest* 112: 554–565, 2003

11. Ronzaud C, Loffing J, Bleich M, Gretz N, Grone HJ, Schutz G, Berger S: Impairment of sodium balance in mice deficient in renal principal cell mineralocorticoid receptor. *J Am Soc Nephrol* 18: 1679–1687, 2007

12. Hummler E, Merillat AM, Rubera I, Rossier BC, Beermann F: Conditional gene targeting of the Scnn1a (alphaENaC) gene locus. *Genesis* 32: 169–172, 2002

13. Nielsen S, DiGiovanni SR, Christensen EI, Knepper MA, Harris HW: Cellular and subcellular immunolocalization of vasopressin- regulated water channel in rat kidney. *Proc Natl Acad Sci U S A* 90: 11663–11667, 1993

14. Kishore BK, Mandon B, Oza NB, DiGiovanni SR, Coleman RA, Ostrowski NL, Wade JB, Knepper MA: Rat renal arcade segment expresses vasopressin-regulated water channel and vasopressin V2 receptor. *J Clin Invest* 97: 2763–2771, 1996

15. Ergonul Z, Frindt G, Palmer LG: Regulation of maturation and processing of ENaC subunits in the rat kidney. *Am J Physiol Renal Physiol* 291: F683–F693, 2006

16. Hughey RP, Bruns JB, Kinlough CL, Harkleroad KL, Tong Q, Carattino MD, Johnson JP, Stockand JD, Kleyman TR: Epithelial sodium channels are activated by furin-dependent proteolysis. *J Biol Chem* 279: 18111–18114, 2004

17. Wang Q, Hummler E, Nussberger J, Clement S, Gabbiani G, Brunner HR, Burnier M: Blood pressure, cardiac, and renal responses to salt and deoxycorticosterone acetate in mice: Role of Renin genes. *J Am Soc Nephrol* 13: 1509–1516, 2002

18. Charles RP, Guitard M, Leyvraz C, Breiden B, Haftek M, Haftek-Terreau Z, Stehle JC, Sandhoff K, Hummler E: Postnatal requirement of the epithelial sodium channel for maintenance of epidermal barrier function. *J Biol Chem* 283: 2622–2630, 2008

19. Coleman RA, Wu DC, Liu J, Wade JB: Expression of aquaporins in the renal connecting tubule. *Am J Physiol Renal Physiol* 279: F874–F883, 2000

20. Hofmeister MV, Fenton RA, Praetorius J: Fluorescence isolation of mouse late distal convoluted tubules and connecting tubules: Effects of vasopressin and vitamin D3 on Ca2+ signaling. *Am J Physiol Renal Physiol* 296: F194–F203, 2009

21. Makhanova N, Lee G, Takahashi N, Sequeira Lopez ML, Gomez RA, Kim HS, Smithies O: Kidney function in mice lacking aldosterone. *Am J Physiol Renal Physiol* 290: F61–F69, 2006

22. Pradervand S, Barker PM, Wang Q, Ernst SA, Beermann F, Grubb BR, Burnier M, Schmidt A, Bindels RJ, Gatzy JT, Rossier BC, Hummler E: Salt restriction induces pseudohypoaldosteronism type 1 in mice expressing low levels of the beta-subunit of the amiloride-sensitive epithelial sodium channel. *Proc Natl Acad Sci U S A* 96: 1732–1737, 1999

23. Meneton P, Loffing J, Warnock DG: Sodium and potassium handling by the aldosterone-sensitive distal nephron: The pivotal role of the distal and connecting tubule. *Am J Physiol Renal Physiol* 287: F593–F601, 2004

24. Loffing J, Korbmacher C: Regulated sodium transport in the renal connecting tubule (CNT) *via* the epithelial sodium channel (ENaC). *Pflugers Arch* 458: 111–135, 2009

25. Malnic G, Klose RM, Giebisch G: Micropuncture study of renal potassium excretion in the rat. *Am J Physiol* 206: 674–686, 1964

26. Frindt G, Palmer LG: Na channels in the rat connecting tubule. *Am J Physiol Renal Physiol* 286: F669–F674, 2004

27. Loffing J, Pietri L, Aregger F, Bloch-Faure M, Ziegler U, Meneton P, Rossier BC, Kaissling B: Differential subcellular localization of ENaC subunits in mouse kidney in response to high- and low-Na diets. *Am J Physiol Renal Physiol* 279: F252–F258, 2000

28. Christensen BM, Kim YH, Kwon TH, Nielsen S: Lithium treatment induces a marked proliferation of primarily principal cells in rat kidney inner medullary collecting duct. *Am J Physiol Renal Physiol* 291: F39–F48, 2006

29. Biner HL, Arpin-Bott MP, Loffing J, Wang X, Knepper M, Hebert SC, Kaissling B: Human cortical distal nephron: Distribution of electrolyte and water transport pathways. *J Am Soc Nephrol* 13: 836–847, 2002

Colon-Specific Deletion of Epithelial Sodium Channel Causes Sodium Loss and Aldosterone Resistance

Sumedha Malsure,* Qing Wang,[†‡] Roch-Philippe Charles,* Chloe Sergi,* Romain Perrier,* Birgitte Mønster Christensen,* Marc Maillard,[†] Bernard C. Rossier,* and Edith Hummler*

*Department of Pharmacology and Toxicology, University of Lausanne, Lausanne, Switzerland; [†]Service of Nephrology, University Hospital of Lausanne (CHUV), Lausanne, Switzerland; and [‡]Division of Physiology, Department of Medicine, University of Fribourg, Fribourg, Switzerland

ABSTRACT

Aldosterone promotes electrogenic sodium reabsorption through the amiloride-sensitive epithelial sodium channel (ENaC). Here, we investigated the importance of ENaC and its positive regulator channel-activating protease 1 (CAP1/*Prss8*) in colon. Mice lacking the αENaC subunit in colonic superficial cells (*Scnn1a*[KO]) were viable, without fetal or perinatal lethality. Control mice fed a regular or low-salt diet had a significantly higher amiloride-sensitive rectal potential difference (ΔPD_{amil}) than control mice fed a high-salt diet. In *Scnn1a*[KO] mice, however, this salt restriction-induced increase in ΔPD_{amil} did not occur, and the circadian rhythm of ΔPD_{amil} was blunted. Plasma and urinary sodium and potassium did not change with regular or high-salt diets or potassium loading in control or *Scnn1a*[KO] mice. However, *Scnn1a*[KO] mice fed a low-salt diet lost significant amounts of sodium in their feces and exhibited high plasma aldosterone and increased urinary sodium retention. Mice lacking the CAP1/*Prss8* in colonic superficial cells (*Prss8*[KO]) were viable, without fetal or perinatal lethality. Compared with controls, *Prss8*[KO] mice fed regular or low-salt diets exhibited significantly reduced ΔPD_{amil} in the afternoon, but the circadian rhythm was maintained. *Prss8*[KO] mice fed a low-salt diet also exhibited sodium loss through feces and higher plasma aldosterone levels. Thus, we identified CAP1/Prss8 as an *in vivo* regulator of ENaC in colon. We conclude that, under salt restriction, activation of the renin-angiotensin-aldosterone system in the kidney compensated for the absence of ENaC in colonic surface epithelium, leading to colon-specific pseudohypoaldosteronism type 1 with mineralocorticoid resistance without evidence of impaired potassium balance.

Sodium and potassium transport across tight epithelia (kidney and colon) is important to keep the body in a constant balance, despite large dietary variations. Aldosterone promotes sodium reabsorption as an electrogenic sodium transport through the amiloride-sensitive epithelial sodium channel (ENaC).[1] Systemic autosomal recessive pseudohypoaldosteronism type 1 (systemic PHA-1) is caused by ENaC mutations and characterized by a severe salt-losing syndrome paralleled with hypotension, hyperkalemia, metabolic acidosis, and high plasma aldosterone levels.[2] Liddle's syndrome is caused by mutations within the PPxY motif (PY) domain of the β- or γENaC subunits and results in severe salt-sensitive hypertension with renal salt retention, alkalosis, and low plasma aldosterone levels.[3]

ENaC was originally identified in rat colon from animals challenged with low salt diet and is made of three homologous subunits: α, β, and γ.[4,5] In the mouse, the constitutive knockout of each subunit is postnatally lethal.[6–8] In the absence of αENaC, the β- and γ-subunits are not transported to the membrane, and no amiloride-sensitive sodium current is measured *in vitro* or *ex vivo*.[6,9]

Along the intestine, sodium absorption occurs through electroneutral sodium transport through the sodium/hydrogen exchanger rather than electrogenic absorption through ENaC that is limited to surface epithelial cells of the distal colon and rectum.[10,11] After proctocolectomy, ENaC starts to be expressed in the distal part of the small intestine (*i.e.*, the ileum), thereby unveiling the importance of an electrogenic amiloride-sensitive transport for the reabsorption of salt and water in the intestine.[12] Thereby, aldosterone stimulates β- and γENaC mRNA transcript expression in rat distal colon.[13–15] If dietary sodium intake is low and plasma aldosterone levels are high, the distal colon can efficiently absorb dietary sodium against a large concentration gradient.[11,16] Enhanced ENaC expression in colon, thus, contributes to sodium retention observed in mice with Liddle's syndrome[17,18] along with increased responsiveness to aldosterone.[19] On the other side, downregulation of ENaC with reduction in sodium reabsorption in colon may contribute to diarrhea associated with inflammatory bowel disease.[20,21]

The membrane-bound serine protease CAP1/*Prss8*, also known as prostasin, activates ENaC by rapidly increasing the open probability.[22–25] CAP1/*Prss8* is coexpressed with ENaC in many salt-absorbing tight epithelia, such as distal colon, urinary bladder, and airways.[23,24] *In vivo* evidence that CAP1/*Prss8* is an important and physiologically relevant activator of ENaC came from the study of mice lacking CAP1/*Prss8* in the alveolar epithelium, unveiling a crucial role for lung fluid balance.[26] In the colon, however, the physiologic role of this membrane-bound serine protease was hitherto unknown, and it was unclear whether CAP1/*Prss8* was implicated in regulating colonic ENaC activity.

In the present study, we, thus, addressed whether suppression of colonic ENaC activity affected sodium and/or potassium balance and what are the compensatory mechanisms that lead to increased renal sodium reabsorption. Finally, we unveiled the role of the positive ENaC activator CAP1/Prss8 in colon. We specifically deleted either αENaC/*Scnn1a* or CAP1/*Prss8* in the colonic surface epithelium and determined *in vivo* the electrogenic sodium transport to correlate plasma electrolytes with fecal sodium loss and plasma aldosterone concentrations.

RESULTS

Intestine-Specific αENaC-Deficient Mice Are Viable and Exhibit Normal Colon Histology

To ablate αENaC expression in colonic superficial cells, we mated *Scnn1a*$^{+/-}$; *villin::Cre*$^{tg/0}$ mice with mice harboring two floxed αENaC alleles (*Scnn1a*^{loxlox}) (Figure 1A). Analysis of a total of 252 offspring at weaning showed no deviation from the expected Mendelian distribution (*Scnn1a*^{Lox}, $n=60$; *Scnn1a*^{Het}, $n=68$; *Scnn1a*^{Hetc}, $n=70$; *Scnn1a*^{KO}, $n=54$). Adult *Scnn1a*^{KO} mice were viable, showed no postnatal mortality, and were indistinguishable in appearance, growth, and body weight (Table 1). In the *Scnn1a*^{KO} mice, colonic superficial cells lack near 99% of *Scnn1a* mRNA transcript expression, whereas heterozygotes (*Scnn1a*^{Het}) exhibit intermediate (71%) expression levels compared with *Scnn1a*^{Lox} ($P<0.05$) (Figure 1B). The expression of β- and γENaC mRNA transcripts was not significantly higher in *Scnn1a*^{KO} mice (Figure 1B). The successful deletion of *Scnn1a* in scraped colonic superficial cells was further confirmed on the protein expression level (Figure 1, C and D). Heterozygotes for the *Scnn1a* allele (*Scnn1a*^{Het} and *Scnn1a*^{Hetc}) showed intermediate expression (70% and 50% of *Scnn1a*^{Lox}, respectively).

Macroscopically, the morphology of the adult distal colon was not different (Supplemental Figure 1). The colon epithelium and mucin-secreting goblet cells appeared normal in knockout mice, without any effect on the number of crypt cells (not shown). The intestine length-to-body weight ratio was not different between the *Scnn1a*^{Lox} (1.97 ± 0.05; $n=5$), *Scnn1a*^{Het} (1.89 ± 0.05; $n=6$), and *Scnn1a*^{KO} (1.83 ± 0.06; $n=6$) groups.

Implication of ENaC in Intestinal Electrogenic Sodium Transport and Sodium Balance

ENaC-mediated sodium transport is electrogenic and generates an amiloride-sensitive transepithelial potential difference (ΔPD_{amil}) that varies on different salt diets and follows a circadian rhythm.[27] We measured ΔPD_{amil}, and the switch from high salt (HS) (Figure 2A) to regular salt (RS) (Figure 2B) and low salt (LS) (Figure 2C) diets induced a progressive increase in plasma aldosterone (Figure 3). On HS diet, plasma aldosterone (0.1–0.2 nmol/L) (Figure 3) and baseline ΔPD_{amil} (Figure 2A) were equally low (-5 to -6 mV) between groups (Figure 2A). On RS diet, plasma aldosterone increased from 0.7 nmol/L in *Scnn1a*^{Lox} to 1.2 nmol/L in *Scnn1a*^{Het} and 1 nmol/L in *Scnn1a*^{Hetc} mice (Figure 3). All mice showed a significant (-10 to -15 mV) increase in ΔPD_{amil} compared with the HS diet. The circadian rhythm expressed as (a.m./p.m.) cyclicity was readily observed (Figure 2, A and B). The highest plasma aldosterone level was observed in the *Scnn1a*^{KO} group (2.4 nmol/L), contrasting with the ΔPD_{amil} that remained low (-6 to -8 mV) and without cyclicity (Figures 2B and 3). On LS diet, plasma aldosterone increased in all groups to reach high values in the *Scnn1a*^{KO} group (8.5 nmol/L) (Figure 3). Despite this drastic increase in plasma aldosterone level, ΔPD_{amil} remained low (-5 to -6 mV) with blunted cyclicity (Figures 2C and 3). In all conditions, a residual amiloride-insensitive negative PD was observed (between -6 and -8 mV; data not shown). The observed hyperaldosteronism suggested that loss of sodium in the feces could have caused a significant hypovolemia and triggered the activation of the renin-angiotensin-aldosterone system (RAAS). We, therefore, analyzed total sodium and potassium in the feces and found
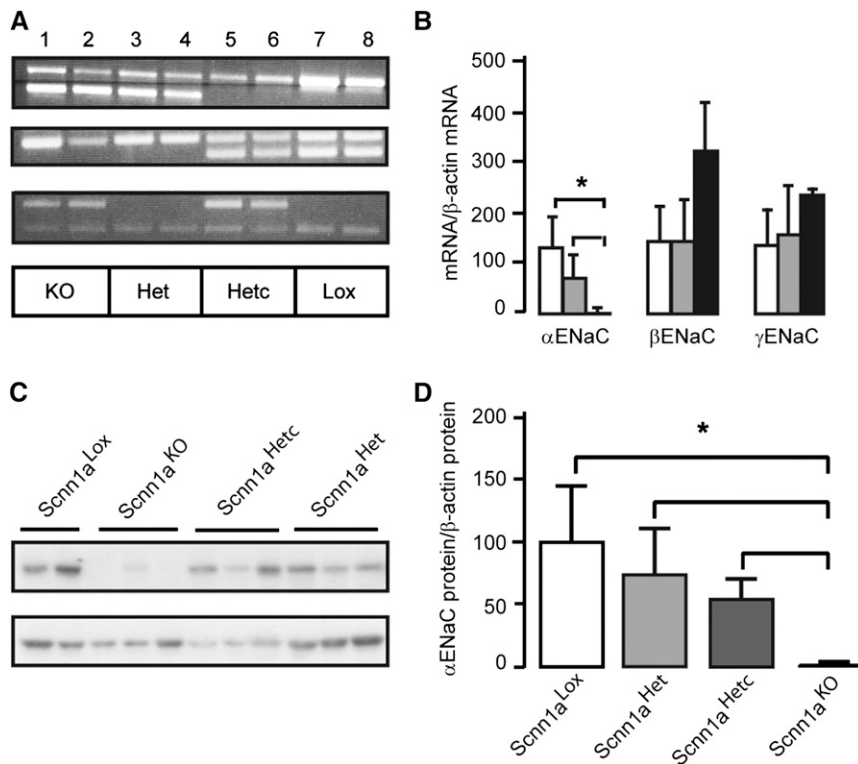
Figure 1. Loss of αENaC mRNA transcript and protein expression in colonic superficial cell-specific *Scnn1a*-deficient mice. DNA, mRNA, and protein samples were analyzed from (A) tissues or (B–D) isolated scraped distal colonic superficial cells. (A) PCR analysis on ear biopsies with primers distinguishes between the lox (580 bp) and the KO (360 bp) allele of the *Scnn1a* gene locus (row 1). In row 2, the primers indicated distinguish between wild type (220 bp) and lox (280 bp) allele in experimental *Scnn1a* $^{lox/-}$; *villin::Cre*$^{tg/+}$ (*Scnn1a*^{KO}) and controls (lanes 1 and 2), *Scnn1a*$^{lox/-}$ (*Scnn1a*^{Het}); lanes 3 and 4, *Scnn1a*$^{lox/+}$; *villin::Cre*$^{tg/+}$ (*Scnn1a*^{Hetc}); lanes 5 and 6, *Scnn1a* $^{lox/+}$ (*Scnn1a*^{Lox}); lanes 7 and 8, littermates. Detection of the *villin::Cre* transgene (upper band) and myogenin (internal control, lower band) (row 3). (B) Quantification of α-, β-, and γENaC mRNA transcripts by quantitative RT-PCR in cells from *Scnn1a*^{Lox} ($n=5$; white), *Scnn1a*^{Het} ($n=4$; light gray), and *Scnn1a*^{KO} mice ($n=4$; black column). Results are expressed as the ratio of mRNA/β-actin mRNA (*$P<0.05$). (C) Representative immunoblot showing the expression of αENaC (row 1) and β-actin (row 2) protein in cells from *Scnn1a*^{Lox}, *Scnn1a*^{Het}, *Scnn1a*^{Hetc}, and *Scnn1a*^{KO} mice. (D) Quantification of αENaC protein expression levels in cells from *Scnn1a*^{Lox} (white), *Scnn1a*^{Het} (light gray), *Scnn1a*^{Hetc} (dark gray), and *Scnn1a*^{KO} (black) mice after analysis with ImageJ software ($n=3$ mice per group; *$P<0.05$). Results are expressed as the ratio of αENaC protein/β-actin protein. Values are mean±SEM.

that, with RS and LS diets, *Scnn1a*^{KO} mice lost significantly more sodium (RS, $P<0.05$; LS, $P<0.001$). This difference was not observed with HS diet (Figure 4A). Fecal potassium was not significantly different among the groups (Figure 4B). Moreover, wet/dry ratio of feces was similar in all groups (*Scnn1a*^{KO}: 0.32±0.02; *Scnn1a*^{Lox}: 0.30±0.02; *Scnn1a*^{Het}: 0.34±0.02).

Lack of Colonic ENaC-Mediated Sodium Absorption Compensated by the Kidney

Scnn1a^{KO} mice should be able to compensate for the fecal sodium loss by an aldosterone-dependent sodium absorption by the distal nephron. Hence, mice were followed in metabolic cages, and on

HS, RS, and LS diets, food and water intake, feces output, urinary volume, and plasma and urinary sodium and potassium were measured (Table 1). On LS diet, cumulative sodium excretion in the *Scnn1a*^{KO} group was significantly diminished compared with all groups ($P<0.05$) (Figure 5, A–C). Cumulative potassium loss was not different, even when challenged with high potassium (5%) (Figure 5, D–F and Table 1).

CAP1/*Prss8* Identified as an *In Vivo* Regulator of ENaC in Distal Colon

To test the role of CAP1/*Prss8* on ENaC in distal colon *in vivo*, intestine-specific CAP1/*Prss8*-deficient mice (*Prss8*^{KO}, *Prss8*$^{\Delta/lox}$; *villin::Cre*$^{tg/0}$) were generated (Figure 6A). At weaning, analysis of a total of 219 offspring showed no deviation from the Mendelian distribution (*Prss8*^{Lox}, $n=55$; *Prss8*^{Het}, $n=55$; *Prss8*^{Hetc}, $n=56$; *Prss8*^{KO}, $n=53$). In *Prss8*^{KO} mice, colonic superficial cells lacked CAP1/*Prss8* mRNA transcript expression ($<1\%$), whereas heterozygotes (*Prss8*^{Het}) exhibited intermediate expression levels compared with *Prss8*^{Lox} cells (70%) (Figure 6B). The mRNA transcript expression of CAP2/*Tmprss4* and CAP3/*Prss14* was not altered (Figure 6B). The successful deletion of CAP1/*Prss8* in scraped colonic superficial cells was further confirmed on the protein level (Figure 6, C and D).

Prss8^{KO} mice did not differ in body weight, food and water intake, urine or feces output, and plasma and urinary sodium and potassium levels (Table 2). Colon histology was normal (Supplemental Figure 2A) without any apparent effect on the number of crypt cells (data not shown). The intestine length-to-body weight ratio was not different between the control (*Prss8*^{Lox}: 2.04±0.14; $n=6$), heterozygotes (*Prss8*^{Het}: 2.16±0.13; $n=6$), and knockout (*Prss8*^{KO}: 1.91±0.1; $n=7$). When we monitored the intestinal permeability after fluorescein isothiocyanate dextran supply in blood plasma, we found no difference amongst the groups, indicating a normal intestinal barrier function in the knockouts ($P=0.09$ to *Prss8*^{Het} and $P=0.39$ to *Prss8*^{Lox}) (Supplemental Figure 2B). When mRNA expression levels of ENaC subunits were quantified in distal colon and the kidney, there was no difference among the groups, with the exception of βENaC mRNA transcripts (KO versus Lox and Het; $P<0.05$) (Supplemental Figure 3, A and B). Western blot analysis using the anti-αENaC antibody revealed the full-length 93 kDa form and its cleaved 30 kDa form (Supplemental Figure 3C). The 95 kDa full-length β- and γENaC, including the cleaved 75 kDa γENaC proteins, are

Table 1. Physiologic parameters of $Scnn1a^{KO}$ mice

Parameters	RS Diet			LS Diet			HS Diet			High Potassium Diet (48 h)		
	$Scnn1a^{Lox}$	$Scnn1a^{Het}$	$Scnn1a^{KO}$	$Scnn1a^{Lox}$	$Scnn1a^{Het}$	$Scnn1a^{KO}$	$Scnn1a^{Lox}$	$Scnn1a^{Het}$	$Scnn1a^{KO}$	$Scnn1a^{Lox}$	$Scnn1a^{Het}$	$Scnn1a^{KO}$
n	7	5	9	5	5	4	4	4	4	4	4	4
Body weight (g)	25.83±1.5	25.92±0.4	26.75±1	25.50±1.2	24.80±0.2	23.83±0.7	25.83±0.6	25.41±0.5	25.13±0.4	26.34±0.3	25.21±0.2	25.23±0.2
Food intake/body weight ratio	0.13±0.02	0.15±0.0	0.14±0.03	0.12±0.01	0.13±0.0	0.13±0.0	0.11±0.02	0.12±0.02	0.11±0.0	0.11±0.03	0.10±0.01	0.11±0.01
Water intake/body weight ratio	0.16±0.01	0.16±0.03	0.22±0.02	0.16±0.04	0.18±0.01	0.22±0.02	0.19±0.01	0.20±0.10	0.21±0.01	0.12±0.03	0.11±0.01	0.12±0.01
Urine output/body weight ratio	0.05±0.01	0.06±0.01	0.08±0.01	0.06±0.02	0.05±0.01	0.06±0.06	1.6±0.01	1.7±0.01	1.75±0.02	0.04±0.03	0.05±0.01	0.04±0.01
Feces output/body weight ratio	0.02±0.0	0.02±0.01	0.02±0.0	0.02±0.0	0.02±0.0	0.02±0.0	0.01±0.0	0.01±0.0	0.01±0.0	0.01±0.0	0.01±0.0	0.01±0.0
Plasma Na$^+$ (mM)	151.6±1.2	149±0.2	161±4.2	148.2±2.2	153±2.4	148±1.07	154±1.2	152±0.2	157±4.3	159.8±3.1	162±4.2	159.7±2.1
Plasma K$^+$ (mM)	5.2±0.2	4.28±0.2	5.1±0.28	4.23±0.2	4.62±0.2	4.83±0.07	5.1±0.29	4.5±0.2	5.1±0.2	4.3±0.1	4.1±0.5	4.4±0.5
Urinary Na$^+$ (mM/24 h)										0.39±0.03	0.34±0.1	0.37±0.1
Urinary K$^+$ (mM/24 h)										3.6±1	3.1±1.1	3.6±1.2

Physiologic parameters in $Scnn1a^{Lox}$, $Scnn1a^{Het}$, and $Scnn1a^{KO}$ mice on different diets. Data are mean±SEM.

equally present in all groups (Supplemental Figure 3, C–F). We finally measured ΔPD_{amil} after HS, RS, and LS diets that induced a progressive increase in plasma aldosterone levels in all groups (Figure 7, A–D). On HS diet, baseline ΔPD_{amil} and plasma aldosterone levels (0.1–0.2 nmol/L) were equally low (−8 to −10 mV), and cyclicity was maintained, although blunted (Figure 7, A and D). On RS diet, ΔPD_{amil} of $Prss8^{Lox}$ and $Prss8^{Het}$ mice increased markedly (−15 to −25 mV) with respect to HS diet, and (a.m./p.m.) cyclicity was readily observed (Figure 7, A and B). Despite increased (0.5 nmol/L) plasma aldosterone levels, the cyclicity of the $Prss8^{KO}$ group was blunted, mainly because of a significant decrease of ΔPD_{amil} in the afternoon. On LS diet, ΔPD_{amil} in $Prss8^{KO}$ remained significantly lower with blunted cyclicity, although plasma aldosterone levels reached comparable high and even significant values ($P<0.05$ to $Prss8^{Lox}$ and $Prss8^{Het}$) (Figure 7, C and D). Interestingly, however, the feces wet/dry ratio was not altered in the knockout ($Prss8^{KO}$: 0.33±0.02 versus controls; $Prss8^{Lox}$: 0.31±0.02 and $Prss8^{Het}$: 0.37±0.02), and sodium, but not potassium, was significantly lost in feces from the knockouts ($P<0.05$) (Figure 7, E and F).

In summary, our data clearly show that *in vivo* stimulation of the amiloride-sensitive ENaC-mediated sodium transport is dependent on the expression of the membrane-bound serine protease CAP1/*Prss8* and more striking in the afternoon, when the RAAS is maximally activated.

DISCUSSION

ENaC-Mediated Electrogenic Sodium Transport Is Limiting for the Final Absorption of Sodium in Distal Colon and Rectum: Evidence for Colon-Specific Haploinsufficiency

In the present study, we studied mice with an efficient deletion of αENaC along the colon and found a strict gene dosage effect at the mRNA transcript and protein expression levels (Figure 1). Electrogenic sodium transport in distal colon was mainly mediated by ENaC, even if a low but significant electrogenic transport was measured after amiloride application (Figure 2). We cannot exclude some residual ENaC activity caused by incomplete recombination, although on a HS diet, mRNA expression of ENaC subunits should be rather repressed. Sodium/hydrogen exchanger 3 that is sensitive to amiloride is electroneutral and thus, undetectable by our PD measurements (Figure 2). On RS diet, despite increased plasma aldosterone levels, the ENaC KO mice remained at a low ΔPD_{amil}. Under LS diet, a significant dissociation between the heterozygotes and the floxed ($Scnn1a^{Lox}$) group was observed, indicating haploinsufficiency possibly caused by upregulation of AT1 receptors, although those mice showed an intact capacity to maintain BP and sodium balance.[28]

Differential Activation of RAAS on Lowering Salt Intake: Evidence for Colon-Specific Mineralocorticoid Resistance

In our study, we varied salt intake from HS to RS (19-fold) and from RS to LS, with an additional 17-fold decrease in salt intake
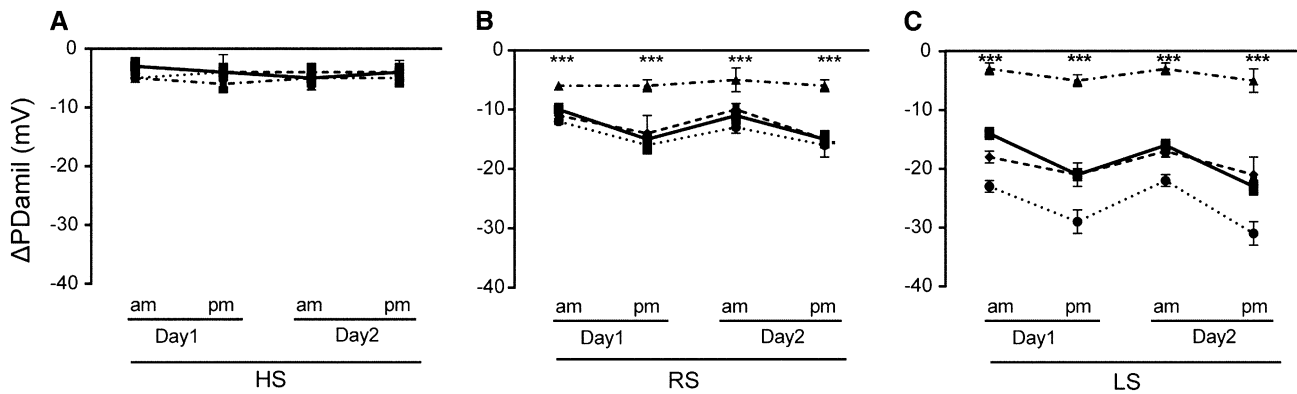
Figure 2. Colonic sodium transport is impaired in $Scnn1a^{KO}$ mice. Morning and afternoon measurements of amiloride-sensitive rectal PD (ΔPDamil) on 2 consecutive days in $Scnn1a^{Lox}$ mice ($n=7$; line), $Scnn1a^{Het}$ ($n=7$; dashed line), $Scnn1a^{Hetc}$ ($n=7$; dotted line), and $Scnn1a^{KO}$ ($n=8$; dashed/dotted line) mice treated with (A) HS, (B) RS, or (C) LS diet. ***$P<0.001$. Values are mean$\pm$SEM.
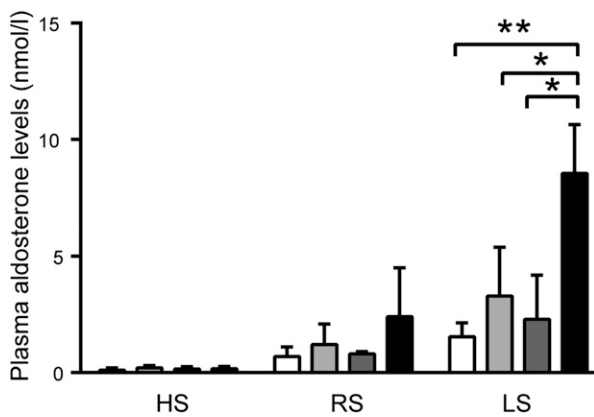

Figure 3. $Scnn1a^{KO}$ mice show elevated plasma aldosterone levels. Plasma aldosterone (nanomoles per liter) concentrations in $Scnn1a^{Lox}$ ($n=6$; white), $Scnn1a^{Het}$ ($n=7$; light gray), $Scnn1a^{Hetc}$ ($n=6$; dark gray), and $Scnn1a^{KO}$ ($n=7$; black) mice were analyzed on various sodium diets. *$P<0.05$; **$P<0.01$. Values are mean$\pm$SEM.

(Supplemental Figure 4). The $Scnn1a^{KO}$ mice showed 14-fold (versus 7-fold in control groups, $P<0.05$; HS to RS) increased aldosterone response that declined on switch from RS to LS to a 4-fold ($P<0.01$; versus 2-fold) induction (Supplemental Figure 4). Absence of ENaC in the colon and consequently, failure of the colon to absorb sodium against an electrochemical gradient might lead to a colon-specific salt-losing syndrome accompanied by high aldosterone response, which was shown by the clear correlation between plasma aldosterone (P_{aldo}) levels and ΔPD$_{amil}$ response; the KO mice remained unresponsive, whereas the $Scnn1a^{Lox}$ mice stayed sensitive to increased P_{aldo}. The response of the heterozygous mice was intermediate ($P<0.05$) (Supplemental Figures 4 and 5). We interpreted these data as indicating a colon-specific mineralocorticoid resistance (or decreased aldosterone responsiveness) that led to a colon-specific PHA-1 phenotype. Interestingly, a mirrored image of this phenotype was observed in the colon of Liddle mice that harbor a point mutation within the βENaC subunit, leading constitutively to hyperactivity of ENaC and an increased aldosterone responsiveness of the sodium transport in colon.[19,29]

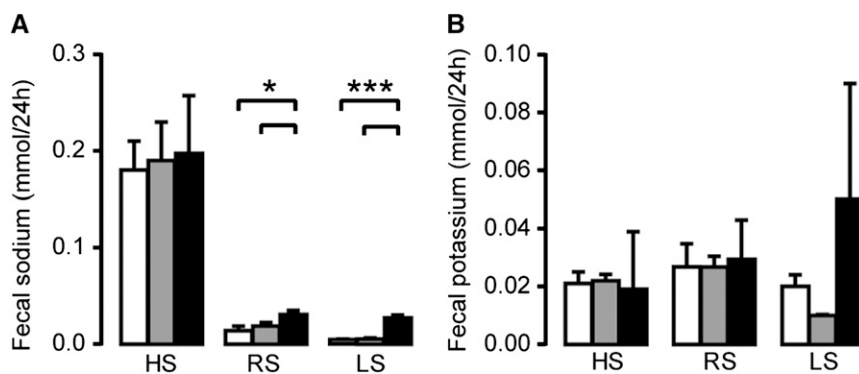### Differential Effect of Colon-Specific αENaC Knockouts on Sodium and Potassium Balance

As summarized in Figure 8, on HS diet, $Scnn1a^{KO}$ mice exhibit a sodium balance, and the total recovery of urinary and fecal sodium accounts for approximately 85% of sodium intake. From HS to LS diet, we found a progressive fecal sodium loss in $Scnn1a^{Het}$, $Scnn1a^{Hetc}$ and $Scnn1a^{KO}$ mice. Under LS, the fecal loss of sodium is compensated for by a maximal retention of sodium in the kidney because of high P_{aldo} (Figures 4 and 8). The missing sodium might be caused by loss into the transcellular fluid compartment, which may account for about 6% along the entire intestine and/or into the skin

Figure 4. Increased sodium loss through feces in $Scnn1a^{KO}$ mice. Measurements of (A) sodium and (B) potassium electrolytes levels in feces from $Scnn1a^{Lox}$ ($n=6$; white), $Scnn1a^{Het}$ ($n=7$; light gray), and $Scnn1a^{KO}$ ($n=7$; black) mice on various sodium diets. Values are mean$\pm$SEM. *$P<0.05$; ***$P<0.001$, $Scnn1a^{KO}$ versus $Scnn1a^{Lox}$ and $Scnn1a^{Het}$ mice.
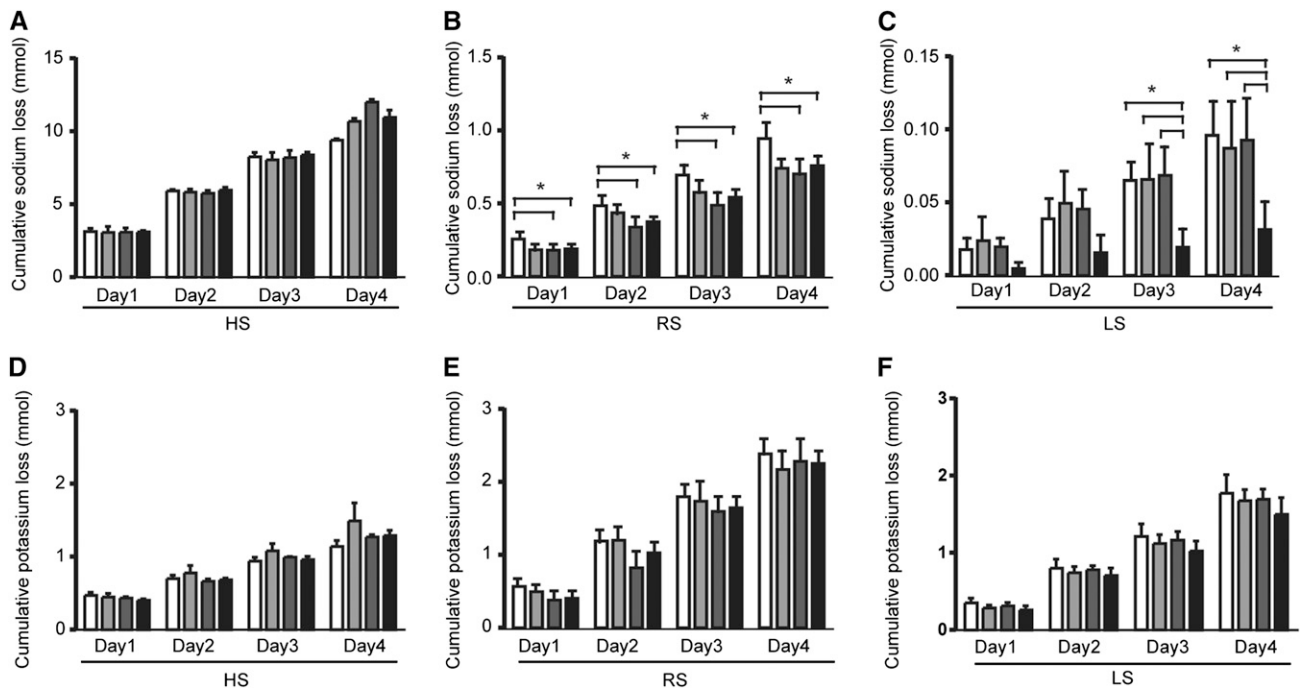
Figure 5. Diet-dependent reduced sodium loss in urine of $Scnn1a^{KO}$ mice. Measurement of cumulative urinary (A–C) sodium and (D–F) potassium electrolyte levels in $Scnn1a^{Lox}$ ($n=8$; white), $Scnn1a^{Het}$ ($n=7$; light gray), $Scnn1a^{Hetc}$ ($n=8$; dark gray), and $Scnn1a^{KO}$ ($n=8$; black) mice on (A and D) HS, (B and E) RS, and (C and F) LS diets; $*P<0.05$. Values are mean±SEM.

compartment.[30] Although systemic PHA-1 is normally also characterized by hyperkalemia, we did not find a shift in the potassium balance in the $Scnn1a^{KO}$ mice (Figures 4 and 5), which may be explained by differentially regulated and spatially separated electrogenic sodium absorption and potassium secretion.[31]

CAP1 Regulates Colon ENaC Activity by Blunting Its Circadian Cyclicity

Previous studies have emphasized the importance of CAP1/Prss8 *in vivo*[32–35] and its implication in ENaC regulation in alveolar fluid clearance and lung fluid balance.[26] In colon, we clearly identify CAP1/Prss8 as a protease activating ENaC *in vivo*, because on RS and LS diets, ENaC-mediated transport becomes limiting in $Prss8^{KO}$ mice (Figure 7). These data are in the same line as recent findings in hairless (fr^{CR}) rats and frizzy (fr/fr) mice harboring spontaneous mutations of CAP1/Prss8.[32] We do not see an implication of CAP1/Prss8 in epithelial barrier formation and permeability in colon (Supplemental Figure 2), which is contrary to mice that specifically lack CAP1/Prss8 in the epidermis and exhibit a severely impaired epidermal barrier caused by defective function of tight junctions.[34] Interestingly, lack of the serine protease in colon superficial cells is not consistent with a failure to cleave ENaC, because the cleaved 75 kDa ENaC fragment is present in $Prss8^{KO}$ mice (Supplemental Figure 3). These data are consistent with previous findings, where the 80 kDa and the cleaved 70 kDa γENaC protein forms were detected when CAP1/Prss8 was absent in lung.[26] This lack of difference in γ-cleavage is maybe not too surprising in view of the relative small difference in ΔPD_{amil} between the KO and the controls.

In conclusion, we showed that, in the colon of mice lacking ENaC and/or CAP1/*Prss8*, amiloride-sensitive sodium transport is drastically diminished. This result leads to increased fecal sodium loss, which is accompanied by mineralocorticoid resistance in ENaC-deficient mice. In patients with PHA-1 mutations, it might become pathophysiologically relevant and aggravate sodium loss, particularly on low dietary salt intake. Because the amount of sodium in the body is the main determinant of extracellular volume, disturbances in sodium balance will lead to clinical situations of volume depletion or overload; the latter will lead to arterial hypertension and heart failure. In CKD, when the ability of the kidneys to excrete sodium decreases, pharmacological inhibition of colonic ENaC may lead to increased intestinal excretion of sodium, which may help to maintain sodium homeostasis in CKD, where diuretics have only limited success.

CONCISE METHODS

Intestine-Specific CAP1/*Prss8* and αENaC-Deficient Mice

Intestine-specific αENaC (*Scnn1a*) or CAP1/*Prss8* knockout mice were generated by interbreeding *Villin::Cre* transgenic mice, which were heterozygous mutant for the αENaC[6] or CAP1/*Prss8*[34] knockout allele, with mice homozygous for the respective conditional alleles $Scnn1a^{loxlox}$[36] or CAP1/$Prss8^{lox/lox}$.[37] To generate an intestine-specific αENaC KO, we mated $Scnn1a^{+/-}$; $villin::Cre^{tg/0}$ mice with mice harboring two floxed αENaC alleles ($Scnn1a^{loxlox}$). Age-matched wild type-like $Scnn1a^{lox/+}$($Scnn1a^{Lox}$), heterozygous mutant $Scnn1a^{lox/-}$ ($Scnn1a^{Het}$),
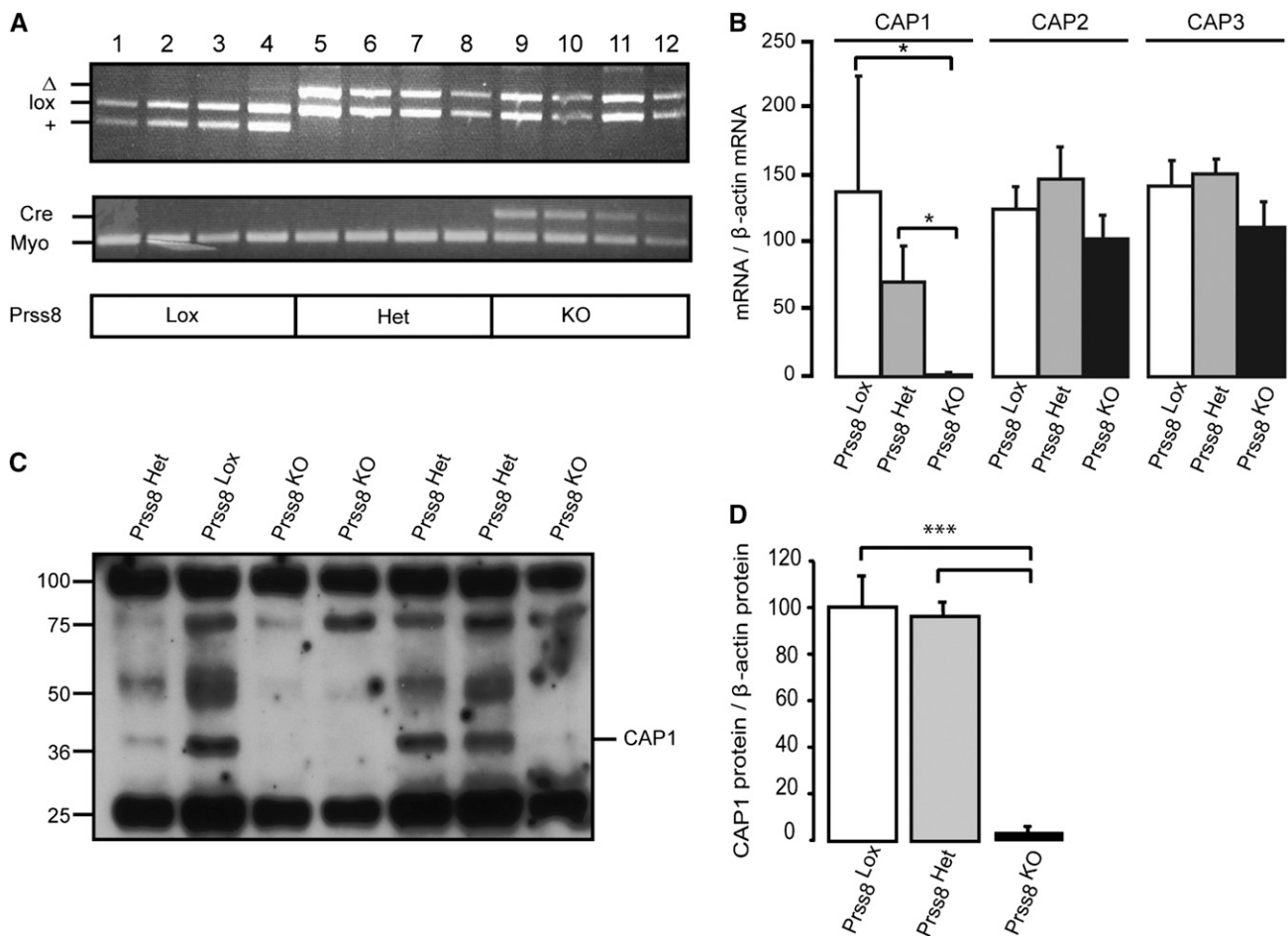
Figure 6. Loss of *Prss8* mRNA transcript and protein expression in colonic superficial cell-specific *Prss8*KO mice. DNA, mRNA, and proteins samples were analyzed from isolated scraped intestinal superficial cells as indicated. (A) DNA-based PCR analysis on ear biopsies using primers distinguishing wild type (+; 379 bp), lox (413 bp), and Δ (473 bp) alleles in *Prss8*lox/+ (*Prss8*Lox; lanes 1–4), *Prss8*lox/Δ (*Prss8*Het; lanes 5–8), and *Prss8*Δ/lox; *villin::Cre*tg/+ (*Prss8*KO; lanes 9–12) littermates. The *villin::Cre* transgene (400 bp) and myogenin (internal control) are detected using specific primers. (B) Quantification of CAP1/*Prss8*, CAP2/*Tmprss4*, and CAP3/*SP14* mRNA transcripts by quantitative RT-PCR in cells from *Prss8*Lox (n=4; white), *Prss8*Het (n=5; gray), and *Prss8*KO (n=8; black) mice. Data are expressed as the ratio of mRNA/β-actin mRNA. *P<0.05. (C) Representative immunoblot showing the expression of CAP1/*Prss8* and β-actin protein in cells from *Prss8*Lox, *Prss8*Het, and *Prss8*KO. (D) Quantification of CAP1/*Prss8* signals in *Prss8*Lox (n=4; white), *Prss8*Het (n=5; gray), and *Prss8*KO (n=6; black) cells analyzed with ImageJ software. ***P<0.001. Results are expressed as the ratio of CAP1/*Prss8* protein/β-actin protein. Values are mean±SEM.

intestine-specific heterozygous mutant *Scnn1a*lox/+; *villin::Cre*tg/0 (*Scnn1a*Hetc), and intestine-specific αENaC knockout *Scnn1a*lox/−, *villin::Cre*tg/0 (*Scnn1a*KO) mice were obtained. To generate intestine-specific CAP1/*Prss8* KO, we mated *Prss8*Δ/+; *villin::Cre*tg/0 mice with mice harboring two floxed CAP1/*Prss8* (*Prss8*loxlox). Age-matched wild type-like CAP1/*Prss8*lox/+ (*Prss8*Lox), heterozygous mutant CAP1/*Prss8*lox/Δ (*Prss8*Het), intestine-specific heterozygous mutant CAP1/*Prss8*lox/+; *villin::Cre*tg/0 (*Prss8*Hetc), and intestine-specific CAP1/ *Prss8* knockout CAP1/*Prss8*lox/Δ; *villin::Cre*tg/0 (*Prss8*KO) mice were obtained.

All animal work was conducted according to Swiss federal guidelines. All mice were kept in the animal facility under animal care regulations of the University of Lausanne. They were housed in individual ventilated cages at 23±1°C with a 12-hour light/dark cycle. All animals were supplied with food and water *ad libitum*. This study

has been reviewed and approved by the "Service de la consommation et des affaires vétérinaires" of the Canton of Vaud, Switzerland. If not otherwise indicated, 6- to 12-week-old age-matched male and female αENaC and CAP1/*Prss8* control and experimental (knockout) mice (homozygous for *Ren-1*c) were fed for at least 3 weeks on an RS (0.17% Na+), HS (3.2% Na+), or LS (0.01% Na+) diet. All diets were obtained from ssniff Spezialdiäten GmbH (Soest, Germany).

Genotyping

Genotyping by PCR was performed using the following primers: **CAP1/ *Prss8*+/lox/Δ:** *Prss8–1* sense (5′-GCAGTTGTAAGCTGTCATGTG-3′); *Prss8–2* sense (5′-CAGCAGCTGAGGTACCACT-3′); *Prss8-3* antisense (5′-CCAGGAAGCATAGGTAGAAG-3′); **αENaC** +/− :αENaC+/− -1 antisense (5′-TTAAGGGTGCACACAGTGACGGC-3′); αENaC+/− -2

Table 2. Physiologic parameters of Prss8^{KO} mice

Parameters	RS Diet			LS Diet			HS Diet		
	Prss8^{Lox}	Prss8^{Het}	Prss8^{KO}	Prss8^{Lox}	Prss8^{Het}	Prss8^{KO}	Prss8^{Lox}	Prss8^{Het}	Prss8^{KO}
n	7	5	9	5	5	4	4	4	4
Body weight (g)	24.95±0.6	24.12±0.3	25.15±0.4	23.93±0.8	22.30±0.2	22.15±0.4	21.30±0.6	21.45±0.4	20.12±0.3
Food intake/body weight ratio	0.12±0.3	0.13±0.3	0.12±0.9	0.12±0.2	0.13±0.3	0.12±0.3	0.12±0.2	0.12±0.2	0.11±0.3
Water intake/body weight ratio	0.15±0.1	0.15±0.3	0.16±0.2	0.16±0.1	0.16±0.1	0.18±0.1	0.17±0.1	0.18±0.1	0.19±0.1
Urine output/body weight ratio	0.04±1.1	0.05±0.4	0.05±0.3	0.05±0.1	0.05±0.1	0.06±0.3	1.8±0.1	1.8±0.1	1.85±0.3
Feces output/body weight ratio	0.02±0.2	0.01±0.0	0.01±0.0	0.02±0.0	0.01±0.0	0.02±0.0	0.01±0.0	0.02±0.0	0.01±0.0
Plasma Na$^+$ (mM)	154±4.3	155±1.5	152±2.9	138±1.5	142±1.2	135±3.8	147±1.8	143±1.02	142±1.02
Plasma K$^+$ (mM)	4.5±0.1	4.7±0.09	4.8±0.1	4.6±0.2	4.3±0.5	4.4±0.1	5±0.1	4.8±0.2	5.08±0.1
Urinary Na$^+$ (mM)	37±1.9	24±1.3	25±8.2	6.6±1.0	6.39±0.34	8.3±0.48	163±10.2	168±14.56	186±11.7
Urinary K$^+$ (mM)	35±1.8	30.2±2.3	30.19±2.4	59±8.1	58±3.23	62±3.05	25.5±3.1	26.34±4.1	26.44±2.8

Physiologic parameters in Prss8^{Lox}, Prss8^{Het}, and Prss8^{KO} mice on different diets. Data are mean±SEM.
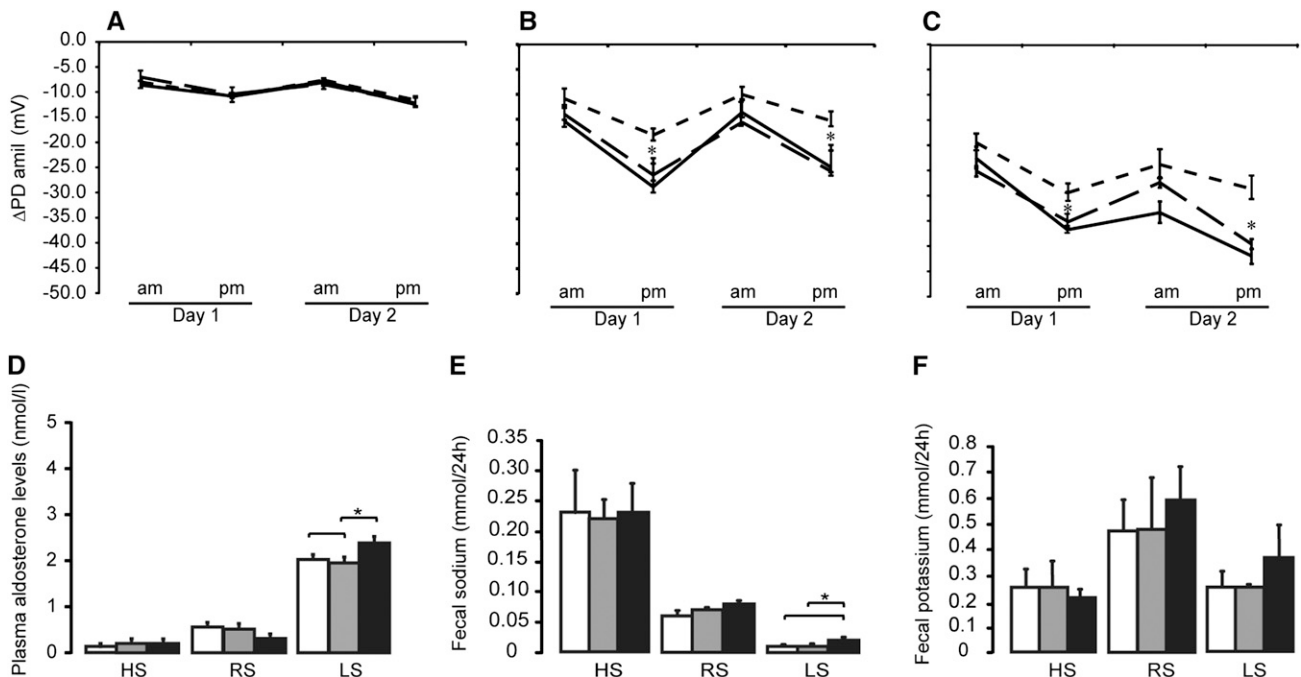

Figure 7. CAP1/Prss8 is as a regulator of ENaC in the colon. (A–C) Morning and afternoon measurements of amiloride-sensitive rectal PD (ΔPD$_{amil}$) on 2 consecutive days in control Prss8^{Lox} (n=8; line), Prss8^{Het} (n=7; long dashed line), and Prss8^{KO} (n=8; dashed line) mice treated with (A) HS, (B) RS, and (C) LS diet. *$P<0.05$. (D) Plasma aldosterone concentrations after various sodium diets. (E) Fecal sodium and (F) fecal potassium concentrations in Prss8^{Lox} (n=5; white), Prss8^{Het} (n=6; gray), and Prss8^{KO} (n=6; black) mice on HS, RS, and LS diets. *$P<0.05$. Values are mean±SEM.

antisense (5′-TTTGTCACGTCCTGCACGACGCG-3′); αENaC$^{+/-}$-3 sense (5′-AACTCCAGAAGGTCAGCTGGCTC-3′); **αENaC$^{+/lox/Δ}$:** αENaC$^{lox/+}$-1 sense (5′-CTCAATCAGAAGGACCCTGG-3′); αENaC$^{lox/+}$-2 sense (5′-GTCACTGTGTGTGCACCCTTAA-3′); αENaC$^{lox/+}$-3 antisense (5′-GCAAAAGATCTTATCCACC-3′).

If not otherwise stated, 35 cycles were run, and each run consisted of 1 minute each at 94°C, 56°C (58°C for ENaC), and 72°C. The *Villin::Cre* transgene was detected by PCR using the following primers: Villin-Cre sense (5′-CCTGGAAAATGCTTCTGTCCG-3′) and Villin-Cre antisense

(5′-CAGGGTGTTATAAGCAATCCC-3′). Myogenin-specific primers (sense, 5′-TTACGTCCTCGTGGACAGC-3′) and (antisense, 5′-TGGGCTGGGTGTTAGTCTTA-3′) were used to control the DNA integrity of each sample.

Quantitative RT-PCR Analysis on Distal Colon and Kidney Samples

Total RNA was prepared from freshly isolated mouse colon superficial cells and whole kidney using the RNeasy Extraction Kit (Qiagen,
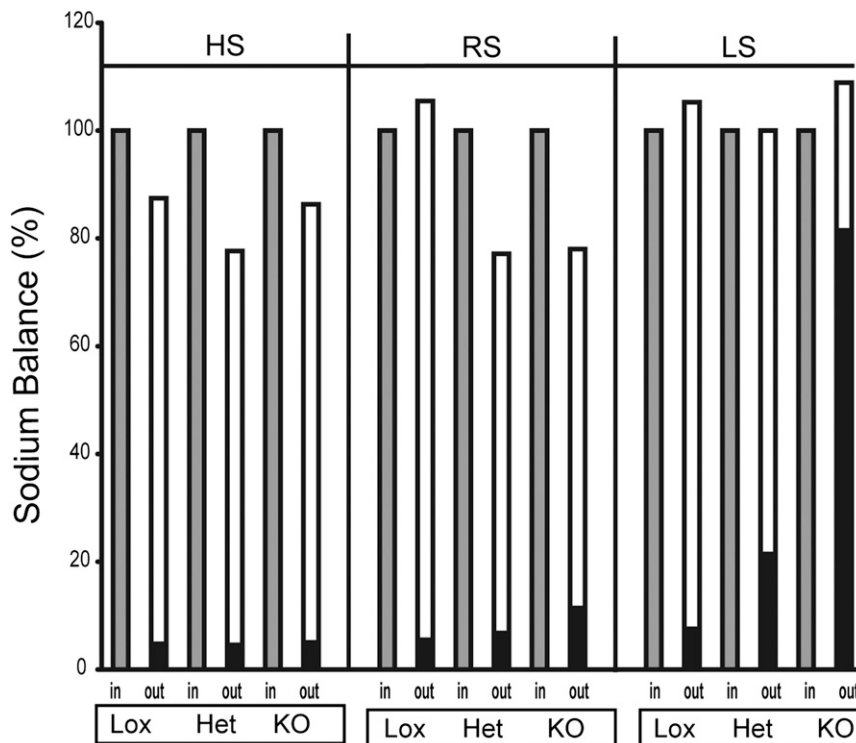
Figure 8. Diet-dependent shift of sodium balance in Scnn1a^KO mice. Sodium balance is considered as the ratio between the quantity of sodium output (in urine or feces) at day 1 normalized by the quantity of sodium intake at day 1. Data were taken from the experiments summarized in Table 1 (food intake), Figure 4 (fecal sodium), and Figure 5 (urinary sodium). For each of the genotypes (Scnn1a^Lox, Scnn1a^Het, and Scnn1a^KO), the average sodium intake through food (gray column) is compared with urinary sodium output (white column) and fecal sodium output (black column) on HS, RS, or LS diet.

BHQ1–3′; ***Prss14***: FOR, 5′-GAAGCTTT-GATGTCGCTCCC-3′, REV, 5′-GGAGGGTGA-GAAGGTGCCA-3′, Probe, 5′-FAM- CCACG-CTGTGGTGCGGCTG-BHQ-1–3′; ***Tmprss4***: FOR, 5′-AGTAGGCATCGTGAGCTGGG-3′, REV, 5′-GGACGGCAGCGTTACATCTC-3′, Probe, 5′-FAM-ATGGATGCGGCGGCCCAA-BHQ1–3′.

Western Blot Analysis

Animals (3–4 months) were kept under an RS or LS diet for 2 weeks. Colon and kidney were freshly isolated and snap frozen in liquid nitrogen. Proteins were extracted by homogenization using polytron and sonication with an IKA sonicator in 8 M urea buffer; then, they were incubated for 30 minutes on ice and centrifuged for 30 minutes at 4°C at 14,000 rpm. The supernatant was taken and centrifuged again for 10 minutes at 4°C at 14,000 rpm. The supernatant was used to detect the protein concentration with a BCA protein kit (PIERCE, Rockford, IL). Samples of protein extracts were separated by SDS-PAGE on 10% acrylamide gels, electrically transferred to polyscreen polyvinylidene difluoride transfer membrane (Perkin Elmer, Boston, MA), and subsequently probed for CAP1/Prss8, Scnn1a (αENaC), Scnn1b (βENaC), Scnn1g (γENaC), and β-actin using primary rabbit antibodies Scnn1a (1:500),[38] Scnn1b and Scnn1g (1:1000),[39] CAP1 (1:1000),[40] β-actin (1:1000; Sigma-Aldrich), and anti-rabbit IgG secondary antibody (1:10,000; Amersham, Burkinghamshire, UK). The signal was developed with the ECL+ system (Hyperfilm ECL; Amersham, Burkinghamshire, UK). Quantification of protein level was obtained using National Institutes of Health image software.

Histologic Analysis of Proximal and Distal Colon

Colon was fixed in 4% paraformaldehyde overnight and subjected to paraffin embedding and sectioning (4-μm sections). Sections were stained with hematoxylin and eosin and examined by light microscopy using an Axioplan microscope (Carl Zeiss Microimaging, Inc., Oberkochen/Jena, Germany), and images were acquired with a high-sensibility digital color camera (Carl Zeiss Microimaging, Inc.).

Determination of Intestine Structural and Functional Parameters

Determination of Length-to-Body Weight.
Length of intestine (centimeters) was measured and normalized to the body weight in 3-month-old mice. Results were determined as mean±SEM.

Feces Wet-to-Dry Weight and Electrolyte Measurements.
Feces samples were collected from age-matched 3-month-old control (n=6), heterozygote mutant (n=6), and knockout (n=7) mice that

Hilden, Germany). The RNA (1 μg/sample) was reverse-transcribed at 37°C for 1 hour using superscript II RNAse H reverse transcriptase (Invitrogen, Basel, Switzerland) and oligo-dT(20) primers (Invitrogen). The products were then diluted 10 times before proceeding with the real-time PCR reaction. Real-time PCRs were performed by Taqman PCR with the Applied Biosystems 7500 (Foster City, CA). The primer and probe mix (2×) (Mm00504792 m1 for mCAP1 and 4352341E for β-actin) was purchased with the Universal Taqman Mix (2×) and used according to the manufacturer's instructions (Applied Bio Systems, Foster City, CA). Quantification of fluorescence was performed with the $\Delta\Delta C_T$ normalized to β-actin. Each measurement was performed in duplicate. Additional primers have been used: ***Scnn1a***: FOR, 5′-GCACCCTTAATCCTTACAGATACACTG-3′ and REV, 5′-CAAAAAGCGTCT-GTTCCGTG-3′, Probe 5′-FAM-AGAG-GATC-TGGAAGAGCTGGACCGCA-BHQ1–3′; ***Scnn1b***: FOR, 5′-GGGTGCTGGTGGACAAGC-3′, REV, 5′-ATGTGGTCTTGGAAACAG-GAATG-3′, Probe, 5′-FAM-CAGTCCCTGCACCATGAA-CGGCT-BHQ1–3′; ***Scnn1g***: FOR, 5′-AACCTTACAGCCAGTGCACAGA-3′, REV, 5′-TTGGAAGCATGAGTAAAGGCAG-3′, Probe, 5′-FAM-AGC-GATGTGCCCGTCACAAA>CATCT-BHQ1–3′; ***Prss8***: FOR, 5′-CCCATCTGCCTCCCTGC-3′, REV, 5′-CCATCCCGTGACAGTA-CAGTGA-3′, Probe, 5′-FAM CCAATGCCTCCTTTCCCAACGGC-

Amersham, Burkinghamshire, UK). The signal was developed with the ECL+ system (Hyperfilm ECL; Amersham, Burkinghamshire, UK). Quantification of protein level was obtained using National Institutes of Health image software.

were kept under RS diet in metabolic cages for 4 consecutive days. Wet-to-dry weight was determined by determining the wet weight feces samples collected within 24 hours, drying the feces at 80°C for another 24 hours, and weighing again to calculate the wet-to-dry feces ratio as described.[32] Sodium and potassium fecal electrolytes were determined from samples as described.[41] Briefly, the feces were collected over 2 consecutive days, weighed, and resuspended overnight into 0.75 N nitric acid at 4°C. After centrifugation, an aliquot of supernatant was measured for Na^+ and K^+ content with a flame photometer (943 Electrolyte Analyzer; Instrumentation Laboratory, UK).

Intestinal Permeability Assay.

In vivo intestinal permeability was determined as described previously.[42] Briefly, mice were kept under RS diet and gavaged with 10 ml/kg solution of 22 mg/ml fluorescein isothiocyanate–dextran (4 kDa; Sigma-Aldrich, St. Louis, MO) in PBS (pH 7.4). Three hours after gavage, plasma was collected at the end of the experiment and centrifuged at 3000 rpm for 20 minutes at 4°C. After a 1:1 dilution in PBS, the concentration of fluorescein was determined using a 96-plate reader with an excitation wavelength at 485 nm and an emission wavelength at 535 nm using serially diluted samples of the tracer as a standard.

Metabolic Cage Studies.

Six- to twelve-week-old age-matched control and knockout mice were individually placed in metabolic cages (Tecniplast, Buguggiate, Italy) for 5 consecutive days to measure urine and feces output. Food and water intake were daily measured. For the entire experiment, mice had free access to food and water. During experimental days, urine and feces were collected. Sodium intake was measured as sodium (millimoles) intake per day in percentage of total food intake. Sodium output was measured as urinary sodium (millimoles) and fecal sodium (millimoles) excretion per day in percentage of total food intake.

High Potassium Diet

Experimental mice and control mice were placed in individual metabolic cages and fed a standard diet for 2 consecutive days (0.95% potassium), which was followed by 2 days on 5% potassium in drinking water (the potassium was added as KCl). During the experiment, the animals had free access to food and water. During experimental days, urine was collected. Blood was collected 2 days after the experiment.

Analyses of Urinary ~~Electrolytes and Blood~~ Plasma ~~Analysis~~

Urine samples (24 hours) were collected in metabolic cages. Blood samples were collected at the end of the experiment. Urine and plasma electrolytes were analyzed using an Instrumentation Laboratory 943 Electrolyte Analyzer, UK.

Blood Collection for Aldosterone Measurements

Control and knockout mice (8–12 weeks old) were kept in standard cages with free access to food and water and fed with RS, LS, or HS diets for 12 consecutive days. At the end of the experiment, blood samples were collected. Plasma aldosterone levels were measured according to standard procedures using a radioimmunoassay (Coat-A-Count RIA Kit; Siemens Medical Solutions Diagnostics,

Ballerup, Denmark).[43] Samples with values >1200 pg/ml were further diluted using a serum pool with a low aldosterone concentration (<50 pg/ml). Aldosterone concentration is indicated as nanomoles per liter.

Amiloride-Sensitive Rectal Transepithelial PD Measurements

Mice were fed a LS or HS diet for 3 weeks. Amiloride-sensitive transepithelial rectal PD measurements were performed as previously described.[27,32] Briefly, rectal PD and amiloride-sensitive rectal PD were measured in the morning (10 a.m. to 12 p.m.) and the afternoon (4 p.m. to 6 p.m.) on 2 days of the same week. The rectal PD was monitored continuously by a VCC600 electrometer (Physiologic Instruments, San Diego, CA) connected to a chart recorder. After stabilization of rectal PD (approximately 1 minute), 0.05 ml saline solution was injected through the first barrel as a control maneuver, and the PD was recorded for another 30 seconds. A similar volume of saline solution containing 25 μmol/L amiloride was injected through the second barrel of the pipette, and the PD was recorded for 1 minute. The PD was recorded before and after the addition of amiloride to determine the amiloride-sensitive PD.

Statistical Analyses

Results are presented as mean±SEM. Throughout the study (if not otherwise stated), data were analyzed by one-way ANOVA. Unpaired *t* test was used for the comparison between two groups (Figure 7D). $P < 0.05$ was considered statistically significant.

DISCLOSURES

None.

REFERENCES

1. Staub O, Loffing J: Mineralocorticoid action in the aldosterone sensitive distal nephron. In: *Seldin and Giebisch's The Kidney*, 5th Ed., edited by Alpern RJ, Moe OW, Caplan M, London, Academic, 2013, pp 1181–1211

2. Zennaro MC, Jeunemaitre X, Boulkroun S: Integrating genetics and genomics in primary aldosteronism. *Hypertension* 60: 580–588, 2012

3. Lifton RP: *Genetic Diseases of the Kidney*, Amsterdam, Elsevier/Academic Press, 2009

4. Canessa CM, Horisberger JD, Rossier BC: Epithelial sodium channel related to proteins involved in neurodegeneration. *Nature* 361: 467–470, 1993

5. Canessa CM, Schild L, Buell G, Thorens B, Gautschi I, Horisberger JD, Rossier BC: Amiloride-sensitive epithelial Na+ channel is made of three homologous subunits. *Nature* 367: 463–467, 1994

6. Hummler E, Barker P, Gatzy J, Beermann F, Verdumo C, Schmidt A, Boucher R, Rossier BC: Early death due to defective neonatal lung liquid clearance in alpha-ENaC-deficient mice. *Nat Genet* 12: 325–328, 1996

7. Barker PM, Nguyen MS, Gatzy JT, Grubb B, Norman H, Hummler E, Rossier B, Boucher RC, Koller B: Role of gammaENaC subunit in lung liquid clearance and electrolyte balance in newborn mice. Insights into perinatal adaptation and pseudohypoaldosteronism. *J Clin Invest* 102: 1634–1640, 1998

8. McDonald FJ, Yang B, Hrstka RF, Drummond HA, Tarr DE, McCray PB Jr, Stokes JB, Welsh MJ, Williamson RA: Disruption of the beta subunit of the epithelial Na+ channel in mice: Hyperkalemia and neonatal death associated with a pseudohypoaldosteronism phenotype. *Proc Natl Acad Sci U S A* 96: 1727–1731, 1999

9. Rubera I, Loffing J, Palmer LG, Frindt G, Fowler-Jaeger N, Sauter D, Carroll T, McMahon A, Hummler E, Rossier BC: Collecting duct-specific gene inactivation of alphaENaC in the mouse kidney does not impair sodium and potassium balance. *J Clin Invest* 112: 554–565, 2003

10. Duc C, Farman N, Canessa CM, Bonvalet JP, Rossier BC: Cell-specific expression of epithelial sodium channel alpha, beta, and gamma subunits in aldosterone-responsive epithelia from the rat: Localization by in situ hybridization and immunocytochemistry. *J Cell Biol* 127: 1907–1921, 1994

11. Kunzelmann K, Mall M: Electrolyte transport in the mammalian colon: Mechanisms and implications for disease. *Physiol Rev* 82: 245–289, 2002

12. Koyama K, Sasaki I, Naito H, Funayama Y, Fukushima K, Unno M, Matsuno S, Hayashi H, Suzuki Y: Induction of epithelial Na+ channel in rat ileum after proctocolectomy. *Am J Physiol* 276: G975–G984, 1999

13. Lingueglia E, Renard S, Waldmann R, Voilley N, Champigny G, Plass H, Lazdunski M, Barbry P: Different homologous subunits of the amiloride-sensitive Na+ channel are differently regulated by aldosterone. *J Biol Chem* 269: 13736–13739, 1994

14. Renard S, Voilley N, Bassilana F, Lazdunski M, Barbry P: Localization and regulation by steroids of the alpha, beta and gamma subunits of the amiloride-sensitive Na+ channel in colon, lung and kidney. *Pflügers Arch* 430: 299–307, 1995

15. Asher C, Wald H, Rossier BC, Garty H: Aldosterone-induced increase in the abundance of Na+ channel subunits. *Am J Physiol* 271: C605–C611, 1996

16. Sandle GI: Salt and water absorption in the human colon: A modern appraisal. *Gut* 43: 294–299, 1998

17. Pradervand S, Wang Q, Burnier M, Beermann F, Horisberger JD, Hummler E, Rossier BC: A mouse model for Liddle's syndrome. *J Am Soc Nephrol* 10: 2527–2533, 1999

18. Pradervand S, Vandewalle A, Bens M, Gautschi I, Loffing J, Hummler E, Schild L, Rossier BC: Dysfunction of the epithelial sodium channel expressed in the kidney of a mouse model for Liddle syndrome. *J Am Soc Nephrol* 14: 2219–2228, 2003

19. Bertog M, Cuffe JE, Pradervand S, Hummler E, Hartner A, Porst M, Hilgers KF, Rossier BC, Korbmacher C: Aldosterone responsiveness of the epithelial sodium channel (ENaC) in colon is increased in a mouse model for Liddle's syndrome. *J Physiol* 586: 459–475, 2008

20. Amasheh S, Barmeyer C, Koch CS, Tavalali S, Mankertz J, Epple HJ, Gehring MM, Florian P, Kroesen AJ, Zeitz M, Fromm M, Schulzke JD: Cytokine-dependent transcriptional down-regulation of epithelial sodium channel in ulcerative colitis. *Gastroenterology* 126: 1711–1720, 2004

21. Zeissig S, Bergann T, Fromm A, Bojarski C, Heller F, Guenther U, Zeitz M, Fromm M, Schulzke JD: Altered ENaC expression leads to impaired sodium absorption in the noninflamed intestine in Crohn's disease. *Gastroenterology* 134: 1436–1447, 2008

22. Vallet V, Chraibi A, Gaeggeler HP, Horisberger JD, Rossier BC: An epithelial serine protease activates the amiloride-sensitive sodium channel. *Nature* 389: 607–610, 1997

23. Vuagniaux G, Vallet V, Jaeger NF, Hummler E, Rossier BC: Synergistic activation of ENaC by three membrane-bound channel-activating serine proteases (mCAP1, mCAP2, and mCAP3) and serum- and glucocorticoid-regulated kinase (Sgk1) in Xenopus oocytes. *J Gen Physiol* 120: 191–201, 2002

24. Vuagniaux G, Vallet V, Jaeger NF, Pfister C, Bens M, Farman N, Courtois-Coutry N, Vandewalle A, Rossier BC, Hummler E: Activation of the amiloride-sensitive epithelial sodium channel by the serine protease mCAP1 expressed in a mouse cortical collecting duct cell line. *J Am Soc Nephrol* 11: 828–834, 2000

25. Adachi M, Kitamura K, Miyoshi T, Narikiyo T, Iwashita K, Shiraishi N, Nonoguchi H, Tomita K: Activation of epithelial sodium channels by prostasin in Xenopus oocytes. *J Am Soc Nephrol* 12: 1114–1121, 2001

26. Planès C, Randrianarison NH, Charles RP, Frateschi S, Cluzeaud F, Vuagniaux G, Soler P, Clerici C, Rossier BC, Hummler E: ENaC-mediated alveolar fluid clearance and lung fluid balance depend on the channel-activating protease 1. *EMBO Mol Med* 2: 26–37, 2010

27. Wang Q, Horisberger JD, Maillard M, Brunner HR, Rossier BC, Burnier M: Salt- and angiotensin II-dependent variations in amiloride-sensitive rectal potential difference in mice. *Clin Exp Pharmacol Physiol* 27: 60–66, 2000

28. Wang H, Garvin JL, Carretero OA: Angiotensin II enhances tubuloglomerular feedback via luminal AT(1) receptors on the macula densa. *Kidney Int* 60: 1851–1857, 2001

29. Pradervand S, Barker PM, Wang Q, Ernst SA, Beermann F, Grubb BR, Burnier M, Schmidt A, Bindels RJ, Gatzy JT, Rossier BC, Hummler E: Salt restriction induces pseudohypoaldosteronism type 1 in mice expressing low levels of the beta-subunit of the amiloride-sensitive epithelial sodium channel. *Proc Natl Acad Sci U S A* 96: 1732–1737, 1999

30. Machnik A, Neuhofer W, Jantsch J, Dahlmann A, Tammela T, Machura K, Park JK, Beck FX, Müller DN, Derer W, Goss J, Ziomber A, Dietsch P, Wagner H, van Rooijen N, Kurtz A, Hilgers KF, Alitalo K, Eckardt KU, Luft FC, Kerjaschki D, Titze J: Macrophages regulate salt-dependent volume and blood pressure by a vascular endothelial growth factor-C-dependent buffering mechanism. *Nat Med* 15: 545–552, 2009

31. Sorensen MV, Matos JE, Praetorius HA, Leipziger J: Colonic potassium handling. *Pflügers Arch* 459: 645–656, 2010

32. Frateschi S, Keppner A, Malsure S, Iwaszkiewicz J, Sergi C, Mérillat AM, Fowler-Jaeger N, Randrianarison N, Planès C, Hummler E: Mutations of the serine protease CAP1/Prss8 lead to reduced embryonic viability, skin defects, and decreased ENaC activity. *Am J Pathol* 181: 605–615, 2012

33. Hummler E, Dousse A, Rieder A, Stehle JC, Rubera I, Osterheld MC, Beermann F, Frateschi S, Charles RP: The channel-activating protease CAP1/Prss8 is required for placental labyrinth maturation. *PLoS One* 8: e55796, 2013

34. Leyvraz C, Charles RP, Rubera I, Guitard M, Rotman S, Breiden B, Sandhoff K, Hummler E: The epidermal barrier function is dependent on the serine protease CAP1/Prss8. *J Cell Biol* 170: 487–496, 2005

35. Frateschi S, Camerer E, Crisante G, Rieser S, Membrez M, Charles RP, Beermann F, Stehle JC, Breiden B, Sandhoff K, Rotman S, Haftek M, Wilson A, Ryser S, Steinhoff M, Coughlin SR, Hummler E: PAR2 absence completely rescues inflammation and ichthyosis caused by altered CAP1/Prss8 expression in mouse skin. *Nat Commun* 2: 161, 2011

36. Hummler E, Mérillat AM, Rubera I, Rossier BC, Beermann F: Conditional gene targeting of the Scnn1a (alphaENaC) gene locus. *Genesis* 32: 169–172, 2002

37. Rubera I, Meier E, Vuagniaux G, Mérillat AM, Beermann F, Rossier BC, Hummler E: A conditional allele at the mouse channel activating protease 1 (Prss8) gene locus. *Genesis* 32: 173–176, 2002

38. Sorensen MV, Grossmann S, Roesinger M, Gresko N, Todkar AP, Barmettler G, Ziegler U, Odermatt A, Loffing-Cueni D, Loffing J: Rapid dephosphorylation of the renal sodium chloride cotransporter in response to oral potassium intake in mice. *Kidney Int* 83: 811–824, 2013

39. Wagner CA, Loffing-Cueni D, Yan Q, Schulz N, Fakitsas P, Carrel M, Wang T, Verrey F, Geibel JP, Giebisch G, Hebert SC, Loffing J: Mouse model of type II Bartter's syndrome. II. Altered expression of renal sodium- and water-transporting proteins. *Am J Physiol Renal Physiol* 294: F1373–F1380, 2008

40. Planès C, Leyvraz C, Uchida T, Angelova MA, Vuagniaux G, Hummler E, Matthay M, Clerici C, Rossier B: In vitro and in vivo regulation of transepithelial lung alveolar sodium transport by serine proteases. *Am J Physiol Lung Cell Mol Physiol* 288: L1099–L1109, 2005

41. Meneton P, Schultheis PJ, Greeb J, Nieman ML, Liu LH, Clarke LL, Duffy JJ, Doetschman T, Lorenz JN, Shull GE: Increased sensitivity to K+ deprivation in colonic H,K-ATPase-deficient mice. *J Clin Invest* 101: 536–542, 1998

42. List K, Kosa P, Szabo R, Bey AL, Wang CB, Molinolo A, Bugge TH: Epithelial integrity is maintained by a matriptase-dependent proteolytic pathway. *Am J Pathol* 175: 1453–1463, 2009

43. Christensen BM, Perrier R, Wang Q, Zuber AM, Maillard M, Mordasini D, Malsure S, Ronzaud C, Stehle JC, Rossier BC, Hummler E: Sodium and potassium balance depends on αENaC expression in connecting tubule. *J Am Soc Nephrol* 21: 1942–1951, 2010

REFERENCES

Agarwal R, Afzalpurkar R, Fordtran JS (1994) Pathophysiology of potassium absorption and secretion by the human intestine. Gastroenterology 107:548-571.

Allan R, Steinberg DM, Dixon K, Cooke WT (1975) Changes in the bidirectional sodium flux across the intestinal mucosa in Crohn's disease. Gut 16:201-204.

Alvarez de la Rosa D, Li H, Canessa CM (2002) Effects of aldosterone on biosynthesis, traffic, and functional expression of epithelial sodium channels in A6 cells. J Gen Physiol 119:427-442.

Alvarez de la Rosa D, Zhang P, Naray-Fejes-Toth A, Fejes-Toth G, Canessa CM (1999) The serum and glucocorticoid kinase sgk increases the abundance of epithelial sodium channels in the plasma membrane of Xenopus oocytes. J Biol Chem 274:37834-37839.

Amasheh S, Barmeyer C, Koch CS, Tavalali S, Mankertz J, Epple HJ, Gehring MM, Florian P, Kroesen AJ, Zeitz M, Fromm M, Schulzke JD (2004) Cytokine-dependent transcriptional down-regulation of epithelial sodium channel in ulcerative colitis. Gastroenterology 126:1711-1720.

Amasheh S, Milatz S, Krug SM, Bergs M, Amasheh M, Schulzke JD, Fromm M (2009) Na+ absorption defends from paracellular back-leakage by claudin-8 upregulation. Biochem Biophys Res Commun 378:45-50.

Anantharam A, Tian Y, Palmer LG (2006) Open probability of the epithelial sodium channel is regulated by intracellular sodium. J Physiol 574:333-347.

Andreasen D, Vuagniaux G, Fowler-Jaeger N, Hummler E, Rossier BC (2006) Activation of epithelial sodium channels by mouse channel activating proteases (mCAP) expressed in Xenopus oocytes requires catalytic activity of mCAP3 and mCAP2 but not mCAP1. J Am Soc Nephrol 17:968-976.

Asher C, Wald H, Rossier BC, Garty H (1996) Aldosterone-induced increase in the abundance of Na+ channel subunits. Am J Physiol 271:C605-611.

Auberson M, Hoffmann-Pochon N, Vandewalle A, Kellenberger S, Schild L (2003) Epithelial Na+ channel mutants causing Liddle's syndrome retain ability to respond to aldosterone and vasopressin. Am J Physiol Renal Physiol 285:F459-471.

Banks MR, Farthing MJ (2002) Fluid and electrolyte transport in the small intestine. Current opinion in gastroenterology 18:176-181.

Barker PM, Nguyen MS, Gatzy JT, Grubb B, Norman H, Hummler E, Rossier B, Boucher RC, Koller B (1998) Role of gammaENaC subunit in lung liquid clearance and electrolyte balance in newborn mice. Insights into perinatal adaptation and pseudohypoaldosteronism. The Journal of clinical investigation 102:1634-1640.

Barmeyer C, Harren M, Schmitz H, Heinzel-Pleines U, Mankertz J, Seidler U, Horak I, Wiedenmann B, Fromm M, Schulzke JD (2004) Mechanisms of diarrhea in the interleukin-2-deficient mouse model of colonic inflammation. American journal of physiology Gastrointestinal and liver physiology 286:G244-252.

Barrett KE, Keely SJ (2000) Chloride secretion by the intestinal epithelium: molecular basis and regulatory aspects. Annu Rev Physiol 62:535-572.

Bassilana F, Champigny G, Waldmann R, de Weille JR, Heurteaux C, Lazdunski M (1997) The acid-sensitive ionic channel subunit ASIC and the mammalian degenerin MDEG form a heteromultimeric H+-gated Na+ channel with novel properties. J Biol Chem 272:28819-28822.

REFERENCES_____

Batlle E, Henderson JT, Beghtel H, van den Born MM, Sancho E, Huls G, Meeldijk J, Robertson J, van de Wetering M, Pawson T, Clevers H (2002) Beta-catenin and TCF mediate cell positioning in the intestinal epithelium by controlling the expression of EphB/ephrinB. Cell 111:251-263.

Berdiev BK, Qadri YJ, Benos DJ (2009) Assessment of the CFTR and ENaC association. Molecular bioSystems 5:123-127.

Bertog M, Cuffe JE, Pradervand S, Hummler E, Hartner A, Porst M, Hilgers KF, Rossier BC, Korbmacher C (2008) Aldosterone responsiveness of the epithelial sodium channel (ENaC) in colon is increased in a mouse model for Liddle's syndrome. J Physiol 586:459-475.

Bhalla V, Daidie D, Li H, Pao AC, LaGrange LP, Wang J, Vandewalle A, Stockand JD, Staub O, Pearce D (2005) Serum- and glucocorticoid-regulated kinase 1 regulates ubiquitin ligase neural precursor cell-expressed, developmentally down-regulated protein 4-2 by inducing interaction with 14-3-3. Molecular endocrinology 19:3073-3084.

Bhalla V, Hallows KR (2008) Mechanisms of ENaC regulation and clinical implications. J Am Soc Nephrol 19:1845-1854.

Bhalla V, Oyster NM, Fitch AC, Wijngaarden MA, Neumann D, Schlattner U, Pearce D, Hallows KR (2006) AMP-activated kinase inhibits the epithelial Na+ channel through functional regulation of the ubiquitin ligase Nedd4-2. J Biol Chem 281:26159-26169.

Binder HJ, Foster ES, Budinger ME, Hayslett JP (1987) Mechanism of electroneutral sodium chloride absorption in distal colon of the rat. Gastroenterology 93:449-455.

Bleich M, Riedemann N, Warth R, Kerstan D, Leipziger J, Hor M, Driessche WV, Greger R (1996) Ca2+ regulated K+ and non-selective cation channels in the basolateral membrane of rat colonic crypt base cells. Pflugers Arch 432:1011-1022.

Blikslager AT, Moeser AJ, Gookin JL, Jones SL, Odle J (2007) Restoration of barrier function in injured intestinal mucosa. Physiological reviews 87:545-564.

Bonny O, Chraibi A, Loffing J, Jaeger NF, Grunder S, Horisberger JD, Rossier BC (1999) Functional expression of a pseudohypoaldosteronism type I mutated epithelial Na+ channel lacking the pore-forming region of its alpha subunit. The Journal of clinical investigation 104:967-974.

Botero-Velez M, Curtis JJ, Warnock DG (1994) Brief report: Liddle's syndrome revisited--a disorder of sodium reabsorption in the distal tubule. N Engl J Med 330:178-181.

Bridges RJ, Newton BB, Pilewski JM, Devor DC, Poll CT, Hall RL (2001) Na+ transport in normal and CF human bronchial epithelial cells is inhibited by BAY 39-9437. Am J Physiol Lung Cell Mol Physiol 281:L16-23.

Broer S (2008) Amino acid transport across mammalian intestinal and renal epithelia. Physiological reviews 88:249-286.

Bruns JB, Carattino MD, Sheng S, Maarouf AB, Weisz OA, Pilewski JM, Hughey RP, Kleyman TR (2007) Epithelial Na+ channels are fully activated by furin- and prostasin-dependent release of an inhibitory peptide from the gamma-subunit. J Biol Chem 282:6153-6160.

Bugaj V, Pochynyuk O, Stockand JD (2009) Activation of the epithelial Na+ channel in the collecting duct by vasopressin contributes to water reabsorption. Am J Physiol Renal Physiol 297:F1411-1418.

Buzza MS, Martin EW, Driesbaugh KH, Desilets A, Leduc R, Antalis TM (2013) Prostasin is required for matriptase activation in intestinal epithelial cells to regulate closure of the paracellular pathway. J Biol Chem 288:10328-10337.

Buzza MS, Netzel-Arnett S, Shea-Donohue T, Zhao A, Lin CY, List K, Szabo R, Fasano A, Bugge TH, Antalis TM (2010) Membrane-anchored serine protease matriptase

REFERENCES_____

      regulates epithelial barrier formation and permeability in the intestine. Proc Natl Acad Sci U S A 107:4200-4205.

Caldwell RA, Boucher RC, Stutts MJ (2004) Serine protease activation of near-silent epithelial Na+ channels. American journal of physiology Cell physiology 286:C190-194.

Caldwell RA, Boucher RC, Stutts MJ (2005) Neutrophil elastase activates near-silent epithelial Na+ channels and increases airway epithelial Na+ transport. Am J Physiol Lung Cell Mol Physiol 288:L813-819.

Canessa CM, Horisberger JD, Rossier BC (1993) Epithelial sodium channel related to proteins involved in neurodegeneration. Nature 361:467-470.

Canessa CM, Merillat AM, Rossier BC (1994a) Membrane topology of the epithelial sodium channel in intact cells. Am J Physiol 267:C1682-1690.

Canessa CM, Schafer JA (1992) AVP stimulates Na+ transport in primary cultures of rabbit cortical collecting duct cells. Am J Physiol 262:F454-461.

Canessa CM, Schild L, Buell G, Thorens B, Gautschi I, Horisberger JD, Rossier BC (1994b) Amiloride-sensitive epithelial Na+ channel is made of three homologous subunits. Nature 367:463-467.

Carattino MD, Passero CJ, Steren CA, Maarouf AB, Pilewski JM, Myerburg MM, Hughey RP, Kleyman TR (2008) Defining an inhibitory domain in the alpha-subunit of the epithelial sodium channel. Am J Physiol Renal Physiol 294:F47-52.

Carattino MD, Sheng S, Bruns JB, Pilewski JM, Hughey RP, Kleyman TR (2006) The epithelial Na+ channel is inhibited by a peptide derived from proteolytic processing of its alpha subunit. J Biol Chem 281:18901-18907.

Cereijido M, Contreras RG, Shoshani L (2004) Cell adhesion, polarity, and epithelia in the dawn of metazoans. Physiological reviews 84:1229-1262.

Chandrashekar J, Kuhn C, Oka Y, Yarmolinsky DA, Hummler E, Ryba NJ, Zuker CS (2010) The cells and peripheral representation of sodium taste in mice. Nature 464:297-301.

Chang SS, Grunder S, Hanukoglu A, Rosler A, Mathew PM, Hanukoglu I, Schild L, Lu Y, Shimkets RA, Nelson-Williams C, Rossier BC, Lifton RP (1996) Mutations in subunits of the epithelial sodium channel cause salt wasting with hyperkalaemic acidosis, pseudohypoaldosteronism type 1. Nat Genet 12:248-253.

Chen CC, England S, Akopian AN, Wood JN (1998) A sensory neuron-specific, proton-gated ion channel. Proc Natl Acad Sci U S A 95:10240-10245.

Chen LM, Skinner ML, Kauffman SW, Chao J, Chao L, Thaler CD, Chai KX (2001) Prostasin is a glycosylphosphatidylinositol-anchored active serine protease. J Biol Chem 276:21434-21442.

Cheng H, Leblond CP (1974) Origin, differentiation and renewal of the four main epithelial cell types in the mouse small intestine. V. Unitarian Theory of the origin of the four epithelial cell types. The American journal of anatomy 141:537-561.

Chraibi A, Horisberger JD (2002) Na self inhibition of human epithelial Na channel: temperature dependence and effect of extracellular proteases. J Gen Physiol 120:133-145.

Chraibi A, Vallet V, Firsov D, Hess SK, Horisberger JD (1998) Protease modulation of the activity of the epithelial sodium channel expressed in Xenopus oocytes. J Gen Physiol 111:127-138.

Christensen BM, Perrier R, Wang Q, Zuber AM, Maillard M, Mordasini D, Malsure S, Ronzaud C, Stehle JC, Rossier BC, Hummler E (2010) Sodium and potassium balance depends on alphaENaC expression in connecting tubule. J Am Soc Nephrol 21:1942-1951.

Clauss W, Schafer H, Horch I, Hornicke H (1985) Segmental differences in electrical properties and Na-transport of rabbit caecum, proximal and distal colon in vitro. Pflugers Arch 403:278-282.

Clayburgh DR, Musch MW, Leitges M, Fu YX, Turner JR (2006) Coordinated epithelial NHE3 inhibition and barrier dysfunction are required for TNF-mediated diarrhea in vivo. The Journal of clinical investigation 116:2682-2694.

Clayburgh DR, Shen L, Turner JR (2004) A porous defense: the leaky epithelial barrier in intestinal disease. Lab Invest 84:282-291.

Cooper HS, Murthy SN, Shah RS, Sedergran DJ (1993) Clinicopathologic study of dextran sulfate sodium experimental murine colitis. Lab Invest 69:238-249.

Corey DP, Garcia-Anoveros J (1996) Mechanosensation and the DEG/ENaC ion channels. Science 273:323-324.

Cortina C, Palomo-Ponce S, Iglesias M, Fernandez-Masip JL, Vivancos A, Whissell G, Huma M, Peiro N, Gallego L, Jonkheer S, Davy A, Lloreta J, Sancho E, Batlle E (2007) EphB-ephrin-B interactions suppress colorectal cancer progression by compartmentalizing tumor cells. Nat Genet 39:1376-1383.

Dawson DC (1991) Ion channels and colonic salt transport. Annu Rev Physiol 53:321-339.

Debonneville C, Flores SY, Kamynina E, Plant PJ, Tauxe C, Thomas MA, Munster C, Chraibi A, Pratt JH, Horisberger JD, Pearce D, Loffing J, Staub O (2001) Phosphorylation of Nedd4-2 by Sgk1 regulates epithelial Na(+) channel cell surface expression. EMBO J 20:7052-7059.

Dijkink L, Hartog A, van Os CH, Bindels RJ (2002) The epithelial sodium channel (ENaC) is intracellularly located as a tetramer. Pflugers Arch 444:549-555.

Donaldson SH, Hirsh A, Li DC, Holloway G, Chao J, Boucher RC, Gabriel SE (2002) Regulation of the epithelial sodium channel by serine proteases in human airways. J Biol Chem 277:8338-8345.

DuBose TD, Jr., Gitomer J, Codina J (1999) H+,K+-ATPase. Curr Opin Nephrol Hypertens 8:597-602.

Duc C, Farman N, Canessa CM, Bonvalet JP, Rossier BC (1994) Cell-specific expression of epithelial sodium channel alpha, beta, and gamma subunits in aldosterone-responsive epithelia from the rat: localization by in situ hybridization and immunocytochemistry. J Cell Biol 127:1907-1921.

Ecelbarger CA, Kim GH, Wade JB, Knepper MA (2001) Regulation of the abundance of renal sodium transporters and channels by vasopressin. Experimental neurology 171:227-234.

el Marjou F, Janssen KP, Chang BH, Li M, Hindie V, Chan L, Louvard D, Chambon P, Metzger D, Robine S (2004) Tissue-specific and inducible Cre-mediated recombination in the gut epithelium. Genesis 39:186-193.

Fakitsas P, Adam G, Daidie D, van Bemmelen MX, Fouladkou F, Patrignani A, Wagner U, Warth R, Camargo SM, Staub O, Verrey F (2007) Early aldosterone-induced gene product regulates the epithelial sodium channel by deubiquitylation. J Am Soc Nephrol 18:1084-1092.

Falin RA, Cotton CU (2007) Acute downregulation of ENaC by EGF involves the PY motif and putative ERK phosphorylation site. J Gen Physiol 130:313-328.

Faresse N, Ruffieux-Daidie D, Salamin M, Gomez-Sanchez CE, Staub O (2010) Mineralocorticoid receptor degradation is promoted by Hsp90 inhibition and the ubiquitin-protein ligase CHIP. Am J Physiol Renal Physiol 299:F1462-1472.

Farquhar MG, Palade GE (1963) Junctional complexes in various epithelia. J Cell Biol 17:375-412.

REFERENCES_____

Feldman GM, Stephenson RL (1990) H+ and HCO3- flux across apical surface of rat distal colon. Am J Physiol 259:C35-40.

Firsov D, Gautschi I, Merillat AM, Rossier BC, Schild L (1998) The heterotetrameric architecture of the epithelial sodium channel (ENaC). EMBO J 17:344-352.

Firsov D, Schild L, Gautschi I, Merillat AM, Schneeberger E, Rossier BC (1996) Cell surface expression of the epithelial Na channel and a mutant causing Liddle syndrome: a quantitative approach. Proc Natl Acad Sci U S A 93:15370-15375.

Foster ES, Budinger ME, Hayslett JP, Binder HJ (1986) Ion transport in proximal colon of the rat. Sodium depletion stimulates neutral sodium chloride absorption. The Journal of clinical investigation 77:228-235.

Foster ES, Dudeja PK, Brasitus TA (1990) Contribution of Cl(-)-OH- exchange to electroneutral NaCl absorption in rat distal colon. Am J Physiol 258:G261-267.

Foster ES, Hayslett JP, Binder HJ (1984) Mechanism of active potassium absorption and secretion in the rat colon. Am J Physiol 246:G611-617.

Frateschi S, Keppner A, Malsure S, Iwaszkiewicz J, Sergi C, Merillat AM, Fowler-Jaeger N, Randrianarison N, Planes C, Hummler E (2012) Mutations of the Serine Protease CAP1/Prss8 Lead to Reduced Embryonic Viability, Skin Defects, and Decreased ENaC Activity. Am J Pathol 181:605-615.

Gaeggeler HP, Gonzalez-Rodriguez E, Jaeger NF, Loffing-Cueni D, Norregaard R, Loffing J, Horisberger JD, Rossier BC (2005) Mineralocorticoid versus glucocorticoid receptor occupancy mediating aldosterone-stimulated sodium transport in a novel renal cell line. J Am Soc Nephrol 16:878-891.

Garovic VD, Hilliard AA, Turner ST (2006) Monogenic forms of low-renin hypertension. Nature clinical practice Nephrology 2:624-630.

Garty H, Palmer LG (1997) Epithelial sodium channels: function, structure, and regulation. Physiological reviews 77:359-396.

Geller DS, Rodriguez-Soriano J, Vallo Boado A, Schifter S, Bayer M, Chang SS, Lifton RP (1998) Mutations in the mineralocorticoid receptor gene cause autosomal dominant pseudohypoaldosteronism type I. Nat Genet 19:279-281.

Gilmore ES, Stutts MJ, Milgram SL (2001) SRC family kinases mediate epithelial Na+ channel inhibition by endothelin. J Biol Chem 276:42610-42617.

Gitter AH, Bendfeldt K, Schulzke JD, Fromm M (2000) Trans/paracellular, surface/crypt, and epithelial/subepithelial resistances of mammalian colonic epithelia. Pflugers Arch 439:477-482.

Gonzales EB, Kawate T, Gouaux E (2009) Pore architecture and ion sites in acid-sensing ion channels and P2X receptors. Nature 460:599-604.

Gormley K, Dong Y, Sagnella GA (2003) Regulation of the epithelial sodium channel by accessory proteins. The Biochemical journal 371:1-14.

Greger R (2000) Role of CFTR in the colon. Annu Rev Physiol 62:467-491.

Greig ER, Boot-Handford RP, Mani V, Sandle GI (2004) Decreased expression of apical Na+ channels and basolateral Na+, K+-ATPase in ulcerative colitis. The Journal of pathology 204:84-92.

Groschwitz KR, Hogan SP (2009) Intestinal barrier function: molecular regulation and disease pathogenesis. J Allergy Clin Immunol 124:3-20; quiz 21-22.

Grunder S, Firsov D, Chang SS, Jaeger NF, Gautschi I, Schild L, Lifton RP, Rossier BC (1997) A mutation causing pseudohypoaldosteronism type 1 identifies a conserved glycine that is involved in the gating of the epithelial sodium channel. EMBO J 16:899-907.

Grunder S, Muller A, Ruppersberg JP (2001) Developmental and cellular expression pattern of epithelial sodium channel alpha, beta and gamma subunits in the inner ear of the rat. The European journal of neuroscience 13:641-648.

Halm DR, Dawson DC (1984) Potassium transport by turtle colon: active secretion and active absorption. Am J Physiol 246:C315-322.

Hansson JH, Schild L, Lu Y, Wilson TA, Gautschi I, Shimkets R, Nelson-Williams C, Rossier BC, Lifton RP (1995) A de novo missense mutation of the beta subunit of the epithelial sodium channel causes hypertension and Liddle syndrome, identifying a proline-rich segment critical for regulation of channel activity. Proc Natl Acad Sci U S A 92:11495-11499.

Harris M, Garcia-Caballero A, Stutts MJ, Firsov D, Rossier BC (2008) Preferential assembly of epithelial sodium channel (ENaC) subunits in Xenopus oocytes: role of furin-mediated endogenous proteolysis. J Biol Chem 283:7455-7463.

Hasegawa H, Skach W, Baker O, Calayag MC, Lingappa V, Verkman AS (1992) A multifunctional aqueous channel formed by CFTR. Science 258:1477-1479.

Hashimoto T, Perlot T, Rehman A, Trichereau J, Ishiguro H, Paolino M, Sigl V, Hanada T, Hanada R, Lipinski S, Wild B, Camargo SM, Singer D, Richter A, Kuba K, Fukamizu A, Schreiber S, Clevers H, Verrey F, Rosenstiel P, Penninger JM (2012) ACE2 links amino acid malnutrition to microbial ecology and intestinal inflammation. Nature 487:477-481.

Hawker PC, McKay JS, Turnberg LA (1980) Electrolyte transport across colonic mucosa from patients with inflammatory bowel disease. Gastroenterology 79:508-511.

Hirt RP, Poulain-Godefroy O, Billotte J, Kraehenbuhl JP, Fasel N (1992) Highly inducible synthesis of heterologous proteins in epithelial cells carrying a glucocorticoid-responsive vector. Gene 111:199-206.

Hoglund P, Haila S, Socha J, Tomaszewski L, Saarialho-Kere U, Karjalainen-Lindsberg ML, Airola K, Holmberg C, de la Chapelle A, Kere J (1996) Mutations of the Down-regulated in adenoma (DRA) gene cause congenital chloride diarrhoea. Nat Genet 14:316-319.

Hollander D, Vadheim CM, Brettholz E, Petersen GM, Delahunty T, Rotter JI (1986) Increased intestinal permeability in patients with Crohn's disease and their relatives. A possible etiologic factor. Annals of internal medicine 105:883-885.

Hooper JD, Clements JA, Quigley JP, Antalis TM (2001) Type II transmembrane serine proteases. Insights into an emerging class of cell surface proteolytic enzymes. J Biol Chem 276:857-860.

Huang M, Chalfie M (1994) Gene interactions affecting mechanosensory transduction in Caenorhabditis elegans. Nature 367:467-470.

Hughey RP, Bruns JB, Kinlough CL, Harkleroad KL, Tong Q, Carattino MD, Johnson JP, Stockand JD, Kleyman TR (2004) Epithelial sodium channels are activated by furin-dependent proteolysis. J Biol Chem 279:18111-18114.

Hughey RP, Mueller GM, Bruns JB, Kinlough CL, Poland PA, Harkleroad KL, Carattino MD, Kleyman TR (2003) Maturation of the epithelial Na+ channel involves proteolytic processing of the alpha- and gamma-subunits. J Biol Chem 278:37073-37082.

Hummler E, Barker P, Gatzy J, Beermann F, Verdumo C, Schmidt A, Boucher R, Rossier BC (1996) Early death due to defective neonatal lung liquid clearance in alpha-ENaC-deficient mice. Nat Genet 12:325-328.

Hummler E, Dousse A, Rieder A, Stehle JC, Rubera I, Osterheld MC, Beermann F, Frateschi S, Charles RP (2013) The channel-activating protease CAP1/Prss8 is required for placental labyrinth maturation. PloS one 8:e55796.

REFERENCES_____

Hummler E, Merillat AM, Rubera I, Rossier BC, Beermann F (2002) Conditional gene targeting of the Scnn1a (alphaENaC) gene locus. Genesis 32:169-172.

Ikuma M, Kashgarian M, Binder HJ, Rajendran VM (1999) Differential regulation of NHE isoforms by sodium depletion in proximal and distal segments of rat colon. Am J Physiol 276:G539-549.

Jaisser F, Coutry N, Farman N, Binder HJ, Rossier BC (1993) A putative H(+)-K(+)-ATPase is selectively expressed in surface epithelial cells of rat distal colon. Am J Physiol 265:C1080-1089.

Kamynina E, Debonneville C, Bens M, Vandewalle A, Staub O (2001) A novel mouse Nedd4 protein suppresses the activity of the epithelial Na+ channel. FASEB J 15:204-214.

Karam SM (1999) Lineage commitment and maturation of epithelial cells in the gut. Frontiers in bioscience : a journal and virtual library 4:D286-298.

Kellenberger S, Gautschi I, Pfister Y, Schild L (2005) Intracellular thiol-mediated modulation of epithelial sodium channel activity. J Biol Chem 280:7739-7747.

Kellenberger S, Gautschi I, Schild L (2003) Mutations in the epithelial Na+ channel ENaC outer pore disrupt amiloride block by increasing its dissociation rate. Molecular pharmacology 64:848-856.

Kiela PR, Ghishan FK (2009) Ion transport in the intestine. Current opinion in gastroenterology 25:87-91.

Kiela PR, Laubitz D, Larmonier CB, Midura-Kiela MT, Lipko MA, Janikashvili N, Bai A, Thurston R, Ghishan FK (2009) Changes in mucosal homeostasis predispose NHE3 knockout mice to increased susceptibility to DSS-induced epithelial injury. Gastroenterology 137:965-975, 975 e961-910.

Kim YS, Ho SB (2010) Intestinal goblet cells and mucins in health and disease: recent insights and progress. Current gastroenterology reports 12:319-330.

Kleyman TR, Carattino MD, Hughey RP (2009) ENaC at the cutting edge: regulation of epithelial sodium channels by proteases. J Biol Chem 284:20447-20451.

Koyama K, Sasaki I, Naito H, Funayama Y, Fukushima K, Unno M, Matsuno S, Hayashi H, Suzuki Y (1999) Induction of epithelial Na+ channel in rat ileum after proctocolectomy. Am J Physiol-Gastr L 276:G975-G984.

Kunzelmann K, Mall M (2002) Electrolyte transport in the mammalian colon: mechanisms and implications for disease. Physiological reviews 82:245-289.

Laubitz D, Larmonier CB, Bai A, Midura-Kiela MT, Lipko MA, Thurston RD, Kiela PR, Ghishan FK (2008) Colonic gene expression profile in NHE3-deficient mice: evidence for spontaneous distal colitis. American journal of physiology Gastrointestinal and liver physiology 295:G63-G77.

Lebowitz J, Edinger RS, An B, Perry CJ, Onate S, Kleyman TR, Johnson JP (2004) Ikappab kinase-beta (ikkbeta) modulation of epithelial sodium channel activity. J Biol Chem 279:41985-41990.

Lee IH, Dinudom A, Sanchez-Perez A, Kumar S, Cook DI (2007) Akt mediates the effect of insulin on epithelial sodium channels by inhibiting Nedd4-2. J Biol Chem 282:29866-29873.

Lencer WI, Cheung G, Strohmeier GR, Currie MG, Ouellette AJ, Selsted ME, Madara JL (1997) Induction of epithelial chloride secretion by channel-forming cryptdins 2 and 3. Proc Natl Acad Sci U S A 94:8585-8589.

Leroy V, De Seigneux S, Agassiz V, Hasler U, Rafestin-Oblin ME, Vinciguerra M, Martin PY, Feraille E (2009) Aldosterone activates NF-kappaB in the collecting duct. J Am Soc Nephrol 20:131-144.

Levitan R, Fordtran JS, Burrows BA, Ingelfinger FJ (1962) Water and salt absorption in the human colon. The Journal of clinical investigation 41:1754-1759.

REFERENCES_____

Leyvraz C, Charles RP, Rubera I, Guitard M, Rotman S, Breiden B, Sandhoff K, Hummler E (2005) The epidermal barrier function is dependent on the serine protease CAP1/Prss8. J Cell Biol 170:487-496.

Lifton RP (1995) Genetic determinants of human hypertension. Proc Natl Acad Sci U S A 92:8545-8551.

Lingueglia E, Renard S, Waldmann R, Voilley N, Champigny G, Plass H, Lazdunski M, Barbry P (1994) Different homologous subunits of the amiloride-sensitive Na+ channel are differently regulated by aldosterone. J Biol Chem 269:13736-13739.

List K, Kosa P, Szabo R, Bey AL, Wang CB, Molinolo A, Bugge TH (2009) Epithelial integrity is maintained by a matriptase-dependent proteolytic pathway. Am J Pathol 175:1453-1463.

Loffing J, Pietri L, Aregger F, Bloch-Faure M, Ziegler U, Meneton P, Rossier BC, Kaissling B (2000) Differential subcellular localization of ENaC subunits in mouse kidney in response to high- and low-Na diets. Am J Physiol Renal Physiol 279:F252-258.

Lohrmann E, Burhoff I, Nitschke RB, Lang HJ, Mania D, Englert HC, Hropot M, Warth R, Rohm W, Bleich M, et al. (1995) A new class of inhibitors of cAMP-mediated Cl-secretion in rabbit colon, acting by the reduction of cAMP-activated K+ conductance. Pflugers Arch 429:517-530.

Loo DD, Zeuthen T, Chandy G, Wright EM (1996) Cotransport of water by the Na+/glucose cotransporter. Proc Natl Acad Sci U S A 93:13367-13370.

Lu C, Pribanic S, Debonneville A, Jiang C, Rotin D (2007) The PY motif of ENaC, mutated in Liddle syndrome, regulates channel internalization, sorting and mobilization from subapical pool. Traffic 8:1246-1264.

Machnik A, Neuhofer W, Jantsch J, Dahlmann A, Tammela T, Machura K, Park JK, Beck FX, Muller DN, Derer W, Goss J, Ziomber A, Dietsch P, Wagner H, van Rooijen N, Kurtz A, Hilgers KF, Alitalo K, Eckardt KU, Luft FC, Kerjaschki D, Titze J (2009) Macrophages regulate salt-dependent volume and blood pressure by a vascular endothelial growth factor-C-dependent buffering mechanism. Nature medicine 15:545-552.

Madara JL, Marcial MA (1984) Structural correlates of intestinal tight-junction permeability. Kroc Foundation series 17:77-100.

Mall M, Bleich M, Kuehr J, Brandis M, Greger R, Kunzelmann K (1999) CFTR-mediated inhibition of epithelial Na+ conductance in human colon is defective in cystic fibrosis. Am J Physiol 277:G709-716.

Mall M, Grubb BR, Harkema JR, O'Neal WK, Boucher RC (2004) Increased airway epithelial Na+ absorption produces cystic fibrosis-like lung disease in mice. Nature medicine 10:487-493.

Mall M, Wissner A, Seydewitz HH, Kuehr J, Brandis M, Greger R, Kunzelmann K (2000) Defective cholinergic Cl(-) secretion and detection of K(+) secretion in rectal biopsies from cystic fibrosis patients. American journal of physiology Gastrointestinal and liver physiology 278:G617-624.

Marunaka Y, Hagiwara N, Tohda H (1992) Insulin activates single amiloride-blockable Na channels in a distal nephron cell line (A6). Am J Physiol 263:F392-400.

McDonald FJ, Yang B, Hrstka RF, Drummond HA, Tarr DE, McCray PB, Jr., Stokes JB, Welsh MJ, Williamson RA (1999) Disruption of the beta subunit of the epithelial Na+ channel in mice: hyperkalemia and neonatal death associated with a pseudohypoaldosteronism phenotype. Proc Natl Acad Sci U S A 96:1727-1731.

Melgar S, Karlsson A, Michaelsson E (2005) Acute colitis induced by dextran sulfate sodium progresses to chronicity in C57BL/6 but not in BALB/c mice: correlation between

symptoms and inflammation. American journal of physiology Gastrointestinal and liver physiology 288:G1328-1338.

Melgar S, Karlsson L, Rehnstrom E, Karlsson A, Utkovic H, Jansson L, Michaelsson E (2008) Validation of murine dextran sulfate sodium-induced colitis using four therapeutic agents for human inflammatory bowel disease. International immunopharmacology 8:836-844.

Meneton P, Schultheis PJ, Greeb J, Nieman ML, Liu LH, Clarke LL, Duffy JJ, Doetschman T, Lorenz JN, Shull GE (1998) Increased sensitivity to K+ deprivation in colonic H,K-ATPase-deficient mice. The Journal of clinical investigation 101:536-542.

Mordasini D, Bustamante M, Rousselot M, Martin PY, Hasler U, Feraille E (2005) Stimulation of Na+ transport by AVP is independent of PKA phosphorylation of the Na-K-ATPase in collecting duct principal cells. Am J Physiol Renal Physiol 289:F1031-1039.

Muller T, Wijmenga C, Phillips AD, Janecke A, Houwen RH, Fischer H, Ellemunter H, Fruhwirth M, Offner F, Hofer S, Muller W, Booth IW, Heinz-Erian P (2000) Congenital sodium diarrhea is an autosomal recessive disorder of sodium/proton exchange but unrelated to known candidate genes. Gastroenterology 119:1506-1513.

Murphy MS, Eastham EJ, Nelson R, Pearson AD, Laker MF (1989) Intestinal permeability in Crohn's disease. Archives of disease in childhood 64:321-325.

Musch MW, Clarke LL, Mamah D, Gawenis LR, Zhang Z, Ellsworth W, Shalowitz D, Mittal N, Efthimiou P, Alnadjim Z, Hurst SD, Chang EB, Barrett TA (2002) T cell activation causes diarrhea by increasing intestinal permeability and inhibiting epithelial Na+/K+-ATPase. The Journal of clinical investigation 110:1739-1747.

Netzel-Arnett S, Buzza MS, Shea-Donohue T, Desilets A, Leduc R, Fasano A, Bugge TH, Antalis TM (2012) Matriptase protects against experimental colitis and promotes intestinal barrier recovery. Inflammatory bowel diseases 18:1303-1314.

Netzel-Arnett S, Currie BM, Szabo R, Lin CY, Chen LM, Chai KX, Antalis TM, Bugge TH, List K (2006) Evidence for a matriptase-prostasin proteolytic cascade regulating terminal epidermal differentiation. J Biol Chem 281:32941-32945.

Nicod M, Michlig S, Flahaut M, Salinas M, Fowler Jaeger N, Horisberger JD, Rossier BC, Firsov D (2002) A novel vasopressin-induced transcript promotes MAP kinase activation and ENaC downregulation. EMBO J 21:5109-5117.

Nielsen MS, Warth R, Bleich M, Weyand B, Greger R (1998) The basolateral Ca2+-dependent K+ channel in rat colonic crypt cells. Pflugers Arch 435:267-272.

Olson TS, Reuter BK, Scott KG, Morris MA, Wang XM, Hancock LN, Burcin TL, Cohn SM, Ernst PB, Cominelli F, Meddings JB, Ley K, Pizarro TT (2006) The primary defect in experimental ileitis originates from a nonhematopoietic source. The Journal of experimental medicine 203:541-552.

Page MJ, Di Cera E (2008) Serine peptidases: classification, structure and function. Cellular and molecular life sciences : CMLS 65:1220-1236.

Palmer LG, Frindt G (1987) Effects of cell Ca and pH on Na channels from rat cortical collecting tubule. Am J Physiol 253:F333-339.

Planes C, Leyvraz C, Uchida T, Angelova MA, Vuagniaux G, Hummler E, Matthay M, Clerici C, Rossier B (2005) In vitro and in vivo regulation of transepithelial lung alveolar sodium transport by serine proteases. Am J Physiol Lung Cell Mol Physiol 288:L1099-1109.

Planes C, Randrianarison NH, Charles RP, Frateschi S, Cluzeaud F, Vuagniaux G, Soler P, Clerici C, Rossier BC, Hummler E (2010) ENaC-mediated alveolar fluid clearance and lung fluid balance depend on the channel-activating protease 1. EMBO Mol Med 2:26-37.

REFERENCES_____

Pochynyuk O, Tong Q, Staruschenko A, Ma HP, Stockand JD (2006) Regulation of the epithelial Na+ channel (ENaC) by phosphatidylinositides. Am J Physiol Renal Physiol 290:F949-957.

Podolsky DK (1999) Mucosal immunity and inflammation. V. Innate mechanisms of mucosal defense and repair: the best offense is a good defense. Am J Physiol 277:G495-499.

Potter GD, Burlingame SM (1986) Ion transport by neonatal rabbit distal colon. Am J Physiol 250:G754-759.

Pradervand S, Vandewalle A, Bens M, Gautschi I, Loffing J, Hummler E, Schild L, Rossier BC (2003) Dysfunction of the epithelial sodium channel expressed in the kidney of a mouse model for Liddle syndrome. J Am Soc Nephrol 14:2219-2228.

Pradervand S, Wang Q, Burnier M, Beermann F, Horisberger JD, Hummler E, Rossier BC (1999) A mouse model for Liddle's syndrome. J Am Soc Nephrol 10:2527-2533.

Quinton PM (1990) Cystic fibrosis: a disease in electrolyte transport. FASEB J 4:2709-2717.

Rajendran VM, Binder HJ (1990) Characterization of Na-H exchange in apical membrane vesicles of rat colon. J Biol Chem 265:8408-8414.

Rajendran VM, Binder HJ (1999) Distribution and regulation of apical Cl/anion exchanges in surface and crypt cells of rat distal colon. Am J Physiol 276:G132-137.

Rajendran VM, Black J, Ardito TA, Sangan P, Alper SL, Schweinfest C, Kashgarian M, Binder HJ (2000) Regulation of DRA and AE1 in rat colon by dietary Na depletion. American journal of physiology Gastrointestinal and liver physiology 279:G931-942.

Rajendran VM, Geibel J, Binder HJ (1995) Chloride-dependent Na-H exchange. A novel mechanism of sodium transport in colonic crypts. J Biol Chem 270:11051-11054.

Rauh R, Soell D, Haerteis S, Diakov A, Nesterov V, Krueger B, Sticht H, Korbmacher C (2013) A mutation in the beta-subunit of ENaC identified in a patient with cystic fibrosis-like symptoms has a gain-of-function effect. Am J Physiol Lung Cell Mol Physiol 304:L43-55.

Rawlings ND, Barrett AJ (1993) Evolutionary families of peptidases. The Biochemical journal 290 (Pt 1):205-218.

Rechkemmer G, Frizzell RA, Halm DR (1996) Active potassium transport across guinea-pig distal colon: action of secretagogues. J Physiol 493 (Pt 2):485-502.

Renard S, Voilley N, Bassilana F, Lazdunski M, Barbry P (1995) Localization and regulation by steroids of the alpha, beta and gamma subunits of the amiloride-sensitive Na+ channel in colon, lung and kidney. Pflugers Arch 430:299-307.

Resta-Lenert S, Smitham J, Barrett KE (2005) Epithelial dysfunction associated with the development of colitis in conventionally housed mdr1a-/- mice. American journal of physiology Gastrointestinal and liver physiology 289:G153-162.

Rocha F, Musch MW, Lishanskiy L, Bookstein C, Sugi K, Xie Y, Chang EB (2001) IFN-gamma downregulates expression of Na(+)/H(+) exchangers NHE2 and NHE3 in rat intestine and human Caco-2/bbe cells. American journal of physiology Cell physiology 280:C1224-1232.

Ronzaud C, Loffing-Cueni D, Hausel P, Debonneville A, Malsure SR, Fowler-Jaeger N, Boase NA, Perrier R, Maillard M, Yang B, Stokes JB, Koesters R, Kumar S, Hummler E, Loffing J, Staub O (2013) Renal tubular NEDD4-2 deficiency causes NCC-mediated salt-dependent hypertension. The Journal of clinical investigation.

Rossier BC, Canessa CM, Schild L, Horisberger JD (1994) Epithelial sodium channels. Curr Opin Nephrol Hypertens 3:487-496.

Rossier BC, Pradervand S, Schild L, Hummler E (2002) Epithelial sodium channel and the control of sodium balance: interaction between genetic and environmental factors. Annu Rev Physiol 64:877-897.

Rossier BC, Staub O, Hummler E (2013) Genetic dissection of sodium and potassium transport along the aldosterone-sensitive distal nephron: Importance in the control of blood pressure and hypertension. Febs Letters 587:1929-1941.

Rossier BC, Stutts MJ (2009) Activation of the epithelial sodium channel (ENaC) by serine proteases. Annu Rev Physiol 71:361-379.

Rotin D (2000) Regulation of the epithelial sodium channel (ENaC) by accessory proteins. Curr Opin Nephrol Hypertens 9:529-534.

Rotin D, Kanelis V, Schild L (2001) Trafficking and cell surface stability of ENaC. Am J Physiol Renal Physiol 281:F391-399.

Ruan YC, Guo JH, Liu X, Zhang R, Tsang LL, Dong JD, Chen H, Yu MK, Jiang X, Zhang XH, Fok KL, Chung YW, Huang H, Zhou WL, Chan HC (2012) Activation of the epithelial Na+ channel triggers prostaglandin E(2) release and production required for embryo implantation. Nature medicine 18:1112-1117.

Rubera I, Loffing J, Palmer LG, Frindt G, Fowler-Jaeger N, Sauter D, Carroll T, McMahon A, Hummler E, Rossier BC (2003) Collecting duct-specific gene inactivation of alphaENaC in the mouse kidney does not impair sodium and potassium balance. The Journal of clinical investigation 112:554-565.

Rubera I, Meier E, Vuagniaux G, Merillat AM, Beermann F, Rossier BC, Hummler E (2002) A conditional allele at the mouse channel activating protease 1 (Prss8) gene locus. Genesis 32:173-176.

Sandle GI (1998) Salt and water absorption in the human colon: a modern appraisal. Gut 43:294-299.

Sandle GI (2011) Infective and inflammatory diarrhoea: mechanisms and opportunities for novel therapies. Current opinion in pharmacology 11:634-639.

Sandle GI, Hayslett JP, Binder HJ (1986a) Effect of glucocorticoids on rectal transport in normal subjects and patients with ulcerative colitis. Gut 27:309-316.

Sandle GI, Perry MD, Mathialahan T, Linley JE, Robinson P, Hunter M, MacLennan KA (2007) Altered cryptal expression of luminal potassium (BK) channels in ulcerative colitis. The Journal of pathology 212:66-73.

Sandle GI, Wills NK, Alles W, Binder HJ (1986b) Electrophysiology of the human colon: evidence of segmental heterogeneity. Gut 27:999-1005.

Schild L (2010) The epithelial sodium channel and the control of sodium balance. Biochim Biophys Acta 1802:1159-1165.

Schild L, Canessa CM, Shimkets RA, Gautschi I, Lifton RP, Rossier BC (1995) A mutation in the epithelial sodium channel causing Liddle disease increases channel activity in the Xenopus laevis oocyte expression system. Proc Natl Acad Sci U S A 92:5699-5703.

Schild L, Lu Y, Gautschi I, Schneeberger E, Lifton RP, Rossier BC (1996) Identification of a PY motif in the epithelial Na channel subunits as a target sequence for mutations causing channel activation found in Liddle syndrome. EMBO J 15:2381-2387.

Schild L, Schneeberger E, Gautschi I, Firsov D (1997) Identification of amino acid residues in the alpha, beta, and gamma subunits of the epithelial sodium channel (ENaC) involved in amiloride block and ion permeation. J Gen Physiol 109:15-26.

Schonhoff SE, Giel-Moloney M, Leiter AB (2004) Minireview: Development and differentiation of gut endocrine cells. Endocrinology 145:2639-2644.

Schultheis PJ, Clarke LL, Meneton P, Miller ML, Soleimani M, Gawenis LR, Riddle TM, Duffy JJ, Doetschman T, Wang T, Giebisch G, Aronson PS, Lorenz JN, Shull GE (1998) Renal and intestinal absorptive defects in mice lacking the NHE3 Na+/H+ exchanger. Nat Genet 19:282-285.

REFERENCES_____

Schultheiss G, Diener M (1997) Regulation of apical and basolateral K+ conductances in rat colon. British journal of pharmacology 122:87-94.

Schweinfest CW, Henderson KW, Suster S, Kondoh N, Papas TS (1993) Identification of a colon mucosa gene that is down-regulated in colon adenomas and adenocarcinomas. Proc Natl Acad Sci U S A 90:4166-4170.

Seidler U, Lenzen H, Cinar A, Tessema T, Bleich A, Riederer B (2006) Molecular mechanisms of disturbed electrolyte transport in intestinal inflammation. Annals of the New York Academy of Sciences 1072:262-275.

Sellin JH, Dubinsky WP (1994) Apical nonspecific cation conductances in rabbit cecum. Am J Physiol 266:G475-484.

Sellin JH, Oyarzabal H, Cragoe EJ (1988) Electrogenic sodium absorption in rabbit cecum in vitro. The Journal of clinical investigation 81:1275-1283.

Shen L (2009) Functional Morphology of the Gastrointestinal Tract. In: Molecular Mechanisms of Bacterial Infection via the Gut, vol. 337 (Sasakawa, C., ed), pp 1-35: Springer Berlin Heidelberg.

Sheng S, Carattino MD, Bruns JB, Hughey RP, Kleyman TR (2006) Furin cleavage activates the epithelial Na+ channel by relieving Na+ self-inhibition. Am J Physiol Renal Physiol 290:F1488-1496.

Sherman MP, Bennett SH, Hwang FF, Sherman J, Bevins CL (2005) Paneth cells and antibacterial host defense in neonatal small intestine. Infection and immunity 73:6143-6146.

Shigaev A, Asher C, Latter H, Garty H, Reuveny E (2000) Regulation of sgk by aldosterone and its effects on the epithelial Na(+) channel. Am J Physiol Renal Physiol 278:F613-619.

Shimkets RA, Warnock DG, Bositis CM, Nelson-Williams C, Hansson JH, Schambelan M, Gill JR, Jr., Ulick S, Milora RV, Findling JW, et al. (1994) Liddle's syndrome: heritable human hypertension caused by mutations in the beta subunit of the epithelial sodium channel. Cell 79:407-414.

Snyder PM, Olson DR, Kabra R, Zhou R, Steines JC (2004) cAMP and serum and glucocorticoid-inducible kinase (SGK) regulate the epithelial Na(+) channel through convergent phosphorylation of Nedd4-2. J Biol Chem 279:45753-45758.

Sorensen MV, Accogli G, Hansen JG (2010a) Postembryonic development of Antygomonas incomitata (Kinorhyncha: Cyclorhagida). Journal of morphology 271:863-882.

Sorensen MV, Grossmann S, Roesinger M, Gresko N, Todkar AP, Barmettler G, Ziegler U, Odermatt A, Loffing-Cueni D, Loffing J (2013) Rapid dephosphorylation of the renal sodium chloride cotransporter in response to oral potassium intake in mice. Kidney international 83:811-824.

Sorensen MV, Leipziger J (2009) The essential role of luminal BK channels in distal colonic K+ secretion. The journal of medical investigation : JMI 56 Suppl:301.

Sorensen MV, Matos JE, Praetorius HA, Leipziger J (2010b) Colonic potassium handling. Pflugers Arch 459:645-656.

Staub O, Dho S, Henry P, Correa J, Ishikawa T, McGlade J, Rotin D (1996) WW domains of Nedd4 bind to the proline-rich PY motifs in the epithelial Na+ channel deleted in Liddle's syndrome. EMBO J 15:2371-2380.

Staub O, Gautschi I, Ishikawa T, Breitschopf K, Ciechanover A, Schild L, Rotin D (1997) Regulation of stability and function of the epithelial Na+ channel (ENaC) by ubiquitination. EMBO J 16:6325-6336.

Stutts MJ, Canessa CM, Olsen JC, Hamrick M, Cohn JA, Rossier BC, Boucher RC (1995) CFTR as a cAMP-dependent regulator of sodium channels. Science 269:847-850.

Sullivan S, Alex P, Dassopoulos T, Zachos NC, Iacobuzio-Donahue C, Donowitz M, Brant SR, Cuffari C, Harris ML, Datta LW, Conklin L, Chen Y, Li X (2009) Downregulation of sodium transporters and NHERF proteins in IBD patients and mouse colitis models: potential contributors to IBD-associated diarrhea. Inflammatory bowel diseases 15:261-274.

Sullivan SK, Smith PL (1986) Bicarbonate secretion by rabbit proximal colon. Am J Physiol 251:G436-445.

Suzuki Y, Kaneko K (1989) Ouabain-sensitive H+-K+ exchange mechanism in the apical membrane of guinea pig colon. Am J Physiol 256:G979-988.

Sweiry JH, Binder HJ (1989) Characterization of aldosterone-induced potassium secretion in rat distal colon. The Journal of clinical investigation 83:844-851.

Szabo R, Uzzun Sales K, Kosa P, Shylo NA, Godiksen S, Hansen KK, Friis S, Gutkind JS, Vogel LK, Hummler E, Camerer E, Bugge TH (2012) Reduced Prostasin (CAP1/PRSS8) Activity Eliminates HAI-1 and HAI-2 Deficiency-Associated Developmental Defects by Preventing Matriptase Activation. PLoS genetics 8:e1002937.

Tibble JA, Sigthorsson G, Bridger S, Fagerhol MK, Bjarnason I (2000) Surrogate markers of intestinal inflammation are predictive of relapse in patients with inflammatory bowel disease. Gastroenterology 119:15-22.

Traykova-Brauch M, Schonig K, Greiner O, Miloud T, Jauch A, Bode M, Felsher DW, Glick AB, Kwiatkowski DJ, Bujard H, Horst J, von Knebel Doeberitz M, Niggli FK, Kriz W, Grone HJ, Koesters R (2008) An efficient and versatile system for acute and chronic modulation of renal tubular function in transgenic mice. Nature medicine 14:979-984.

Trezise AE, Buchwald M (1991) In vivo cell-specific expression of the cystic fibrosis transmembrane conductance regulator. Nature 353:434-437.

Tsukita S, Furuse M (2000) The structure and function of claudins, cell adhesion molecules at tight junctions. Annals of the New York Academy of Sciences 915:129-135.

Tsukita S, Furuse M, Itoh M (2001) Multifunctional strands in tight junctions. Nature reviews Molecular cell biology 2:285-293.

Vallet V, Chraibi A, Gaeggeler HP, Horisberger JD, Rossier BC (1997) An epithelial serine protease activates the amiloride-sensitive sodium channel. Nature 389:607-610.

Vallet V, Horisberger JD, Rossier BC (1998) Epithelial sodium channel regulatory proteins identified by functional expression cloning. Kidney international Supplement 67:S109-114.

Vallet V, Pfister C, Loffing J, Rossier BC (2002) Cell-surface expression of the channel activating protease xCAP-1 is required for activation of ENaC in the Xenopus oocyte. J Am Soc Nephrol 13:588-594.

van der Flier LG, Clevers H (2009) Stem cells, self-renewal, and differentiation in the intestinal epithelium. Annu Rev Physiol 71:241-260.

van Es JH, Jay P, Gregorieff A, van Gijn ME, Jonkheer S, Hatzis P, Thiele A, van den Born M, Begthel H, Brabletz T, Taketo MM, Clevers H (2005) Wnt signalling induces maturation of Paneth cells in intestinal crypts. Nature cell biology 7:381-386.

Verrey F (1999) Early aldosterone action: toward filling the gap between transcription and transport. Am J Physiol 277:F319-327.

Vuagniaux G, Vallet V, Jaeger NF, Hummler E, Rossier BC (2002) Synergistic activation of ENaC by three membrane-bound channel-activating serine proteases (mCAP1, mCAP2, and mCAP3) and serum- and glucocorticoid-regulated kinase (Sgk1) in Xenopus Oocytes. J Gen Physiol 120:191-201.

REFERENCES_____

Vuagniaux G, Vallet V, Jaeger NF, Pfister C, Bens M, Farman N, Courtois-Coutry N, Vandewalle A, Rossier BC, Hummler E (2000) Activation of the amiloride-sensitive epithelial sodium channel by the serine protease mCAP1 expressed in a mouse cortical collecting duct cell line. J Am Soc Nephrol 11:828-834.

Wagner CA, Loffing-Cueni D, Yan Q, Schulz N, Fakitsas P, Carrel M, Wang T, Verrey F, Geibel JP, Giebisch G, Hebert SC, Loffing J (2008) Mouse model of type II Bartter's syndrome. II. Altered expression of renal sodium- and water-transporting proteins. Am J Physiol Renal Physiol 294:F1373-1380.

Wang H, Garvin JL, Carretero OA (2001) Angiotensin II enhances tubuloglomerular feedback via luminal AT(1) receptors on the macula densa. Kidney international 60:1851-1857.

Wang J, Cortina G, Wu SV, Tran R, Cho JH, Tsai MJ, Bailey TJ, Jamrich M, Ament ME, Treem WR, Hill ID, Vargas JH, Gershman G, Farmer DG, Reyen L, Martin MG (2006) Mutant neurogenin-3 in congenital malabsorptive diarrhea. N Engl J Med 355:270-280.

Wang Q, Horisberger JD, Maillard M, Brunner HR, Rossier BC, Burnier M (2000) Salt- and angiotensin II-dependent variations in amiloride-sensitive rectal potential difference in mice. Clin Exp Pharmacol Physiol 27:60-66.

Warnock DG (2001) Liddle syndrome: genetics and mechanisms of Na+ channel defects. The American journal of the medical sciences 322:302-307.

Warth R, Bleich M (2000) K+ channels and colonic function. Reviews of physiology, biochemistry and pharmacology 140:1-62.

Warth R, Riedemann N, Bleich M, Van Driessche W, Busch AE, Greger R (1996) The cAMP-regulated and 293B-inhibited K+ conductance of rat colonic crypt base cells. Pflugers Arch 432:81-88.

Weinman EJ, Steplock D, Donowitz M, Shenolikar S (2000) NHERF associations with sodium-hydrogen exchanger isoform 3 (NHE3) and ezrin are essential for cAMP-mediated phosphorylation and inhibition of NHE3. Biochemistry 39:6123-6129.

Welsh MJ, Smith PL, Fromm M, Frizzell RA (1982) Crypts are the site of intestinal fluid and electrolyte secretion. Science 218:1219-1221.

Wilson CL, Ouellette AJ, Satchell DP, Ayabe T, Lopez-Boado YS, Stratman JL, Hultgren SJ, Matrisian LM, Parks WC (1999) Regulation of intestinal alpha-defensin activation by the metalloproteinase matrilysin in innate host defense. Science 286:113-117.

Winter DC, Schneider MF, O'Sullivan GC, Harvey BJ, Geibel JP (1999) Rapid effects of aldosterone on sodium-hydrogen exchange in isolated colonic crypts. J Membr Biol 170:17-26.

Woollhead AM, Baines DL (2006) Forskolin-induced cell shrinkage and apical translocation of functional enhanced green fluorescent protein-human alphaENaC in H441 lung epithelial cell monolayers. J Biol Chem 281:5158-5168.

Wyatt J, Vogelsang H, Hubl W, Waldhoer T, Lochs H (1993) Intestinal permeability and the prediction of relapse in Crohn's disease. Lancet 341:1437-1439.

Yang H, Jiang W, Furth EE, Wen X, Katz JP, Sellon RK, Silberg DG, Antalis TM, Schweinfest CW, Wu GD (1998) Intestinal inflammation reduces expression of DRA, a transporter responsible for congenital chloride diarrhea. Am J Physiol 275:G1445-1453.

Yu JX, Chao L, Chao J (1994) Prostasin is a novel human serine proteinase from seminal fluid. Purification, tissue distribution, and localization in prostate gland. J Biol Chem 269:18843-18848.

Yu JX, Chao L, Chao J (1995) Molecular cloning, tissue-specific expression, and cellular localization of human prostasin mRNA. J Biol Chem 270:13483-13489.

REFERENCES_____

Yun CH, Oh S, Zizak M, Steplock D, Tsao S, Tse CM, Weinman EJ, Donowitz M (1997) cAMP-mediated inhibition of the epithelial brush border Na+/H+ exchanger, NHE3, requires an associated regulatory protein. Proc Natl Acad Sci U S A 94:3010-3015.

Zeidel ML, Kikeri D, Silva P, Burrowes M, Brenner BM (1988) Atrial natriuretic peptides inhibit conductive sodium uptake by rabbit inner medullary collecting duct cells. The Journal of clinical investigation 82:1067-1074.

Zeissig S, Bergann T, Fromm A, Bojarski C, Heller F, Guenther U, Zeitz M, Fromm M, Schulzke JD (2008) Altered ENaC expression leads to impaired sodium absorption in the noninflamed intestine in Crohn's disease. Gastroenterology 134:1436-1447.

Zhou Z, Duerr J, Johannesson B, Schubert SC, Treis D, Harm M, Graeber SY, Dalpke A, Schultz C, Mall MA (2011) The ENaC-overexpressing mouse as a model of cystic fibrosis lung disease. Journal of cystic fibrosis : official journal of the European Cystic Fibrosis Society 10 Suppl 2:S172-182.